THE UNIVERSITY *of* EDINBURGH

THE UNIVERSITY *of* EDINBURGH

Diode Pumped Liquid Crystal Lasers

Calum M. Brown

A thesis submitted for the degree of Doctor of Philosophy

The University of Edinburgh

2022

This thesis is dedicated in memory of Lilias C. Tyre *(1925 – 2021)*; my biggest supporter and a frustrated academic whose education was interrupted by WWII and who would have otherwise pursued a career in medical science. Her determination and passion for learning are an inspiration and her unwavering support is greatly missed.

Abstract

Liquid crystal (LC) lasers have received much interest in photonics research for over twenty years. Their self-organising micro-scale structure, emission wavelengths spanning the visible spectrum and low thresholds offer many advantages over competing technologies. However, despite such benefits, LC lasers remain a lab-based curiosity. This is primarily due to the use of Q-switched lasers as the typical excitation source; the complexity, cost and size of which are orders of magnitude greater than the LC lasers they are pumping.

There has been much conjecture in the literature that a semiconductor-based pump source would offer a major step forward in the field. This thesis addresses this challenge, by demonstrating optical excitation using a laser diode (LD). Cleanroom fabrication processes and optical benchtop arrangements are presented to respectively produce and test LC lasers. A 445 nm LD was used to demonstrate the first unequivocal evidence of diode-pumped band-edge LC lasing, exhibiting a low threshold of 12.3 nJ/pulse and a narrow spectral linewidth (< 1.5 nm) at 610 nm. LC laser emission in the blue (480 nm) and green (530 nm) regions of the spectrum were also realised using the same 445 nm LD pump source.

An experimental investigation found that an increase in pump pulse length caused an increase in LC laser threshold and decrease in LC laser slope efficiency, thus verifying, for the first time, the theoretically hypothesised and anecdotally observed results of previously published work. It is only with the success of LD pumping that such an investigation was possible. LD pumping experiments also revealed the existence of an upper limit to the LC laser pulse length – irrespective of pump pulse durations that exceed this upper limit – with a value of 3.5 (± 0.1) ns for the DCM-based laser in this work. This phenomenon is attributed to the rate of intersystem crossing of the organic dye molecules.

Finally, the design, build and testing of the first diode-pumped LC laser prototype was realised, capable of producing up to 90 μW at 15 kHz at wavelengths ranging from 480 nm to 610 nm. This low-cost (< £3,000) and small-footprint (20 cm × 12 cm) laser was successfully used to image dye-doped LC droplets in a biomedical imaging lab, demonstrating the application potential of diode-pumped LC lasers. The novel results presented in this thesis are anticipated to have a significant impact on the development of LC lasers, regarding pump source selection, performance optimisation and application potential.

Lay summary

Laser beams of different colours are desirable in many applications, such as medical diagnostics and biological imaging. However, lasers that are capable of producing a wide range of colours (known as tuneable lasers) are often size and cost prohibitive, owing to the complexity of the technology. Liquid crystal (LC) lasers offer an attractive alternative to such systems. Compared to many tuneable lasers, they are significantly simpler and more compact, and do not require manual alignment. Furthermore, by simply varying the chemicals inside the LC laser (and their relative concentrations), colours spanning the spectrum from the ultraviolet to the near-infrared can be produced. One challenge with this technology, is the energy source used to produce laser emission, known as the pump source. Q-switched lasers have been exclusively used as the pump source for LC lasers, as they produce high peak powers in short timescales; a prerequisite for successful LC laser emission. However, they are significantly larger and more expensive than the LC laser component. Consequently, LC lasers have yet to be commercialised and remain in a lab-based research environment.

In this thesis, a blue laser diode (LD), capable of operating with a high current, was combined with high specification electronics to pump a well-fabricated LC laser. For the first time, LC laser emission using an alternative pump source was unequivocally demonstrated, with similar (and in some cases, identical) performance to the Q-switched pump regime. This long-awaited breakthrough also enabled an investigation into the performance limitations of LC lasers by controlling the LD's pulse duration – a feature not possible with Q-switched lasers.

The results from this work showed that decreasing the pump pulse duration benefitted LC laser performance, as evidenced by a lower threshold and higher slope efficiency. A novel investigation into the temporal dynamics of LC lasers was also conducted, to observe the effect that the pump pulse duration had on the LC laser pulse. The LC laser pulse length was found to be independent of pump pulse length (for long pump pulse lengths), with the upper limit to the LC laser pulse depending upon the laser dye. This could have profound implications on the application of LC lasers in the future.

The final part of the work in this thesis focussed on delivering the world's first diode-pumped LC laser prototype, for demonstrating the benefits of this technology in a practical setting. The laser beam from the prototype was successfully used in a medical imaging lab, highlighting the application potential of this breakthrough.

Declaration of authorship

I declare that the work presented in this thesis is entirely my own. Any exceptions are acknowledged accordingly.

I declare that:

a) This thesis has been composed entirely by myself, except where stated otherwise by reference or acknowledgment.
b) The work in this thesis was conducted solely by myself, except where stated otherwise by reference or acknowledgment.
c) That the work has not been submitted for any other degree or professional qualification.

Calum M. Brown
The University of Edinburgh
2022

Acknowledgments

Returning to academia after seven years in industry is one of the best decisions I've made, and I couldn't have done it without the support of my family, friends and colleagues.

I would like to thank my fellow liquid crystal laser researchers, Daisy, Jason & Ieva: Daisy for providing access to the microscope at the IGMM, and for distracting me with football at the adjacent desk in our office; Jason for his insightful feedback, and for constantly reminding me of how much older I am than the rest of the group; and Ieva for doing an excellent job programming the laser testing software and writing the code for the prototype motor, and for introducing me to Lithuanian mead.

Many thanks to Richard Scott, Iain Gold and Jamie Graham in the electronics workshop and Mark Mason in the mechanical workshop for their assistance in the construction of the laser diode modules and prototype. Thanks to Alistair Gorman and Hanning Mai for their respective advice on optical components and electronics. Thanks also to Danial Chitnis and Jonathan Terry for their advice and feedback during my annual reviews. I am very grateful to all the cleanroom and admin staff at the SMC for their assistance. A special thanks to Axel Thomson at Edinburgh Innovations for sharing his enthusiasm for my work and for his funding advice and support.

I would like to thank my parents, Jill and Davy, and sister, Tricia, for their ongoing support and for always taking an interest in my work. And many thanks to Adam, Bryony, Chris, Ellie, Jack, Joanna & Richard, for their friendship and advice.

There are two people to whom I am particularly grateful.
The first is my supervisor, Dr Philip Hands, whose enthusiasm, advice, support and mentorship throughout my PhD has been invaluable. We have spent many hours discussing liquid crystal lasers, research collaborations, funding opportunities, career options, (and electric cars!) and I am very grateful for his advice, feedback and generosity with his time.
The second is my wife, Allie, who has patiently listened to my ideas, sat through presentations, read my papers and always taken an interest in my work. During my PhD we endured lockdown together, we got engaged and married, and we bought our first home. I will always be grateful for her support during a very busy few years.

Lastly I would like to acknowledge Robert Greene's book, *Mastery*. This book reignited my passion for science and learning, and was partly responsible for my decision to quit a comfortable job to pursue a doctorate. While I'm sure I won't make it into the history books alongside the case-studies featured in *Mastery*, I hope that my PhD will enable me to make a positive contribution to science throughout my career.

Publications

C. M. Brown, D. K. E. Dickinson, and P. J. W. Hands, *"Advancing multi-wavelength liquid crystal laser microcavities in a compact prototype device using a laser diode pump source,"* in SPIE 11987, Laser Resonators, Microresonators, and Beam Control XXIV, vol. 1198703, 2022

P. J. W. Hands, C. M. Brown, D. K. E. Dickinson, S. M Morris and J. Lin, "*36-1: Invited Paper: Liquid-Crystal Lasers: Recent Advances and Future Opportunities",* SID Symposium Digest of Technical Papers, 53: 440-443, 2022

C. M. Brown, D. K. E. Dickinson, and P. J. W. Hands, *"Diode pumping of liquid crystal lasers,"* Opt. Laser Technol., vol. 140, p. 107080, 2021

C. M. Brown, I. Pakamorytė , and P. J. W. Hands, *"Exploring the temporal dynamics of liquid crystal lasers"*, 2022, (in preparation for submission to Optics Express)

C. M. Brown, I. Pakamorytė , and P. J. W. Hands, *"Investigating the effect of pump pulse length on liquid crystal laser threshold and slope efficiency"*, 2022, (in preparation for submission to Optics Letters)

Conference Presentations

Conference Presentation: C. M. Brown, D. K. E. Dickinson, J. Norman, P. J. W. Hands, *"Towards Commercialisation of Liquid Crystal Lasers"*, Rank Symposium: Liquid Crystals for Light, 2022

Conference Presentation: C. M. Brown, D. K E. Dickinson, P. J. W. Hands, *"Advancing multi-wavelength liquid crystal laser microcavities in a compact prototype device using a laser diode pump source"*, Photonics West Digital Forum, 2022

Invited Speaker: C. M. Brown, *"Why should(n't) I do a PhD?"*, IEEE Webinar, 2020

Conference Presentation: C. M. Brown, *"Liquid crystal lasers"*, School of Engineering Postgraduate Conference, 2020

Poster presentation: C. M. Brown, M. C. Normand, P. Chen, P. J. W. Hands, *"Improving repetition rates and tuning capabilities of liquid crystal lasers"*, Annual Conference of the British Liquid Crystal Society, 2019

Awards and Funding Grants

C. M. Brown & P. J. W. Hands, University of Edinburgh Principal's Innovation Award for *"Liquid crystal tuneable microlasers: A research project with transformative potential"* (£10,000), 2020

C. M. Brown, *Proof of Principle Funding Call in Optical Imaging for Life Sciences and Medicine* (£4,500), awarded by SINAPSE, SULSA and SUPA, 2019

Acronyms

ASE	Amplified spontaneous emission
CAD	Computer-aided design
CW	Continuous wave
DC	Direct current
DDN*LC	Dye-doped chiral nematic liquid crystal
DPLCL	Diode-pumped liquid crystal laser
DPSS	Diode-pumped solid-state
FRET	Forster resonant energy transfer
FWHM	Full width at half maximum
GUI	Graphical user interface
HTP	Helical twisting power
IPA	Isopropyl alcohol
IR	Infrared
ITO	Indium tin oxide
KOH	Potassium hydroxide
LC	Liquid crystal
LCD	Liquid crystal display
LD	Laser diode
LED	Light emitting diode
LTS	Laser testing software
ND	Neutral density
NIR	Near infrared
NLC	Nematic liquid crystal
N*LC	Chiral nematic liquid crystal
OPO	Optical parametric oscillator
PBG	Photonic band-gap
PC	Personal computer
PCB	Printed circuit board
PI	Polyimide
POM	Polarised optical microscopy
QSPLCL	Q-switch-pumped liquid crystal laser
SMC	Scottish Microelectronics Centre
TEM	Transverse electromagnetic
UV	Ultraviolet
VECSOL	Vertical external cavity surface-emitting organic laser
Nd:YAG	Neodymium-doped yttrium aluminium garnet

Contents

List of figures

List of tables

Chapter 1

Introduction

"Dare to be honest and fear no labour."

Robert Burns

1.1 Introduction

When the laser was invented by Ted Maiman in 1960, he described it as "a solution seeking a problem" and speculated on its potential usefulness in the medical industry [1]. Sixty-two years on, and the laser is now globally ubiquitous. From laser pointers to astronomical interferometry; from metal cutting to corrective eye surgery, the laser has revolutionised many fields, industries and professions throughout the world. It has enabled the detection of gravitational waves [2], facilitated global fibre optic communications [3] and allowed physicists to probe the fundamental constituents of matter [4]. As technology has advanced, so have the capabilities of lasers: a laser pulse with a duration of 43 attoseconds was observed in 2017 [5]; the world's most powerful laser (10 PW) was demonstrated in 2020 [6]; and a laser smaller than the wavelength of light was invented in 2009 [7]. Such examples highlight the ongoing endeavour to push the boundaries of laser technology and to introduce new lasers to new markets and applications. One such opportunity is in the development of liquid crystal (LC) lasers, which have the potential to revolutionise photonics in the form a compact, low-cost and wavelength selectable device.

1.2 Liquid crystal lasers

1.2.1 Historical context and performance characteristics

The concept of an LC laser was first introduced in a patent, published in 1973, by the United States Department of Navy [8]. However, it took another seven years before the first working LC laser was produced [9] and over ten years after that before the first theoretical explanation [10] and demonstration [11] of LC band-edge lasing. Band-edge LC lasers are therefore a relatively new and unexplored field in photonics, compared to dye lasers and solid state lasers for example, but they offer great potential in addressing the limitations of current laser technologies. The appeal of LC lasers is their simplicity; comprising a chiral nematic liquid crystal (N*LC) and an organic dye which, when mixed and sealed within a cell (consisting of two substrates with microscale separation), self-organises to form a laser cavity. A separate Q-switched laser is typically used to optically pump the laser cell to induce LC laser emission.

LC lasers perform in pulsed operation, with pulse lengths typically in the order of nanoseconds, and have been shown to deliver mW of average power at kHz repetition rates [12], [13]. Furthermore, they exhibit many features desirable from laser technology, such as: compact size (< 1 cm^2 cross-sectional area); low-cost; ability to emit wavelengths from the ultraviolet (UV) [14] to the near-infrared (NIR) [15]; self-assembling microstructure; low thresholds; and high efficiencies [16]–[18]. The wavelength accessibility of LC lasers can be achieved by wavelength tuning (whereby a gradual change in wavelength can occur, for example, by applying an electric field [19] or a change in temperature [12]) or wavelength selectivity (whereby multiple different wavelengths can be addressed in quick succession [13]).

Such characteristics exemplify the main advantages of LC lasers over competing technologies. Although LC lasers are not capable of generating the same pulse energies or peak powers as diode-pumped solid state (DPSS) lasers or laser diodes, they can emit wavelengths not currently accessible from either, in a single device [20]. And compared to other tuneable lasers, such as supercontinuum lasers, optical parametric oscillators and dye lasers, LC lasers are significantly smaller and lower cost.

1.2.2 Potential applications

The unique properties of LC lasers could be useful in many applications and have the potential to rival competing technologies. While the current limitations of LC lasers (with regards to output power and repetition rates) restrict the range of possible applications, the advantages they offer in terms of wavelength selectability, small footprint, low cost and hands-off alignment could be applied in several areas.

One example is in medical diagnostics. Laser-based technologies with different wavelengths have been shown to detect changes in the retina that indicate the onset of health conditions such as age-related macular degeneration, cardiovascular disease, strokes and neurodegenerative diseases including Alzheimer's disease, multiple sclerosis and Parkinson's disease [21], [22]. If diagnosed early enough, it can have a profound impact on the prognosis of patients. There is a limit to the number of single-wavelength lasers that can be integrated within a diagnostic system, however, particularly in a clinical environment where compact

and/or portable systems are often required. Thus, there is a finite number of wavelengths at the clinicians' disposal. The low power and broad wavelength range (387 – 850 nm [14], [15]) of LC lasers could be invaluable for addressing this challenge. This wavelength range could result in an improved detection range of retinal anomalies and the low powers of LC lasers (≤ mW) could be advantageous, as there are strict limits to the maximum optical power permissible in ophthalmic imaging.

In fluorescence microscopy, wavelength selectability is particularly important for targeting specific fluorophores and therefore reducing cross-talk [23]. Light sources such as broadband mercury or xenon arc lamps, light emitting diodes (LEDs), laser diodes (LDs) and supercontinuum lasers are typically used, with each having advantages and drawbacks [24]: arc lamps suffer from stability issues, and the broadband emission (~ 300 – 1000 nm) requires filters for accessing the desired wavelengths; LEDs, although a promising alternative to arc lamps, as they are robust and produce more stable emission, exhibit broadband emission (20 – 50 nm [25]) which can affect the image resolution; and although the narrow spectral linewidth of LDs and supercontinuum lasers can overcome this issue, the former has a limited range of wavelengths and the latter is large, expensive and suffers from non-uniform intensity across the spectrum. If the wavelength accessibility of LC lasers could be combined with minimising the cost and footprint of the pump-LC system, they would offer an attractive alternative to competing laser devices.

Other applications such as displays and holography have also been shown as promising candidates for LC laser applications. In displays, it has been shown that the colour gamut (that is, the range of perceivable colours available) in a hypothetical three-wavelength LC laser display would be higher than that of most modern television screens [26], [27]. In holography, although the spatial and temporal coherence of LC lasers have not been investigated in great detail, the work that has been done has indicated an intrinsic ability to reduce speckle while maintaining high resolution [28]. This is a subject worthy of further investigation that could lead to LC lasers being the light source of choice in holographic displays.

1.2.3 Technology challenges

Despite their many desirable features and application potential, at the time of writing this thesis, LC lasers have not been commercialised – they remain a lab-based curiosity. Moreover, there are many scientific questions regarding the performance of LC lasers that remain unanswered.

There could be several reasons for this:

1. The requirement for optical pumping by a Q-switched laser has a detrimental impact on the size and expense of what would otherwise be a low-cost and compact laser system.
2. Device optimisation requires a scaled-up manufacturing process, whereas research is currently limited to hand-made devices fabricated in limited-run batches.
3. There is very little evidence of LC lasers in an application-based setting, despite the numerous suggestions and predictions of their commercial potential in the research literature.
4. The limited performance capabilities of Q-switched lasers have rendered many LC laser characteristics difficult to experimentally investigate, such as the effect of pump pulse duration on LC laser pulse duration. Anecdotal experimental results [29] and theoretical hypotheses [30], [31] have therefore been required to predict the temporal performance of LC lasers.
5. Few research groups are investigating this technology, possibly because of the points above, resulting in slow dissemination and progress in the field.

Such scientific and commercial challenges offer exciting opportunities for developing LC laser technology. Until some solutions are demonstrated, LC lasers are unlikely to be considered a viable alternative to competing technologies. It is the purpose of the work presented in this thesis to address some of these limitations.

1.2.4 Limitations of Q-switched pumping

Since the advent of LC lasers, successful optical pumping has typically been achieved by Q-switched lasers. They are well suited as the pump source because of their ability to produce high-energy pulses in short timescales (nanoseconds and below). Thermal damage, optical reorientation and population of non-radiative energy states of the organic dyes are possible detrimental effects caused by longer pulse lengths, high repetition rates or high pulse energies [32]–[34]. The effects vary from gradual degradation of output intensity that recover over time, to immediate and permanent damage of the cell area undergoing optical excitation. Thus, while the short pulse durations of Q-switched lasers are ideal for mitigating against the deleterious effects caused by long pulse durations, their high pulse energies can also damage the organic dyes. Q-switched lasers have two further limitations regarding their suitability as an LC laser pump source: size and cost. They are typically one or two orders of magnitude larger than the LC laser cells, limiting the possibility of integrating the overall system with pre-existing devices. At costs varying from ~ £2,000 (for passive Q-switched nanosecond lasers) to > £100,000 (for active Q-switched picosecond lasers), the financial accessibility of such lasers is limited. The low cost and small footprint of LC lasers become irrelevant when they can only function when combined with these more complex Q-switched lasers. As stated in Ref. [35], an alternative pump source to overcome the limitations of the "unwieldy YAG[1] lasers" would greatly benefit the field. Furthermore, if this, as yet elusive, compact pump source were of a sufficiently short wavelength such that all wavelengths in the visible spectrum could be produced by LC lasers, it would offer a major step forward in small-footprint wavelength selective/tuneable technology.

[1] This abbreviation is referring to a Q-switched diode-pumped solid state (DPSS) laser based on a neodymium-doped yttrium aluminium garnet (Nd:YAG) crystal.

1.3 Aims and hypotheses

The work presented in this thesis aims to contribute to the knowledge, understanding and application potential of LC lasers by addressing the following hypotheses:

1. **Demonstrate an alternative pump source**
   An alternative to Q-switched pumping of LC lasers has been sought over the past few decades [31], [35]–[37]. The few attempts at achieving this using semiconductor-based technology have proven unsuccessful [12], [38]. By optimising the fabrication process and experimental arrangement, and combining a laser diode (capable of high current operation) with specialist electronics, it is hypothesised that LD-pumped LC lasing ought to be possible.

2. **Advance the understanding of the temporal dynamics of LC lasers**
   In addition to their size and cost limitations, the pulse duration of Q-switched lasers cannot be varied. Investigation into the effect of pump pulse duration on LC laser output is important for determining the optimum performance conditions. Only limited anecdotal evidence [29] and theoretical predictions [30] of the effect of pump pulse length on LC laser slope efficiency and threshold have therefore been possible, and even less work has explored LC laser temporal characteristics [31], [39]. A more rigorous investigation into such performance parameters would be feasible if semiconductor-based pumping were achieved, as this would allow temporal variation of the pump pulse.

3. **Develop the next generation of LC laser system for application demonstration**
   Some success has previously been achieved in reducing the size of LC laser arrangements for demonstration purposes [40]–[42]. However, the lower limit to size and cost has been dictated by the Q-switched pump source. Successful demonstration of a semiconductor-based pump source would enable the development of the next generation of LC laser demonstration systems in a smaller and lower-cost package. This could facilitate future LC laser integration into existing applications that currently require more expensive and complex lasers. Future favourable evaluation of LC laser performance in these areas could leverage commercialisation opportunities.

1.4 Thesis outline

This thesis begins with a theoretical background of LC lasers (Chapter 2), highlighting the key performance parameters upon which the experimental work in this thesis expands. The research responsible for the development of the LC laser over the past few decades is reviewed, with particular emphasis on the LC laser characteristics relevant for achieving optical excitation with a non-Q-switched pump source. Chapter 3 describes the experimental methodology throughout the work in this thesis. This focusses on the LC laser cell fabrication process and the laser lab experimental arrangements. Chapter 4 characterises the performance of an LC laser under Q-switched laser excitation. The concept of LD pumping is introduced and evidence of the first diode-pumped LC laser emission is presented. Chapters 5 and 6 build upon the work in Chapter 4, by determining the effect that the pump pulse duration has on the LC laser threshold and efficiency (Chapter 5) and the LC laser temporal characteristics (Chapter 6). Chapter 7 incorporates LD pumping with high repetition rate optical excitation, in the design, build and testing of the first diode-pumped LC laser prototype device. A potential application of this system is demonstrated in fluorescence microscopy. In Chapter 8, the conclusions from this work are drawn and the future of LC lasers is considered.

Chapter 2

Theoretical background and motivation

"In every branch of knowledge the progress is proportional to the amount of facts on which to build, and therefore to the facility of obtaining data."

James Clerk Maxwell

2.1 Introduction

This chapter reviews and critically analyses liquid crystal (LC) laser literature, with a focus on the performance parameters investigated in this thesis. Of particular interest, are the temporal dynamics of LC lasers; a subtopic that is introduced in this chapter and reviewed in greater depth in later chapters. The various tuning mechanisms that have been demonstrated in the literature are summarised, as motivation towards commercialisation of LC lasers. Finally, the limited attempts at demonstrating non-Q-switched lasers as pump sources are discussed, and motivate the principal aim of this thesis. Before this, however, the properties of LCs are presented and placed in a historical context.

2.2 Introduction to liquid crystals

2.2.1 Historical context and commercial motivation

The existence of LCs has been known for over 100 years, with their discovery attributed to the Austrian botanist, Friedrich Reinitzer, in 1888 [43]. Reinitzer observed two melting points in a cholesterol; one at 145.5 °C and another at 178.5 °C, which were accompanied by a change from a solid to a cloudy liquid at the first temperature, and a cloudy liquid to a clear liquid at the second temperature. Reinitzer sent samples of this material to Otto Lehmann; a professor of physics in Germany who specialised in constructing microscopes to observe the crystallisation properties of materials [44]. He also observed the same two-step temperature change upon melting, which agreed with observations he had made with his own samples. This led him to the realisation that there was an intermediate phase between the solid and liquid states when the material was opaque, which he called a liquid crystal. In 1889, he published his findings in a paper entitled “Über fliessende Krystalle” [45] (which translates as “On Flowing Crystals” [46]).

It wasn’t until 1972 that LCs became commercially available, when George Gray *et al.* synthesised the first alkylcyanobiphenyls, which exhibited liquid crystalline properties at room temperature [47]. Their paper was written towards applying LCs to display applications and, throughout the 1970s, this application was realised in commercial devices such as watches, calculators, and personal organisers [48]. Their small scale, low weight and low-voltage

operation made them particularly attractive for replacing cathode-ray technology (previously used in televisions and computer monitors) with compact and high definition liquid crystal displays (LCDs).

The advancement of LCs has coincided with the development of other areas in science and technology such as organic chemistry, physics, electronics, device engineering and fabrication facilities. Of particular relevance to this thesis, is their impact in photonics. A report published in 2022 valued the global LCD market at $148 billion in 2021, with a predicted value of $1,422 billion by 2029 [49]. This not only demonstrates the investment in LC-based applications, but presents an opportunity for introducing new LC-based technologies to a growing market. The technological revolution that LCs brought to the display sector in terms of mass production capabilities and reduction in size, cost and power consumption compared to the previous state of the art, can be compared to the significant advantages that LC-based lasers offer over competing technologies. It took seventy years for LCs to be translated from a research environment to a commercial setting; the aim of this thesis is to bring a similar success closer to realisation for LC lasers, and do so in a shorter timescale.

2.2.2 Liquid crystal mesophases

The most common states of matter (i.e. solids, liquids and gases) are distinguished by the relative position, orientation and separation of the atoms or molecules within the structure. In a solid, the constituent particles are closely spaced together and movement is limited by rigid bonds; in liquids, the movement of particles is less restricted than in solids; and in gases, the particles experience greater separation than in solids and liquids, and are able to flow freely. Crystals are solid materials in which the atoms or molecules are highly ordered and form an isotropic lattice structure (Figure 2.1a). It is this positional order that differentiates crystals from liquids. In liquids, the molecules are able to flow with random positional and orientational ordering throughout the sample (Figure 2.1d). In comparison, rigid crystals have positional (and often also orientational) molecular ordering.

An LC mesophase can be exhibited by some materials, in which the particles move as if in a liquid state, but exhibit some degree of positional and/or orientational order. They can either be thermotropic or lyotropic, with the former having temperature dependent phase transitions,

and the latter's formation being dependent upon solvent concentration [50]. LC molecules (mesogens) can also be described in terms of their shape, such as calamitic (rod-like) and discotic (disc-like). The general molecular structure of a calamitic LC consists of a rigid core, typically comprising linearly linked ring systems of aromatic groups, at the end of which are flexible alkyl or alkoxy chains which are often polar [44]. This gives rise to molecular anisotropy, depicted by the rod-like shapes in Figure 2.1.

Further categorisation defines the mesogens' orientational and positional order, including nematic, smectic and cholesteric LCs [44]. The nematic mesophase (NLC) is the least ordered, with no positional order but some orientational order, with the time-averaged preferred orientation described by a unit vector, $\hat{\mathbf{n}}$, known as the director. This lack of positional order means that NLCs have a high degree of fluidity, allowing easy manipulation. The smectic mesophase has positional and orientational order and occurs at a lower temperature than the nematic mesophase. Figure 2.1 shows the phase transitions for a hypothetical thermotropic LC with calamitic mesogens: at low temperatures, a crystalline solid is formed, with smectic and nematic mesophases occurring as the temperature is increased above the melting point, before reaching the clearing temperature, above which the material becomes an isotropic liquid [3].

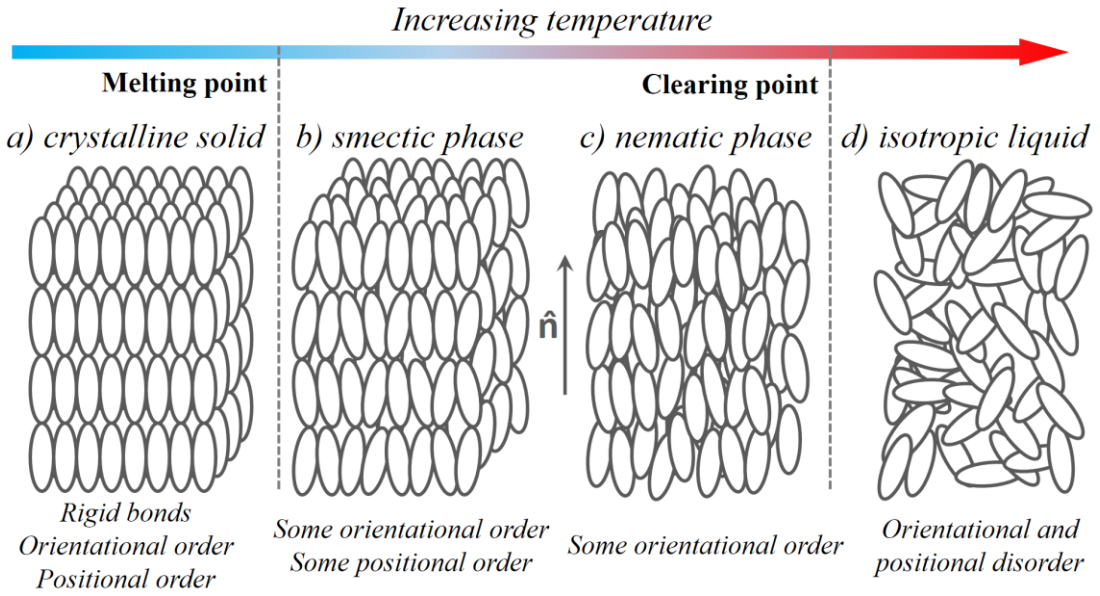

Figure 2.1. Representation of calamitic molecules in different phases where a) is a crystalline solid b) is a smectic phase LC, c) is a nematic phase LC and d) is an isotropic liquid. The time-averaged preferred orientation for the smectic and nematic phases are shown by the vertical unit vector, $\hat{n}$. (Image adapted from Ref. [48]*.)*

The degree of orientational order of an LC is defined by the order parameter, S, given by [44]:

$$S = \left\langle \frac{3}{2}\cos^2\theta - \frac{1}{2} \right\rangle \qquad \text{Equation 2.1}$$

where θ is the angle between the director and a given molecular axis. For example, a solid (or a perfectly aligned LC) has an order parameter $S = 1$ and, for a liquid, $S = 0$, where the molecules are randomly oriented.

The cholesteric mesophase (so-called for historical reasons, as this phase was first discovered in cholesterol [48]) is similar to the nematic, in that it exhibits long-range orientational order, but differs in that the director varies regularly throughout the medium, resulting in a helical structure. The distance over which the director rotates by 360 ° is known as the pitch, P, and is perpendicular to the LC director (Figure 2.2).

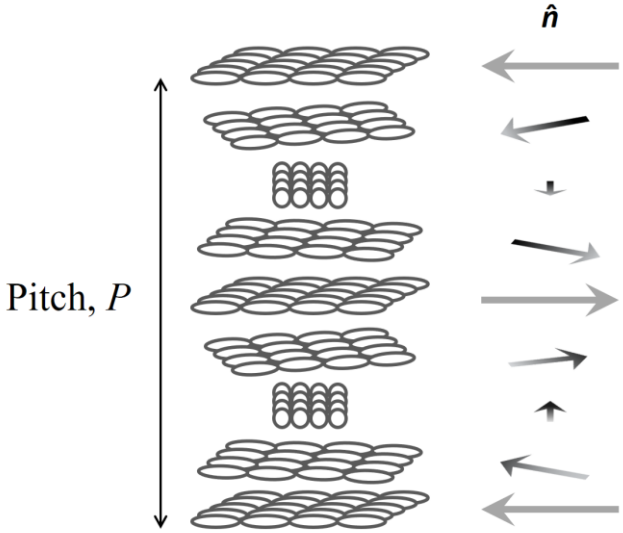

Figure 2.2. Impression of the cholesteric mesophase, exhibiting a full 360° degree twist, with a pitch the length, P. The twist is highlighted by the rotation of the director, n̂.

An NLC can form a helical structure, similar to a cholesteric, by adding a chiral dopant. This induces a twist in the nematic structure, resulting in a chiral nematic LC (N*LC). The pitch of the N*LC is controlled by the concentration of the chiral dopant relative to the NLC; a property exploited throughout this thesis. The ability of a chiral dopant to induce a twist in the nematic phase is quantified by the helical twisting power (HTP) [51]. For a given mixture for which the HTP is known, the pitch is calculated by:

$$P = \frac{1}{HTP * ee * [C]} \qquad \textit{Equation 2.2}$$

where ee is the enantiomeric excess (defined as the purity of the chiral dopant) and $[C]$ is the concentration of the chiral dopant.

2.2.3 Optical properties

The optical properties of NLCs and N*LCs vary, depending upon how they are orientated relative to the substrates they are confined between. This is known as surface anchoring or surface alignment, and is determined by the interaction of the LCs with the confinement material [52]. If the director is parallel to the surface, this is termed *planar alignment*, whereas perpendicular orientation of the director to the surface is *homeotropic alignment* [53]. For completeness, the different alignment regimes of NLCs and N*LCs are summarised in Figure 2.3, with the standing helix alignment (Figure 2.3d) of particular importance for this thesis. The ability of LCs to self-assemble when confined between alignment layers is a key feature with respect to this work.

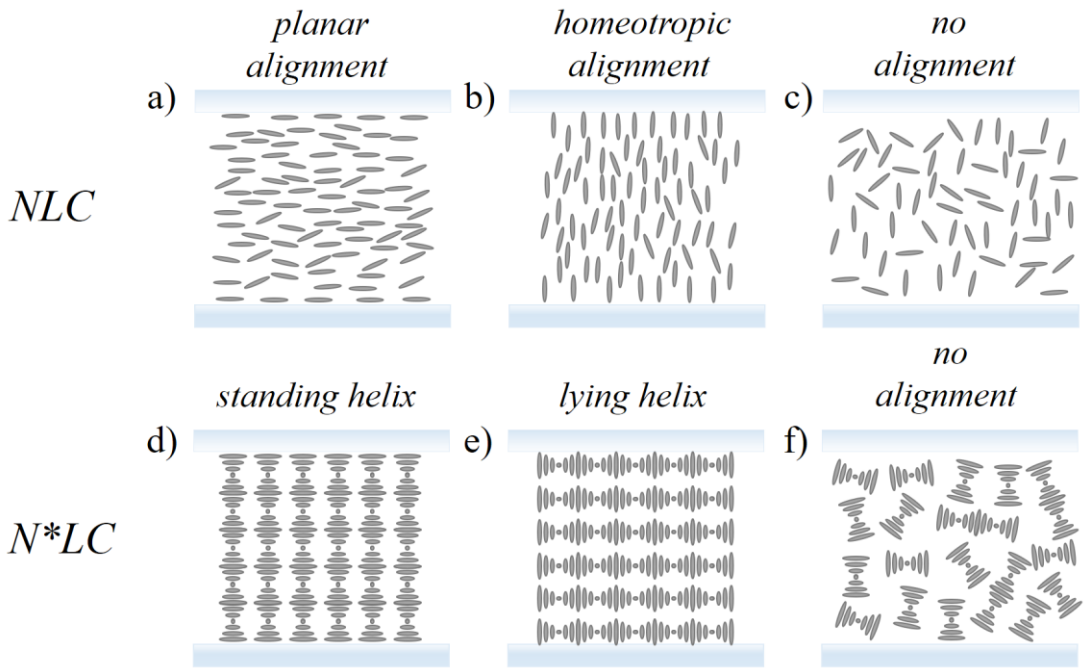

*Figure 2.3. Alignment of LCs under varying surface anchoring conditions showing an a) NLC with planar alignment, b) NLC with homeotropic alignment, c) NLC with no alignment, d) N*LC with planar alignment resulting in a standing helix (aka Grandjean texture), e) a uniform lying helix* [54] *and f) N*LC with no alignment (aka focal-conic texture).*

LC mesophases are optically anisotropic due to the uniaxial nature of the molecules. The long axis of calamitic mesogens is referred to as the optic axis or extraordinary axis with refractive index n_e, and is rotationally symmetric around the director axis. The short axis, known as the ordinary axis, has refractive index n_o and is perpendicular to the director. This difference in refractive index gives rise to birefringence, whereby the propagation of light through the material is polarisation dependent [55].

The birefringence, Δn, is defined by:

$$\Delta n = n_e - n_o \qquad \textit{Equation 2.3}$$

As previously mentioned, the addition of chiral dopant to an NLC results in a chiral structure, with the concentration of the dopant determining the helical pitch. In an N*LC, the periodic rotation of the director gives rise to a periodic variation in refractive index. As a consequence, wavelength-selective Bragg reflection occurs along the helical axis for circularly polarised light of the same handedness as the chiral helix for a range of wavelengths, $\Delta\lambda$. This is dependent upon the birefringence, Δn, such that [56]:

$$\Delta\lambda = \Delta nP \qquad \textit{Equation 2.4}$$

where P is the helical pitch given by:

$$P = \frac{\lambda_c}{\bar{n}} \qquad \textit{Equation 2.5}$$

and where λ_c is the central wavelength in the $\Delta\lambda$ range. $\bar{n}$ is the average refractive index defined as:

$$\bar{n} = \frac{n_e + n_o}{2} \qquad \textit{Equation 2.6}$$

The wavelength range, $\Delta\lambda$, is known as the photonic band-gap (PBG) and is observed in the transmission spectrum of unpolarised white light (which can be considered as comprising a combination of 50 % left circularly polarised and 50 % right circularly polarised light) through an N*LC in a standing helix configuration, an example of which is shown in Figure 2.4.

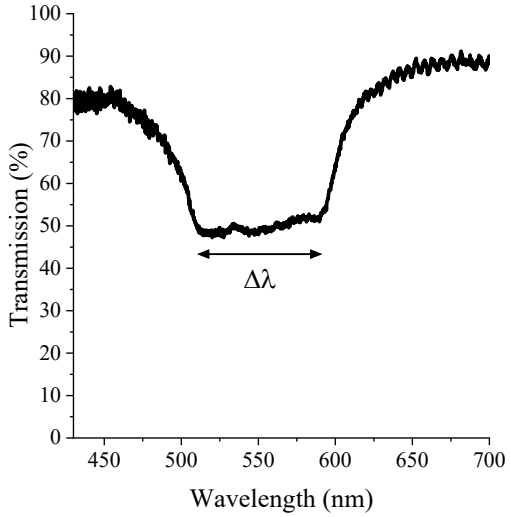

*Figure 2.4. Unpolarised white light transmission spectrum of an N*LC, showing the characteristic photonic band-gap across the wavelength range, Δλ. This N*LC comprised the LC BL006 (Merck) with 4.35 wt% of the chiral dopant BDH-1281 (Merck).*

While circularly polarised light of the same handedness as the chiral helix is reflected by the PBG, all other polarisation states and wavelengths outside the PBG are transmitted [57]. This property of N*LCs contributes to the lasing mechanism presented throughout this thesis. Before this is elaborated upon, however, the basic principle of lasing is presented.

2.3 Introduction to laser operation

The classical design of a laser in its most fundamental form, is based on two mirrors, a gain medium, and an energy source [58] (Figure 2.5). The mirrors form a resonant cavity, known as a Fabry-Perot cavity, with one mirror 100% reflective and the other, known as the output coupler, partially transmissive at the lasing wavelength. Within the cavity, the gain medium is responsible for energy absorption and photon emission. Depending on the type of laser, this gain medium can be a solid crystal, a liquid dye solution or a gas. Optical or electrical energy is provided by a pump source and is absorbed by the gain medium.

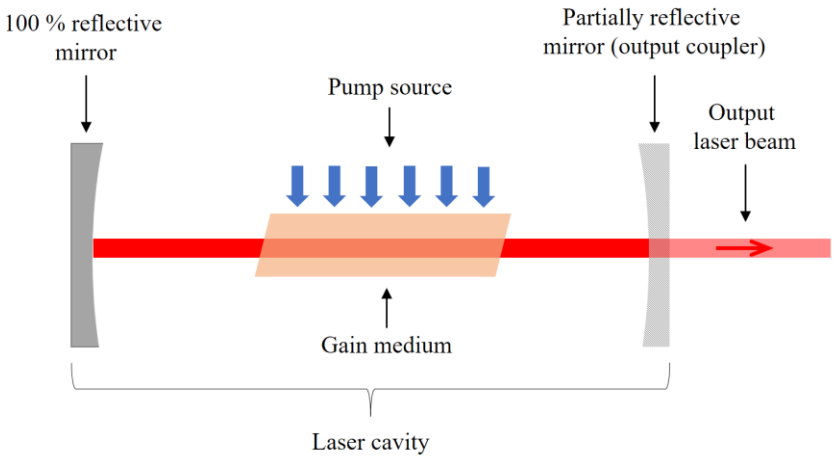

Figure 2.5. Basic design of a Fabry-Perot laser cavity.

Absorption of the pump source causes the electrons in the gain medium to transition to a higher energy state; a process known as excitation (Figure 2.6a). Electrons in this excited state can decay/de-excite to a lower energy level, emitting a photon via spontaneous emission (Figure 2.6b). As pumping continues, the population of electrons in the excited state continues to increase until the number of electrons in the excited state exceeds the electron population in the ground state. This is known as a population inversion and is the condition required for laser emission. When an electron in the excited state decays to emit a photon, this photon can cause other excited electrons to decay and emit photons, resulting in optical amplification. The photons exhibit the same wavelength, phase and direction as the photons that caused the decay. This is known as stimulated emission (Figure 2.6c). The purpose of the mirrors is to form a resonant cavity, which enables optical feedback to promote further stimulated emission. The partial reflectivity of the output coupler allows some of the light to leave the cavity in the form

of a laser beam. The minimum pump energy required to form a population and induce stimulated emission is known as the laser threshold [59]. Depending upon the pumping technique and cavity design, the laser output can be a continuous stream of photons, known as continuous wave (CW) lasing, or it can be pulsed. An example of the latter is a Q-switched laser (of particular interest with respect to a pump source used in this thesis), whereby an intracavity optical "switch" prevents the laser light from being coupled out of the system, resulting in a build-up of photons [60]. When the state of this switch is changed, the photons are emitted from the device in a short (nanoseconds or shorter), intense light pulse, often with a peak power typically in the order of kilowatts or higher.

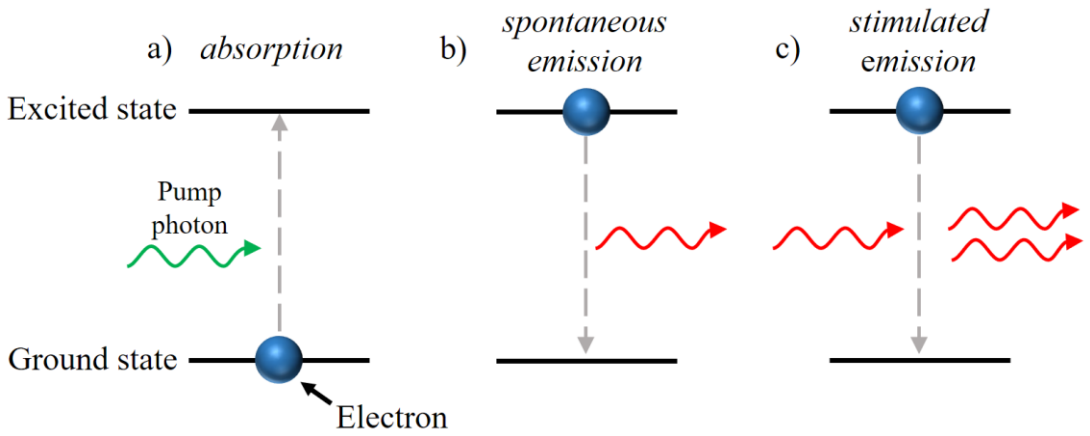

Figure 2.6. Simplified diagram of energy level transitions showing absorption, spontaneous emission and stimulated emission.

2.4 Liquid crystal band-edge lasers

2.4.1 Theory of operation

In an LC laser, the mechanism for lasing is different to the laser based on a Fabry-Perot cavity, but is based on the same fundamental principles of optical resonance in the presence of a gain medium.

With reference to the one-dimensional PBG of a self-assembling standing helix N*LC introduced in Section 2.2.3, Kopp *et al.* showed that the density of photonic states, i.e. the number of allowed reflections, tends to infinity at the band-gap edges (known as the band edges) for an infinitely large structure, or is maximum for a structure of finite thickness [61]. The maximum density of photonic states corresponds to a maximum photon dwell time in the N*LC. Therefore, it is at the band edges where optical amplification is maximum and, in the presence of an appropriate gain medium, laser emission is possible. This is known as photonic band-edge lasing. Unlike the Fabry-Perot laser where optical resonance occurs between two mirrors, the optical resonance in band-edge lasing is based on the principal of distributed feedback, whereby Bragg reflections, caused by the periodic refractive index change of the N*LC, result in optical feedback. Lasing typically occurs at the long band edge, λ_{long}, given by [62]:

$$\lambda_{long} = n_e P \qquad \textit{Equation 2.7}$$

although short band-edge lasing is also possible [63], in which case the laser wavelength is found by:

$$\lambda_{short} = n_o P \qquad \textit{Equation 2.8}$$

Organic dyes are typically used as the gain media in LC lasers due to their solubility in LCs, and for their broad fluorescence spectra which enable a range of laser wavelengths, spanning the full visible spectrum and beyond [14], [15]. The choice of dye in an LC laser is dependent upon the dye's absorption and fluorescence spectra, whereby the absorption spectrum is selected to coincide with the wavelength of the optical pump source (or conversely, the pump source is selected to match the absorption spectrum of the dye), and the desired LC laser

wavelength is within the dye fluorescence spectrum. When the dye fluorescence spectrum overlaps with the (typically long) band edge of the PBG, laser emission is possible, provided that the pump pulse energy density is sufficiently high to overcome threshold. Under this condition, LC laser emission occurs along both directions of the N*LC helical axis. An appealing feature of LC lasers is that the lasing wavelength can be easily defined during fabrication, simply by changing the concentration of the chiral dopant (provided that the band edge remains within the dye fluorescence spectrum). The condition for band-edge lasing is summarised in Figure 2.7, whereby optical excitation is provided by a 532 nm laser which overlaps with the absorption of the organic dye, and the long band edge of the PBG overlaps with the fluorescence spectrum of the dye, resulting in laser emission at 610 nm.

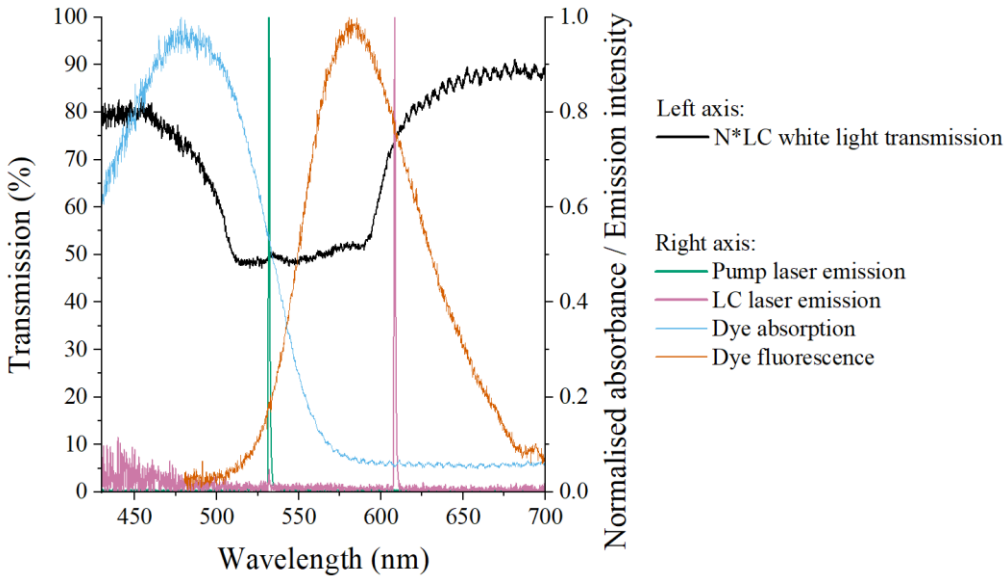

*Figure 2.7. Band-edge lasing condition showing the white light transmission of an N*LC (black line), and the absorption (blue line) and fluorescence spectra (orange line) of DCM. The long band edge of the N*LC coincides with the fluorescence spectrum of the dye, resulting in narrow-linewidth laser emission (pink line) under optical excitation with a 532 nm pump source (green line)* [2].

Organic dye molecules typically operate in a four-level energy system in which radiative and non-radiative energy transitions occur upon optical excitation [64]. This can be represented in a Jablonski diagram (Figure 2.8).

[2] Although LC laser emission is produced, this system is not optimised, as the pump wavelength does not coincide with the absorption maximum, and the long band-edge does not overlap with the fluorescence maximum of the dye.

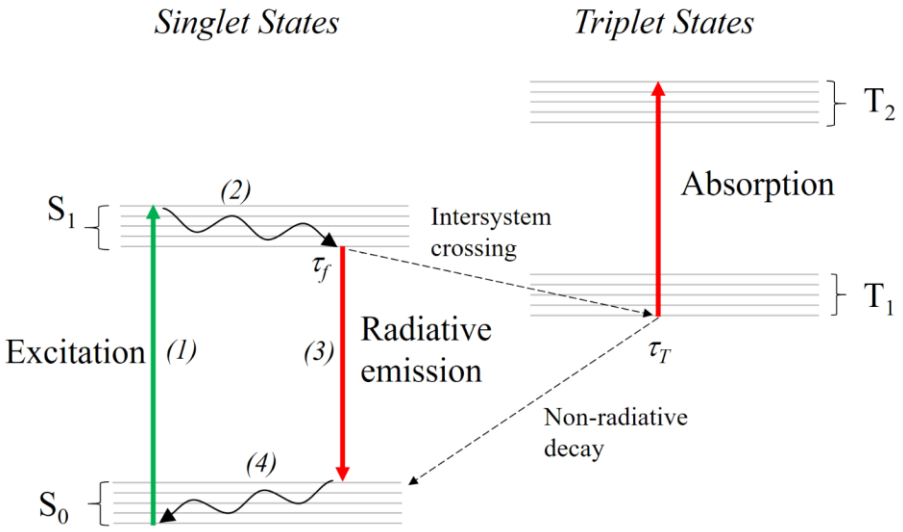

Figure 2.8. Four-level Jablonski diagram showing allowed energy level transitions within and between singlet and triplet states.

The ground state and first excited state of the singlet and triplet energy levels can be used to explain the mechanisms that both enable and inhibit stimulated emission from LC lasers under optical excitation. In Figure 2.8, S_0 is the ground singlet state, S_1 is the first excited singlet state, T_1 is the ground triplet state, and T_2 is the first excited triplet state [65]. When the energy of the pump source is absorbed by a dye molecule, optical excitation promotes the molecule from the lowest vibrational level of S_0 to the highest vibrational level within S_1 (*(1)* in Figure 2.8). Through a non-radiative process, the molecule decays to the lowest vibrational level in S_1 *(2)* before decaying to an upper energy level of S_0 *(3)*, emitting a photon in the process. In a laser operating at or above threshold, this decay mostly occurs via stimulated emission. Below threshold, this decay happens through spontaneous emission, also known as fluorescence, and can occur to/from different energy levels, thus giving rise to a broader fluorescence spectrum. The molecule then non-radiatively decays back to the lowest state of S_0 *(4)*.

Radiative emission is only permitted within either singlet to singlet state transitions or triplet to triplet state transitions. However, non-radiative transitions between an excited singlet state to a lower-energy triplet state can also occur. This intersystem crossing has a finite probability of occurring and is detrimental to laser operation. T_1 is a metastable state, as the transition from this state to the lower energy state S_0 is statistically forbidden but *can* occur, meaning the lifetime is orders of magnitude longer than the lifetime of the molecule in S_1. This has two

implications that are detrimental to laser performance: firstly, molecules in T_1 will accumulate, meaning fewer molecules are available to participate in stimulated emission; and secondly, the optical energy absorption required for triplet excitation from T_1 to T_2 corresponds to the fluorescence associated with singlet radiative decay. Thus, the photons in S_1 that would be available for stimulated emission can be absorbed by the triplet state, resulting in optical losses that can quench lasing. This can be minimised by ensuring that optical excitation occurs over a timescale shorter than the inverse of the rate of intersystem crossing [66]. This validates the pumping of LC lasers with nanosecond-scale Q-switched pulses, as the rate of intersystem crossing of organic dyes falls within the range of $10^6 – 10^8$ s^{-1}. The lifetime of the dyes' triplet ground state, τ_T, typically of the order of 10^{-3} s, is of importance when considering the repetition rate, *f*, of the pump laser. Provided $1/f > \tau_T$, the population of T_1 should not cause significant degradation in lasing performance [32].

2.4.2 Liquid crystal laser performance parameters

2.4.2.1 Slope efficiency & threshold

The slope efficiency of a laser, η_s, is the ratio of output energy to input (pump) energy, expressed as a percentage:

$$\eta_s(\%) = \frac{E_{out}}{E_{in}} * 100 \qquad \textit{Equation 2.9}$$

This is a common figure of merit for laser systems. Often, a graph showing output energy as a function of input energy is plotted to determine and visualise the efficiency (Figure 2.9). Usually for band-edge LC lasers, there are two distinct gradients. As the input energy is increased from zero, there is a gradual increase in the spontaneous emission from the system. This region is characterised by a shallow gradient and a broad emission spectrum. When the input energy reaches a certain value, the emission spectral bandwidth narrows and the efficiency gradient increases as stimulated emission becomes the dominant process. The point at which the gradient changes and stimulated emission dominates is the threshold energy, E_{th}.

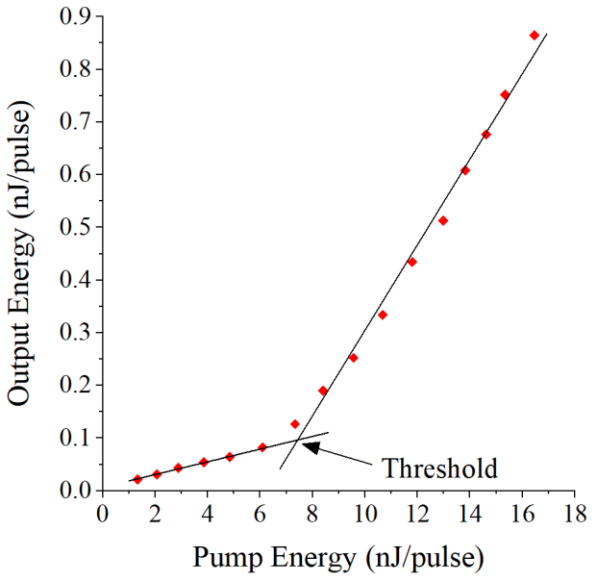

Figure 2.9. Plot of output pulse energy as a function of the input pump pulse energy. Lasing begins at threshold, with the slope efficiency calculated from the gradient of the line above threshold.

Increasing the efficiency and reducing the threshold have been two of the main focuses of LC laser research. A common and longstanding goal within the field is to achieve lasing using low energy light sources such as light emitting diodes or laser diodes, as this could enable the use of low cost and compact dye-doped (DD) N*LC lasers in applications ranging from displays, fundamental physics and chemistry research and medical diagnostics [34], [37], [67]. The following paragraphs detail some of the achievements to-date in improving the efficiency and threshold of LC lasers.

When the DDN*LC is confined between two substrates, this is known as the laser cell[3]. The design of the laser cell containing the DDN*LC has been shown to impact the efficiency and threshold of LC lasers, to varying degrees. There are two cell geometries that can be used – transmissive and reflective, both of which result in light emission perpendicular to the substrate. In a transmissive geometry, the output beam is circularly polarised and bidirectional along the helical axis, whereas a reflective cell has a reflective coating on the inner surface of one of the substrates, resulting in uni-directional emission. In this regime, LC laser emission is linearly polarised, caused by the superposition of left-handed and right-handed circularly polarised light [68].

[3] A detailed discussion of the typical composition and fabrication of an LC laser cell is presented in Chapter 3.

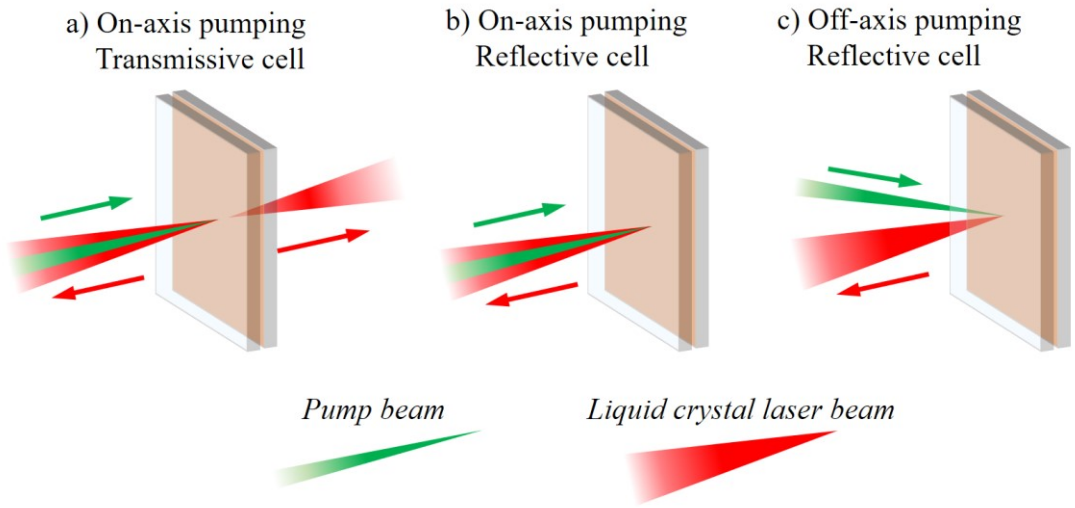

Figure 2.10. Different LC laser cell pumping regimes with a) on-axis transmissive cell, showing bi-direction output, b) on-axis reflective cell with uni-directional output parallel to the input and c) off-axis reflective cell geometry. Arrows indicate beam direction of travel.

Several studies have demonstrated the benefits of a reflective cell geometry. Amemiya *et al.* observed an eight-fold increase in output intensity when one of the inside surfaces of the cells was coated in aluminium [69]. However, there was no noticeable reduction in threshold when compared to a transmissive cell in this work, nor was a quantitative analysis of efficiency increase offered, even though the data presented suggested an apparent improvement. A similar experiment was carried out by Zhou *et al.* in which the doubling of efficiency of a reflective cell was presented when compared to the transmissive equivalent [70]. Again, no specific value for the efficiency was provided. However, a more thorough experiment was carried out by Mowatt *et al.* [71]. Their results offer more conclusive evidence of performance improvements resulting from a reflective cell geometry. Here, an increase in efficiency from 39% to 60% was found for the transmissive and reflective geometries respectively. At the time of writing this thesis, this is believed to be the highest recorded efficiency to-date. Furthermore, a reduction in threshold was found for the same data. An interesting feature of the three papers detailing these findings is the similarities in experimental configuration and laser design. All are pumped at low repetition rates (1 – 10 Hz) with near-identical pump pulse lengths (4 – 6 ns) and use aluminium as the reflective surface. An obvious question is, therefore, what are the differences between these experiments? There were two significant differences in Ref. [71] compared to the Refs. [69] and [70]. The first was the material onto which the aluminium layer was applied. Mowatt *et al.* used a conductive silicon substrate, as opposed to a standard glass substrate referenced in the other two papers. This, according to

Mowatt *et al.*, improved the thermal conductivity, thus allowing heat to be conducted away from the cell area undergoing optical excitation. The second difference was the application of a broadband anti-reflection coating on the outer surfaces of the cell to prevent reflection of the pump beam. While such a high efficiency was measured, it must be noted that their standard transmissive cell had an efficiency of 39 %; an already exceptional value which increased by less than a factor of two when the aluminium later and anti-reflective coating were present.

It can be concluded from these papers that a reflective cell geometry improves the output intensity and efficiency of the cells, as a result of the double-pass of the pump beam increasing the absorption, and the superposition of the reflected output beam with the unreflected beam.

There are further design considerations that can also have an impact on threshold and slope efficiency. Several experimental and theoretical studies have been carried out to determine the impact of the substrate separation (/cell spacing/thickness) on the slope efficiency and threshold of DDN*LCs. Cao *et al.* derived an expression to quantify the effect of cell spacing, which suggested that the optimum value would fall within the range of 15 – 25 μm [29]. Morris *et al.* applied this theoretical derivation to their own experimental work and found similar results, showing that the cell spacing for which the threshold was minimised and efficiency was maximised was within a range of 10 – 15 μm [63]. This was corroborated by Sans-Enguita *et al.* who demonstrated optimum laser performance with a cell thickness of 14 μm and found that the spacing had a more profound impact on the efficiency than the threshold [37]. Interestingly, their results showed that the peak efficiency did not coincide with the lowest measured value for threshold. This contradicts the evidence presented in other works, for example Refs. [29], [63], [71], in which $E_{th} \propto 1/\eta_s$. This thesis experimentally explores this in greater detail.

The experimental work presented by Cao *et al.* in Ref. [29] included another interesting result that has had limited attention from the LC laser community, and motivated much of the work in this thesis. In addition to the effect of cell thickness on efficiency and threshold, both parameters were investigated in relation to the pulse length of the pump laser, τ_{pump}. The pulse length of Q-switched lasers (the preferred pump source for LC lasers) is determined by the cavity design and cannot be varied. In Ref. [29], a Q-switched laser with $\tau_{pump} = 7.5\ ns$ was compared to a mode-locked laser with $\tau_{pump} = 40\ ps$ (both at 532 nm) when pumping

the same cell. The data show a decrease in threshold from 53 nJ/pulse to 4.13 nJ/pulse, respectively. This is in good agreement with the theory presented in Ref. [37], which showed that the threshold is proportional to the pulse length. It is believed that the work in Ref. [29] is the only example of experimental results showing the effect of pump pulse length on threshold. However, the pulse lengths used were dependent upon the pump sources and the study was therefore limited to these two arbitrary durations. No incremental studies with multiple pulse lengths have ever been made (due to the aforementioned limitations of the pump sources) to determine the nature of the impact of pulse length on threshold, nor have there been any investigations into the effect on LC laser slope efficiency.

In a theoretical model by Shtykov *et al.* (which will be explored in greater detail in Chapters 5 and 6), an increasing linear trend in threshold and an inverse trend in efficiency were also predicted, but as a function of the rise time of a trapezoidal pulse, in anticipation of a semiconductor-based pump source being successfully demonstrated [30]. While this agrees with the limited experimental evidence of Ref. [29], the two sources cannot be directly compared due to the difference in the pumps' temporal characteristics.

In addition to the lack of published evidence of the effect that pump pulse duration has on LC laser threshold and efficiency, the characterisation of LC laser pulse length as a function of pump pulse length is not believed to have been investigated. This would offer greater insight into the optimum performance requirements of LC laser pump sources and the performance limitations of LC lasers.

2.4.2.2 Repetition rate

A parameter of Q-switched lasers that *can* often be varied is the pulse repetition rate, *f*, often ranging from 1 Hz to > 100 kHz. High frequency operation of DDN*LC lasers is desirable to achieve higher average powers. However, as elaborated upon in Section 2.4.3, degradation at high frequencies has been demonstrated, with various studies offering compelling reasons for this effect. Most research into LC lasers is conducted at low repetition rates < 10 Hz, so as not to degrade the performance during data acquisition. While this allows investigations into performance parameters, high frequency operation is advantageous (and even necessary) for practical applications. Conventional dye lasers typically flow the dye-solvent mixture to allow

high repetition rate, or even CW operation, to minimise thermal effects [72], [73], [67]. This hydrodynamic flow has been attempted with DDN*LC lasers but with limited success [74]. The maximum repetition rate achieved was 1 kHz, and did exhibit a more stable output when the LC mixture was flowed, compared to a conventional DDN*LC laser cell. However, flow-induced LC domain variations produced multiple wavelengths simultaneously.

The highest repetition rate published (at the time of writing this thesis) was realised by Normand *et al.* in 2018 [13]. By positioning the pump beam at a radius of 20 mm from the centre of a spinning laser cell, a stable output at 10 kHz was achieved for over 1 hour. While this was an order of magnitude improvement upon previous results, there is clearly a limit to this technique, as an impractical cell radius (> 1 m) would be required for pumping in the MHz regime, for example.

In 2012, a paper was published by Munoz *et al.* in which CW LC lasing was claimed [38]. According to the authors, by using a fabrication method known as polymer templating, a temperature independent N*LC structure resulted in the cell's ability to withstand CW pumping from a 532 nm laser. However, this claim is disputed, as the output did not have the characteristic narrow linewidth commonly observed in a band-edge laser, and instead showed a narrow linewidth feature as part of a broader fluorescence; behaviour, according to Ortega *et al.* [31], more akin to amplified spontaneous emission (ASE)[4]. When attempting to show the typical change in gradient of the slope efficiency often used to identify laser threshold, only a few data points were used to determine a point of intersection and there was a continuous curvature in the efficiency graph rather than a distinct change in gradient. Therefore, only weak evidence of lasing above threshold was provided. Crucially, no temporal stability data were presented – the acquisition time was simply given as "> 5 sec". To the author's best knowledge, no papers have been published since Ref. [38] that claim CW emission from an LC laser, suggesting that this challenge has not been overcome. The fundamental mechanisms which limit the performance of LC lasers are discussed later in Chapters 5 and 6, as they relate to the experimental work presented therein. At this stage, it is

[4] ASE is the interaction of photons emitted from singlet states excited along the optical path in the gain material [156]. Unlike the highly-directional narrow linewidth intrinsic to lasing, ASE can emit photons in all directions and at any wavelength permitted by the fluorescence spectrum of the gain material [157]. However, the higher gain at certain wavelengths results in a more limited wavelength range and directionality but without the single mode associated with lasing.

sufficient to note that the population of triplet states in organic dyes during prolonged optical excitation poses significant challenges for achieving long pulse duration or CW pumping [60].

2.4.2.3 Wavelength tuning

The accessible wavelength range spanning the full visible spectrum is one of the main advantages DDN*LC lasers offer over competing technologies. Not only can laser cells be fabricated for lasing at a specific wavelength simply by varying the DDN*LC mixture constituents, but many methods of wavelength tuning have been achieved. While advancing tuning mechanisms is not an aim of this thesis, a brief summary of tuning techniques is provided in this section, as this is a feature that would likely be exploited in a commercial setting.

Perhaps the simplest form of wavelength selectivity is by using multiple cells with different DDN*LC mixtures, or a single cell with multiple partitions containing different DDN*LC mixtures, and rotating/moving the cell(s) relative to the pump beam [13], [41], [75]. For example, by rotating sixteen cells, each with different dyes and chiral dopant concentrations, P. Chen achieved a wavelength range of 120 nm [75].

Another method used to achieve multiple wavelengths by moving the LC laser cell relative to the pump beam is in the form of a spatially-tuned gradient-pitch cell, in which DDN*LC mixtures are optimised for different emission wavelengths and introduced into opposite sides of an empty cell [20], [26], [76]–[78]. As the different DDN*LC mixtures move through the cell during the annealing process, the LC directors are aligned such that a continuous pitch gradient occurs. By translating the position of the cell relative to the pump beam, different output wavelengths are accessible from the same cell.

Controlling the diffusion of DDN*LC mixtures can present a challenge to gradient-pitch cell tuning, however, and there are perhaps better alternative methods that are more reliable. Furthermore, both of the previously described tuning techniques require moving parts, which are often undesirable within laser systems, as they will invariably introduce vibrations, produce fluctuating outputs, increase complexity and consume more power. There are, however, active tuning mechanisms which address some of these issues.

Some studies have demonstrated photo-induced wavelength tuning: the photoreactive property of a chiral dopant was demonstrated by Chanishvili *et al.* upon exposure to a UV source, achieving a 35 nm tuning range; a 110 nm tuning range via time-dependent exposure with a UV source by adding a photoreactive chemical to the DDN*LC was demonstrated by Lin *et al.* [79]; and a 405 nm (blueshift-inducing) LED and a 465 nm (redshift-inducing) LED to reversibly tune > 100 nm in less than 10 minutes was achieved by Chilaya *et al.* [80], among other notable works [81], [82]. There are also some limitations to this tuning mechanism however; the DDN*LC laser output wavelength stability cannot always be maintained and the time taken to reach the required wavelengths may be too long for practical use.

A more reliable method of wavelength selectivity has been demonstrated by applying an electric field across the laser cell. An early publication claiming to demonstrate electric field-induced tuning showed a 40 nm wavelength change, with a microsecond-scale switching response, but did not provide evidence of wavelength reversibility, nor the impact of a varying electric field on laser output intensity [83]. Another early study used an electric field to vary the intensity of a DDN*LC laser, simultaneously shifting the wavelength, although this was not discussed in detail [84]. The undesirable decrease in intensity in the presence of an increasing electric field in conventional DDN*LC lasers has been shown to be caused by distortions in the N*LC structure [19], [85]. This can be overcome by using an oblique heliconical N*LC, whereby the LC director is tilted at an acute angle relative to the helical axis (as opposed to conventional perpendicular alignment) [19]. Under the influence of an electric field, the chiral pitch shortens without rotating the structure and a tuning range of 100 nm has been be realised. An even higher tuning range > 110 nm was achieved by using a negative dielectric polymer structure with a pitch gradient, where the full wavelength range was accessed and returned to the original wavelength within two minutes [86].

While improvements in wavelengths tuning mechanisms are not addressed in this thesis, this is an area of LC laser research that presents interesting engineering and material challenges that, in the author's opinion, are worthy of future work.

2.4.2.4 Laser dyes

The performance of DDN*LC lasers is largely dependent on the choice of dye used for the gain medium. In particular, the pump wavelength and required output wavelength determine the most suitable dye, depending upon the absorption and emission spectra, respectively. The solubility of dyes in the host material (N*LCs in this case) determines the success of a particular dye as a gain medium. Pyrromethene groups, coumarins and 4-(dicyano-methylene)-2-methyl-6-(4-dimethylaminostryl)-4H-pyran (DCM) are the most commonly used dyes in LC lasers, as their combined emission spectra emit across the full visible range and they are soluble in their LC hosts [20], [35]. Moreover, their quantum efficiencies, that is, the number of photons emitted *vs.* the number of photons absorbed, is high, in particular for pyrromethenes [87]. For the purposes of this thesis, the discussion of dyes will be limited to DCM, Coumarin 504 (C504) and Coumarin 540A (C540A), as they exemplify output wavelengths spanning the visible spectrum. The pyrromethenes are not include, as their absorption spectra do not overlap with the emission wavelength of the pump laser used throughout most of this work.

Intramolecular charge transfer between electron-donating and electron-accepting units is typically responsible for the photon emission from a dye, while intermolecular interactions with the host can affect the efficiency of this process [87]. The dye-host combination therefore impacts the thresholds and efficiencies of LC lasers, as the quantum efficiency and fluorescence lifetimes of laser dyes dispersed in an LC host are likely to differ from solvents used in conventional dye lasers [88]. An extensive study was carried out by Morris *et al.* [89] to confirm and quantify this, by mixing DCM with ten different LC hosts. It was found that the greater the order parameter, *S*, and the higher the birefringence, Δn, of the LC (as defined by Equation 2.1 and Equation 2.3 respectively), the lower the threshold and the higher the efficiency. A further figure of merit that was used to characterise the dye-host interaction was the order parameter of the transition dipole moment, S_d, of the dye. This is analogous to the LC molecular order parameter, S, and describes the alignment of the dipole moment of dye relative to the LC the director, $\hat{\mathbf{n}}$, and is given by [90]:

$$S_d = \left\langle \frac{3}{2}\cos^2\theta_d - \frac{1}{2} \right\rangle \qquad \textit{Equation 2.10}$$

where θ_d is the angle between $\hat{\mathbf{n}}$ and the transition dipole moment and for which the maximum (S_d = 1) corresponds to the idealised case where the dipole moment is parallel to the director, resulting in preferential laser emission at the long band edge [91]. S_d = 0 corresponds to an isotropic orientational distribution and S_d = -0.5 is the case for which the transition dipole moment is perpendicular to the director, resulting in preferential emission at the short band edge. Morris *et al.* showed that S_d was (inversely) proportional to the (threshold) efficiency [89]. It has been shown that laser dyes can be synthesised to improve such performance parameters [92]–[95], while others have shown performance improvements by deliberately using negative order parameters [16], [19], [62], [86], [96]. However, dye synthesis and experimentation with different LCs were beyond the scope of the work required for this thesis; off-the-shelf LCs and dyes were used exclusively.

One of the most commonly used dyes in LC lasers is DCM. It has a high quantum yield, it is soluble in many LCs [90] and its broad absorption spectra enables the use of a wide range of pump wavelengths for optical excitation [87], [97]. Furthermore, the broad emission spectra can be exploited for wavelength tuning [77], [79], [98], ranging from ~ 500 – 700 nm (depending upon the host) with a peak emission at 590 nm, (Figure 2.11). The Stokes shift (the spectral difference between the absorption and emission maxima) for DCM, is considered large (~ 150 nm – again, dependent upon the host) [99], [100] and is therefore suited to producing a range of wavelengths well beyond the excitation wavelength, as will become apparent through experimental evidence later in this thesis.

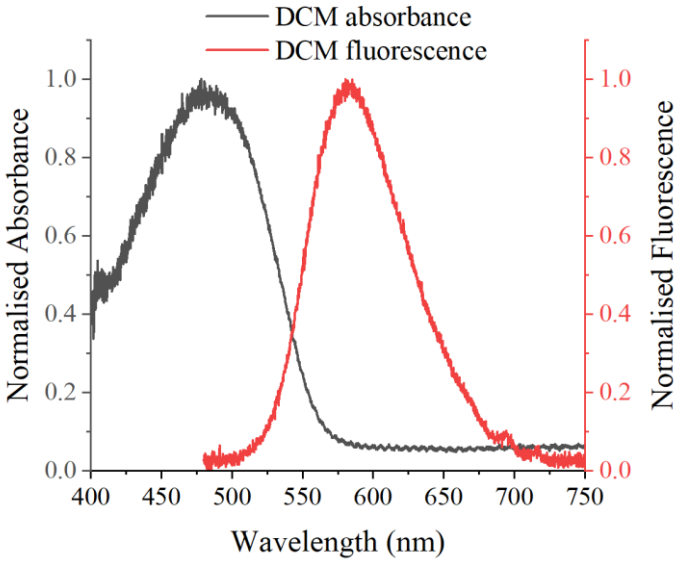

Figure 2.11. Absorption and fluorescence spectra of 1.5 wt% of DCM dye dissolved in NLC (BL006, Merck).

A method used to improve the tuning range of an LC laser without changing the pump source is through dye mixing. A broader turning range is achieved via a non-radiative excitation energy transfer from a shorter wavelength-absorbing "donor" dye molecule to a longer wavelength-absorbing "acceptor" dye[5] [101]. This process, known as Förster resonant energy transfer (FRET), is possible provided that there is good overlap between the donor emission spectrum and acceptor absorption spectrum [102].

2.4.3 Liquid crystal laser performance limitations

The causes of LC laser performance degradation have been investigated within the LC laser research community in recent years. Morris *et al.* carried out a detailed investigation into the causes of reduced laser emission for varying pulse energies and repetition rates [32]. They concluded that optical reorientation of the LC director caused by the presence of the organic dye distorts the chiral helix and reduces the efficiency of the laser. They showed that, as the pump laser repetition rate was increased, the time between pulses was insufficient to allow recovery from molecular reorientation, resulting in an exponential reduction in output. While Morris *et al.* discounted thermal effects as the cause of this, Varanytsia and Palffy-Muhoray concluded that localised heating caused by the pump source resulted in a reversible drop in emission as the repetition rate and pulse energy were independently increased [33]. They also

[5] the donor can also be known as the "sensitiser", and the acceptor can also be known as the "emitter"

noted a threshold beyond which the thermal effects were irreversible, and that a permanent localised focal conic texture of the LC replaced the well-aligned planar texture. While they do not address the conclusions of optical orientation drawn by Morris *et al.*, the authors of Ref. [33] present compelling evidence of thermal distortion through changes in emission wavelength.

Not all emission loss by high repetition rate pumping is accompanied by a shift in wavelength, however. Etxebarria *et al.* showed that, when pumped at 100 Hz for 15 minutes, a DDN*LC laser output intensity dropped until it was fully extinguished, during which time the wavelength remained stable [34]. The authors argued this could not be caused by dye bleaching[6], nor because of a temperature increase in the DDN*LC, but was a result of scattered pump light from small imperfections in the material. Somewhat confusingly, they hypothesise that this scattering effect is due to a local temperature increase, having just dismissed localised heating in the same study.

It is apparent from these studies that there is no consensus as to the cause of the output intensity degradation of DDN*LC lasers under different pump conditions. Most probably, dye bleaching, triplet state population, thermally induced scattering, optical reorientation and thermal damage are simultaneously present, occurring on different timescales and are a result of different pump parameters (repetition rate, pulse energy, pulse length) and LC laser cell constituents (dyes, LCs, substrate material). Understanding the effects different parameters can have on LC laser performance is important for optimising and developing this technology towards a practical application.

2.4.4 Laser diodes: an alternative pump source

The complexity, cost and size of Q-switched pump lasers is one of the foremost causes in preventing the adoption of LC laser technology as an alternative to more established laser

[6] The authors of Ref. [34] use the term *dye bleaching* to describe triplet state population (a reversible phenomenon). However, *dye bleaching* is also often used to describe irreversible photodestruction of dyes, such as in Refs. [135], [158]. For the work in this thesis, a clear distinction between reversible and irreversible LC performance degradation mechanisms is required, as evidence of both is apparent under different experimental conditions. Therefore, **for the experimental results presented in this thesis *dye bleaching* will be used exclusively to refer to permanent photo-induced destruction. Reversible phenomena such as triplet state population will be referred to accordingly.**

systems. Ideally, if a simpler, more compact pump source at a significantly lower cost could be demonstrated, it would offer a major step forward for LC laser development.

Many papers have alluded to the possibility of employing semiconductor-based technology in the form of light emitting diodes (LEDs) or laser diode (LDs) to pump LC lasers [30], [35]–[37], [103]. Attempts have been made towards achieving successful LC laser emission using such pump sources, however none have thus far succeeded [12], [38]. The challenge results from the high fluence and short pulse duration necessary to induce LC lasing; hence the ubiquitous use of Q-switched lasers within LC laser research. This is one of the primary motivators for reducing the threshold and increasing the efficiency of LC lasers, as it would allow the use of low-energy pump sources.

The peak power of Q-switched lasers is often > 1000 times higher than most semiconductor-based sources, with complex intracavity electro-optics required for achieving the short pulse durations, such as acousto-optic modulators, electro-optic modulators or Pockels cells [60]. Conversely, there are no intracavity methods for enabling high-intensity pulse build-up in semiconductor-based devices – they can either be "on" or "off", as determined by the driver electronics used to control the current flow. It is possible to deliver currents to laser diodes higher than their specified tolerances, provided the duration is short enough so as not to thermally damage the device [104]. This can produce higher output peak powers than the average powers specified for CW operation. Therefore, to reach the requirements needed for LC lasing, the electronics would need to produce a high current (~ Amps) in nanoseconds or shorter.

An example of the currents required to produce a high enough optical power for pumping, was demonstrated by Yang *et al.* when they attempted to pump a semiconducting polymer with an LED [105]. They provided a range of currents up to 160 A with pulse a duration of 36 ns. However, although they stated that the narrow linewidth output from the semiconducting polymer was indicative of lasing, they conceded that improvements in pump design, driver electronics and the laser resonator would be required for improved laser performance, as the narrow linewidth emission appears as a feature upon a broader photoluminescence spectrum. Coles *et al.* applied a similar idea of LED pumping, but to an LC laser, resulting in narrow multimodal emission spectra, again superimposed upon a broader fluorescence spectra [12].

The paper in which Munoz *et al.* claimed the first CW DDN*LC laser, also attempted to demonstrate optical pumping with an LED, for which they also alleged success [38]. However, upon inspection of their intensity results, the output emission again appears as a feature of a broader fluorescence spectrum – not the typical narrow-linewidth emission associated with band-edge lasing. Furthermore, there are no data presented showing the slope efficiency with the characteristic gradient change indicative of laser threshold. Their results closely resemble those of Refs. [12] and [105] which do not claim lasing, as evidenced by the broad (> 10 nm) output spectra with narrow linewidth features. Further confirmation that the results presented in Ref. [38] fall short of LC laser emission was demonstrated by Stranks *et al.* [106], in which the emission of organic-inorganic perovskites upon optical excitation was analysed using a similar methodology often applied to DDN*LC lasers. They showed a polarised emission output, but conclude that the unstable emission, combined with the broadband spectrum, was ASE and not lasing; contrary to the conclusion drawn by Munoz *et al.* for similar results. Although LD pumping of conventional dye lasers has been demonstrated [73], it is apparent that no equivalent evidence has yet been published for bandedge lasing from a DDN*LC laser.

Ortega *et al.* argue that there is a threshold limit, below which it is impossible to successfully pump an LC laser, as a result of intrinsic cavity losses associated with DDN*LCs, and that improvements can therefore only come with new, improved dyes [31]. However, with advances in LD technology and driver electronics, it is conceivable that conventional DDN*LC mixtures *could* be used, provided that the LC laser fabrication and experimental arrangements are optimised.

Recent developments in LD technology have resulted in output powers moving from the mW regime [107], [108] to operating in the order of Watts [104]. Furthermore, they can be manufactured in bulk and are millimetres in size. While such practical advantages are obvious, their performance parameters must also be considered with respect to their potential application as pump sources. High power laser diodes exhibit multi-wavelength behaviour, albeit with sub-nanometre mode separation [109]. Single mode operation is achievable by introducing external optical components such as etalons or diffraction gratings [110], [111], but this often sacrifices output power for a narrower linewidth, and may not be necessary, depending upon the intended application. The shape of the beam is another factor to consider. The rectangular shape and micro-scale geometry of the edge-emitting region of typical LDs results in a divergent elliptical or rectangular beam profile, with the divergence occurring at a

different rate for the *x* and *y* axes (hence the use of the terms “fast” and “slow” divergence axes).

Among other wavelengths, laser diodes operating at 445 nm have successfully been used to pump organic dye lasers [111]–[116]. Within these studies, multi-mode and single-mode pumping have succeeded (as have pulsed and CW operation) in producing single wavelength and tuneable wavelength outputs and, perhaps most relevantly, the dyes used to achieve this have often been the same as those used in DDN*LC lasers.

It is the many references over the past few decades stating the advantages that a semiconductor pump source would bring to the field of LC lasers, in addition to the near-successful attempts, that provided the motivation to overcome this challenge and formed the principal aims of this thesis.

Chapter 3
Experimental methodology

"Anybody who has been seriously engaged in scientific work of any kind realises that over the entrance to the gates of the temple of science are written the words: 'Ye must have faith.'"

Max Planck

3.1 Introduction

The success of the experimental work in this thesis was dependent upon the quality of the LC laser cells that were fabricated for each investigation. Furthermore, the optical arrangement used for testing the quality of the cells and conducting experimental investigations was configured to optimise LC laser performance.

This chapter presents the cell fabrication process, a typical optical arrangement and an overview of the methods used to measure the LC laser threshold, slope efficiency and the pump beam spot size. The emission characteristics for varying cell qualities are compared, with the aim of demonstrating a well-fabricated laser cell for the experimental work to follow. Investigation-specific experimental configurations and methods are presented in the relevant chapters.

3.2 Liquid crystal laser fabrication

3.2.1 Introduction

High performance lasing from an LC laser cell is dependent upon the fabrication process. Constructing the cell, mixing the dye-doped chiral nematic LC (DDN*LC), filling the cell with the DDN*LC mixture, and cooling and sealing the cell, all required specific processes. The risk of contamination during fabrication was minimised by constructing the LC laser cell in a cleanroom to minimise variations in quality (and hence performance) from one cell to another.

This section presents the steps required to produce LC Laser cells. Analysis and testing of the cells are also discussed, with concluding remarks suggesting further improvements to the fabrication process. Substrate cleaning and fabrication, DDN*LC mixing and cell filling were based on the research perfected and documented by previous members of the group [41], [75]. The details below largely emulate this previous work, with additions/redactions/changes explicitly stated where improvements were possible.

3.2.2 Cell fabrication

The first part of the process was the construction of the empty laser cell (i.e. without the DDN*LC). For the in-house fabricated lasers used in this work, cell fabrication took place in the Class 10 cleanroom at the Scottish Microelectronics Centre (SMC), based at the University of Edinburgh.

3.2.2.1 Overview of cell architecture

A diagram of a fully-constructed empty laser cell is shown in Figure 3.1. It comprises two glass substrates, one of which has a coating of aluminium to form a reflective cell geometry. The inside surfaces of each substrate are coated with a polyimide (PI) alignment layer. The alignment layers are rubbed to facilitate in-plane alignment of the LC director across each surface. The substrates are glued together with the top substrate orientated such that the rubbing direction of the PI is antiparallel to the PI of the bottom substrate. The glue that bonds the two substrates together contains spacer spheres, 10 μm in diameter, to ensure a 10 μm gap in which the DDN*LC is later added. Each step of this process is elaborated upon below. The specifications and manufacturers of the equipment and chemicals are tabulated in Appendix C.

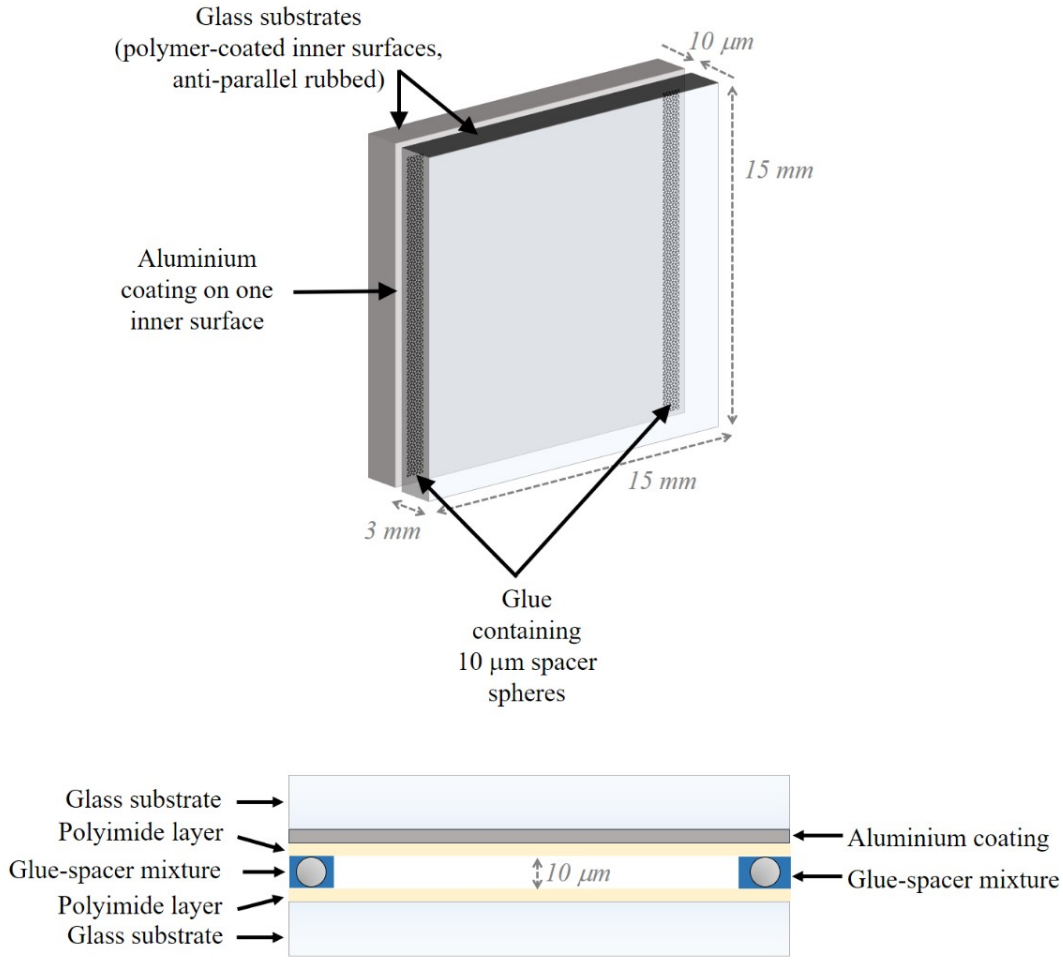

Figure 3.1. Structure and dimensions of an in-house fabricated reflective LC laser cell (top), with a profile view (bottom) to highlight the layers (not to scale).

3.2.2.2 Cleaning the substrates

The specifications for the glass substrates (*Laser 2000)* used throughout the work in this thesis are given in Table 3.1. A detailed study was carried out in Ref. [41], in which it was found that a scratch-dig specification of at least 40-20 was required, in addition to a surface flatness of $\leq \lambda/2$. When specifications lower than these were used, a poor LC texture was observed and multi-modal emission occurred.

Table 3.1. Specifications of substrates supplied by Laser 2000 used to make the LC laser cells.

	Plain glass	Aluminium-coated
Dimensions (l × w × d) (mm)	15 × 15 × 3	15 × 15 × 3
Surface flatness	< λ/4	< λ/2
Scratch-dig	40-20	40-20

The substrates were cleaned before they were coated with the PI. The chemicals used to clean the aluminium-coated substrates were less abrasive than those used for cleaning the plain substrates to prevent damage to the aluminium layer.

The plain glass substrates were cleaned using the following process:

1. Dissolve potassium hydroxide (KOH) pellets in deionised (DI) water (approximate volume ratio of 1:1).
2. Soak a lint-free tissue in the KOH solution and use to rub the surfaces of the glass substrates. This is done to remove any grease from the substrates.
3. Rinse the substrates in DI water.
4. Place substrates in a 'piranha' solution, comprising sulphuric acid (98 %) and hydrogen peroxide (35 %) in a ratio of 3:1 for 10 minutes. This removes all remaining contaminants from the glass surfaces.
5. Rise the substrates in DI water and store in DI water until needed, to prevent contamination.

The aluminium-coated substrates were cleaned using the following process:

1. Submerge aluminium-coated substrates in a beaker of isopropyl alcohol (IPA).
2. Place in an ultrasonic bath at 50 °C for 10 minutes.
3. Renew IPA and repeat for a further 10 minutes.
4. Remove substrates from IPA and dry with nitrogen.
5. Store in DI water to prevent contamination.

3.2.2.3 Spin-coating the substrates with polyimide

The polyimide *(SE-1410, Nissan Chemical Industries)* was chosen for the alignment layer as it is commonly used in LC displays and provides good planar alignment with a low pre-tilt angle. It was mixed at room temperature in a ratio of 1:1 with a solvent (N-Methyl-2-Pyrrolidone (NMP), *OM Group Ultra Pure Chemicals Ltd*) in preparation for spin-coating. The mixture was made in a beaker containing a magnetic stirrer. The beaker was placed on a stirring hotplate at room temperature and set to spin at 200 rpm for half an hour. The mixture was then filtered through a 0.22 μm syringe filter and left for an hour to reduce the bubbles in the mixture. (The presence of bubbles was found to result in streaks upon spin-coating the substrates [41].)

The following steps were performed for coating the plain glass and the aluminium-coated substrates:

1. Place the substrate in the centre of the spin-coater (*LIT-016, Polos*) and activate the vacuum to secure the substrate in place.
2. Using a pipette, apply 2-3 drops of the PI-NMP mixture to the substrate. Ensure sufficient covering of the substrate but ensure that excess mixture does not spill over the sides.
3. Activate the spinner. (Settings: 500 rpm for 5 seconds, immediately followed by 4000 rpm for 60 seconds.) These settings ensured an even distribution of PI across the surface of the substrate.
4. Deactivate the vacuum and remove the substrate from the spin-coater.

3.2.2.4 Curing the polyimide

Upon completion of PI-coating, the substrates were pre-baked on a hotplate set to 80 °C for 5 minutes to evaporate the NMP solvent from the substrate surface. Prior to hard-baking the PI, a visual inspection with a white light microscope (*MET-019, Leica*) was useful to assess the quality of the substrates. Occasionally, some defects were found. The quality of the substrates and PI coating was either deemed sufficient for continuing on to the next stage of baking, or else the cleaning process was restarted and the PI reapplied. This depended upon the source of

the defect. If it was caused by a micro-scale particle, the substrate was re-cleaned. If the defect was caused by a manufacturing fault such as a scratch or chip, then the process could continue, provided that the defect didn't dominate the active area or affect the cell spacing. Rarely, a manufacturing defect appeared across the active area. In this instance, the substrate was discarded.

Having confirmed that the substrates appeared to be contaminant-free, the PI was hard-baked to solidify the layers. An oven set to 220 °C was used to cure the plain substrates for 1.5 hours, while a lower temperature of 140 °C was used to hard-bake the aluminium-coated substrates for 3 hours, as higher temperatures were found to tarnish the reflective coating [41].

3.2.2.5 Rubbing the polyimide

Rubbing the PI layer was necessary to promote planar alignment of the LCs. The cells were placed on the vacuum stage of a rubbing machine (*HO-IAD-BTR-01, Holmarc)* and passed beneath a rotating cloth specifically designed for LC rubbing. Previous work found that a high roller rotation speed (900 rpm) damaged the PI layer [41]. A roller speed of 200 rpm was therefore set, and the substrate passed beneath the roller three times at a speed of 2 mm/s. The height of the roller above the cell was set so that only the tips of the cloth fibres touched the PI layer to prevent over-rubbing. Static build-up on the surface of the substrates that developed during rubbing was dissipated using an anti-static nitrogen gun.

3.2.2.6 Cell assembly

A robotic gluing machine (*JR-2304N, Nordson EFD with JR2000N desktop robot, Janome)* was used to apply a UV-curable optical adhesive (*NOA68, Norland)* to the aluminium-coated substrate. Spacer spheres, 10 μm in diameter (*Nanjing Jianzun Glass Microsphere Plant Company Ltd),* were mixed with the glue at 2 wt%. This quantity ensured sufficient distribution of spheres in the glue such that, when the two substrates made contact, there was a uniform cell separation. A higher concentration of spheres risked the spheres overlapping and thus causing an uneven cell gap. A syringe was attached to the gluing machine with a 0.2 mm tip and the glue dispenser was programmed to deliver a pressure of 1.2 bar and a line speed of 8 mm/s. This produced glue lines of approximately 1 mm thickness when the

substrates made contact. The plain glass substrate was manually placed on top of the aluminium-coated substrate such that the rubbing directions of the PI were antiparallel. The substrates were gently pressed together to ensure that the glue was distributed uniformly, such that the spacers formed an even 10 μm gap between the two substrates. The assembly was then UV-cured (*UV-1250, Loctite*) for 3 minutes to ensure the glue solidified.

3.2.3 Making a chiral nematic liquid crystal mixture

The desired output wavelength from an LC laser dictated the concentration of chiral dopant and the choice of dye. The dopant concentration defined the position of the long band-edge and hence the location in the spectrum for which lasing was optimised. The laser dye was selected such that its emission spectrum coincided with the band-edge.

To make the N*LC, a 2 ml UV-blocking vial was placed on digital scales which were then reset to zero. Approximately 200 mg of LC (BL006 [n_e = 1.815, n_o = 1.530, Δn = 0.285], *Merck*) was added to the vial using a micropipette; this was a sufficient quantity for filling multiple cells (if required). The weight of the LC was measured and used to calculate the mass of the right-handed chiral dopant, BDH-1281 (*Merck)*, needed for obtaining the desired position of the long band-edge. For example, the majority of the work in this thesis used DCM dye, which has a fluorescence peak at ~ 590 nm. For the long band-edge to overlap with this, a mass of chiral dopant equal to 4.5 % of the weight of LC was required (see Figure 3.5). The chiral dopant was added to the vial, followed by a magnetic stirrer to assist with mixing. The vial was then placed on a stirring hotplate at 140 °C and set to stir at 200 rpm for 3 hours until the dopant had fully dissolved. This temperature was used as it was above the clearing point of the LC (113 °C for BL006) but not so high that it damaged the LC or chiral dopant. Above the clearing temperature, the viscosity of the LC dropped, thus assisting with mixing. Mixing at temperature < 140 °C was found to result in incomplete dissolution of the chiral dopant [41] After this stage was completed, the band-gap position was confirmed and the dye was added to the N*LC.

3.2.4 Verifying the band-gap position

The position of the band-gap was usually verified before the dye was added to the mixture to ensure that the long band-edge was positioned in the spectral location required for lasing[7]. Off-the-shelf anti-parallel rubbed transmissive cells (*LC2-20.0, Instec*), with a cell gap of 20 μm, were used to test the N*LC band-gap position by measuring the white-light transmission of the sample using a custom-built microscope and a spectrometer. Using an Instec cell was a more time-efficient and cost-effective method of testing the sample, rather than using in-house fabricated cells[8].

An empty cell was placed on a hotplate and a Pasteur pipette was used to add the N*LC to the cell via capillary action. A microcontroller with a touchscreen interface was integrated with the control electronics of the hotplate [117]. This was programmed to allow the user to define the starting and finishing temperatures. A feedback loop controlled the cooling rate which was fixed at 0.3 °C/min. Once at room temperature, the band-gap of the N*LC was tested in the laser lab using the optical configuration shown in Figure 3.2.

[7] Testing the band-gap was required less frequently with experience, especially if the mixture being made was a repeat of a previous mixture. This made the process quicker and more economical. Only when a new wavelength or dye was required was it beneficial to test the band-gap to ensure that the band-edge was positioned correctly.

[8] The Instec cells could also be used for lasing once the dye was added to the N*LC mixture but, unlike the in-house cells which had the glue-spacer mixture positioned along two narrow lines at the edge of the active area, the Instec cells microspheres were randomly distributed throughout the active area. This meant that there were fewer positions available for lasing within the cell, which posed a problem when uninterrupted emission across the cell was required. The work in this thesis therefore used in-house fabricated cells for laser experiments.

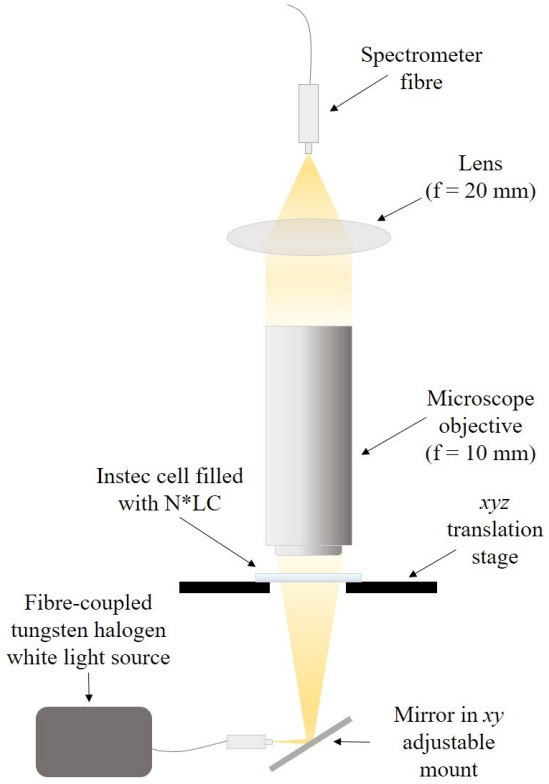

*Figure 3.2. Microscope arrangement used for measuring the band-gap position of N*LC in Instec cells.*

Before the transmission spectrum of the N*LC was measured, the dark spectrum was recorded on the spectrometer (*USB4000, Ocean Optics*) and the white light transmission of a tungsten halogen lamp (*HL-2000-HP-FSHA, Ocean Optics, 360 nm to 2400nm*) through an empty cell was measured to account for losses from the cell surfaces. The transmitted light was collimated by the microscope objective and focussed onto a fibre (*P600-1-VIS-NIR, Ocean Optics*) connected to the spectrometer, the signal from which was analysed on the spectrometer software (*Spectrasuite v2.0.162*). These spectra enabled a normalised transmission spectrum of the N*LC to then be measured when the empty cell was replaced with the filled cell.

The white-light transmission of three Instec cells containing different chiral dopant concentrations can be seen in Figure 3.3. The blue-shift in the band-gap associated with an increase in chiral dopant concentration can clearly be seen. The signal-to-noise ratio < 400 nm was low due to the fibre optic, which was specified for transmission from 400 nm to 2100 nm.

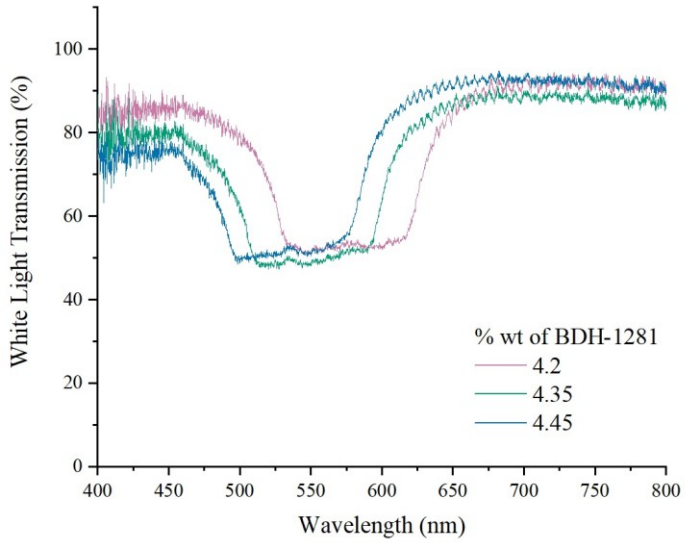

Figure 3.3. White light transmission spectra of three Instec cells with chiral dopant concentrations of 4.45 % wt (blue line), 4.35 % wt (green line) and 4.2 % wt (pink line).

The cell resulting in the transmission spectrum shown by the green line in Figure 3.3 is shown in Figure 3.4, in which the effect of the photonic band-gap on the transmission and reflection of white light is apparent. Here, light in the green-yellow part of the spectrum is reflected by the band-gap, while wavelengths in the blue and red regions are transmitted.

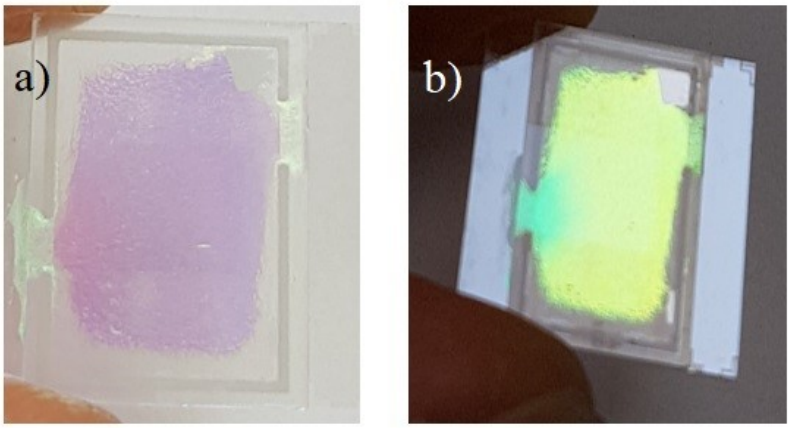

Figure 3.4. Transmissive Instec cell used for testing the band-gap position, showing the effect that the band-gap has on a) transmission and b) reflection of white light.

The position of the band-gap is important to measure prior to adding dye to the mixture for two reasons. Firstly, it allows the position of the long band-edge to be verified to ensure it overlaps with the fluorescence peak of the dye. Secondly, the position of the reflection band dictates whether or not a quarter waveplate is required in the optical arrangement when lasing.

As can be seen from Figure 3.3, 50 % of the unpolarised light from the white light source is reflected by the band-gap. This corresponds to light with a circular polarisation with the same handedness as the chiral twist of the LC. When pumping a DDN*LC for LC lasing, if the pump laser wavelength falls within the PBG, then the loss caused by this reflection can be overcome by using a quarter-waveplate to circularly polarise the pump beam to the opposite handedness of the chiral helix. This ensures that all of the pump light is transmitted into the cell (assuming there are no additional losses, for example, from surface scattering). However, there would be no advantage in circularly polarising the pump beam with a wavelength outside the PBG. In this instance, the optical arrangement can be simplified by removing the quarter waveplate.

The effect of chiral dopant concentration on the band-edge position is shown in Figure 3.5. This graph was used throughout the work in this thesis to calculate the concentration of chiral dopant needed for achieving a specific LC laser wavelength.

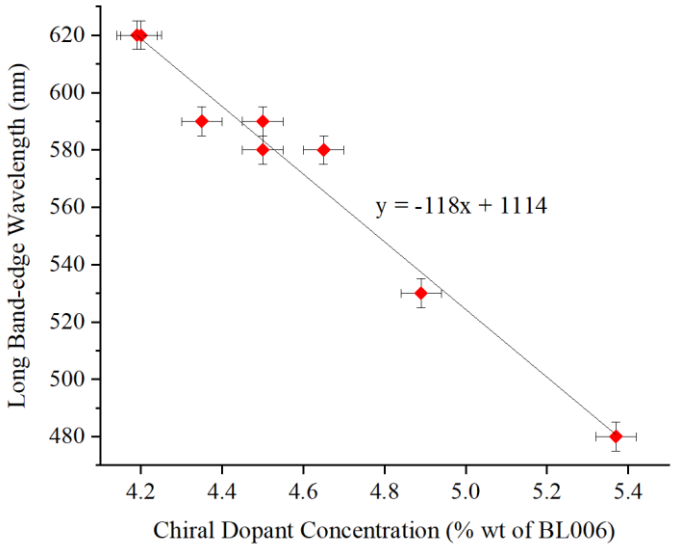

Figure 3.5. Chiral dopant (BDH-1281) concentration in the LC, BL006, used to predict the LC laser wavelength when mixed with an appropriate organic dye and added to an LC laser cell.

Having verified the band-gap position, an appropriate dye was added to the N*LC (assuming that the long band-edge was positioned at the desired wavelength).

3.2.5 Characterising and adding the dye

The absorption and fluorescence of the dyes were measured before adding the dyes to the N*LC. 1.5 wt% of dye was added to the NLC at 100 °C and mixed on a hotplate for 3 hours at 200 rpm. The mixture was added to an Instec cell and the same arrangement for measuring the band-gap position was used. The absorption was measured by observing the transmission of the white light source through the sample. The fluorescence was measured by illuminating the sample with the pump laser (Figure 3.6). The pump beam was coupled into the microscope arrangement and focussed onto the sample by reflecting the beam from a dichroic mirror and through the microscope objective. The fluorescence emission from the DDNLC was transmitted by the dichroic mirror and detected by the spectrometer. (Figure 2.11 exemplified the absorption and fluorescence spectra measured for DCM.)

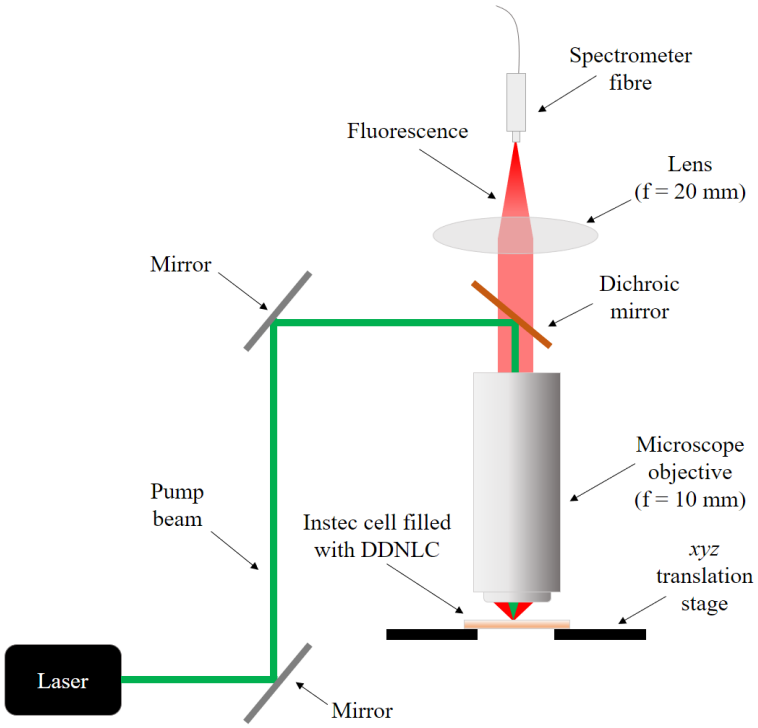

Figure 3.6. Microscope arrangement for measuring the fluorescence spectrum an organic dye when mixed with an NLC and added to an Instec cell.

To make the DDN*LC, the dye was added to the N*LC at a concentration selected to optimise the LC laser performance. This was typically in the range of 0.5 – 2.0 wt%. At lower concentrations, laser emission was weak or non-existent, and at higher concentrations, the dye

was found to agglomerate in the LC. The dye (in powder form) was added to the vial containing the N*LC on a hotplate set at a temperature of 100 °C (higher temperatures were found to cause irreversible damage to the dyes). The dye was mixed on the hotplate at 200 rpm for 3 hours before heating in the oven overnight. Previous work in the group had found that overnight heating of the mixtures in an oven at 100 °C before cell filling improved the uniformity of the DDN*LC texture when added to the cells [75]. After heating overnight, the vial was removed from the oven and immediately placed on a hotplate at 100 °C in preparation for adding to an empty cell.

3.2.6 Filling, cooling and sealing the cells

The final step to the construction of an LC laser was to fill, cool and seal the cell. This usually took place immediately after a new mixture had been heated overnight, although it was possible to reheat a previously made mixture, using the heating process previously described in Section 3.2.5.

The DDN*LC mixture was removed from the oven and placed on the hotplate (integrated with the microcontroller) and set to 100 °C, along with an empty cell. A Pasteur pipette was used to draw a small volume of mixture from the vial, and capillary action was used to transfer the mixture from the pipette into the cell until the gap between the substrates was filled with DDN*LC. The hotplate was then set to cool to room temperature at 0.3 °C/min. Anecdotal evidence found that manually rubbing the cells during the cooling process, by firmly running a piece of plastic across the top surface of the top substrate in the direction of the cloth-rubbing, appeared to improve the DDN*LC texture. It is hypothesised that this improved the alignment of the LC director through shearing effects. Finally, an epoxy resin (*TS10, Varian)* was applied around the sides of the cell to prevent leaking and oxidation of the mixture.

A diagrammatic illustration of the cell production process is shown in Figure 3.7.
Further details of the cleanroom fabrication and dye mixing processes are given in Appendix A and Appendix B, respectively.

1. Clean substrates

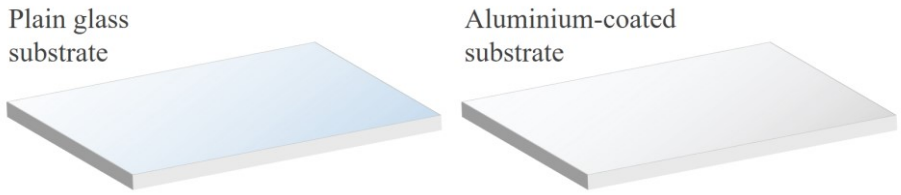

2. Spin-coat an even layer of polyimide onto one surface of each substrate.

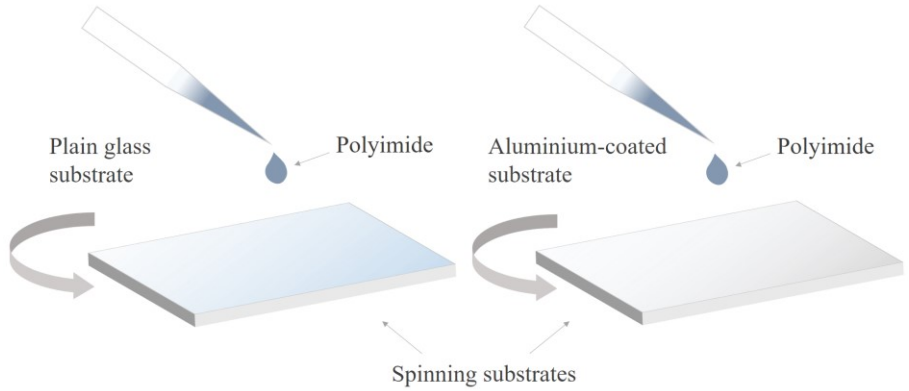

3. Rub the polyimide layer on both substrates then remove any static build-up using an anti-static gun.

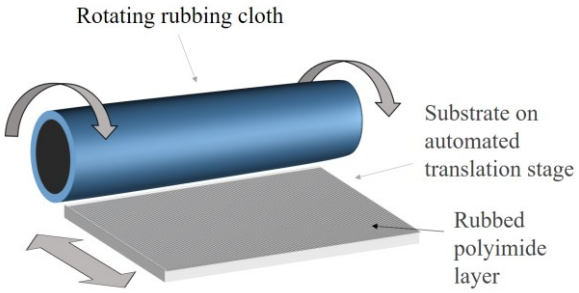

4. Apply optical adhesive mixed with spacers to the aluminium-coated substrate. Place the plain glass substrate ontop and cure with UV illumination.

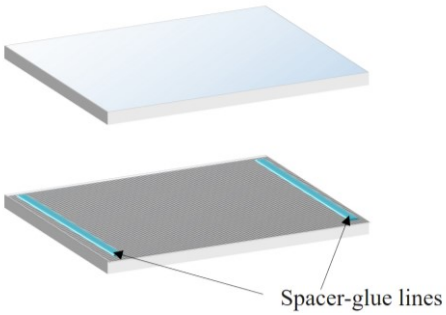

5. Use a Pasteur pipette to capillary fill the cell at 100 °C.

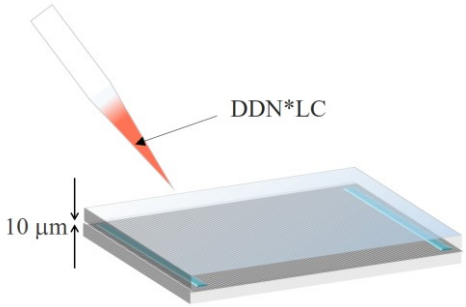

6. Once filled, cool to room temperature at 0.3 °C/min then seal the edges with an epoxy.

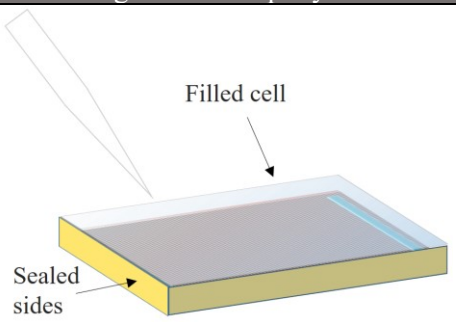

Figure 3.7. Pictorial description of fabrication and filling process.

The complete LC laser production procedure is summarised in the flow chart in Figure 3.8.

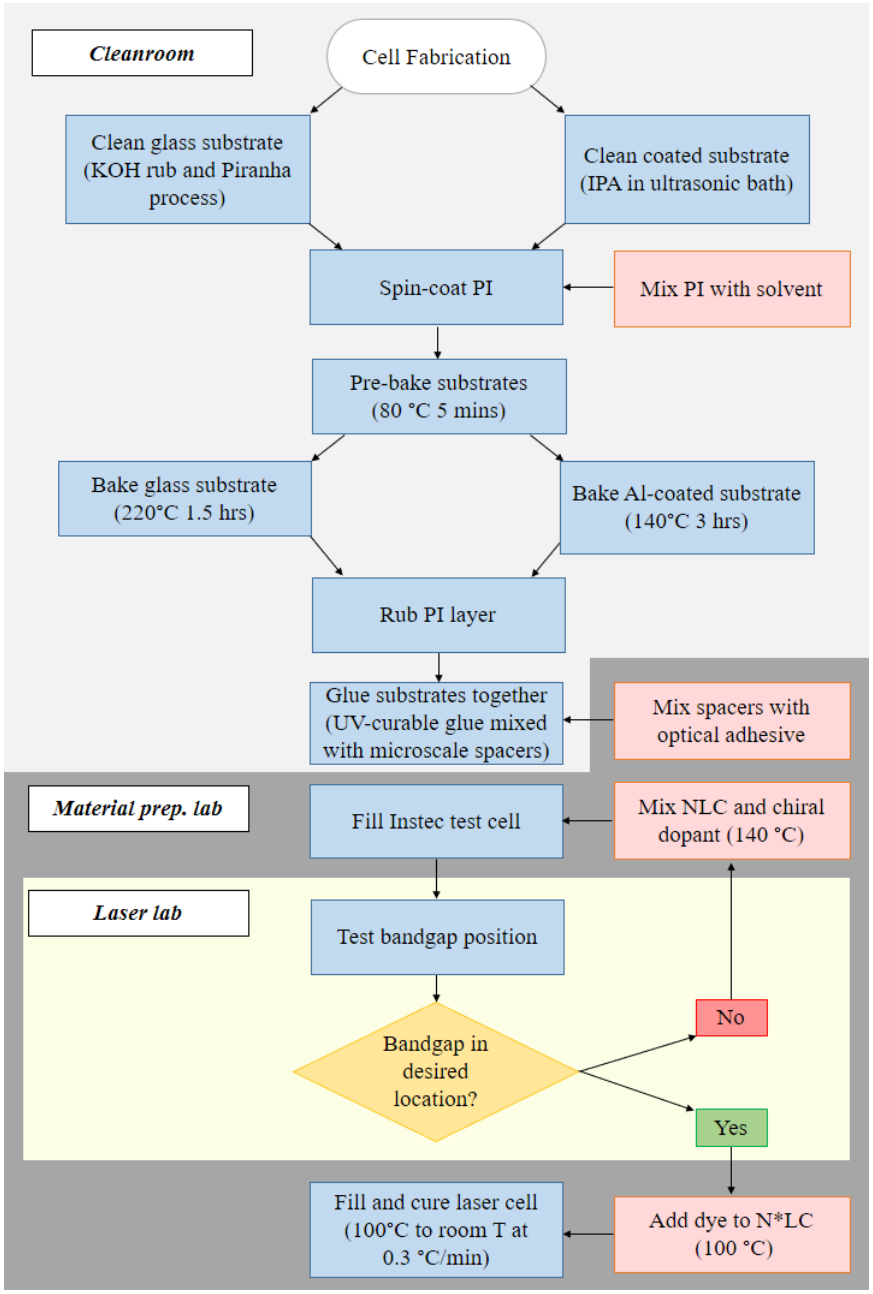

Figure 3.8. Flow chart of LC laser cell production.

3.2.7 Visually inspecting the quality of filled cells

In the context of LC laser cell fabrication, the "quality" of the cells refers to how well they were made for optimising laser performance. The quality was only assessed visually during the fabrication process, with the ultimate verification of quality carried out post-fabrication, by how well the cell lased. The best cells were those that produced single longitudinal mode emission, with a high laser slope efficiency and with the least variation in LC laser wavelength and intensity across the active region. However, as these tests could only be made after the cell fabrication process, alternative means of evaluating the cell quality during fabrication were required.

Once the substrates were baked, rubbed, bonded and the cells were filled DDN*LC, the quality of the cells could be visually assessed. A mostly uniform texture with large monodomain areas was a good indicator that a cell would work (if appropriately pumped). Cells were also inspected under a white-light microscope *(Leica, DM12000 M)* before attempting lasing. LC textures are typically inspected using polarised optical microscopy (POM) whereby the LC sample is positioned between crossed polarisers [50]. However, as the LC laser cells fabricated throughout the work in this thesis used a reflective geometry, POM was not possible. Although this limited the degree to which the cell quality could be verified prior to lasing, white-light microscopy remained a useful tool to provide a qualitative indication of the cells' condition. Examples of a poorly made cell (Figure 3.9) and a well-made cell (Figure 3.10) are shown below.

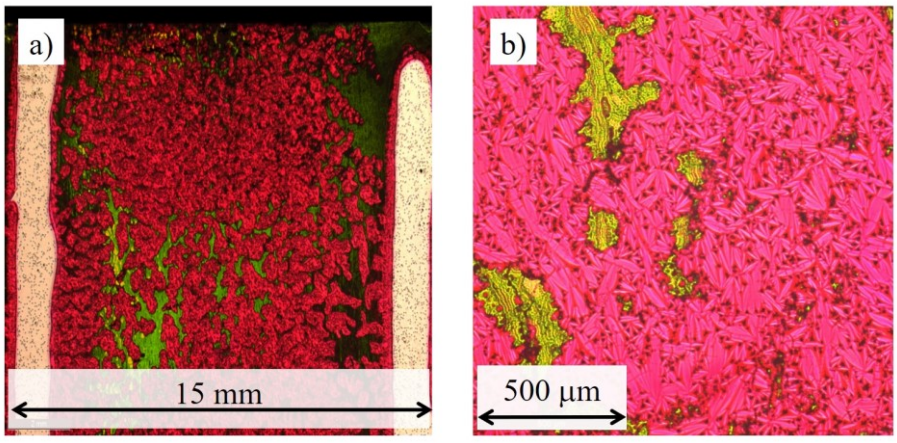

*Figure 3.9. A poorly fabricated cell with the magnified image in b) exhibiting a defective (possibly focal conic) texture, likely due to poor alignment of the DDN*LC with the alignment layer.*

Figure 3.9 is an example of LC texture, in which the N*LCs are randomly orientated with weak or no surface anchoring. This would imply LC alignment with the PI layer was unsuccessful. This could have been caused by a poorly coated PI layer (possibly a result of insufficient cleaning), contamination during baking or an error during the rubbing process. This cell did not lase.

With more practice and care, particularly during the spin-coating and rubbing processes, the cell quality was improved (Figure 3.10).

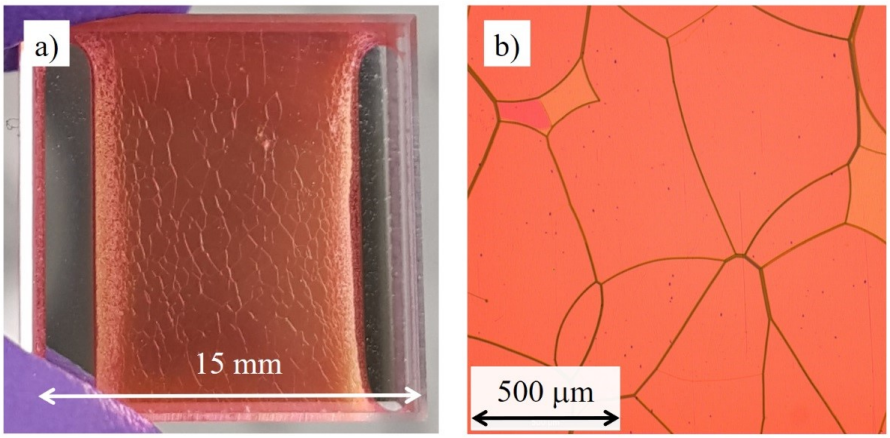

*Figure 3.10. Images of the same cell under different magnifications, showing a well-aligned DDN*LC with large monodomains.*

The well-aligned N*LC in Figure 3.10 exhibited large (> 500 µm) monodomains. The characteristic 'oily streaks' indicative of a well-aligned N*LC when viewed using POM may also be shown here, although this could not be verified due to the limitations of the reflective cell geometry [42]. This cell lased well, with little variation in output wavelength between domains separated by the apparent oily streaks. The main fabrication changes made between the cells in Figure 3.9 and Figure 3.10 that resulted in the improved cell quality were:

1. Using IPA instead of acetone to clean the substrates. The use of acetone at the early stages of perfecting the fabrication process was based on an inherited procedure that was used to clean the aluminium-coated substrates. Upon inspection under the microscope, however, it appeared that the acetone was damaging the aluminium, thus resulting in an uneven surface.

2. Removing the IPA-soaked swab from the process. Another inherited step was to draw a non-shedding swab soaked in IPA across the aluminium-coated substrate prior to spin-coating the PI. This was also found to sometimes damage the surface.
3. Reducing the amount of PI. For the poorer performing cells, it was found that there was a sticky residue caused by the PI on the sides of the substrates. This suggested that there was too much PI being applied to the substrates, likely resulting in an uneven surface onto which the spacer-glue mixture was applied and causing poor LC alignment.

However, whilst this showed an improvement in cell fabrication, ideally the surface would be one large monodomain, rather than a polydomain structure (albeit with minimal pitch variation between each domain). Morris *et al.* attribute the less desirable polydomain structure to a fast cooling rate and demonstrated a large monodomain when the cooling rate was reduced from 50 °C/min to 5 °/min [118]. As the cells shown in Figure 3.10 were cooled at a rate of 0.3 °/min, the presence of a polydomain structure was unlikely caused by the cooling rate. Furthermore, it was observed that the polydomain structure appeared immediately when the cell was capillary-filled with the DDN*LC, and mostly remained this way throughout the cooling process. In some cases, (Figure 3.15) the cell *was* one large monodomain structure, despite the exact same process being followed throughout the fabrication. This would suggest that it is not just the cooling rate that affects the resultant domain size of the DDN*LC. This requires further investigation. For the purposes of the work presented in in this thesis, cells displaying a polydomain structure were used, provided that the domains were sufficiently larger than the pump spot diameter and that there was minimal variation in emission wavelength between adjacent domains.

3.2.8 Measuring cell performance and analysing cell quality

The LC laser cells were tested in the laser lab once they were visually inspected. The optical configuration described in Section 3.3 was used to test the cells' performance.

The first measurement of a newly-fabricated LC laser cell was to confirm that it was lasing at the desired wavelength i.e. at the long edge of the photonic band-gap measured earlier in the process. The spectrometer was also used to measure the uniformity of the DDN*LC by moving the cell to different positions along the plane perpendicular to the pump beam and observing

the variation in wavelength and intensity. A well-fabricated cell ought to have little or no variation in both, and produce single longitudinal mode emission (to within the resolution limit of 1.5 nm of the spectrometer). If there were random jumps in wavelength > 5 nm (Figure 3.11), or many positions with no laser emission (Figure 3.12), or multiple wavelengths emitted within the same pump spot (black lines in graphs shown in Figure 3.12 and Figure 3.13), or apparent variations in pitch length (Figure 3.14) then the cell was considered to be of poor quality and was not used for experimental purposes.

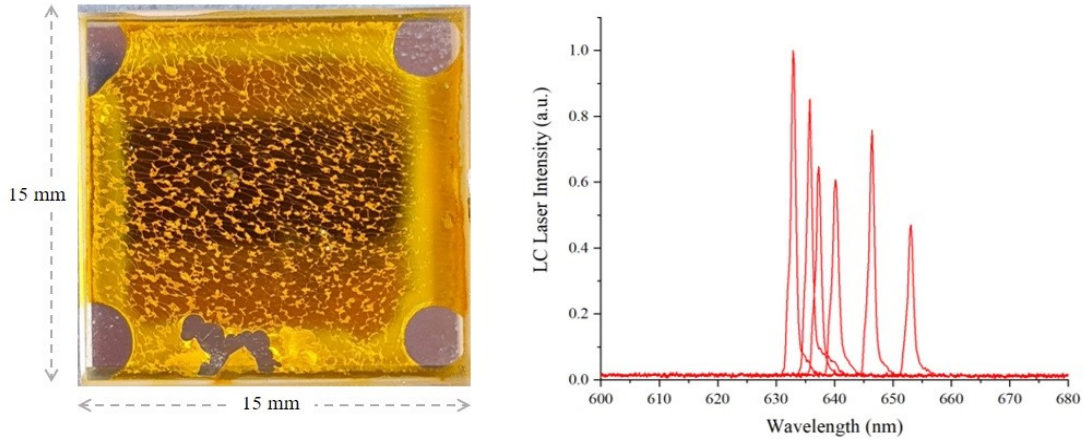

Figure 3.11. Example of multiple discrete laser wavelengths emitted from different cell positions of a polydomain cell. Multiple disclinations can be seen throughout the active area of the cell, possibly due to insufficient shearing to induce large monodomain areas. (Accidental glue deposition can be seen at the bottom of the cell. The dark band across the centre of the cell is a reflection from the camera.)

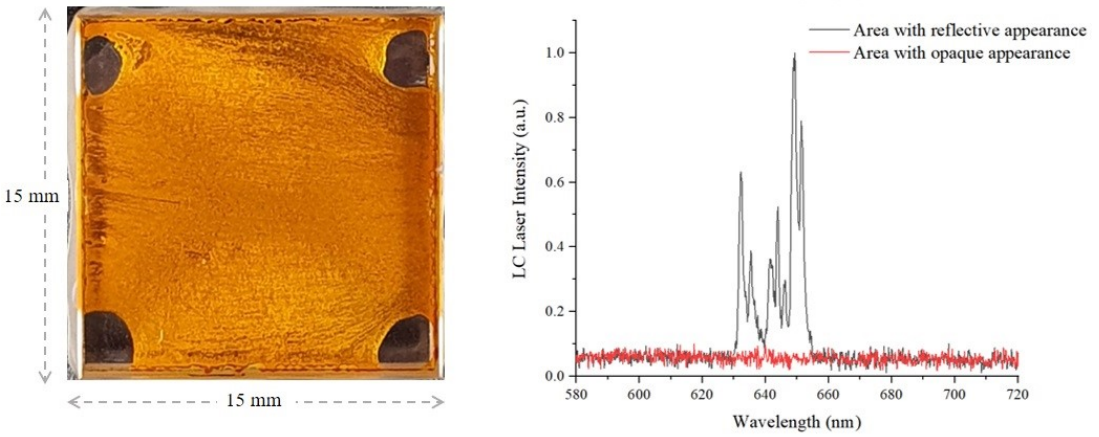

Figure 3.12. A poorly fabricated cell, with a cloudy appearance across most of the active area, resulting in no laser emission (red line in graph) except for the small areas with a reflective appearance, for which multimode emission was produced (black line in graph). The poor quality may be due to weak anchoring caused by poor rubbing.

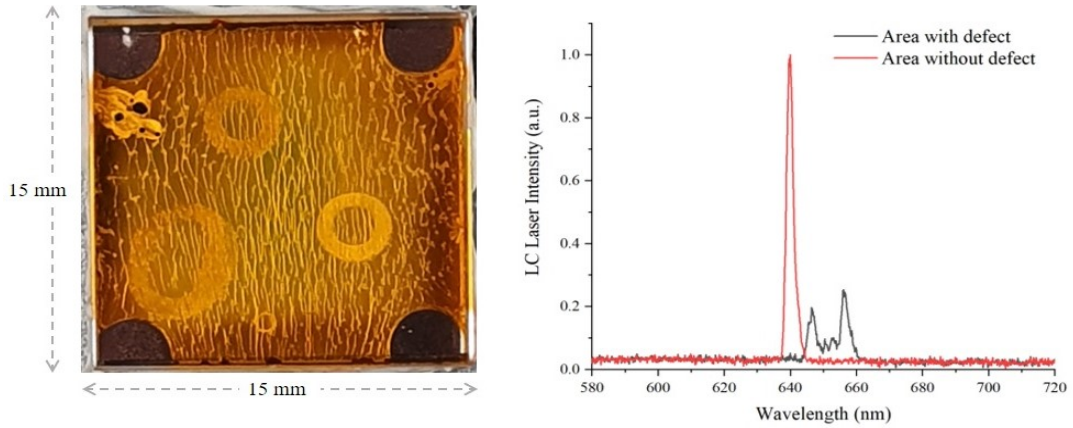

Figure 3.13. Laser cell containing large defects of unknown origin, likely due to insufficient cleaning or post-cleaning contamination. Narrow linewidth laser emission was produced in many areas of the cell (red line in graph) but the defects caused multimodal behaviour (black line in graph).

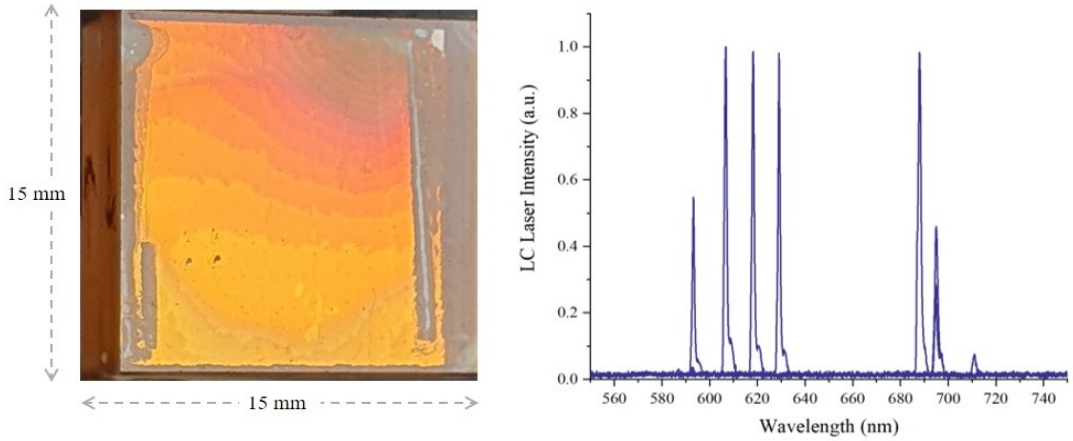

Figure 3.14. This cell appears to show regions of varying colour consistent with a wedge cell, likely caused by a contaminant preventing parallel alignment of the substrates. An apparent change in pitch length across the cell area can be seen from the cell colour changing from yellow to dark red, resulting in a wavelength range spanning > 100 nm.

The cells show in Figure 3.11 – Figure 3.13 used small spots of the glue-spacer mixture in the corners, instead of two glues lines (Figure 3.14), in an attempt to increase the useable area of the cell. However, this appeared to detrimentally affect the cell quality and was not used in future work.

An example of a well-fabricated cell with a corresponding narrow spectral linewidth, coinciding with little variation in wavelength and intensity across the active area, is shown in Figure 3.15.

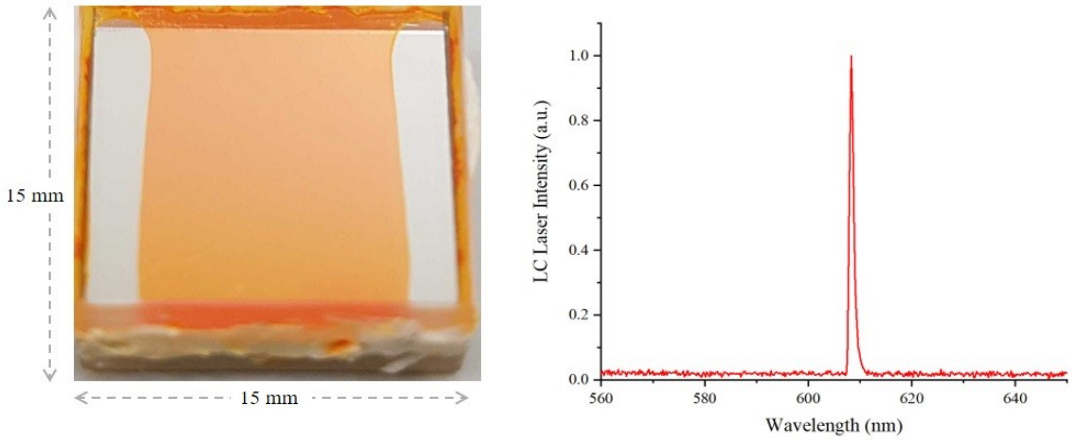

Figure 3.15. A well-fabricated cell with a largely monodomain texture, resulting in single mode LC laser emission.

Once the spectral profiles had been used to identify high-quality cells, additional tests could be made for further performance indicators. For example, the threshold and slope efficiency (Section 3.3) were often measured to determine LC laser performance under different optical excitation conditions.

Figure 3.11 – Figure 3.14 show examples of cell fabrication outcomes that led to poor laser performance. With practice, cells like those in Figure 3.15 were achieved more frequently. However, this was not always the case, despite the process remaining unchanged. Throughout this work, the same batch of substrates, the same cleaning chemicals, LC, chiral dopant, PI and PI solvent were used; and yet variation in cell quality sometimes occurred. The most likely source of inconsistency was human intervention, for example off-centre placement of the substrates on the spinner, too much or too little PI applied to the substrates prior to spinning or accidental introduction of contaminants when transferring the substrates from one piece of equipment to another – all of which could contribute to poorly performing cells.

This highlights the benefit that an automated fabrication process could have on laser performance. Much of this process has already been perfected in the manufacture of displays using NLCs [119]. It is conceivable that a similar process ought to be possible with DDN*LCs with minimum disruption to the process. Thus, if LC lasers are to be considered an enabling technology in a commercial setting, the up-scaling of their manufacturing ought not to present a significant challenge in the route to market – provided a similar quality can be achieved with DDN*LCs as with the typical NLCs.

A feature that is present in Figure 3.11 – Figure 3.13 is the change in colouration near the exposed edges of the cells. This was initially thought to be caused by oxidation or moisture ingress, which motivated the introduction of an epoxy resin to seal the cells. However, this was not always effective at preventing this edge effect. Further investigation would be required to determine the cause of this and alternative approaches to cell filling could be considered. For example, the spacer-glue lines could extend around the cell further, leaving only a small gap for the DDN*LC to enter and another for the air to leave (similar to the design of the Instec cells in Figure 3.4). If it transpired that the edge effect *were* caused by a reaction to the air, vacuum filling or filling in a nitrogen glove-box could also be considered. Here, the DDN*LC would first be de-gassed under low pressure to remove gaseous impurities, before being filled into cells whilst still in the vacuum chamber (or glove-box). Cells would also be sealed after filling before exposure to the air. The edge effect typically occurred over several weeks/months and did not affect the central areas of the cell. Investigating this effect further was therefore not considered a priority in this work.

3.2.9 Summary and future improvements

The purpose of the work in Section 3.2 was to present the cell fabrication process with the aim of achieving repeatable, high quality LC laser cells. This was realised by refining the fabrication process such that narrow linewidth LC laser emission was consistently demonstrated across multiple areas of the same cell. Furthermore, a chiral dopant calibration plot enabled the photonic band-edge position to be determined prior to mixing with the laser dye. It was not the aim of this work to make significant changes to the fabrication process, as this would have dominated the research in this thesis and would not have addressed the main research aims. Continuous improvement of the process was sought throughout the cell production, but was done so within the time and resources allocated for this part of the research. There is an ongoing effort in LC and LC laser research for improving the quality of cells. Techniques such as thermal treatment to reduce oily streaks [120], photopolymerisation to remove the need for rubbing [121] and acoustic streaming to change a focal conic texture to a planar alignment, have been investigated [122]. Consultation with a display manufacturer would also be useful, as similar techniques are applied in the display sector.

Visual inspection of the substrates at each stage of the cleanroom process was likely not sufficient in determining how well they had been cleaned, coated, baked and rubbed. For example, measurement variation of the PI thickness would be useful for optimising the PI and the spin-coating process. Furthermore, the rubbing machine did not provide feedback for the pressure it was exerting on the substrates. Considering the pile of the cloth will degrade with use, a pressure feedback mechanism would be expected to improve the rubbing consistency.

Automation of the production process would benefit the LC laser cell quality and repeatability, as human intervention at each stage of fabrication is suspected as being the main contributor to the variation in laser performance. It is unrealistic to expect an automated process at this stage in the development of LC lasers, but if larger-scale production were required, this would merit a more streamlined approach to fabrication. An example of this could be to clean and PI-coat larger substrates (wafers, for example) which could then have pre-programmed spacer-glue line geometries applied, followed by a dicing procedure to produce individual cells. Such wafer-scale fabrication (compared to the current chip-scale fabrication) would not only increase the scale and efficiency of production, but would also improve the consistency between cells. However, the flatness and surface quality of alternative, larger-scale substrates would need to be consistent with the specifications used here; there would be no benefit in upscaling cell production at the expense of the optical quality. Until there is an appetite for large-scale LC laser manufacture, the current methods used for small-scale fabrication are sufficient, as has been demonstrated by the high quality cells presented in this chapter.

The spectral quality of the LC laser emission was used to demonstrate that a high-quality laser cell was successfully produced using the fabrication process presented. In addition to the spectral profile, the spatial profile of a laser beam is also often provided in the specifications for commercial laser systems. This usually takes the form of a heat map or transverse electromagnetic (TEM) mode value, which describe the Gaussian profile energy distribution of a laser beam perpendicular to the direction of travel. A TEM_{00} mode indicates the desired fundamental mode of a laser, with additional modes taking non-zero values [60]. TEM_{00} modes have been demonstrated for LC lasers as a means of comparison to commercial laser systems [31], [103], [118], [123]. It was not possible to measure the spatial mode for the work in this thesis due to limitations in equipment, but for completeness it ought to be acknowledged as an additional figure of merit for quantifying the performance of LC lasers in the future.

3.3 Experimental investigations

3.3.1 Optical arrangement

The optical configuration for lasing LC laser cells was dependent upon the aims of each experimental investigation presented in this thesis. However, the general arrangement (Figure 3.16) remained the same throughout.

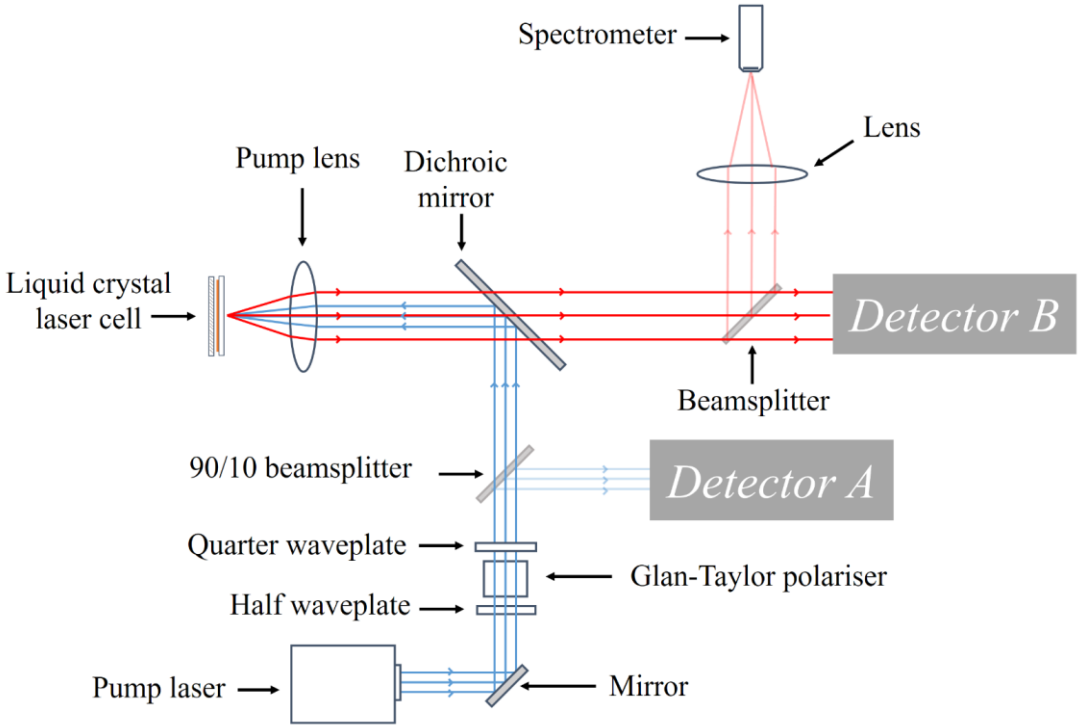

Figure 3.16. General optical arrangement for LC laser experiments.

A pump laser was used to induce LC laser emission and was varied depending upon the experiment. A Glan-Taylor polariser (*GT5-A, Thorlabs, 350 – 700 nm*) was fixed in an orientation such that it allowed maximum transmission of the linearly polarised pump source. Rotation of a zero-order half-waveplate rotated the polarisation of the pump beam relative to the Glan-Taylor polariser, and thus provided a mechanism for varying the pump beam energy incident upon the LC laser cell. A quarter waveplate was used to change the pump polarisation from linear to circularly polarised light with the opposite handedness of the chiral helix. This ensured maximum transmission of the pump laser by the N*LC and hence maximum

absorption of the pump beam by the laser dye. A 90/10 beamsplitter (*BSN10, Thorlabs, 400 – 700 nm*) enabled measurements of the pump beam on detector *A* whist 90 % of the pump emission was transmitted. A dichroic mirror reflected the pump beam which was then focussed onto the LC laser cell by a short focal length lens – the 'pump lens'. Emission from the LC laser cell was transmitted by the dichroic mirror whereupon a beamsplitter enabled simultaneous detection by a spectrometer and detector *B*. Detectors *A* and *B* were varied depending upon the experiment and comprised any permutation of two energy meters (*PD10-C, Ophir*), two photodiodes (*DET025A/M, Thorlabs*) or a spectrometer (either *USB4000, Ocean Optics, resolution < 1.5 nm* or *CCS100/M, Thorlabs, resolution < 0.5 nm*). The choice of pump lens, dichroic mirror, beamsplitter, and waveplate also varied depending upon the experiment. Details of the components required for specific experiments are specified in the relevant chapters.

3.3.2 Measuring LC laser threshold and slope efficiency

LC laser threshold and slope efficiency measurements are used throughout this thesis to quantify the LC laser performance under different experimental conditions. The slope efficiency was found by calculating the gradient of the slope of LC *laser* energy as a function of the pump energy. LC laser threshold is the minimum pump energy required to produce LC laser emission and coincides with a change in gradient of the slope efficiency (Section 2.4.2.1). For the work in this thesis, the pump energy[9] was controlled by varying the angle of the half-waveplate. This was accomplished either by *manually* rotating the waveplate (having calibrated the pump energy as a function of the waveplate angle) and recording the energy output from the LC laser (Chapter 4), or by using an *automated* configuration with two energy meters recording the pump and LC laser energies simultaneously (Chapter 5). In both cases, the intersection of the lines of best fit for the two distinct gradients present in the data (pre-threshold data and post-threshold data) defined the LC laser threshold. An alternative approach for determining the threshold was to observe the spectral and/or temporal profiles of the LC emission (Chapter 6). The appearance of a narrow spectral output (limited by the

[9] The term *energy* is ambiguous in this work, as *energy* was controlled by independently varying the peak power **and** the pulse duration with the introduction of laser diode pumping. For the purposes of this work, the change in pump pulse energy with angular displacement of the half-waveplate was due to a change in **peak power**. *Energy* is used when discussing efficiency and threshold data, firstly because this is typically used throughout the literature, and secondly, because *energy* was the quantity measured by the energy meters.

resolution of the spectrometer), and narrow spiking features on the photodiode upon increasing the pump energy, indicated the onset of LC laser emission, at which point the pump energy was measured. Further details and justifications for each method are presented in the relevant chapters.

3.3.3 Measuring the pump laser spot size

The diameter of a laser beam is typically referred to as the spot size. The spot size of the pump was required throughout much of the work in this thesis as it was used for calculating the area of the pump spot. The pump area was necessary to calculate the fluence and intensity of the pump (Chapter 4), and for calculating the maximum number of pump spots incident upon a spinning LC laser cell (Chapter 7). It was also useful for measuring the effect of different focusing optics on the pump beam, as the optics used to focus the pump onto the LC laser cells varied from an expensive multi-element microscope objective to a standard, low-cost aspheric lens. A beam profiler is often used to measure the energy distribution of a laser beam in the *xy* plane and scan along the *z*-axis/optical axis (the direction of beam propagation), thus determining a laser beam's spot size at any given position along the optical axis. In the absence of such a device, as was the case for the work in this thesis, the spot size was measured using the knife-edge technique [124]. This method assumes a Gaussian beam profile and uses a sharp edge (for example, the edge of a knife blade) to incrementally block the laser beam in the *x* or *y* axis (Figure 3.17). The energy is plotted as a function of the blade position and the process is repeated at different positions along the *z*-axis to find the spot size at the focus.

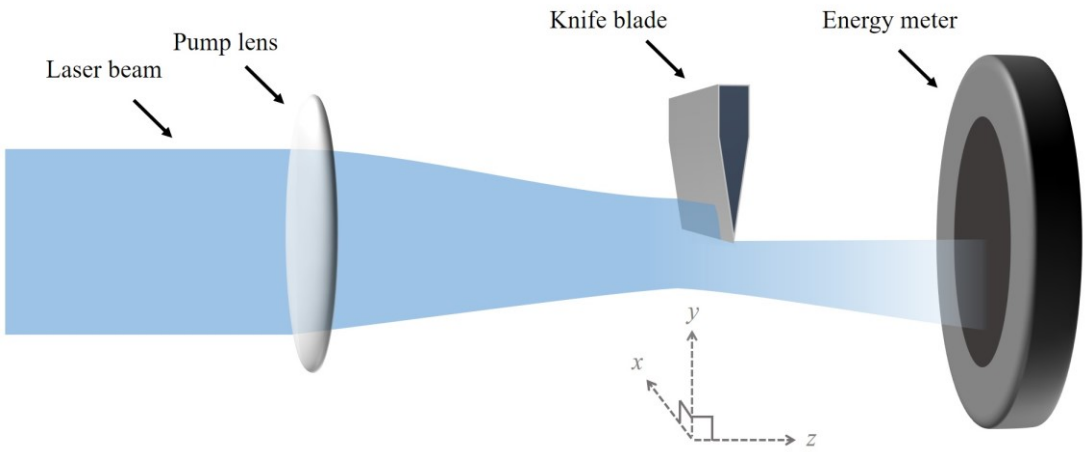

Figure 3.17. Knife edge experiment, showing the attenuation of the laser beam energy caused by the incremental translation of the knife blade in the y-axis.

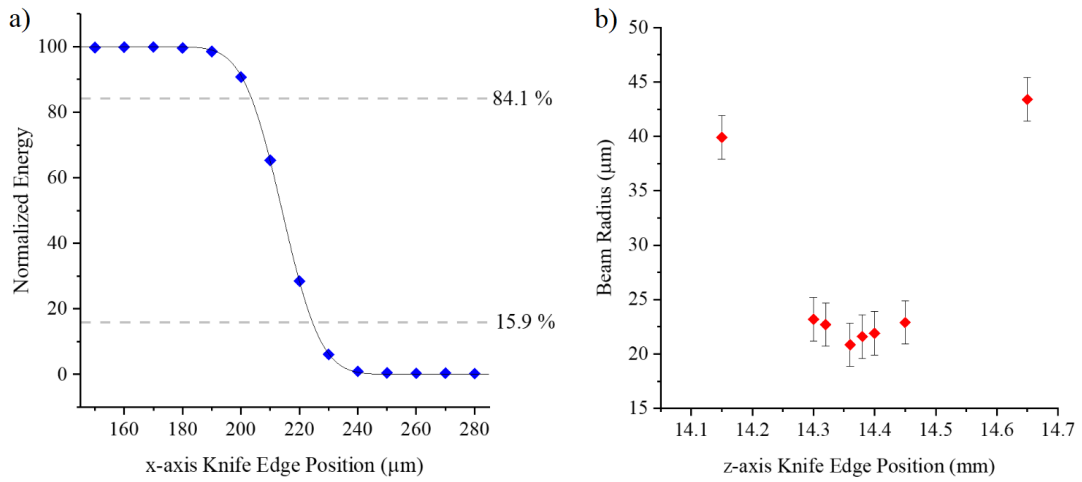

Figure 3.18. Knife-edge measurement to determine the spot size of a laser diode beam at the focal point of an aspheric lens (f = 10.5 mm). a) Shows the normalised energy as a function of the knife blade position as it is translated across the x-axis of the beam and b) is a plot of the beam radius at different positions along the optical axis.

Figure 3.18 shows the results of a knife-edge measurement for the 445 nm laser diode described in Section 4.4.3. The plot in Figure 3.18a shows the energy as a function of the knife blade position as it was translated across the *x*-axis of the laser beam in 10 µm increments when focussed by a 10.5 mm focal length aspheric lens. The beam radius is calculated from the difference between the positions where 81.4 % and 15.9 % of the total energy was detected. This distance corresponds to $1/e^2$ of the total energy [124]. In the case of Figure 3.18a, the radius was found to be 20.8 (± 0.2) µm which was also the smallest spot size measured for this

pump-lens configuration. Figure 3.18b shows the results of multiple knife-edge measurements taken along the optical axis which were used to determine the smallest spot size, as this was the spot size used to maximise the slope efficiency when pumping an LC laser. This method was repeated for the *x* and *y* axes for all combinations of pump beam and focussing optics used throughout this thesis to calculated the area of the spots (Table 3.2)[10].

Table 3.2. Spot area data for the 532 nm Q-switched YAG laser and 445 nm laser diode used throughout the work in this thesis.

Pump Source	**Pump Lens**	**Spot Area (μm^2)**
532 nm YAG	Microscope objective (f = 10 mm)	106.8 ± 5.3
445 nm LD	Microscope objective (f = 10 mm)	78.4 ± 4.5
445 nm LD	Aspheric lens (f = 10.5 mm)	797 ± 15

3.4 Summary

This chapter presented the LC laser fabrication process for making the LC laser cells used throughout this thesis. The ability to produce reliable, repeatable and wavelength-specific LC laser cells was essential to fulfil the research aims. A well-made LC laser cell ought to exhibit a uniform LC texture and produce narrow-linewidth laser emission, with minimum wavelength variation across the cell's active area. These performance criteria were achieved and exemplified, and validated the suitability of this process for making the high-quality laser cells required for novel and impactful experimental investigation. While an automated process that incorporated intermittent fabrication quality inspection would be beneficial for producing consistent, high quality cells on a large scale, the small scale manual fabrication process detailed in this chapter was sufficient in the context of this work. The experimental arrangement presented in this chapter for optically pumping an LC laser (in an on-axis configuration using a reflective cell) is a standard approach used in LC laser research. The

[10] The microscope objective focusses the pump beams to a smaller area than the aspheric lens by an order of magnitude. This is to be expected, as the objective comprises a multi-element arrangement of lenses designed to minimise optical aberrations

details of the interchangeable optical and optomechanical components, and the different detectors, were investigation-specific, and are presented at the beginning of each experimental chapter (Chapters 4, 5, 6 and 7); all are based upon the general arrangement presented here. A qualitative summary of the experimental approach for measuring the LC laser slope efficiency and threshold was provided and the knife-edge technique for calculating the pump area at the LC laser was presented.

Chapter 4

Laser diode pumping of liquid crystal lasers

"You are looking at a laser which emits an extraordinary light, not to be found in nature."

Auric Goldfinger (Gert Fröbe)

4.1 Introduction

As discussed in Chapter 1, the complexity, expense and bulk of Q-switched pump lasers have contributed to preventing LC laser technology from becoming a competitive alternative to more established tuneable laser systems. Ideally, if a simpler, more compact pump source at a significantly lower cost could be found, it would offer a major step forward for LC laser development.

It is the aim of the work presented in this chapter to demonstrate the first successful laser diode-pumped LC laser. The conjecture for many years that an alternative pump source would be a major breakthrough in the field and the attempts by other research groups provided the motivation for this investigation. The drive to commercialise LC lasers and establish this technology as a viable alternative to competing tuneable sources was further incentive to carry out this research.

In this chapter, an LC laser is fabricated, optimised for low-threshold behaviour, and tested using a standard Q-switched pump source. The performance is quantified and used to justify testing a laser diode (LD) with the aim of replicating the Q-switch-pumped laser results. Performance and design specifications are considered for the construction of an LD module, including the LD and the specialised driver electronics required to deliver a high current in a nanosecond time-scale. The performance of an LD-pumped LC laser is presented and compared to the Q-switched pumping regime.

The results from this chapter are published in:

- The peer-reviewed journal, Optics and Laser Technology, vol. 140, p. 107080, 2021; “Diode pumping of liquid crystal lasers” and;
- An invited paper for the Society for Information Display, vol. 53, no. 2, pp. 440–443, 2022; “Liquid-Crystal Lasers : Recent Advances and Future Opportunities”.

4.2 Making the liquid crystal laser

4.2.1 Cell fabrication

The first objective towards demonstrating a diode-pumped LC laser, was to quantify the performance of a well-made LC laser. Optimisation for low threshold behaviour was required to maximise the chances of successful LC laser emission. An in-house fabricated cell was best-suited to ensure a low threshold, by building upon previously published results for optimal performance such as: the use of a reflective cell geometry by using aluminium-coated substrates [70], [71]; optimising the cell spacing using 10 μm diameter silica spheres[11] *(Nanjing Jianzun Glass Microsphere Plant Company Ltd*); and the use of a high quantum efficiency laser dye. The cell fabrication process was as described in Chapter 3.

4.2.2 Dye-doped chiral nematic mixture

An extensive study by Mowatt *et al.* showed that the pyrromethene-597 dye (*PM597, Exciton*) exhibited excellent laser performance, in terms of emission intensity and threshold, attributed to the dye's high quantum efficiency and order parameter [87]. However, compared to DCM (which has a similar order parameter to PM597), the absorption spectrum of PM597 is narrower. At this stage of the investigation, the wavelength of the LD had not been determined, so a broad dye absorption was preferable to provide a greater choice of pump wavelengths. Furthermore, the peak absorption of PM597 is at 530 nm and an alternative pump source at a shorter wavelength was preferable for enabling a greater range of LC laser wavelengths in the visible spectrum. DCM (*Exciton*) was therefore selected for the preliminary investigation, in which the performance of a DCM-doped LC laser was quantified using a 532 nm Q-switched laser *(FDSS532-Q2, Crylas, pulse duration $\tau \leq 1.3$ ns)*. The absorbance and fluorescence spectra of DCM, first shown in Section 2.4.2.4, are shown again in Figure 4.1.

[11] To the author's knowledge, the optimum spacing for a *reflective* cell geometry has not been established in the literature. Morris *et al.* [63] and Mavrogordatos *et al.* [159] determined an optimum cell spacing of 10 – 15 μm for a transmissive cell and Sanz-Enguita *et al.* corroborated this by measuring an optimum performance with a cell spacing of 14 μm [37]. It could be that the optimum cell spacing for a reflective cell is less than this, due to the double-pass of the pump beam. A cell spacing of 10 μm was therefore considered a reasonable compromise until future work (beyond this thesis) identifies an optimum value (or range of values).

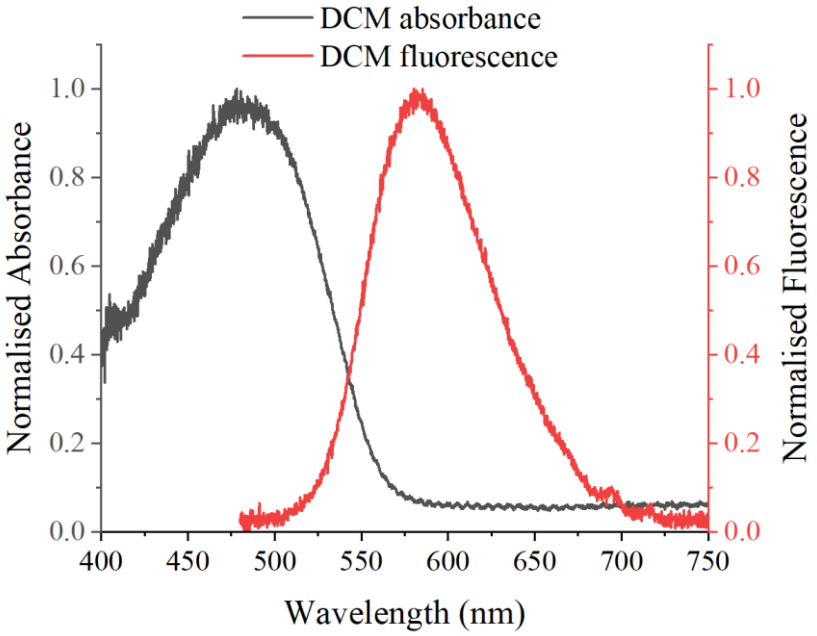

Figure 4.1. Absorption and fluorescence spectra of DCM when dissolved in BL006 LC.

A chiral dopant concentration of 4.35 wt% (relative to the LC) was used to produce a bandgap with the long band-edge at the peak emission of the DCM (590 nm) and was experimentally verified by measuring the transmission of white light through the chiral nematic sample in an Instec cell (Figure 4.5), as described in Section 3.2.4.

The DCM was then added to the mixture at a concentration of 1.5 wt%; a concentration based on published data [87] and in-house experimental evidence of optimum performance for DCM[12]. The in-house fabricated cell was filled with the mixture and cured from 100 °C to room temperature at 0.3 °/min.

[12] A more rigorous DCM dye concentration investigation was carried out later in the project which resulted in an optimum concentration of 0.5 % wt. The results of this study are shown in Appendix D.

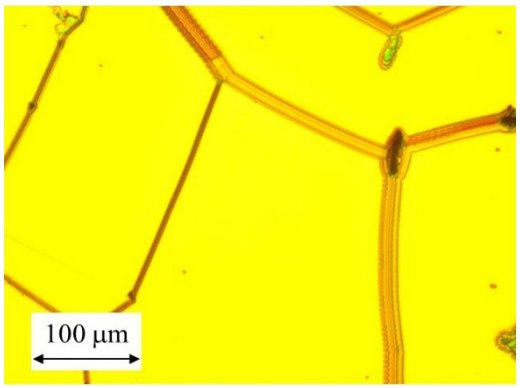

*Figure 4.2. White-light illuminated microscope image of the reflective DCM-doped N*LC laser cell.*

The cell was visually inspected under the white-light microscope *(Leica, DM12000 M)* before attempting lasing. In the sample shown in Figure 4.2, the DDN*LC within the laser cell shows full dissolution of the dye and chiral dopant and a uniform texture with large monodomains > 200 µm, (significantly larger than the area of the focussed pump spots described in Table 3.2). The characteristic oily streak defect lines, often found between well aligned neighbouring chiral domains using POM analysis [125], also appear to be present here. The cell was therefore considered to have been well prepared and was predicted to yield lasing emission with a low threshold and narrow linewidth when appropriately excited.

4.3 Preliminary investigation with the Q-switched pump

The performance of the LC laser cell was first verified using the 532 nm Q-switched YAG laser, having fabricated the cell for low threshold performance and visually checked it to confirm a well prepared sample.

4.3.1 Experimental procedure

The optical arrangement presented in Chapter 3 was used for pumping the LC laser. Components specific to this investigation are shown in Figure 4.3. The pump lens in this arrangement was a microscope objective[13] (*MY20X-804, Mitutoyo*), the half-waveplate (*WPH05M-532, Thorlabs*) and quarter-waveplate (*WPQ05M-532, Thorlabs*) were anti-reflective coated for 532 nm and the long-pass dichroic mirror (*DMLP550R, Thorlabs*) had a cut-off wavelength at 550 nm (i.e. light above this wavelength was transmitted). The beamsplitter at the output of the LC laser was a 50/50 non-polarising beamsplitter *(BS004, Thorlabs)* which enabled simultaneous measurement of the wavelength and energy using the spectrometer *(USB4000, Ocean Optics, resolution < 1.5 nm)* and energy meter *(PD10-C, Ophir),* respectively. This optical configuration was used to determine the minimum pulse energy required to induce LC lasing (i.e. the laser threshold) to estimate the LD specifications that would be needed to overcome the same threshold.

[13] A microscope objective was used because, at the time of this investigation, the experimental arrangement allowed integration with a camera for imaging the cells. It was found, however, that a microscope (*MET-019, Leica*) provided higher image quality, so there was no need for the objective to remain in the arrangement for focussing the pump laser onto the LC laser. The microscope objective was later replaced with an aspheric lens, as discussed in Chapter 6.

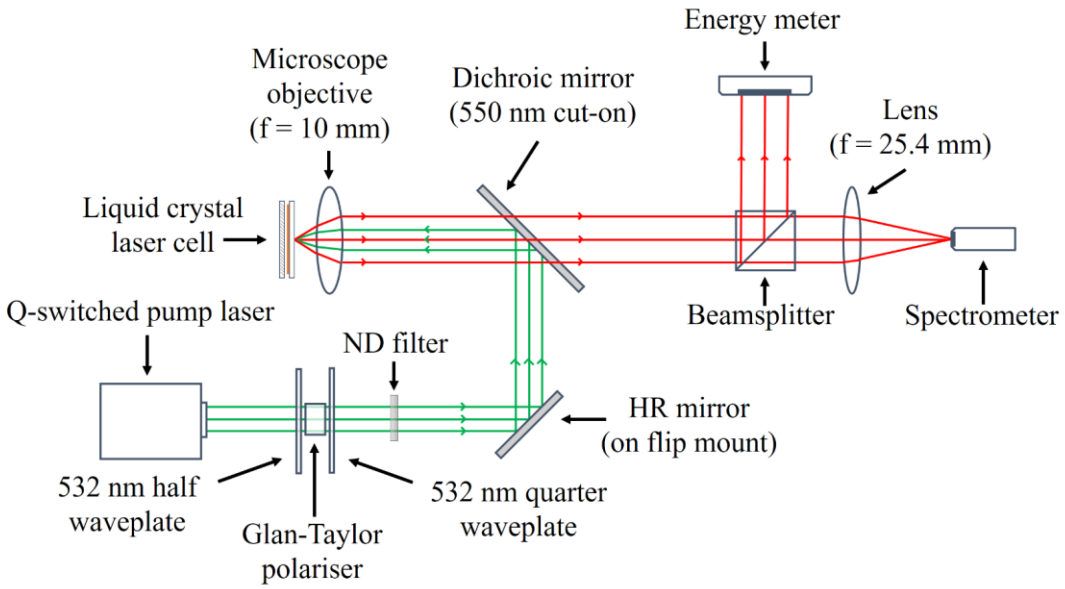

Figure 4.3. Experimental layout for optically pumping an LC laser with a 532 nm Q-switched laser.

A calibration graph for the pump energy as a function of half-waveplate position was required, as the energy could not be measured at the same time as pumping the LC laser cell[14]. The half-waveplate was rotated in 2 ° increments and the transmitted pump energy was measured at each wave-plate position, with the energy meter placed infront of the LC laser. With the input energy known for a given waveplate position, the energy meter was repositioned at the output of the LC laser, as shown in Figure 4.3. The repetition rate of the Q-switched laser was set to 1 Hz to minimise the risk of thermal and optical damage of the cell during data acquisition. The position of the LC laser relative to the microscope objective was optimised by maximising the LC laser beam intensity measured by the spectrometer. The half-waveplate was returned to its initial position and the average LC laser output energy over a 60 second period was recorded for each 2 ° waveplate rotation. This was plotted against the corresponding input energy to determine the slope efficiency and threshold.

It was found that the pulse energy of the Q-switched laser was such that, even when the waveplate was positioned only a few degrees from minimum transmission, LC lasing was

[14] At this stage of the project, the input and output energies could not be measured simultaneously, as only one energy meter was available, hence the need for a waveplate calibration curve. An additional energy meter was procured later in the project to enable simultaneous measurement of the pump and LC laser emission by adding a beamsplitter to the arrangement. This is introduced in Chapter 5. An additional energy meter was not necessary for this experiment and the data collected using the method explained here were fit for purpose.

detected. The fact that LC lasing occurred so close to minimum transmission, was testament to the high quality of the cell, resulting in a low LC laser threshold (yet to be quantified) and thus fulfilling the preliminary objective. This initially prevented acquisition of pre-threshold data, thus preventing threshold from being determined, as there were not enough pre-threshold data points to establish the gradient change of slope efficiency expected at threshold. This was addressed by placing a neutral density (ND) filter between the quarter-waveplate and dichroic mirror to attenuate the beam. The waveplate calibration curve with the ND filter in place (and obeying Malus' Law), is shown in Figure 4.4.

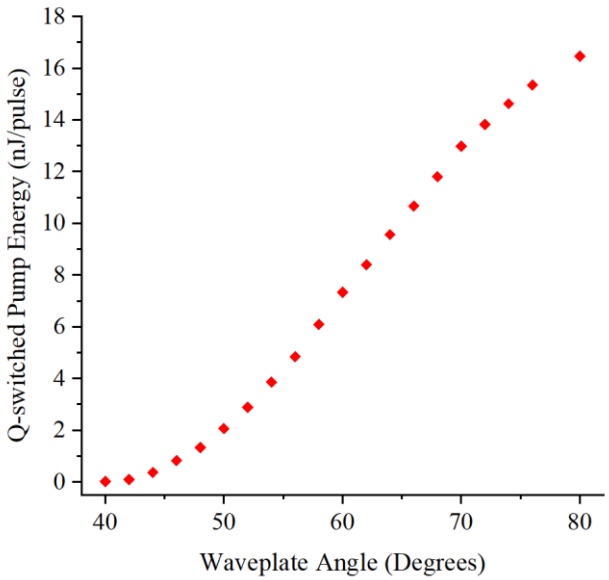

Figure 4.4. Waveplate calibration curve for the Q-switched laser with the neutral density filter in place.

4.3.2 Q-switched pumping results

A narrow linewidth (< 1.5 nm full width half maximum (FWHM), limited by the resolution of the spectrometer) LC laser output at 610 nm was observed, close to the fluorescence maximum and coincident with the measured band-edge position (Figure 4.5).

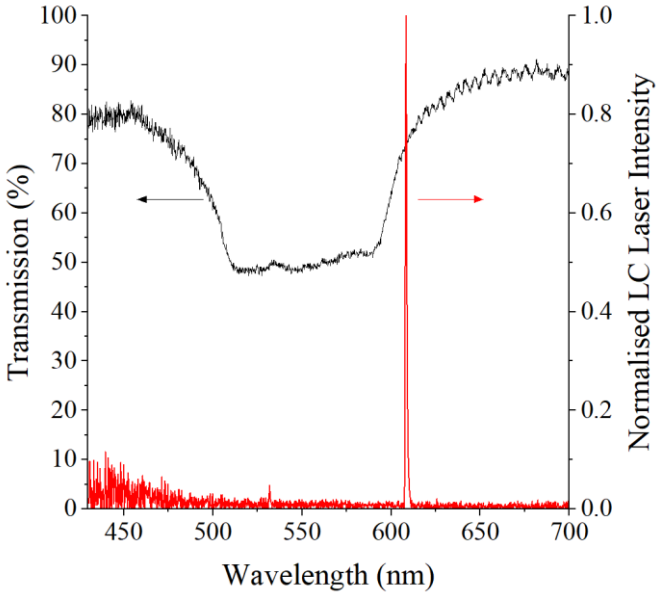

*Figure 4.5. White light transmission spectrum of the N*LC (black), showing the photonic bandgap. Also shown is 610 nm LC laser emission at the long bandedge (red) when pumped by the 532 nm Q-switched laser.*

An obvious change in the gradient of the slope efficiency was observed (Figure 4.6) and, above threshold, a slope efficiency of 8.1 % was measured, similar to efficiencies presented in Refs. [63] and [87] for equivalent 532 nm Q-switch-pumped DCM-doped LC lasers. As expected, a low threshold [16], [126] was confirmed, and calculated to be 7.4 nJ/pulse (6.93 mJ/pulse/cm^2), corresponding to a peak power of 5.7 W[15]. This data confirmed the presence of photonic band-edge lasing and, more importantly, verified low-threshold lasing in anticipation of demonstrating LD pumping.

[15] At this stage in the research, it was unclear if pulse energy or peak power was the more important quantity for determining LC laser threshold, so both were calculated based on the pump parameters.

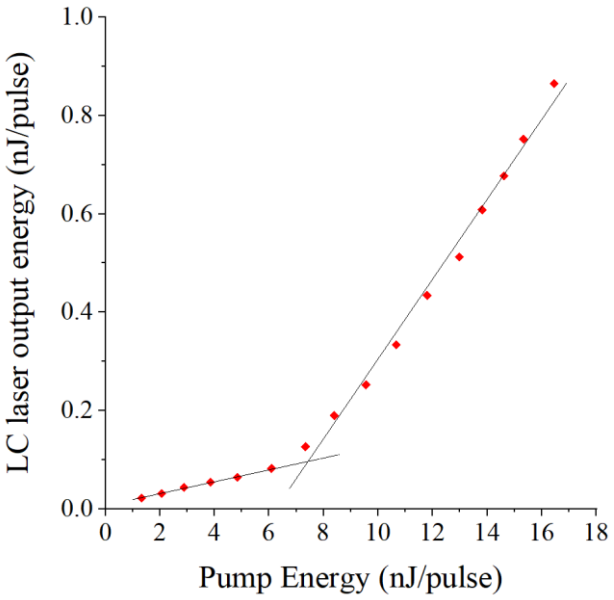

Figure 4.6. LC laser efficiency graph when pumped with the 532 nm Q-switched laser, showing a clear gradient change at the laser threshold.

4.4 Laser diode selection and characterisation

4.4.1 Feasibility study

4.4.1.1 Laser diode

Having determined the performance parameters of the threshold-optimised LC laser cell with the Q-switched pump, a feasibility study was required to determine if the pump properties could be replicated using LD technology.

The LD had to have as similar characteristics as possible to the Q-switched laser to maximise the chances of successful LC laser emission. The Q-switched laser specifications and resultant LC laser performance characteristics are summarised in Table 4.1a and 1b respectively.

Table 4.1. a) Q-switched laser specifications and b) resultant LC laser performance characteristics

a)

Q-switched Laser Specifications	
Wavelength	532 nm
Pulse duration	1.3 ns
Max peak power	4.5 kW
Spot area at focus	106.8 (± 5.3) μm^2

b)

LC Laser Performance Parameters	
Threshold	7.4 nJ/pulse 6.93 mJ/pulse/cm^2 (5.7 W/pulse)
Slope efficiency	8.1 %
Wavelength	610 nm

The LD peak power was not expected to match the > kW peak power of the Q-switched laser, as there are no mechanisms by which this power can be achieved with a single LD; a LD is either on or off, with the peak power determined by the maximum current tolerable without damaging the diode. A LD with the highest possible output power specifications was therefore desirable to overcome LC laser threshold which, when pumped with the Q-switched laser, was 5.7 W (peak power).

Another key consideration in selecting the LD was the wavelength. To directly compare the LD with the Q-switched laser, a 532 nm LD was desirable. However, a lower-wavelength LD, such as an emitter in the blue/violet region of the visible spectrum, had the advantage of

maximising the range of LC laser emission wavelengths not possible with 532 nm excitation. Furthermore, the LD wavelength had to overlap with the absorption of DCM (approximately 400 – 560 nm).

Different LDs and suppliers were investigated. It was apparent that a 532 nm LD was not a viable option, as this wavelength was not available at the fundamental wavelength output from a LD device, and those sources that could produce 532 nm in a compact package *(DJ532-40, Thorlabs,* for example*)* had a maximum power rating of milliwatts (40 mW in the case of the *DJ532-40*). Alternatives at a shorter wavelength of 520 nm were more common, the specifications of which are shown in Table 4.2.

Table 4.2. Specifications for different LDs with output wavelengths at 520 nm. Note that power ratings are for continuous wave operation.

LD Manufacturer	**Model**	**Power Output**	**Current Rating**
Osram	PLT3 520D	140 mW	330 mA
Sharp	GH05C01A9G	600 mW	1.1 A
Thorlabs	L520G1	900 mW	1.6 A
Nichia	NDG7575	1 W	1.6 A

Despite the greater prevalence of LDs at 520 nm, the maximum output powers available were still not suitably high to maximise the chances of overcoming threshold (assuming that the maximum specified power at CW operation was also the maximum peak power that could be achieved in pulsed operation).

The semiconductor material gallium nitride (GaN) is used as the gain medium in blue LDs and can tolerate higher power densities than the semiconductor materials used in other LDs. Furthermore, the emission wavelength of 445 nm is suitable for optically pumping some commonly used dyes in LC lasers, including DCM. A study by Stylogiannis *et al.* showed that a Nichia LD operating at 445 nm worked in nanosecond pulsed operation at a current 40 times greater than the specified CW current rating [127]. Their work confirmed that an increase in operating current resulted in an increase in optical output power from the LD without it being

damaged. This suggested that the same 445 nm LD ought to be capable of overcoming the threshold of the LC laser discussed above if driven in a pulsed mode operation.

Table 4.3. Specifications for different LDs with output wavelengths at 445 nm. Note that power ratings are for continuous wave operation.

LD Manufacturer	Model	Power output	Current Rating
Osram	PLPT9 450LA_E	3.0 W	2.5 A
Thorlabs	L450G1	3.2 W	2.5 A
Nichia	NDB7K75	3.5 W	3 A
Nichia	NUBM44	6 W	3 A

Based on the specifications of common 445 nm LDs (Table 4.3), the Nichia NUBM44 LD (Figure 4.7b) was selected as the most likely to overcome LC laser threshold as it had the highest power output of any LD available. This was also similar in specification to the LD used in ref [127] in which a high current was used in pulsed operation.

Figure 4.7. Pump lasers used throughout this work with a) the 532 nm Q-switched laser being more than ten times larger than b) the 445 nm laser diode [128].

4.4.1.2 Driver electronics

An additional advantage of LDs from a research perspective is the controllability of the performance parameters. Unlike Q-switched lasers which deliver a fixed pulse length determined by the optoelectronics, the output characteristics of an LD (such as pulse length, peak power and repetition rate) can be independently controlled by the driver electronics. Off-the-shelf LD driver electronics vary in cost and size, depending upon the performance requirements. In the case of the work presented here, nanosecond-scale pulse lengths, and

currents ≥ 3 A (based on the specifications in Table 4.3) were required to ensure the LC laser threshold was reached.

One of the leading manufacturers of LD driver electronics is PicoLAS GmbH. They specialise in making compact drivers that deliver high currents over multiple times-scales, including within the nanosecond regime, and have successfully been used in other work for high-power LD applications [112], [129]. They also provide compact pulse generators that can be "piggybacked" onto their driver electronics to form a single compact device. For this work, the *LDP-V 50 100 V3.3* driver was used with pulse generator *PLCS-21*. The specifications of this combination of driver electronics and signal generator are summarised in Table 4.4.

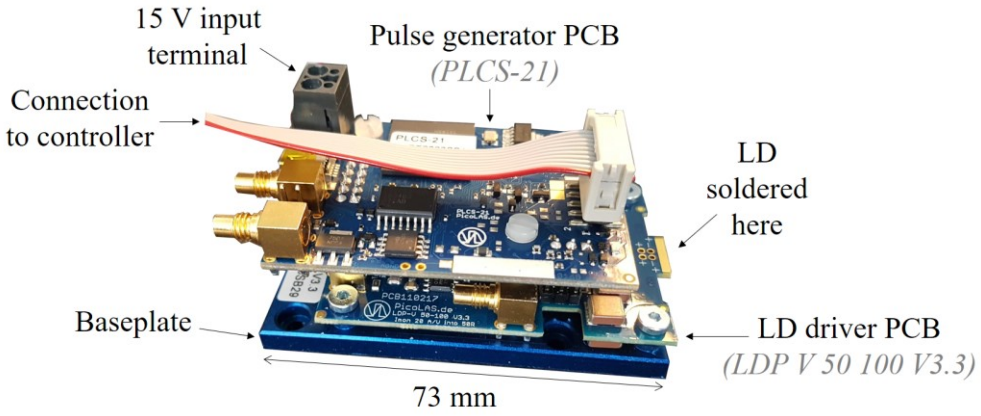

Figure 4.8. Pulse generator PCB piggybacked onto the LD driver electronics. The LD is not yet soldered onto the electronics at this stage of the LD module construction.

Table 4.4. LD driver electronic specifications.

Output Current	3 A – 50 A
Repetition Rate	1 Hz – 2 MHz
Pulse Length	12 ns – 1 µs
Rise Time	2.3 ns
Supply Voltage	15 V
Current Monitor	20 A/V into 50 Ω
Operating Temperature	- 20 °C to + 55 °C

Although the minimum specified pulse duration of the driver electronics was not as short as the Q-switched laser (12 ns and 1.3 ns respectively), it was still considered suitable, as other work has successfully demonstrated LC laser emission with a pump pulse duration of 14 ns [31], [37], [39].

4.4.2 Laser diode module design

4.4.2.1 Design considerations

The design of the LD pump module had to be considered before its construction. Firstly, it had to be integratable with the LC laser experimental arrangement used with the Q-switched laser to allow direct comparisons between the two pumping techniques. Furthermore, easy access to the LD and electronics was also necessary, firstly for alignment optimisation and secondly to allow modifications or adjustments to the components. For example, access to a potentiometer on the driver board was required, as this limited the maximum current delivered to the LD.

Compliance with laser safety regulations was also required. The NUBM44 LD at full power in CW mode is classified as a Class IV laser device, requiring key-switch operation in an interlocked room. The ability to secure the module to the optics bench was necessary to prevent accidental misalignment and/or dangerous exposure of the laser beam during operation. The output leads and capacitors on the driver printed circuit board (PCB) were connected to an internal 100 V supply, so needed to be physically inaccessible during operation to prevent accidental damage to the device and electrocution of the user.

A cooling mechanism to prevent the electronics from overheating at high repetition rate operation was desirable to prolong the lifetime of the components and prevent temperature-induced noise fluctuations in the optical output of the LD.

Finally, direct connection of the LD to the driver electronics (without the presence of long wires) was important to minimise parasitic stray inductance, which detrimentally affects the pulse rise time and hence the overall LD pulse length.

4.4.2.2 Design solutions

An off-the-shelf box *(517-3793, RS)* was used to house the electronics and LD, as the aim at this stage of the project was to demonstrate LD pumping, rather than to optimise finer design details that would, for example, be more relevant for designing a prototype device. The module was easily modified, and featured flanges for clamping to the optics table and a lid to prevent accidental access to the electronics during use. It also had sufficient internal space for the electronics, key-switch, alignment mechanics and surge protection circuitry.

The output height of the LD was designed to match the Q-switched laser output so that the two pump sources could be co-aligned for performance comparison and to minimise disruption to the experimental arrangement.

The LD was fixed in a copper cylinder which contained an adjustable long focal length lens. Unlike the circular spot from the Q-switched laser, LDs often produce a divergent elliptical beam due to the rectangular geometry at the output from the semiconductor material (as discussed in Section 2.4.4). The half-angle divergence of the *x* and *y* axes of the LD differed (hence the ellipticity) and were stated in the Nichia specifications as 23° and 7° respectively [128]; hence the presence of a long focal length lens (hereafter referred to as the 'LD lens') positioned immediately after the output of the LD to control the beam's divergence. The beam shape and size were controllable by varying the distance between LD and LD lens. The LD anode and cathode were shortened to ~ 2 mm and soldered directly onto the *LDP-V 50-100 V3.3* driver board to minimise stray inductance. The baseplate of the driver board was then mounted onto adjustable legs to optimise the height of the LD inside the module. The electronics were connected to a control unit (*PLB-21, PicoLAS*) via a 2 A fuse (for surge protection) and a double pole single throw keyswitch (*S286A-1, Farnell*). This switched on/off the electronics and a small cooling fan to assist heat dissipation from the electronics[16]. The keyswitch was laser-safety compliant such that the key could not be removed during operation.

[16] Given the short duty cycle (< 0.0001 %) operation expected for the LD experiments, water cooling or Peltier cooling was ruled out due to the expense, complexity and bulk. Fan cooling was considered the most appropriate option.

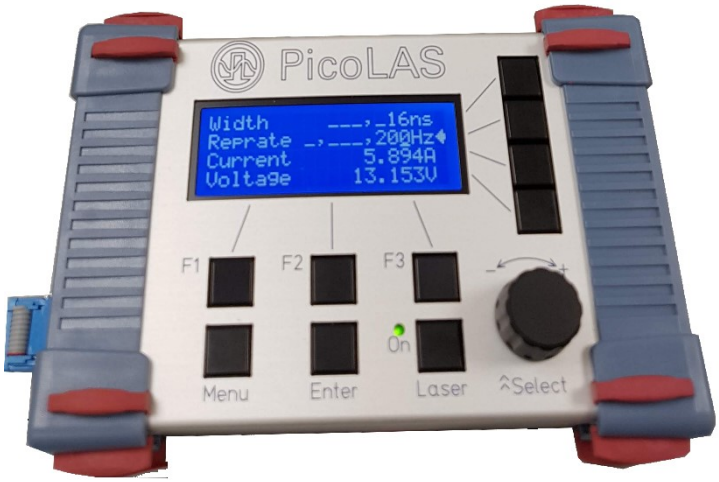

Figure 4.9. PLB-21 controller unit that can be calibrated to the specific LD in use and allows the user to independently control the pulse length, rep rate and current. The LED indicator on the unit shows when the LD is active.

The controller unit (Figure 4.9) was powered via the 15 V supply to the driver and enabled LD calibration, temperature monitoring and LD pulse parameter adjustment. A BNC connection for monitoring the driver current output was also included in the design of the module. The LD module is shown in Figure 4.10.

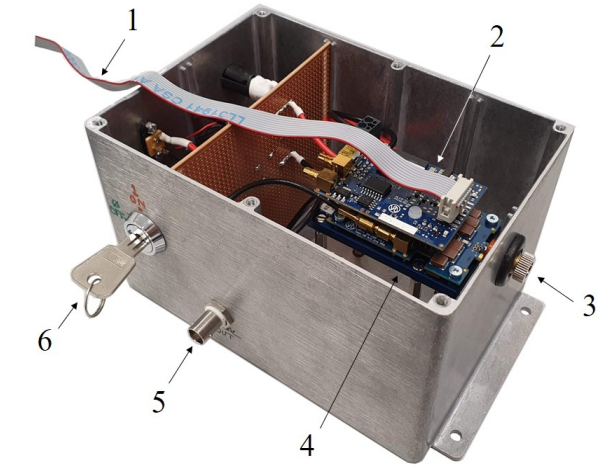

1	Controller power and signal cable
2	Pulse generator PCB
3	LD focussing lens
4	LD driver PCB
5	Current monitor output
6	Key switch

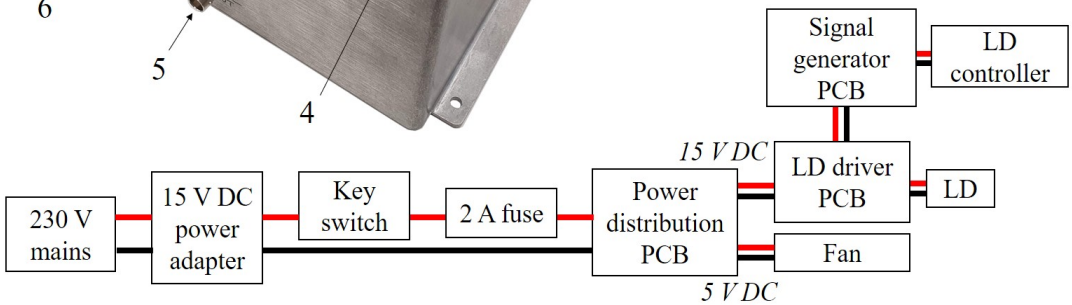

Figure 4.10. LD pump module (top left) with components detailed in the table (top right) and schematic diagram of electrical components (bottom).

4.4.3 Laser diode performance characterisation

The LD output was first characterised before attempting to pump the LC laser. The minimum performance specifications were set on the control module ($I = 5.89$ A, $\tau = 12$ ns, $f = 1$ Hz) in order to measure the minimum output energy from the LD. However, it was only when the pulse length was increased to a set value of 16 ns that laser emission was produced. At these settings, an energy of 53 nJ/pulse was measured. This was encouraging, as it exceeded the LC laser threshold determined by the Q-switched laser (7.4 nJ/pulse). The specified wavelength of 445 nm was confirmed by the spectrometer (Figure 4.11).

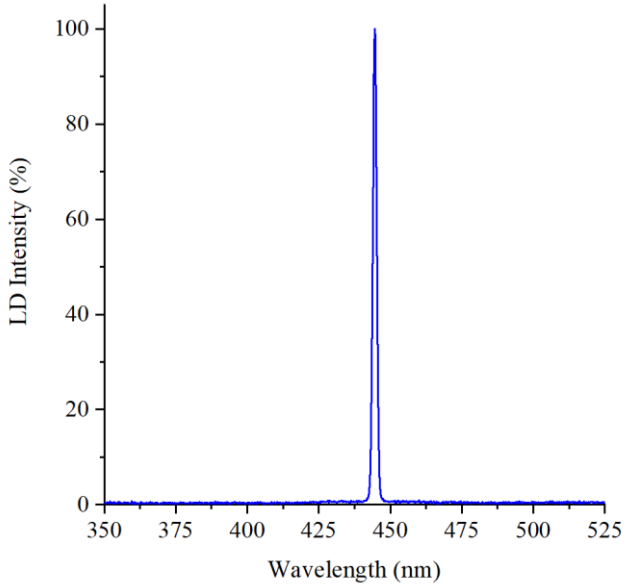

Figure 4.11. LD spectrum showing peak wavelength at 445 nm.

An energy stability measurement was also recorded to determine the LD warm-up time required before any experiments were conducted. The LD parameters were set to deliver a pulse length of 16 ns, a repetition rate of 10 Hz and a current of 5.89 A (the maximum current permissible at this stage of the investigation, as determined by the potentiometer on the driver electronics). The pulse energy was recorded for three hours and the results were plotted as a function of time (black data in Figure 4.12). An adjacent-averaging plot (red data in Figure 4.12) was overlaid in addition to the raw data to observe any fluctuations or noise bursts that would otherwise have been obscured by the pulse-to-pulse energy variation.

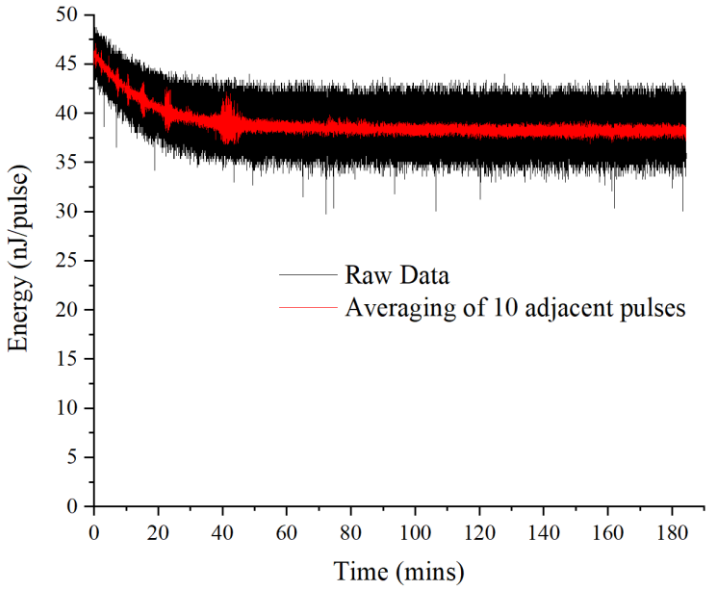

Figure 4.12. LD temporal stability recorded for 3 hours. A 10-point adjacent averaging function (red) was applied to the raw data (black) to observe any energy spikes hidden in the noise.

An exponential decrease in pulse energy was present for the first hour and was accompanied by noise bursts during the same time period. After this time, the energy stabilised with a pulse-to-pulse variation of ± 7 %. The LD energy stability measurement was repeated (after allowing the LD to cool down for a day), with the repetition rate increased from 10 Hz to 100 Hz. It was thought that increasing the frequency would reduce the time required for the LD pulse energy to stabilise. There was, however, no difference in the time taken for the pulse energy to plateau when compared to the lower repetition rate. This suggested that the warm-up time, before a steady output was reached, was independent of the repetition rate; at least for the limited repetition rates tested here. The LD was therefore run for one hour before any data were taken for the work presented in this chapter and for the remainder of this thesis. The pulse-to-pulse variation was also measured at different currents to determine if the fluctuations were absolute or a percentage of the average pulse energy. It was found that the pulse energy fluctuations ranged between 6 % and 8 % of the average pulse energy, rather than by an absolute value.

Unlike Q-switched lasers, which have a fixed pulse energy, the LD's pulse energy could be varied by two different means: pulse duration and pulse peak power (via current control). The effect of varying the pump pulse length on the output energy was characterised.

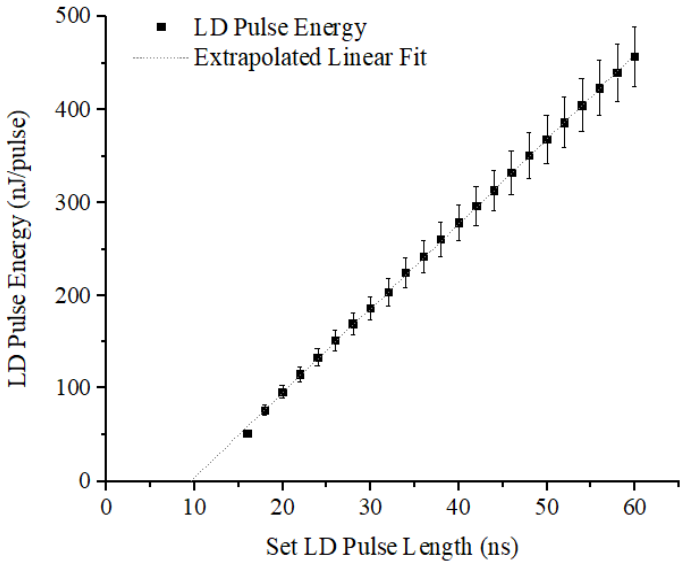

Figure 4.13. Measurement of the LD pulse energy as a function of the pulse length set on the controller unit.

Figure 4.13 shows a linear trend between the pulse length set on the LD controller and the output energy. An unexpected feature, was that the extrapolated trend did not pass through the origin, which suggested either a discrepancy between the LD pulse length set on the controller and the true optical pulse length output, or a calibration issue with the energy meter. The latter was discounted by recording the same data set using a different energy meter and measuring the same trend. The temporal profiles of the electrical and optical signals were therefore investigated and compared to the pump pulse length set on the controller.

The electrical signal supplied to the LD was measured via the current output monitor of the driver electronics and the resultant optical pulse from the LD was measured simultaneously using a photodiode *(DET025A/M, Thorlabs, rise and fall time = 150 ps)*. Both signals were displayed on an oscilloscope *(WavePro 735Zi, LeCroy, response time = 120 ps)*. The experimental arrangement for these measurements is shown in Figure 4.14.

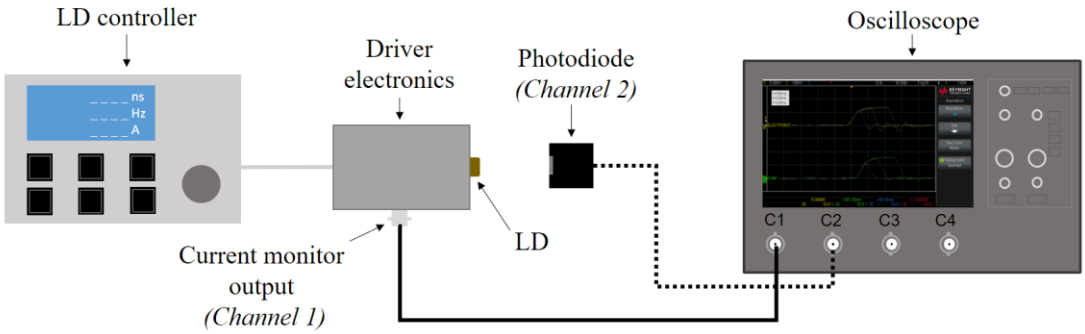

Figure 4.14. Arrangement for comparing the electrical signal from the LD driver electronics to the resultant optical signal from the LD.

The current was set to 5.89 A and the repetition rate to 10 Hz. The scope was set to measure the FWHM for both the electrical and optical signals. Two hundred pulses were recorded and an average value for both measured parameters was calculated. The results are shown in Figure 4.15.

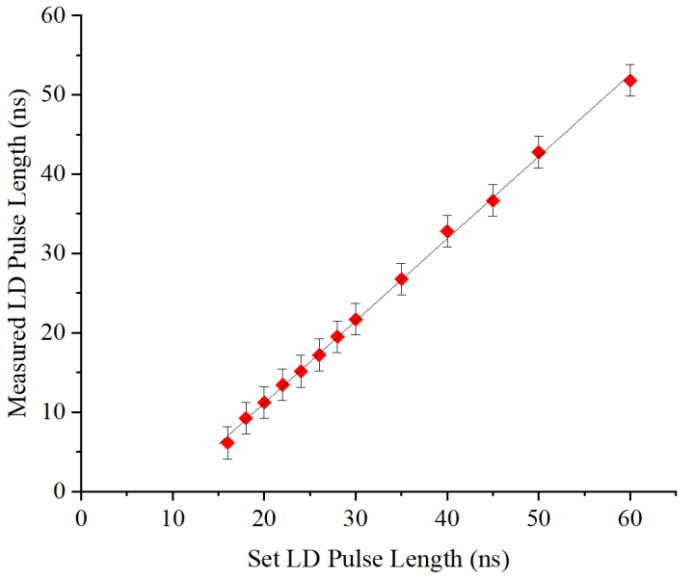

Figure 4.15. Comparison of the measured optical pulse length to the pulse length set on the LD controller. The error bars were calculated from the standard deviation of the mean of 200 pulses recorded for each pulse length.

From Figure 4.15, it can be seen that the set pulse length, τ_{set}, is linearly proportional to optical pulse length, $\tau_{optical}$, but that $\tau_{optical} < \tau_{set}$. An example of a temporal profile for a pulse with $\tau_{set} = 20\ ns$ can be seen in Figure 4.16, which explains the discrepancy between the two pulse lengths. Within the 20 ns duration, the electrical pulse rises to its maximum amplitude,

falls below zero, then returns to zero. The LD only emits a pulse during the time the electrical signal is operating above zero.

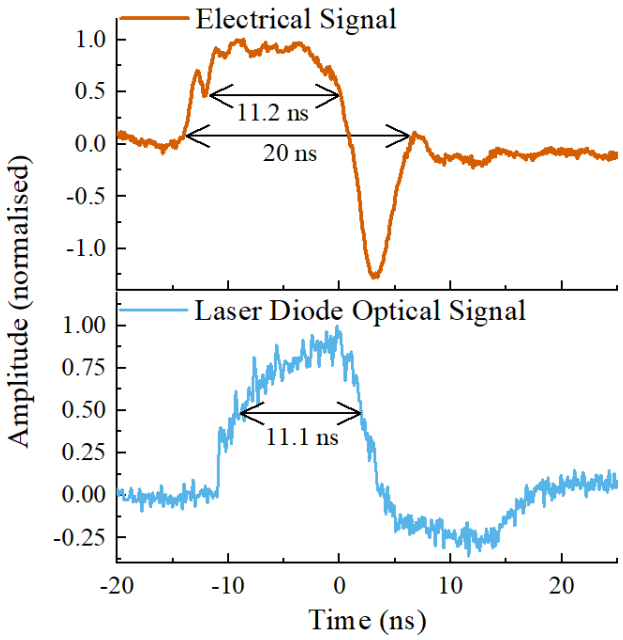

Figure 4.16. Comparison between electrical signal (top) and optical temporal profile of the LD pump (bottom) when the controller was set to 20 ns.

The disparity between the electrical and optical pulses explains the offset from the origin on the *x*-axis in Figure 4.13. When the measured value of the LD pulse length was used in place of the set value, the red data in Figure 4.17 showed the effect of increasing the pulse length on the LD output energy, with the extrapolated linear fit now intersecting the origin as expected. This was used throughout the work in this thesis to determine the true pulse length for a given set pulse length.

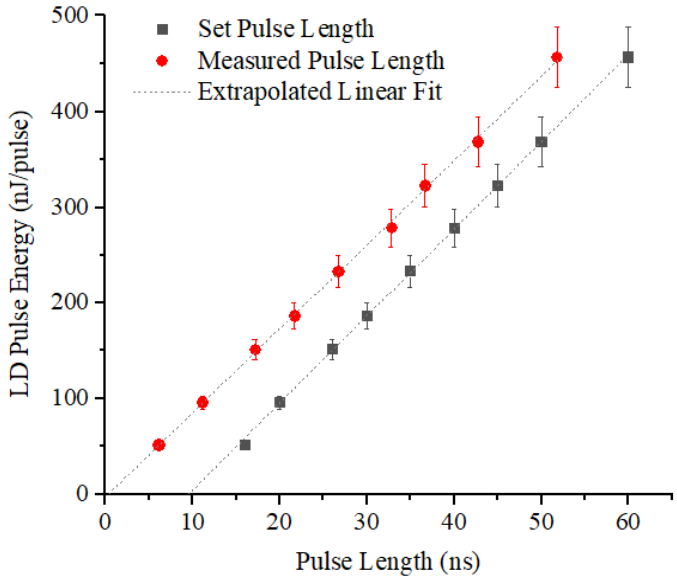

Figure 4.17. LD pulse energy as a function of measured LD pulse length (red), with the set pulse plotted for comparison (black).

The first data point in Figure 4.13 and Figure 4.15, corresponding to a set pulse length of 16 ns, deviates slightly from the linear trend, such that its output pulse energy and optical pulse length are lower/shorter than expected. The reason for this was investigated and found to be caused by a limitation in the response of the electronics when set to deliver the shortest possible pulse lengths. It was found that at a set value of 16 ns, the maximum voltage was not reached within the duration of the pulse. This measurement was repeated for increasing set pulse lengths and it was found that the maximum voltage was reached and remained approximately constant for all set pulse lengths ≥ 20 ns. This can be seen in Figure 4.18 which shows the peak voltage reached by the electronics and resultant optical signal for pulse lengths ranging from 16 ns – 50 ns. The optical signal followed a similar trend to the electrical signal, as expected.

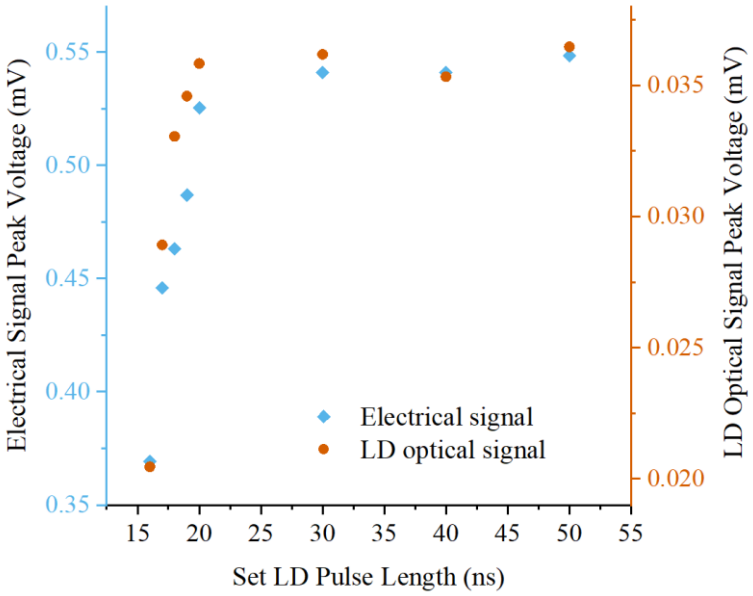

Figure 4.18. Effect of the LD pulse length on the peak voltage reached by the electrical pulse (blue) and the resultant optical pulse from the LD (orange).

Despite the maximum voltage not being reached when $\tau_{set} = 16\,ns$, and consequently, the LD pulse energy being slightly lower than expected, this pulse length was used for the initial attempt at LC laser pumping, as theoretical predictions showed a proportionality between threshold and pump pulse length [30]. Thus, $\tau_{set} = 16\,ns$ (corresponding to an actual pulse length of ~ 8 ns) was expected to maximise the chances of successful LC lasing (within the performance limitations of the equipment).

4.4.4 Laser diode characterisation summary

A 445 nm Nichia LD was selected in an attempt to demonstrate an alternative pump source to a Q-switched laser. This particular LD was chosen due to its ability to produce the highest output powers compared to other LDs, and because of the suitability of its wavelength for use with the organic laser dye, DCM. Driver electronics capable of delivering up to 50 A in nanosecond-scale pulse durations were used to deliver a pulse with specifications as close as possible to the Q-switched laser.

The performance of the LD was characterised prior to its use as an LC laser pump source. It was found that operation for one hour was required before the LD output energy was stable. This was likely due to thermal stabilisation between the LD and the copper housing which was

needed to mount the LD lens. The effect of increasing the pulse length on laser pulse energy was found to be linear, as expected. A discrepancy between the set duration of the electrical pulse supplied to the LD and resultant optical pulse duration was found, and upon comparison between the temporal profiles of the two pulses, the reason for this was attributed to the time taken for the electrical signal to stabilise after producing the pulse. A look-up table was populated for the remainder of the work in this thesis so that the duration of the optical pulses used to pump the LC laser could be found for a given set pulse length. The maximum output voltage (set by the current on the LD driver electronics) was reached for pulse lengths with a set value ≥ 20 ns.

4.5 Laser diode pumping of a liquid crystal laser

4.5.1 Experimental arrangement

As before with the Q-switched pump, the experimental arrangement presented in Section 3.3.1 was used to pump the LC laser, but with optics suitable for use with the LD (Figure 4.19). A half-waveplate (*WPH05M-445, Thorlabs*), quarter waveplate *(WPQ05M-445, Thorlabs)* and long-pass dichroic mirror *(ZT442rdc, Chroma)* were introduced. The dichroic mirror reflected the LD pump beam and transmitted LC laser emission at wavelengths > 459 nm, whilst also blocking any residual pump beam scattered from the focussing lens. The LD was co-aligned with the Q-switched laser and a flip mirror mount was used to switch between the two pump sources.

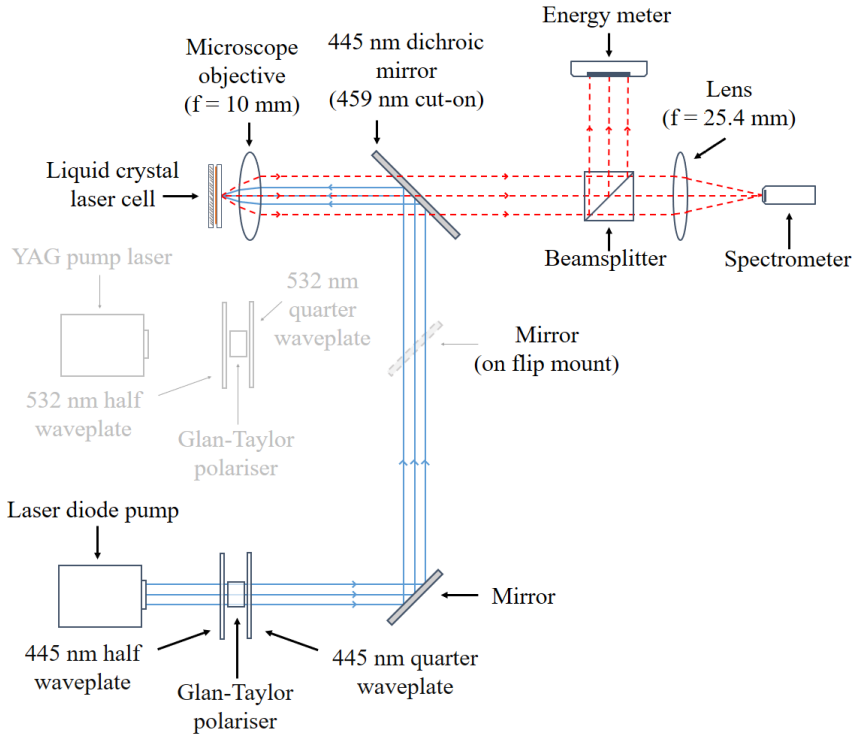

Figure 4.19. Experimental configuration for optically pumping an LC laser with the 445 nm LD. (The Q-switched pump that was co-aligned with the LD for directly comparing the LC laser performance using the different pump sources is included in the diagram. A different dichroic mirror was used when pumping with 532 nm, as shown in Figure 4.3.)

Using the same LC laser cell as characterised in the Q-switched experiment (Section 4.3.2), the LD parameters were set to:

Table 4.5. LD parameters first used to demonstrate successful pumping of an LC laser.

Current	5.89 A
Set Pulse Length	16 ns
Repetition Rate	1 Hz

4.5.2 Spectral output and polarisation

No immediate signal was detected on the spectrometer nor on the energy meter. There were two factors contributing to this. Firstly, the position of the LC laser cell along the optical axis needed adjusting to optimise the cell position at the focus of the microscope objective. Secondly, the position of the LD lens relative to the LD needed to be optimised. At optimum alignment, a signal appeared on the spectrometer, along with a pJ-scale reading on the energy meter. The repetition rate, pulse length and cell position were arbitrarily adjusted to confirm that the spectrometer signal was indeed laser emission.

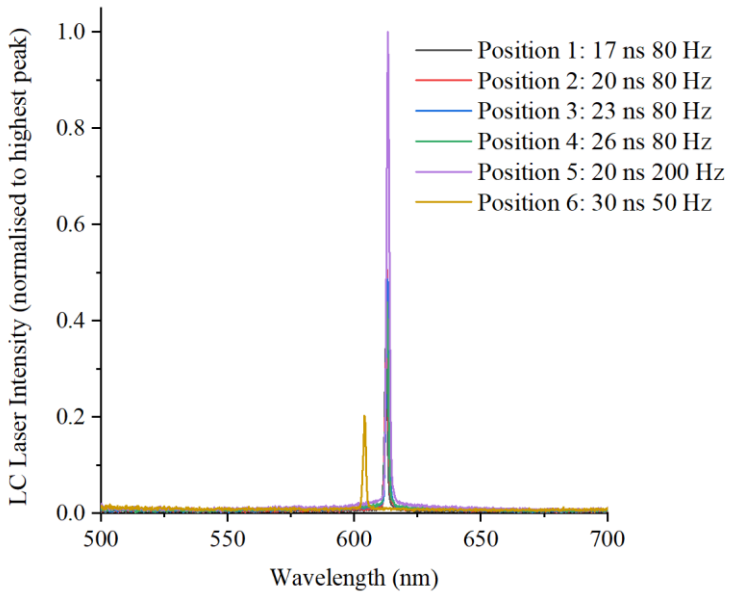

Figure 4.20. Spectra of the first data set of diode-pumped LC laser emission.

The spectra recorded from this initial attempt (Figure 4.20) showed consistently narrow-linewidth emission. As shown in Section 3.2.8, one possible outcome of a poorly made cell is a multi-domain LC texture, whereby a variation in pitch length between domains results in different wavelengths. In Figure 4.20, however, the fact that only one of the six positions tested had a different wavelength from the rest confirmed that the cell had been well fabricated with a uniform texture, resulting in a mostly consistent wavelength across the cell.

The emission properties were then considered in greater detail. Not only did band-edge emission appear at 610 nm – the same wavelength as when the same cell was pumped with the

Q-switched pump source – but the linewidth also appeared to be identical in nature (< 1.2 nm) (Figure 4.21).

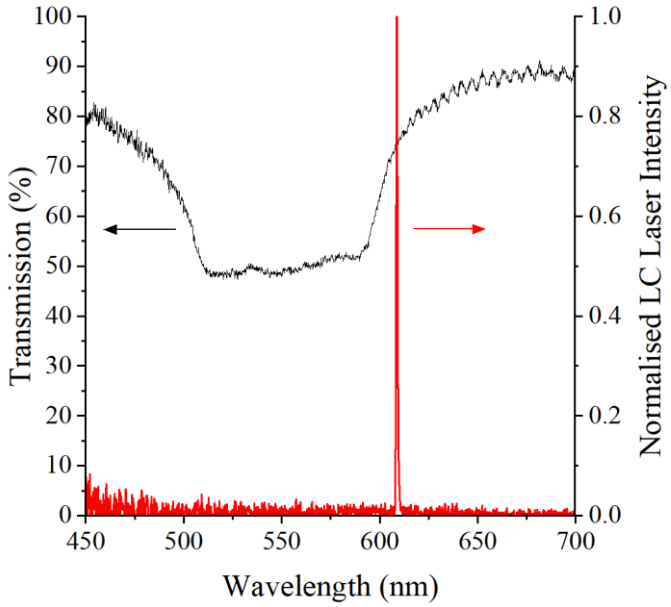

Figure 4.21. The same white light transmission spectrum of the chiral nematic LC as shown in Figure 4.5 (black). When pumped with the LD, 610 nm LC laser emission results at the long bandedge (red) and is spectrally identical to that obtained with the Q-switched pump.

Unlike previous attempts at semiconductor-based pumping of LC lasers [12], [38], the narrow linewidth signal was not dominated by the simultaneous presence of a broad fluorescence band. This narrow linewidth emission is the first evidence of successful LC bandedge lasing using a LD pump source. Furthermore, at this repetition rate of 1 Hz and set pump pulse duration of 16 ns, the LC laser linewidth and intensity were constant for ≥ 30 minutes.

Additional investigations were made to provide further evidence that band-edge lasing had been achieved with the LD.

Previous work has shown that the polarisation state of a photonic band-edge LC laser with a reflective geometry is mostly linear, as a consequence of the reversal of circular polarisation upon reflection at the mirrored surface resulting in the superposition of left-handed and right-handed polarised light [68]. A linear polariser was therefore placed before the beamsplitter at the output of the LC laser to replicate this result as further evidence of band-edge laser emission from a reflective cell. The intensity of the LC output was measured on the spectrometer, firstly with the polariser set at an angle of 0° relative to the polarisation

output of the LC laser and then again at 90°. The results are shown in Figure 4.22a are compared to the same measurement with the Q-switched pump (Figure 4.22b).

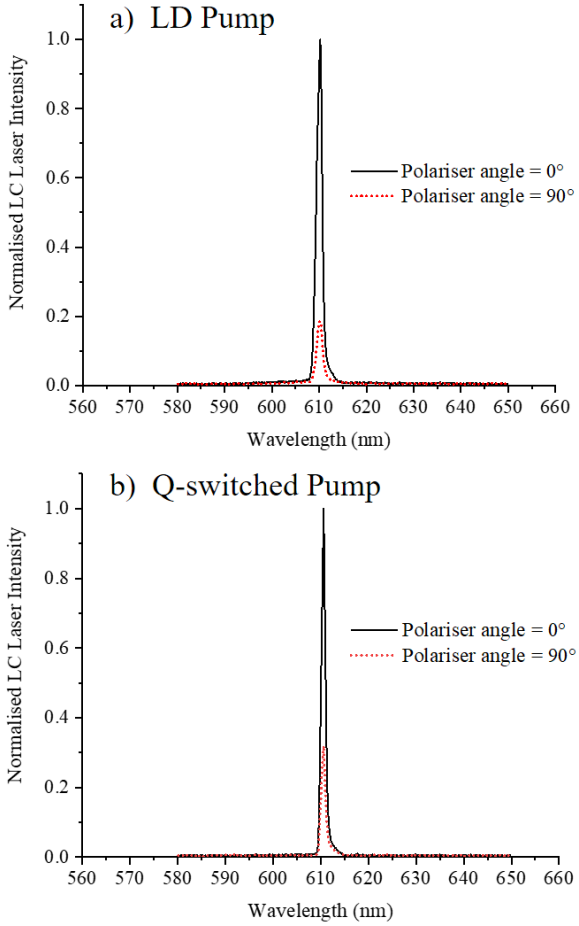

Figure 4.22. Confirmation of linear polarisation of LC laser output when pumped with a) the 445 nm LD and b) the 532 nm Q-switched laser.

It can be seen that both pumping regimes resulted in a near-identical degree of linear polarisation of the LC laser output. As there is no known mechanism for linearly polarised emission from an N*LC laser, other than photonic band-edge lasing from a reflective cell, this this had to be responsible for the data in Figure 4.22. When the polariser was rotated by 90°, the transmission dropped by at least 70 %. The fact that 100 % extinction was not observed was attributed to an unequal combination of left-handed and right-handed light, possibly due to imperfections in the reflective aluminium surface.

4.5.3 Slope efficiency and threshold

In addition to the linewidth and polarisation data, the distinct gradient change in slope efficiency at threshold (associated with bandedge lasing and observed with the Q-switch-pumped LC laser) was sought with the LD. As before, the pump pulse energy was calibrated with respect to the half-waveplate angle. Unlike the Q-switched pumping regime, the pulse energy of the LD was sufficiently low to not require attenuation by an ND filter. The repetition rate of the LD was set to 1 Hz and the half waveplate was rotated in 2 ° increments from the lowest detectable LC output pulse energy to the maximum pulse energy. The average pulse energy output from the LC laser was measured for 60 seconds for each waveplate angle.

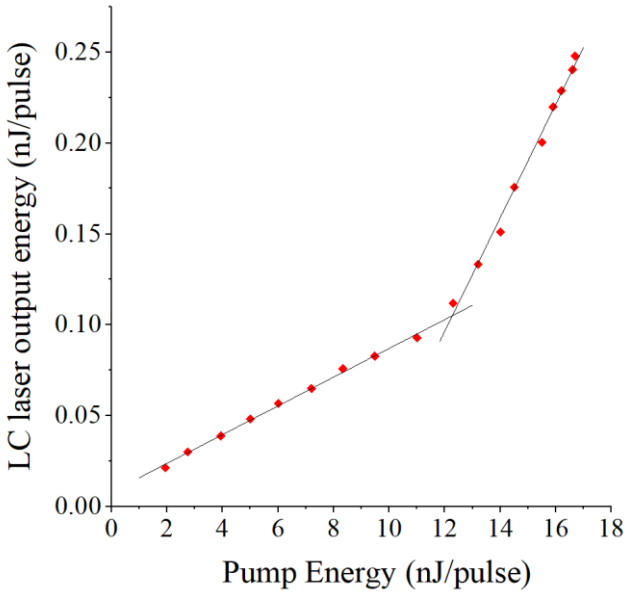

Figure 4.23. Slope efficiency plot for the LD pumped LC laser showing a distinct gradient change at the laser threshold.

The resultant slope efficiency (Figure 4.23) showed the same characteristic change in gradient at LC laser threshold. From the point of intersection of the lines that best fit the below and above threshold data, the threshold of the LD pumped LC laser was found at 12.3 nJ/pulse (15.7 mJ/pulse/cm^2) with a slope efficiency above threshold of 3.1 %.

The Q-switch-pumped LC laser efficiency data, with a clear gradient change at threshold, is typical behaviour for a band-edge laser. The near-identical behaviour of the LD-pumped regime is therefore the first unequivocal evidence of successful diode-pumped LC lasing.

Furthermore, the narrow linewidth output, identical for both pumping regimes is additional verification that the LC laser was operating above threshold, along with a similar degree of polarisation measured for both cases. The nanosecond-scale pulsing of the LD is what distinguishes this work from previous attempts at semiconductor-based pumping [12], [38], and is likely the principal reason for successful LC laser emission. The higher power output of the LD compared to the LEDs used in previous work is also a significant factor.

4.5.4 Multi-wavelength emission

To further validate the results and demonstrate the capabilities of this pump source, two more LC laser cells were fabricated using different dyes and chiralities to lase at different wavelengths when pumped with the same 445 nm LD. Table 4.6 below details the cell composition and lasing properties of the two additional cells (B and C). The DCM cell (A) used above in the Q-switched and LD investigation is also included for completeness.

Table 4.6. Relative chiral dopant and dye concentrations for Cell A used to prove LD pumping, with additional cells B and C fabricated to further demonstrate LD-pumped LC lasing at additional wavelengths.

Cell	**Chiral Dopant Concentration (wt%)**	**Dye**	**Dye Concentration (wt%)**	**LC Laser Wavelength (nm)**	**Pitch Length (nm)**
A	4.35 ± 0.05	DCM	1.50 ± 0.05	610	336
B	5.37 ± 0.05	C504	0.89 ± 0.05	480	264
C	4.89 ± 0.05	C540A	1.00 ± 0.05	530	292

Cells B and C were fabricated using the same method as Cell A, with the chiral dopant concentrations chosen to position the long bandedge as close as possible to the peak emission of dyes Coumarin-504 and Coumarin-540A respectively. Both dyes were chosen for their absorption properties that coincide with the 445 nm emission from the LD (Figure 4.24).

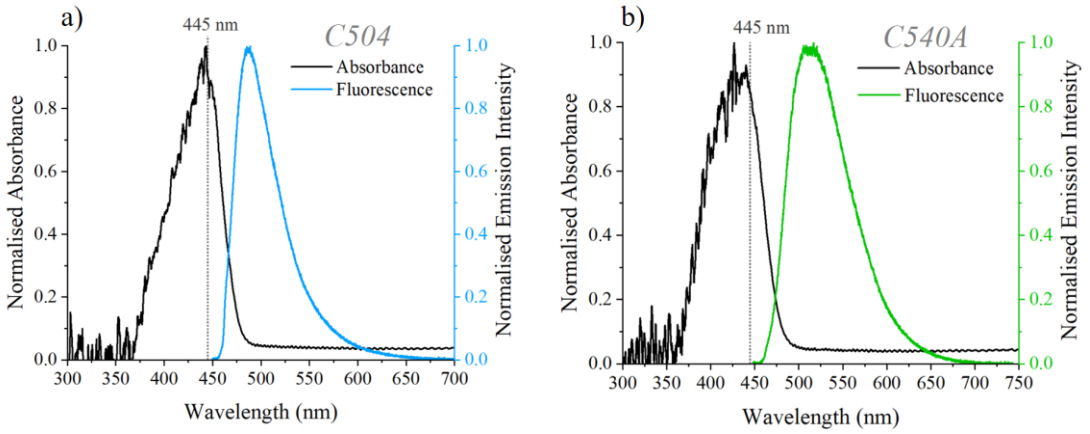

Figure 4.24. Absorbance and fluorescence spectra of a) C504 and b) C540A in nematic LC BL006.

The relative concentrations of the dyes in cells B and C were based on best available data and in-house experimental evidence of optimum performance for C504 and C540A [26].

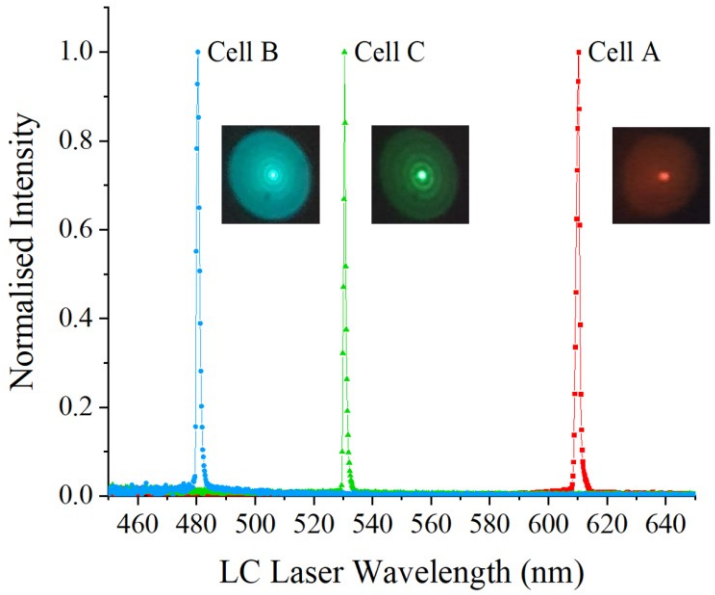

Figure 4.25. LC laser spectra for three different cells when pumped with the 445 nm LD (lines overlaid as a guide) with inset images of each beam spot as illustrative examples.

The results in Figure 4.25 show successful narrow linewidth LC laser emission at 480 nm, 530 nm and 610 nm. Intermediate wavelengths were also possible through the use of different chiralities and (if necessary) other dyes [15], but were not fabricated here. Whilst red, green and blue lasing from LC lasers have been demonstrated previously [12], [18], [76], these works required the use of a tuneable optical parametric oscillator (OPO) pump laser, a nitrogen pump laser and a frequency tripled Q-switched pump laser, respectively, which are much larger and more expensive than the LD pump source used here. The ability to produce LC laser emission

spanning this wavelength range using a single LD pump source is an important demonstration of the capabilities of this LD pumping breakthrough.

4.5.5 Further analysis

Given the slightly higher absorption of DCM at 445 nm compared to 532 nm (Figure 4.1), it might be considered reasonable to expect a lower threshold and higher efficiency with the LD than with the Q-switched pump. However, the opposite trend is found here. This can be attributed to the LD's longer pulse length (16 ns compared to 1.3 ns), which has previously been shown to negatively impact LC laser thresholds [29], [32], [34], [37], and appears to be the dominant effect here. The effect of pump pulse length on LC laser performance is investigated further in the following chapters.

Another contrasting feature between the two pumping regimes is that the maximum output pulse energy of the LD-pumped LC laser was lower than with the Q-switched pump. This was to be expected due to the higher peak powers associated with Q-switching, compared with LDs. A technique for increasing the peak power of LDs has been demonstrated for material processing applications, by combining LDs into clusters [130]. This could be applied to pumping LC lasers to increase the peak pump power and thus the peak output power. Although this was beyond the scope of this thesis, it could present future research opportunities. Increasing the current to produce a higher LD peak power is also possible and is explored in Chapter 5.

The position of the LD lens was critical for successful LC laser pumping. Specifically, the LD cross-sectional beam diameter relative to the microscope entrance pupil determined if LC laser emission could be achieved. A simulation tool *(Light Machinery Optical Design Cloud)* was used to replicate the experimentally observed effects that adjusting the position of the LD lens had on the LD spot size and shape. The experimental parameters (Table 4.7) were specified in the software, and included the measured optical path length from the LD lens to the microscope objective and the manufacturers' specifications for the LD and the LD lens.

Table 4.7. LD lens and LD beam parameters used to simulate the beam propagation from the lens to the microscope objective.

LD lens diameter	6.33 mm
LD lens thickness	3.3 mm
LD lens material	Glass, n = 1.466
Front focus	4.8 mm
Back focus	- 4.02 mm
x-axis beam half-angle divergence	23 °
y-axis beam half-angle divergence	7 °
Distance from LD lens to microscope objective	900 mm

At approximately 3 mm from the LD, the LD lens was capable of collimating the light, but the resultant beam spot was larger than the input aperture of the microscope objective. Under this condition, 65 % of light was lost (Figure 4.26b), assuming a Gaussian energy distribution[17]. This was the case when the LD was first set up and no LC laser output was produced.

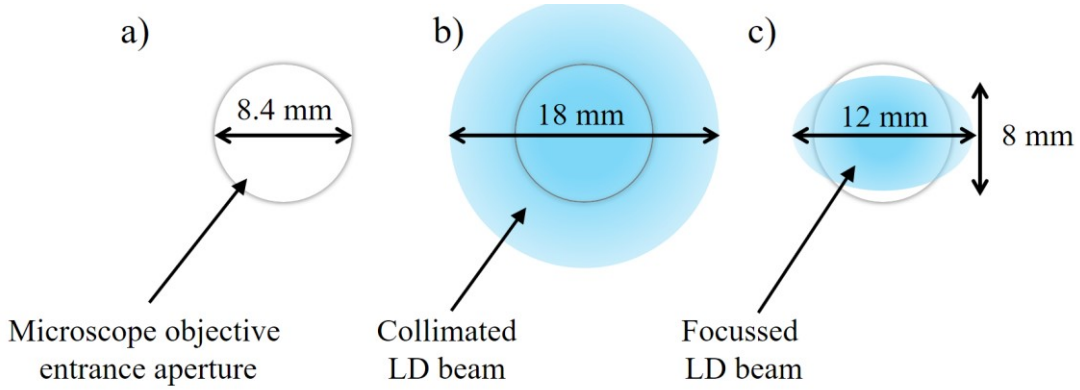

Figure 4.26. Diagram indicating the microscope objective entrance aperture showing b) the LD beam when collimated by the LD lens and c) the elliptical beam shape when focussed by the LD lens.

Ideally, the collimated beam would have been recollimated to a smaller beam diameter by using a telescopic arrangement of lenses. However, the addition of such optics would have introduced undesirable optical losses and was therefore not attempted, since as much light as possible was required to overcome the LC laser threshold. By increasing the distance between the LD and the LD lens by approximately 0.3 mm, the beam diameter was reduced at the input

[17] The transverse energy distribution from a LD is not a perfect Gaussian, owing to the complex structure of the semiconductor layers [140]. However, a Gaussian distribution is a valid approximation for most applications.

aperture of the microscope objective, albeit with a slightly elliptical beam shape (Figure 4.26c). This immediately resulted in LC laser emission when the cell was positioned at the focus of the microscope objective. The spot size at the plane of the LC laser was found to have major and minor axes of 11.6 and 8.6 μm respectively.

The effect that the pump spot size has on the LC laser threshold is often overlooked or omitted in LC laser literature, despite it being well-understood to be an important factor; an investigation by Morris *et al.* showed that the threshold is linearly proportional with the cross-sectional area of the pump beam [63]. This makes it difficult to compare thresholds from one publication to another if spot size data are omitted. Figure 4.27 below shows the efficiency data for both pumping regimes on the same graph. The input data are expressed in terms of a) pulse energy and b) fluence (energy per pulse per unit area), typically in units of mJ/pulse/cm^2, such that:

$$Fluence = \frac{Pulse\ energy}{Cross\ sectional\ area\ of\ pump} \qquad \textit{Equation 4.1}$$

where the pump beam spot sizes for the Q-switched laser and LD were calculated as 106.8 μm^2 and 78.4 μm^2 respectively. For the examples presented Figure 4.27, converting the efficiency data from pulse energy to fluence has a negligible effect on the trends in threshold and efficiency, as both have spot sizes of a similar order of magnitude. If the pulse energy data had been acquired with significantly different spot sizes, visual representation of this in terms of fluence may highlight more contrasting features.

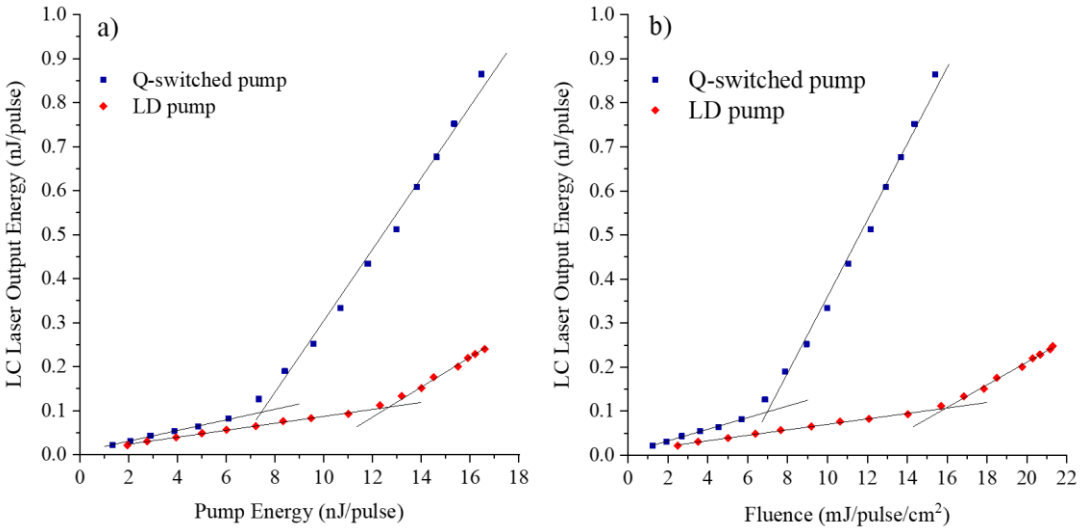

Figure 4.27. The same efficiency data are plotted for both graphs but a) shows the input in terms of pulse energy and b) shows the input in terms of pulse energy per unit area. Note the different units between the x-axes.

Consideration of threshold in terms in fluence enables hypothetical performance parameter comparisons to be drawn, for example: the LD spot size would need to be reduced from 78.4 μm^2 to 47.16 μm^2 if the same LD pulse energy were to be used as the Q-switched laser to reach threshold; or alternatively, the LD pulse energy would need to be increased from 12.3 nJ to 16.8 nJ to reach threshold if the LD had the same spot size as the Q-switched laser. Such comparisons of thresholds in different pumping regimes are not possible without knowledge of the pump laser spot sizes. The threshold will continue to be expressed in units of energy per pulse throughout the thesis to conform to the commonly accepted practice, but it would be remiss not to acknowledge the fluence as an important factor to consider when stating laser threshold. The spot size is, however, recalculated when different optical arrangements are used, to enable fluence comparisons, when required.

4.6 Conclusions

This chapter set out to demonstrate LC laser emission using a semiconductor-based pump source – a much sought-after development by the LC laser community that has remained elusive for more than twenty years. After verifying low-threshold behaviour from a well-fabricated LC laser cell using standard Q-switched pumping, a 445 nm LD was selected as the most likely alternative pump source to replicate the results. The LD was integrated with electronics capable of delivering nanosecond pulse durations and high currents in an optical arrangement optimised for 445 nm. Not only was LC laser emission detected upon exposure of the LC cell to the focused LD emission, but it showed near identical linear polarisation, narrow linewidth, slope efficiency and low threshold performance when compared with the Q-switch-pumped data. This provided unequivocal evidence that the first demonstration of diode-pumped photonic band-edge lasing was successfully achieved. Both pump regimes resulted in LC laser spectral linewidths < 1.5 nm, and threshold and efficiencies of 7.4 nJ/pulse and 8.1 % respectively for the Q-switched laser and 12.3 nJ/pulse and 3.1 % respectively for the LD. The discrepancy in performance between the two pump sources was attributed to differences in their spot sizes and pulse lengths. Blue, green and red LC laser emission were all demonstrated using the same LD pump source, highlighting the wavelength range achievable from this pump-LC laser combination.

The breakthrough demonstrated in this chapter is applied throughout the following chapters, by exploring a parameter space previously not possible with Q-switched lasers. The ability to vary the LD pulse duration is exploited, by determining how the LC laser threshold and efficiency (Chapter 5), and the LC laser pulse length (Chapter 6) are affected. The performance parameters are characterised, leading to previously undocumented results, and enable the design and construction of the first LD-pumped LC laser prototype (Chapter 7).

Chapter 5

Effect of pump pulse length on liquid crystal laser threshold and slope efficiency

"Don't let anything stand in the way of the light that shines through this form. Risk being seen in all of your glory."

Jim Carrey

5.1 Introduction

Until now, only theoretical models, or individual pump sources with different specifications, have been capable of demonstrating the effect of pump pulse length on LC laser threshold and slope efficiency. Consequently, the available data on these effects is limited and difficult to compare. LD pumping provides a unique opportunity to continuously vary the pump pulse length within a single experimental arrangement. This chapter provides the first evidence of the effect that the pump pulse length has on the LC laser threshold and efficiency, and compares the experimental data using a LD pump source to a theoretical hypothesis that has been shown to reliably predict LC laser behaviour. The expectation was that a deeper understanding of the performance limitations would be achieved, which would not only provide motivation for follow-on research, but would also bring practical applications of LC lasers closer to realisation.

5.2 Background and motivation

The effect of LC laser parameters such as dye concentration, cell architecture and choice of materials on LC laser threshold and slope efficiency have been reported (as discussed in Section 2.4.2), but very little has been explored experimentally to determine the effect of pump pulse length. Cao *et al.* showed an order of magnitude improvement in threshold when a picosecond pump source was used compared to a nanosecond source [29], and Shtykov *et al.* simulated LC laser threshold and slope efficiency under optical excitation from a hypothetical semiconductor-based pump source by deriving and solving differential rate equations [30]. However, rather than varying the pump pulse length, the authors of Ref. [30] varied the duration of the leading edge of a trapezoidal-shaped pulse, which resulted in a gradual increase in threshold and a steeper decline in slope efficiency. Ortega *et al.* presented an argument, based on Shtykov *et al.'s* rate equations, which predicted proportionality between pump pulse length and threshold [31]. This has yet to be experimentally verified.

Chapter 4 demonstrated the first unequivocal evidence of successful LC laser emission when pumped with a LD. The investigation was conducted with the LD driver electronics set to the

lowest performance settings[18] to minimise the risk of damaging the electronics and LD at the early stage of the investigation. The fact that LC laser emission was successfully demonstrated with the pump parameters minimised was encouraging, as it allowed further exploration at longer pulse lengths, higher currents and faster repetition rates. This versatility offered by the LD is exploited in this chapter. The first experimental evidence of the effect of pump pulse length on LC laser threshold and slope efficiency is presented, by varying the pulse length in the lower regime of the LD driver's temporal capabilities. To achieve this, an automated data acquisition and processing feature was introduced to the experimental arrangement to control the pump pulse energy and plot the resultant pre-threshold and post-threshold LC laser energy. Using different pump pulse lengths, the LC laser energy data were acquired alongside the LC laser spectra to substantiate the results. The results were further validated by repeating the experiments using different laser cells containing different organic dyes. Where possible, the conclusions were compared to previously published hypotheses and results.

[18] The pulse duration of the LD was set to the minimum value at which it produced laser emission (τ_{set} = 16 ns), the current was set to a minimum of ~ 6 A and the repetition rate set to the lowest frequency of 1 Hz.

5.3 Experimental

5.3.1 LC laser cell requirements

A DCM-doped LC laser cell was fabricated as described in Chapter 3. The reasons for choosing this dye, were firstly its strong absorption at the wavelength of the LD (445 nm) and secondly that it has often been used throughout studies relevant to the work presented in this chapter, enabling valuable comparisons. A reflective cell geometry was used, with a chiral dopant concentration of 4.35 wt% relative to the BL006 LC, and a dye concentration of 0.5 wt%. The cell spacing was 10 μm.

5.3.2 Laser testing software and benchtop configuration

The apparatus shown in Figure 5.1 was used for the automated efficiency measurements with the LD. This relied upon the electrical control of a motorised piezo rotation stage *(AG-PR100, Newport)* containing the half-waveplate, the angle of which dictated the LD pump energy[19]. The rotator was connected to a PC (*Windows 10, Microsoft)* via a controller unit *(AG-UC8, Newport)* which allowed the angle of the waveplate, and hence the pump energy, to be controlled. Two energy meters (*PD10-pJ-C, Ophir*)[20], connected to the lab PC via an interface module (*Pulsar-2, Ophir*), measured the pump energy (recorded on the first energy meter, EM1) and LC laser energy (recorded on the second energy meter, EM2) (*Starlab v3.62, Ophir*). A 10 mm focal length aspheric lens *(ACL1210U-A, Thorlabs)* was used in place of the microscope objective in order to simplify the arrangement and reduce the optical losses.

[19] Unlike the Q-switched laser which had a fixed pulse energy that could only be controlled with extra-cavity optics changing the peak power, the LD pulse energy could also be controlled by adjusting the peak power (via the current delivered to the LD) and by controlling of pulse duration. Here, the half-waveplate controlled the pump energy by changing the peak power of the pump pulse.

[20] This second energy meter was procured *after* the initial set of LD-pumping experiments in Chapter 4 were carried out. The second energy meter removed the need for the calibration table of pump energy as a function of waveplate angle previously required, as both the input and output energies could be recorded simultaneously with the use of a beamsplitter.

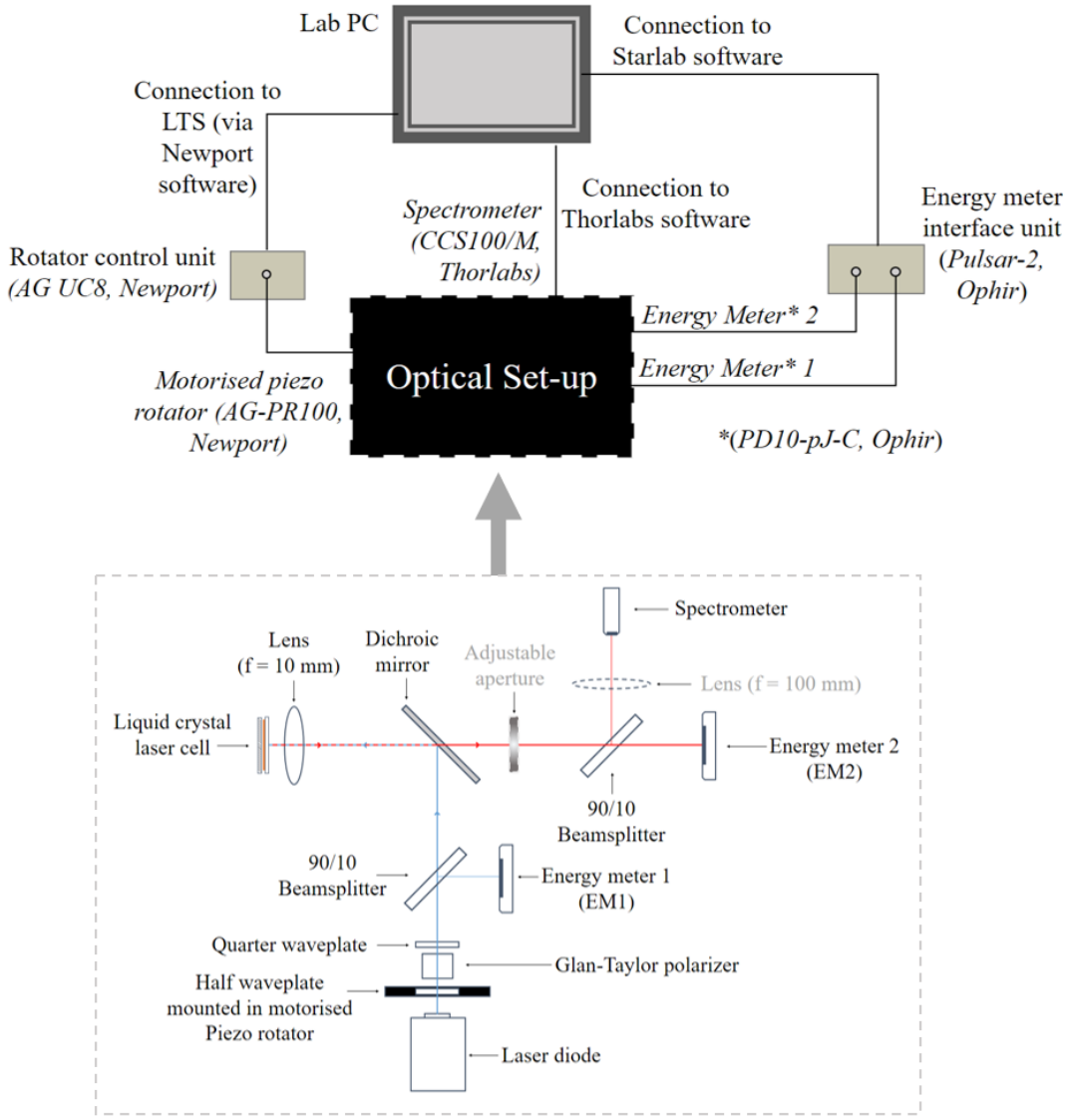

Figure 5.1. Experimental arrangement used to measure the effect of pump pulse length on threshold and efficiency. The optical configuration 'black box' in the top diagram is expanded upon in the bottom diagram.

Custom-built software (henceforth referred to as the laser testing software, LTS)[21] was used to automate the data acquisition for measuring the slope efficiency of the LC laser. The LTS was written in Python, with a graphical user interface (GUI) (Figure 5.2) installed on the lab PC. The LTS controlled the position of the piezo rotator and thus, controlled the pump energy. The LTS recorded and processed the energy metre data to calculate the LC laser threshold and slope efficiency using a least-squares fit algorithm (Appendix E).

[21] This software was built in collaboration with Ieva Pakamorytė; a University of Edinburgh physics undergraduate summer internship student (2019) funded by Equate Scotland.

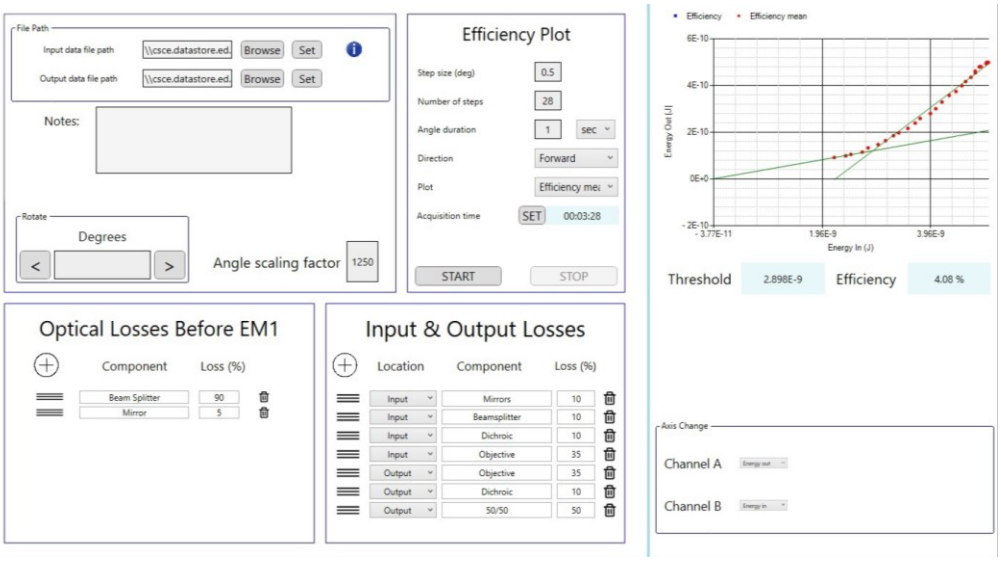

Figure 5.2. Laser testing software graphical user interface, with the user-defined configuration inputs on the left, and the efficiency plot and calculated threshold and efficiency values on the right.

The LTS was designed to allow the user to configure the:

- Step size (measured in degrees) by which the waveplate was rotated, between each data acquisition position.
- Number of waveplate step changes in a full data set.
- Time spent at each waveplate position.
- Experimentally-determined optical losses of each component present in the experimental arrangement.

The LTS created an output file in which the unprocessed energy meter data were recorded, in addition to the processed data, which took into account the optical losses (Appendix F). The data were exported to Origin (*v.2018b, OriginLab*) for analysis. The LTS data file stored all user-defined parameters for future reference, with the option to include experimental notes. The software also allowed independent adjustment of the half-waveplate position via the piezo rotator software (*AG-UC2-UC8-2.0.1, Newport*).

The LTS enabled controlled, repeatable and more rapid data acquisition than the method of manually rotating the half-waveplate and recording the average input and output energy values at each waveplate position, as was required in Chapter 4.

Once the software was configured, the data acquisition process was started and a slope efficiency graph (top right of Figure 5.2) was plotted in real-time. The LC laser spectrum was observed throughout (*CCD Spectrometer Software v2.9, Thorlabs*) to confirm that the threshold value calculated by the LTS corresponded to the pump energy at which the narrow-linewidth laser emission was detected by the spectrometer (USB spectrometer *CCS100/M*, *Thorlabs*).

For the slope efficiency data presented in this chapter, the LD was set to the desired pulse length at a repetition rate of 10 Hz. This repetition rate was sufficiently low to prevent immediate performance degradation of the LC laser associated with higher repetition rates [13]. The LTS was programmed to record data at each pump energy for 1 second, thus an average energy for 10 pulses was calculated for each waveplate position. The number of waveplate positions ranged from 10 – 16 positions, depending upon the energy resolution window of the energy meter (Appendix G). Each data set was recorded by starting with the lowest detectable LC laser energy and incrementally rotating the half-waveplate to increase the pump energy incident upon the LC laser cell. This process was continued beyond the LC laser threshold until the number of data points below and above threshold was approximately the same. This method of data acquisition of *increasing* the pump energy (as opposed to starting at high pump energies and *decreasing* the pump energy to below LC laser threshold) was done to mitigate erroneous results caused by cell fatigue which was more prevalent at higher pump energies. Pump pulse lengths ranging from the minimum possible set value of 16 ns up to a set value of 100 ns were used in 10 ns increments to obtain a sufficiently large data set for observing trends in threshold and slope efficiency measurements. Five data sets were recorded for each pulse length at different cell positions to account for variations in performance across the laser cell and thus allowed average values for the threshold and slope efficiency to be calculated.

5.4 Observations from a preliminary investigation

The investigation began by measuring the slope efficiency for the shortest set pump pulse duration of 16 ns. The measurement process was then repeated with increasing pump pulse lengths. However, as the pump pulse length increased, the change in gradient at threshold became increasingly difficult to identify, despite the spectrometer displaying a distinct emergence of narrow-linewidth LC laser emission at a specific pump energy. An example of this near-indistinguishable change in gradient is shown by the red data points in Figure 5.3 for a pump pulse length of 60 ns.

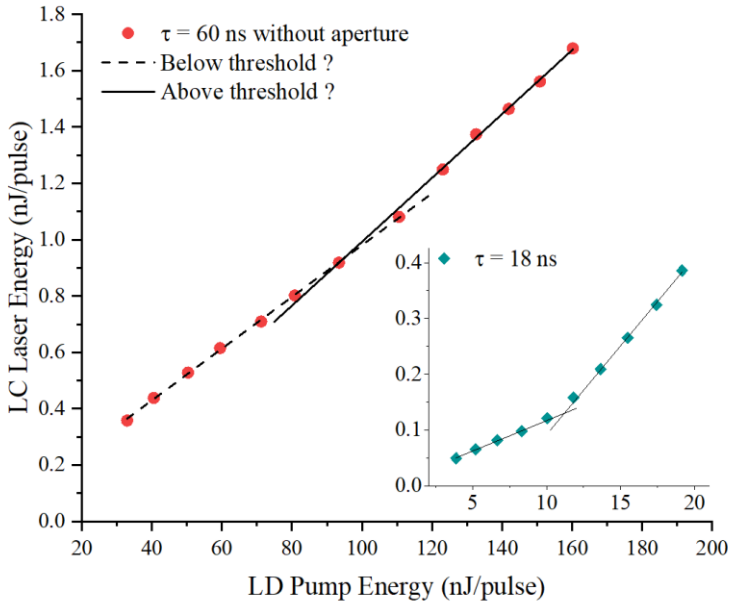

Figure 5.3. Efficiency data for a pump pulse length of 60 ns (red circles), without the obvious change in gradient expected at threshold. The inset is shown for comparison for a shorter pump pulse length of 18 ns (green diamonds) with a more distinct change in gradient at threshold.

The 60 ns data in Figure 5.3 was plotted by *manually* rotating the half-waveplate and recording the LC laser output energy at different waveplate positions, as the LTS was unable to distinguish pre- and post-lasing behaviour. The signal on the spectrometer verified the energy at which a narrow-linewidth spectrum emerged, therefore enabling the pre-threshold and post-threshold data points to be distinguished and the respective lines of best fit to be added. As the LC laser intensity on the spectrometer grew with increasing pump energy, the linewidth remained narrow (< 1.5 nm). Visual observation of the emission from the LC cell, however, revealed off-axis emission that was being detected by the energy meter (Figure 5.4a) but was

not being captured by the spectrometer (Figure 5.4b). This had not been present, or at least not been obvious, at shorter pulse lengths and required further investigation.

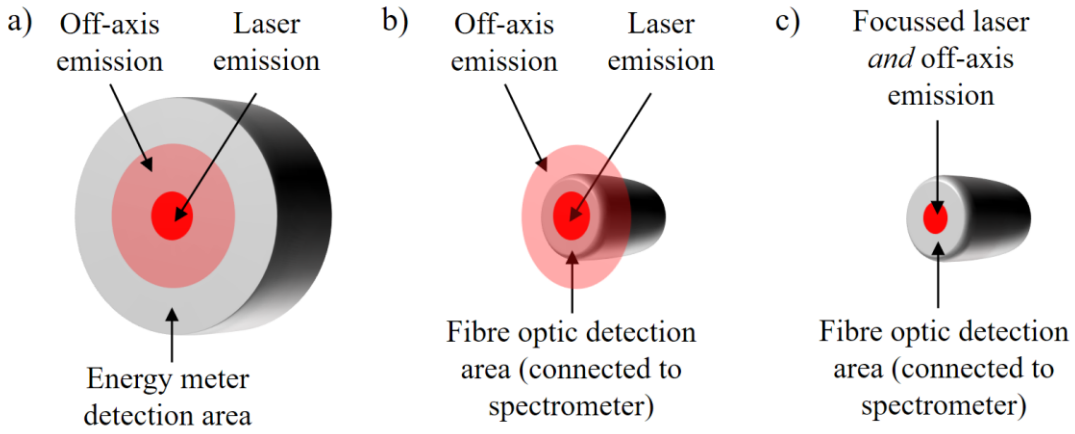

Figure 5.4. On- and off-axis emission as detected by a) the energy meter, b) the spectrometer ***without*** *a lens in place and c) the spectrometer* ***with*** *a lens in place.*

It was hypothesised that the off-axis emission was either caused by an increase in emission angle with increasing pulse length, or that the spectral content of the output was changing with increasing pump pulse length such that there was an increase in contribution from non-lasing emission, i.e. fluorescence or ASE.

A spectral measurement of on-axis *and* off-axis emission was made to determine which hypothesis was correct. A 100 mm focal length lens was placed before the optical fibre connected to the spectrometer (Figure 5.1) to collect the emission at all pulse lengths and focus it onto the fibre (Figure 5.4c).

A broad fluorescence signal (black profile, Figure 5.5) immediately appeared at the base of the laser spectrum when the lens was added. It was this fluorescence signal being detected by the energy meter, in addition to the laser emission, which had resulted in a false interpretation of the LC laser pulse energy. It was concluded that this off-axis emission was caused by fluorescence (as per the second hypothesis), as the spectrum coincided with the fluorescence of DCM (Figure 4.1). If the off-axis emission had been due to an increase in cone angle of the *laser* emission (as per the first hypothesis), the addition of the lens would have caused an increase in intensity of only the laser emission. Fluorescence emission from an LC laser would be expected to be highly divergent. Here, however, although considerably more divergent than

the laser emission, it appeared as a concentrated pool of light with a larger diameter than the laser beam due to the presence of the lens used to focus the pump beam immediately before the LC laser cell. This not only focussed the pump beam onto the LC laser cell, but also acted to approximately collimate both the stimulated *and* spontaneous emission from the LC laser cell.

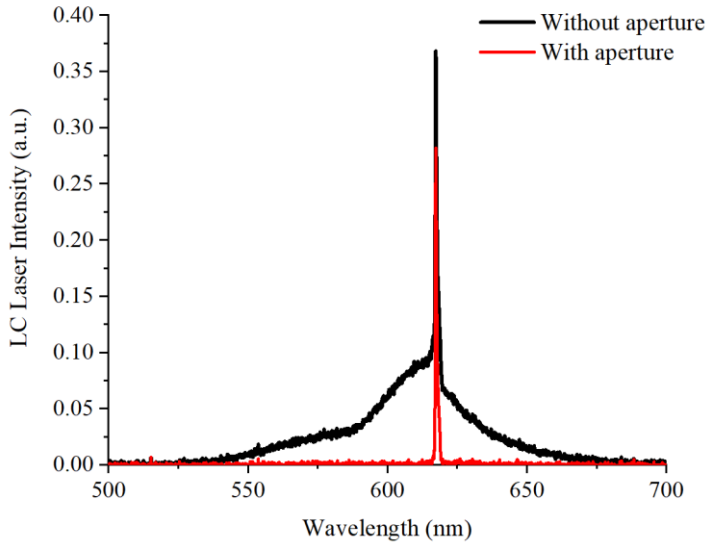

Figure 5.5. Effect of the presence of a lens positioned at the input of the spectrometer with (red line) and without (black line) an aperture present at the output of the LC laser. The pump pulse length was set to 60 ns.

An adjustable aperture was positioned after the dichroic mirror along the LC laser beam path (Figure 5.1), the diameter of which was adjusted until the fluorescence was removed from the spectrum (red line, Figure 5.5). This visually coincided with the removal of the off-axis emission, with only the laser spot remaining, thus validating the second hypothesis that the increase in energy was caused by an increase in fluorescence.

The slope efficiency measurement for the 60 ns data was repeated with the aperture in place. There was an immediate difference in the slope efficiency (Figure 5.6), with an obvious change in gradient at threshold, again, simultaneously verified by the appearance of the laser spectrum detected by the spectrometer.

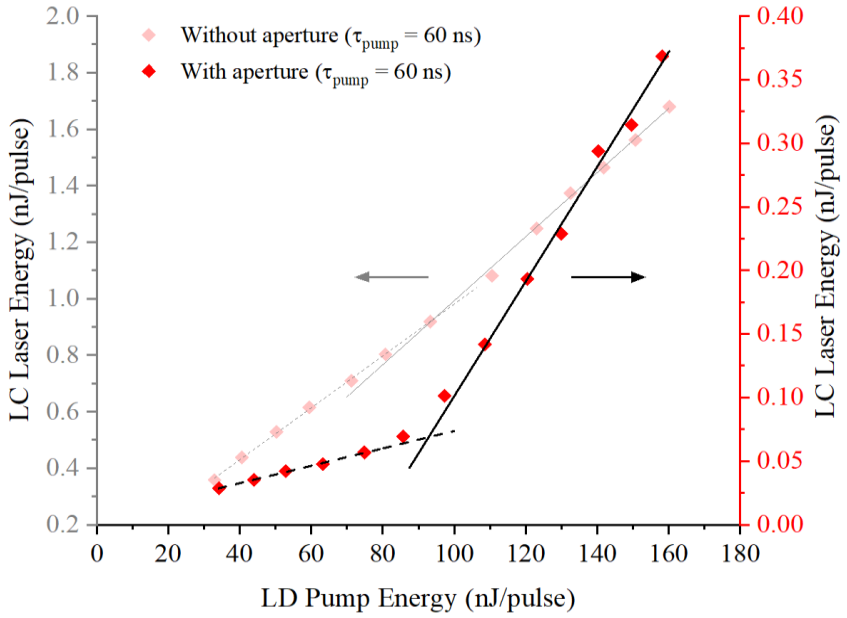

Figure 5.6. Repeat of efficiency plot for a pump pulse length of 60 ns, now with an aperture present at the LC laser output to attenuate the fluorescence. The previous data without the aperture present is shown (faded) for comparison.

Adding the aperture to the experimental arrangement confirmed that the fluorescence was distorting the efficiency data. The aperture allowed detection of LC laser emission only (on EM2 and the spectrometer) by blocking the fluorescence. The aperture size was determined by monitoring the signal on the spectrometer as the aperture was closed. As the diameter was reduced, the broad fluorescence signal was attenuated. A diameter of approximately 2 mm was set such that the fluorescence signal was minimised, while maintaining the LC laser intensity (red line, Figure 5.5). This diameter was specific to the location of the aperture along the LC laser beam path, as the LC laser beam exhibited a gradual divergence. Collimating optics were not used to correct the divergence, as it was negligible over the experimental distances, and minimisation of optical losses was desired. For measurements at longer distances along the beam path, the aperture diameter would need to be adjusted accordingly to accommodate the beam divergence. Alternatively, lenses would be required to collimate the LC laser beam.

To summarise, a distortion in a measurement of LC laser slope efficiency led to an investigation that identified off-axis fluorescence as being the cause. This appeared to be more prevalent at longer pump pulse lengths. The addition of an aperture to block the fluorescence and allow mostly laser emission to be detected by the energy meter and spectrometer resulted in the expected gradient change in slope efficiency at threshold. The cause of the increase in

fluorescence at longer pulse lengths required further investigation before the threshold and slope efficiency at different pulse lengths could be investigated.

5.5 Further characterisation of fluorescence

This section presents two investigations that were undertaken to determine the cause of the increase in LC fluorescence with pump pulse duration. The experimental procedure and results from each investigation are presented separately, followed by a combined concluding statement.

5.5.1 Investigation 1 – Measuring the liquid crystal emission pulse energy as a function of pump pulse length

5.5.1.1 Experimental procedure

The first investigation built upon the initial fluorescence observation, by measuring the effect of the aperture on LC emission energy across a 50 ns range of pulse lengths. The LC laser pulse energy was measured for increasing pump pulse lengths without the aperture present at the output. This was then repeated with the aperture present to allow detection of only laser emission. Spectral data were also recorded to observe the effect the pump pulse length had on the LC laser linewidth and intensity.

5.5.1.2 Results and discussion

Figure 5.7 shows the LC laser pulse energy (red sold circles) increasing proportionally with the increasing pump pulse length (black solid diamonds), when there was no aperture in the experimental arrangement. When the same measurement was made with the aperture present at the LC laser output, the LC laser pulse energy remained approximately constant (red hollow squares). This indicated that the increase in energy associated with increasing the pump pulse length did not result in an increase in LC *laser* output energy and that the additional energy from the pump contributed only to LC *fluorescence* emission. This substantiated the initial results showing a distortion of the efficiency curve caused by the presence of fluorescence using a 60 ns pump pulse.

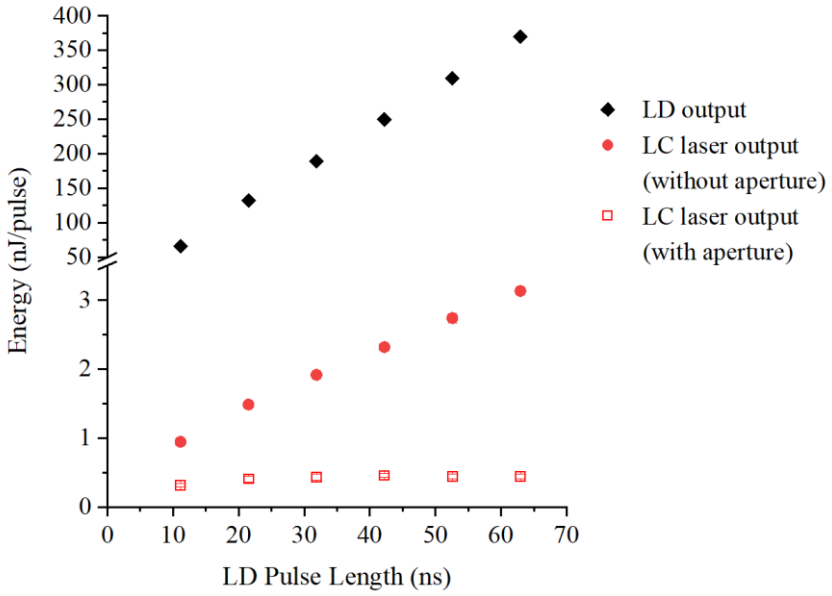

Figure 5.7. Effect of pump pulse length on LC laser energy without an aperture present (red solid circles) and with an aperture present (red hollow squares) at the output of the LC laser.

The increase in pump pulse energy associated with an increase in pump pulse length was not accompanied by an increase in the pump pulse peak power (Figure 5.8). The LD energy data (black diamonds, Figure 5.7) is presented as the shaded areas in the temporal pulses in Figure 5.8. The temporal data were acquired by replacing EM1 with a photodiode (*DET025A/M, Thorlabs*) connected to an oscilloscope (*WavePro 735Zi, LeCroy)*.

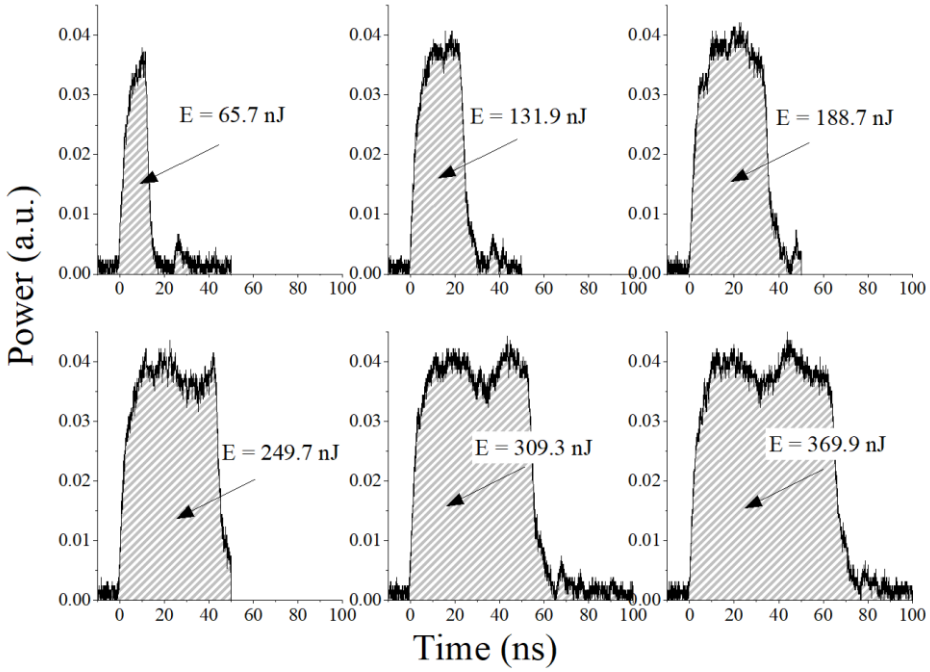

Figure 5.8. Effect of increasing the pump pulse length on total pulse energy (shown by the shaded area), whilst the peak power remains approximately constant.

The temporal data in Figure 5.8 highlights an important feature of this work, regarding pulse energy. *Energy* is used throughout LC laser literature, both with respect to the pump laser and the LC laser emission. However, until now, any change in energy has been due to a change in peak power, as determined by the optics typically used to attenuate the pump beam. In this work, however, the energy can be varied through variation of peak power *and* pulse duration. The importance of this distinction is exemplified in the following investigation and throughout the work presented in Chapter 6.

5.5.2 Investigation 2 – Measuring the liquid crystal emission pulse energy as a function of pump pulse peak power

5.5.2.1 Experimental procedure

As an increase in laser pulse length is accompanied by an increase in pulse energy, a second investigation was carried out to separate the two parameters. This involved maintaining a constant pump pulse length while the pump pulse energy was changed. The change in pulse energy was accomplished by changing the pump pulse peak power through control of the current delivered to the LD. A pump pulse length of 13 ns was used and the LD driver current was incrementally increased from 6.5 A to 14 A to increase the peak power (and hence also the pulse energy). This pump pulse length was chosen, as it was sufficiently long to show obvious signs of fluorescence but not so long as to rapidly fatigue the cell. The same position of the cell was used throughout for consistency, thus the LD repetition rate was set to 1 Hz to minimise cell degradation associated with high repetition rates. The LC emission energy was measured for each current, firstly without the aperture and then with the aperture present.

5.5.2.2 Results and discussion

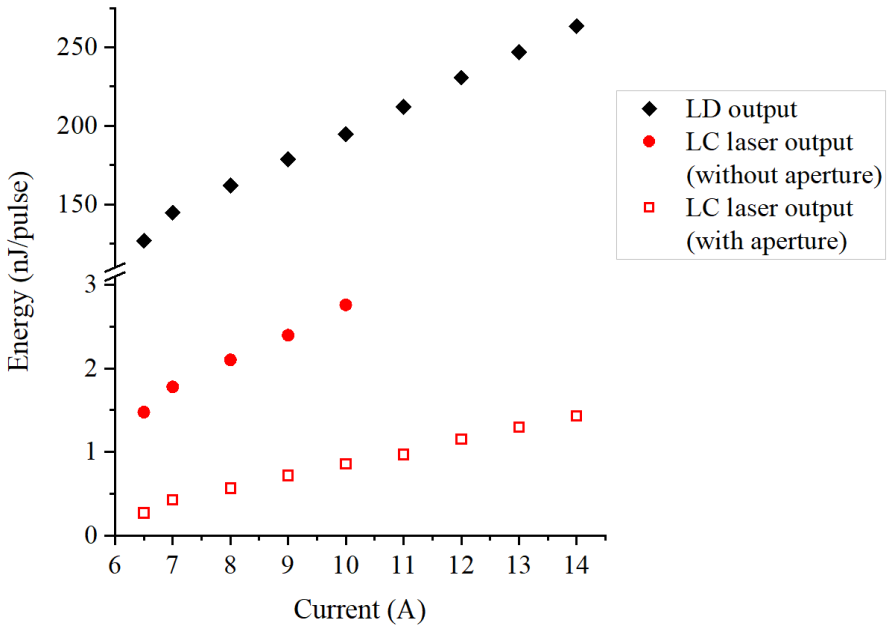

Figure 5.9. Effect of increasing the pump pulse energy (by increasing peak power, but maintaining a fixed pulse length of 13 ns), on the LC laser pulse energy a) without an aperture and b) with an aperture positioned at the LC laser output.

Figure 5.9 shows the effect that increasing the pump peak power had on the pump energy (black diamonds). Without the aperture present, the resultant LC laser pulse energy increased (red solid circles)[22], as was the case when the pump pulse energy was increased via an increase in pulse length in Investigation 1.

However, unlike when the aperture was added to the optical arrangement in Investigation 1, the LC laser emission *increased* as the pump peak power was increased. This showed than an increase in pump energy via pump peak power increased the LC *laser* emission output. This is in contrast to the increase in pump energy caused by an increase in pump pulse duration, which only increased the LC *fluorescence* emission.

[22] The reason for no LC emission data without the aperture beyond 10 A was because the LC laser spectrum was simultaneously being recorded and, at currents higher than 10 A, the spectrometer saturated. The beam was therefore blocked at the output. In hindsight, the signal to the spectrometer ought to have been attenuated with a neutral density filter and the energy data set should have continued up to a current of 14 A. Nonetheless, there is adequate data to show the expected proportionality between the pump energy and LC emission energy.

5.5.3 Spectral summary of results

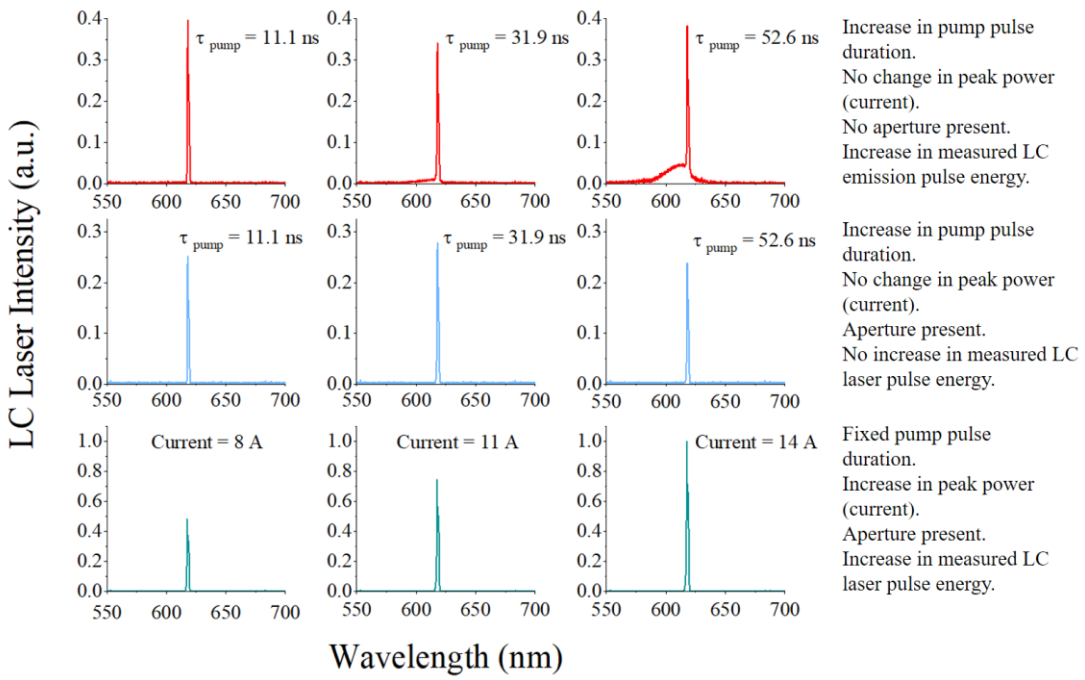

Figure 5.10. LC laser spectra for: increasing pump pulse length (and hence pump energy) without an aperture present (red data); increasing pump pulse length (and hence pump energy) with an aperture present (blue data); and increasing pump peak power (and hence pump energy) with an aperture present (green data).

The data in Figure 5.10 summarise the effects that varying the pump pulse energy (through variation of either pulse length or peak power) had on LC laser emission. The top row (red data) shows the effect on the LC emission spectrum by increasing the pump pulse length (whilst maintaining a constant pump peak power). The intensity of the narrow-linewidth emission remains approximately constant, but a broadband feature (coinciding with the fluorescence spectrum for DCM) begins to emerge around the base of the laser emission. The addition of an aperture removes this feature, as shown in the second row (blue data) without influencing the intensity of the narrowband laser emission. This verified that the increase in energy measured for increasing pump pulse durations was caused by the broadband fluorescence signal. A distinction between pump pulse length and pump pulse energy was made in the second investigation. The spectral data of this is shown in the bottom row of graphs in Figure 5.10 (green data) in which an increase in laser intensity can be seen as the pump peak power is increased. This concurred with the corresponding energy data (Figure 5.9), showing that LC *laser* energy is increased with an increase *pump peak power*; *not* through

pump pulse length which acts to increase the fluorescence (at least, for the range of pump pulse durations tested here).

5.5.4 Conclusions

Several conclusions can be drawn from these investigations:

1. The effects on LC laser performance due to changes in pump pulse energy are ambiguous, and need to be characterised instead as changes in pump peak power or in pump pulse duration.
2. Increasing the duration of the pump pulse has the effect of introducing spectral noise into the output in the form of fluorescence.
3. For the range of pump pulse lengths tested here, increasing the pump pulse length did not achieve a proportionally higher LC laser pulse energy, as the associated increase in pump energy only contributed to increased fluorescence emission from the LC laser. This suggests that shorter pump pulse durations are desirable to optimise the efficiency of laser emission. The lower limit of this (if one exists) is yet to be determined.
4. Finally, an aperture at the output of the LC laser is necessary for investigating LC laser emission, as the existence of fluorescence distorts the results. This ought to be accounted for when analysing LC output data reported elsewhere, which may have over-estimated emission energies, especially if longer pump pulses and/or wide-angle collection optics were used.

The investigation into the effect of increasing the pump peak power was repeated multiple times using different pump pulse lengths, and the same trends in the data were observed. Furthermore, a second laser cell with Coumarin 504 (C504) dye was fabricated to ensure that the observations were not unique to DCM. The effect of increasing the pump pulse length and pump peak power, and the consequences of adding an aperture to the optical arrangement were all measured using the C504-doped cell. All exhibited the same behavioural trends as with the DCM.

The results from this investigation are not believed to have been reported in LC laser literature until now. It would be reasonable to assume that increasing the pulse energy from the pump

source would lead to an increase in the LC laser pulse energy. However, this work demonstrates that the way in which the energy is increased is critical to the output from the LC laser. This work shows that it is the pulse energy associated with an increase in pump peak power that leads to an increase in LC laser emission, rather than an increase in the pump pulse energy associated with the an increase in pump pulse duration.

5.6 Effect of pump pulse length on liquid crystal laser slope efficiency and threshold

Having established that an aperture was required at the LC laser output, the investigation into the effect of pump pulse length on LC laser[23] threshold and slope efficiency was pursued. The LTS was used throughout this investigation in which the slope efficiency for a 90 ns range of wavelengths was measured. Data were acquired using the method described in Section 5.3.2.

5.6.1 Results

Results from efficiency plots for each pump pulse length showed that the pump energy required for LC laser emission increased with pump pulse length, coinciding with a decrease in the gradient of the slope above threshold (Figure 5.11).

[23] LC laser emission is henceforth defined as the on-axis stimulated emission, with the accompanying off-axis fluorescence blocked by the aperture (unless explicitly stated otherwise).

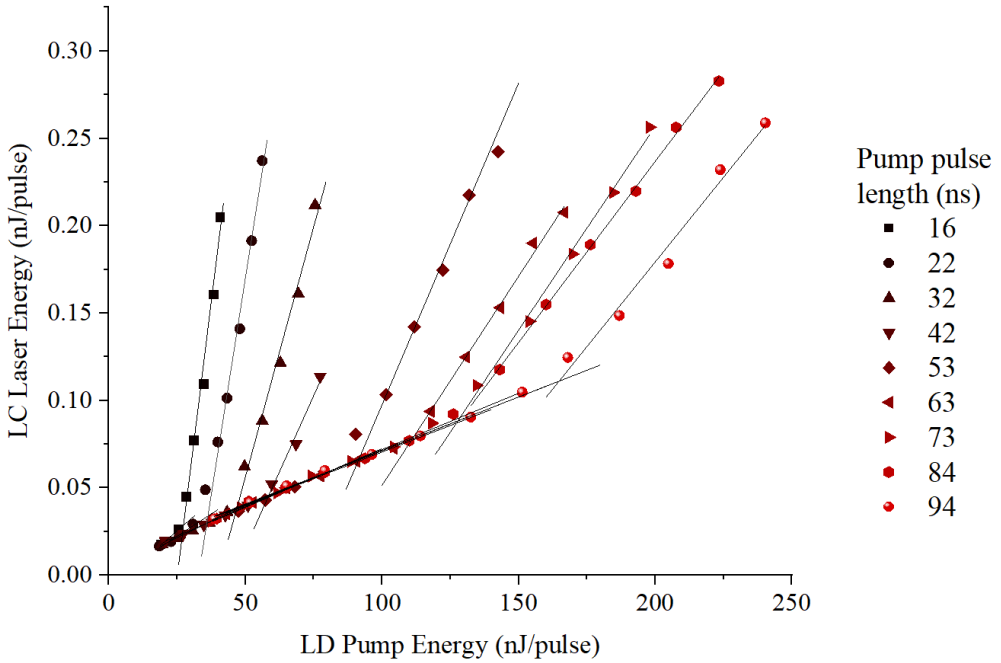

Figure 5.11. Sample of efficiency data for increasing pulse lengths. A clear increase in threshold and decrease in slope efficiency above threshold and can be seen with increasing pulse length.

The full data set, comprising forty-five separate efficiency measurements (nine pulse lengths recorded at five different cell positions) were individually analysed, from which the LC laser threshold and slope efficiency values were calculated. The results of this can be seen in Figure 5.12 and show, for the first time, a distinct trend in LC laser threshold and slope efficiency as a function of pump pulse length.

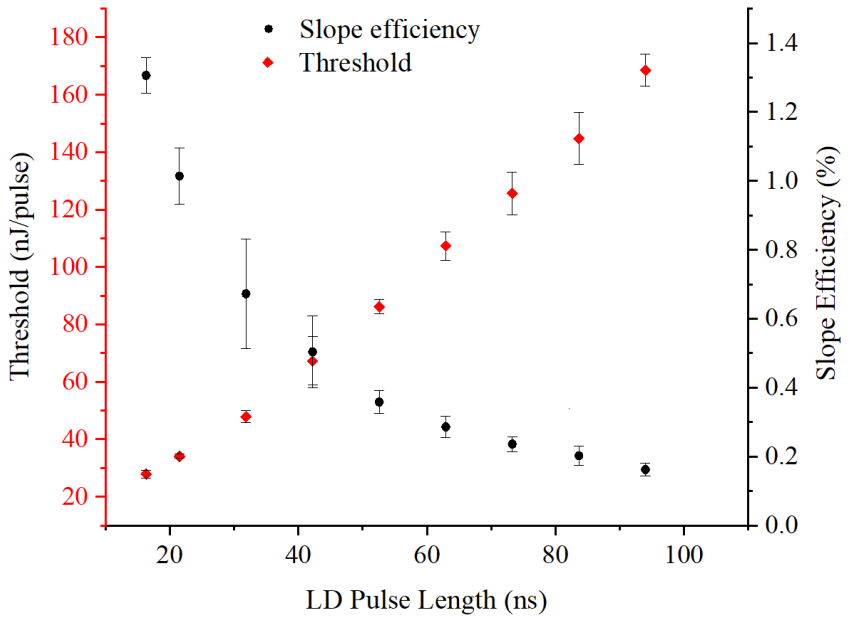

Figure 5.12. Effect of pump pulse length on LC laser threshold (red diamonds) and efficiency (black circles). The error bars were calculated from the standard deviation of the mean of the five data sets recorded for each pump pulse length.

5.6.2 Analysis

This is believed to be the first investigation in which a controlled, incremental increase in pump pulse duration shows the adverse effects on LC laser performance. Not only does an increase in pump pulse length result in a decrease in LC laser slope efficiency, but the threshold also increases. Comparing the theoretical predictions by Shtykov *et al.* [30] to the experimental results, a similar decrease in efficiency and increase in threshold was found for the same range of pump pulse lengths. Although a *direct* comparison cannot be made (as Shtykov *et al.* present threshold in terms of *pump power for the rising edge of a trapezoidal pulse*, whereas the work presented here is given in terms of *pump pulse energy across the full width half maximum of the LD pulse*), the proportionality between threshold and pump pulse length is in good agreement with the theoretical work by Ortega *et al.* [31], in addition to the anecdotal experimental evidence by Cao *et al.* [29].

The following chapter explores the temporal dynamics of the pump pulse and resultant LC laser pulse. However, observing the temporal behaviour of the pump laser at LC laser threshold in the context of this chapter offers further insight into the experimental results.

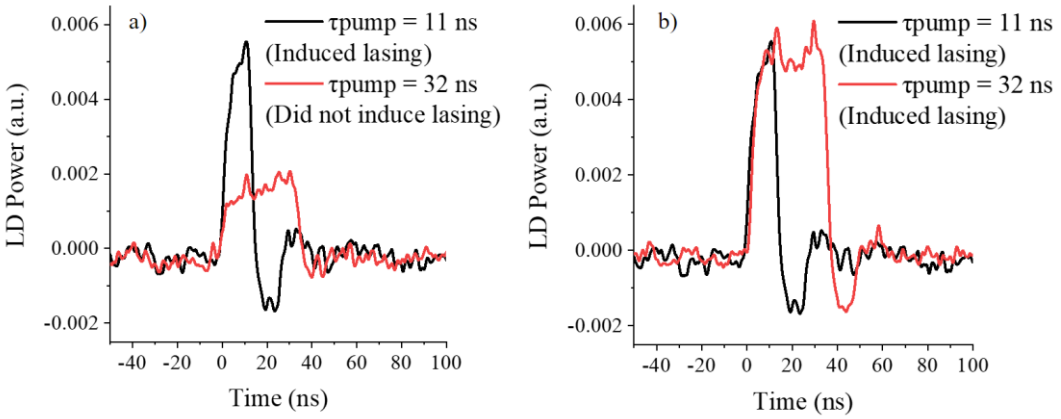

Figure 5.13. Temporal characteristics of LD pump beam with a pulse duration of 11 ns (black line) and 32 ns (red line) with a) the same pulse energy and b) the same peak power.

Figure 5.13 shows the temporal profile of the pump beam with a pulse duration of 11 ns (black data) and 32 ns (red data). In Figure 5.13a, the 11 ns pulse illustrates the peak power required to induce LC laser emission. The area under the peak is the threshold energy. The 32 ns data has the *same energy* (i.e. the area under both profiles is equal) but this did *not* result in LC laser emission.

The energy of the 32 ns pump laser was increased by increasing the peak power, through the rotation of the half-waveplate (equivalent to increasing the LD current) until threshold was reached. LC laser emission occurred when the peak power of the 32 ns pulse coincided with the peak power of the 11 ns pulse, as can be seen in Figure 5.13b. This was repeated for all of the pulse durations in Figure 5.12, whereby the energy was increased from below threshold for each pulse length until threshold was reached and the temporal pump pulse observed (Figure 5.14). A near-identical peak power was reached for each pulse length.

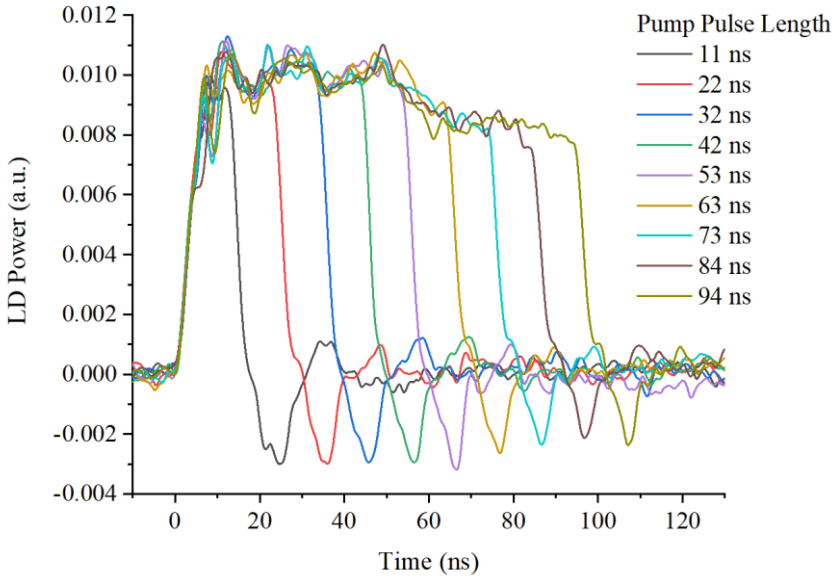

Figure 5.14. Temporal profile of LD pump required to reach LC laser threshold for different pump pulse durations. Note the near-identical peak intensity for all pulse lengths accompanied by an increasing energy (area under each pulse). Note also the identical rising edge of all pulses. The gradually decreasing gradient of the peak is a feature of the driver electronics; not the laser diode.

It is therefore not only the energy of the pump pulse that dictates its ability to reach LC laser threshold, but a combination of the energy *and* the time over which the pulse is delivered.

A brief qualitative hypothesis of this behaviour is offered here, with a more thorough analysis presented after further experimental work in Chapter 6. The proportionality between pump pulse length and threshold can likely be attributed to the increasing population of the triplet states of the DCM molecules with *increasing pump pulse length*. As the pump pulse length is increased, more energy is absorbed by the dye over an ever-longer duration, resulting in an increase in the probability of molecules transferring to the triplet state. Thus, fewer molecules are available to contribute to stimulated emission. Therefore, more pump photons are required to form a population inversion as the duration of the pump pulse is increased. This would explain the requirement of increasing the pump's peak power. This also accounts for the decrease in efficiency with pump pulse length (black data, Figure 5.12), since more energy is required to reach the same peak height for longer pump pulse durations. This was also exemplified when the increase in pump pulse length resulted in a greater intensity of fluorescence without a corresponding increase in LC stimulated emission. In other words, the process of converting pump light to stimulated emission became *less efficient* as the pump pulse length was increased.

On the other hand, for a *fixed pump pulse length* operating below threshold, the only way to increase the pump energy incident upon the LC laser is by increasing the peak power of the pulse until LC laser threshold is reached. In this experimental arrangement, this was achieved either through intensity control by rotating the half-waveplate or by increasing the current delivered to the LD. An increase in peak power means an increase of molecules in the excited state, but the proportion that populate the triplet state with increasing peak power will be constant.

5.7 Comments on laser threshold

At the end of Chapter 4, it was highlighted that the spot size of the pump is a factor often overlooked when defining the threshold of an LC laser and that direct comparisons between LC laser systems are difficult to make without knowing the spot size. Thresholds should therefore be defined in terms of fluence rather than energy per pulse. However, this chapter has shown that pump pulse **duration** *also* affects the threshold. From Figure 5.14, the threshold is approximately constant in terms of peak power (or peak intensity if the spot size is taken into account) with increasing pump pulse length, but that there is a linear increase in threshold with an increase in pump pulse energy (Figure 5.12). It can therefore be concluded that the way in which threshold is defined is important.

One might reasonably expect that the threshold of a laser is an intrinsic property of that particular system. When threshold is stated, there should be sufficient information to compare one pumping regime to another without ambiguity. In other words, there should be a single value of the threshold associated with a particular LC laser in terms of the energy per pulse per unit area per unit time. However, there are additional parameters that make expressing threshold non-trivial.

For the work in this chapter, the pump spot area was 78.4 (± 3.3) μm^2. Therefore, replotting the threshold data in Figure 5.12 with respect to the spot size and pump pulse duration results in the blue data points shown in Figure 5.15.

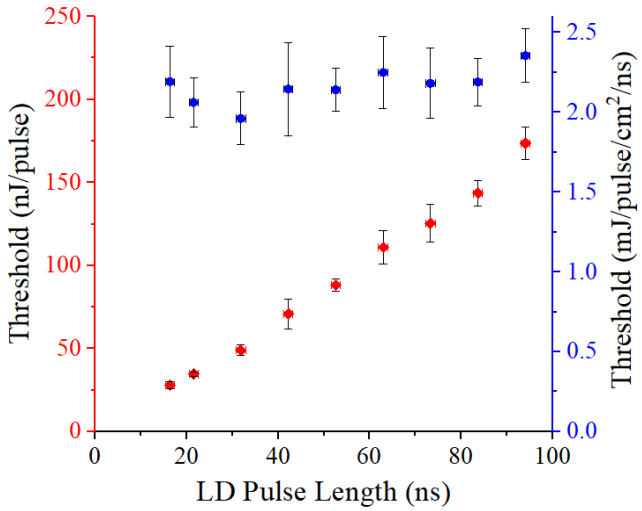

Figure 5.15. Graph showing the effect of redefining the units for threshold in terms of pump spot size and pump pulse length to demonstrate that the threshold is an intrinsic property of the laser cell. The blue data show the threshold in terms of energy per pulse per unit area per unit time. The red data is a repeat of the threshold data in Figure 5.12 for comparison.

With reference to Figure 5.15, it can now be seen that the threshold is constant (within the error bounds) once the spot size and pump pulse length are considered. In the case of this laser cell, the threshold can now be defined as 2.2 (± 0.2) mJ/pulse/cm^2/ns (2.2 (± 0.2) MW/cm^2/pulse).

There are two further parameters that have an impact on the threshold, which have not been considered in this definition. The first is the wavelength of the pump source. The threshold of the laser will be affected by the spectral proximity of the pump wavelength to the absorption spectra of the dye. The proposed method above of defining the threshold assumes the same wavelength when comparing different pump sources. Secondly, the theoretical work by Shtykov *et al.* showed a dependency on threshold with the *rise time* of the pump pulse, such that an increase in the pump pulse rise time resulted in an increase in LC laser threshold [30]. The results from an experimental study by Herrnsdorf *et al.*, in which the rising edge of a similar LD source was varied and used to pump an organic solid-state laser, agreed with this theoretical hypothesis, albeit for a different laser architecture [131]. In the case of the work presented in this chapter, it can be seen in Figure 5.14 that the rising edge for all pump pulse durations is near-identical, thus enabling a direct comparison of the LC laser thresholds for the different pump pulse lengths. However, for a pump pulse with a fixed duration, an increase in pulse energy due to increasing the peak power results in a decrease in rise time, i.e. the gradient of the rising edge of the pump pulse increases. For a fixed peak power and fluence, the rise

time is determined by the driver electronics and cannot be independently varied (at least, not in the electronics used here). Therefore, the effect of rise time on threshold cannot be directly measured here.

Within the pumping regime discussed so far with respect to the laser diode's pulse duration, it can be argued that the peak power is the critical parameter for determining the threshold, as exemplified in Figure 5.13b, where the pump energy was increased until the pulse peak power required to induce LC lasing was reached. If, however, the pulse duration is decreased further while maintaining the same peak power, logic dictates that there will be a pump pulse duration for which the energy within the pulse will not be sufficient to overcome threshold. In this instance, it is the energy that will become the critical parameter for determining the threshold. This hypothesis could not be tested here due to the limitations of the driver electronics. However, the hypothesis is in good agreement with the conclusions drawn by Herrnsdorf *et al.*, which state the different pumping scenarios for which different threshold definitions are appropriate [131]. The same authors state that the duration of the pump pulse relative to the fluorescence lifetime and intersystem crossing time of the gain medium explains the existence of a transition between describing threshold in terms of fluence (energy) and intensity (peak power). The next chapter will elaborate on this, and place further significance on the temporal characteristics of the pump source for optimising LC laser performance.

The work presented in this chapter shows that threshold is minimised by reducing the pump pulse duration, and work by others has shown that the pump spot size and rise time ought also to be minimised. It can therefore be concluded that the way in which the threshold is defined is non-trivial and must take into account the excitation pulse wavelength, fluence, intensity and rise time.

5.8 Conclusions

The aim of this chapter was to investigate the effect of the pump pulse length on LC laser threshold and slope efficiency. The ability to control the pulse duration of the 445 nm LD pump source was exploited and bespoke software was used to automate slope efficiency data acquisition.

This investigation verified what, until now, has been limited to theoretical conjecture and anecdotal discussion in LC laser literature. By controlling the pulse length of the LD pump source, the increase in LC laser threshold and decrease in slope efficiency with increasing pump pulse length was, for the first time, experimentally demonstrated. This behaviour is in good agreement with the theory and was qualitatively attributed to the population of non-radiative triplet states. A manifestation of the deleterious effect that longer pulse lengths had on the LC laser threshold and efficiency was observed in the increase in fluorescence intensity that accompanied the LC laser emission. The pump pulse energy increase caused by an increase in pump pulse duration was found to be the cause of the increase in fluorescence intensity, by independently measuring the effect of pump pulse length and pump peak power on the LC laser energy and spectrum. An adjustable aperture was added to the optical arrangement to block the fluorescence, thus enabling accurate measurement of the effect of pump pulse duration on LC laser threshold and slope efficiency. The introduction of an aperture to control the fluorescence may benefit applications that require spatial coherence control, for example in holographic imaging. This would be an interesting investigation for future work.

Based on the evidence in this chapter, it is apparent that the pump pulse duration ought to be minimised, within the limits of the values tested in this work, in order to maximise the slope efficiency and minimise the threshold. The pump pulse intensity, fluence, wavelength and rise time must all be considered when defining LC laser threshold, and when selecting and comparing suitable pump sources. This chapter has primarily focussed on the energy behaviour of the LC laser with respect to the input energy. The following chapter builds upon this work by observing the temporal characteristics of the LC laser to gain further insight into the optimum operating conditions.

Chapter 6

Investigating the temporal dynamics of liquid crystal lasers

"It doesn't matter how beautiful your theory is, it doesn't matter how smart you are. If it doesn't agree with experiment, it's wrong."

Richard Feynman

6.1 Introduction

In Chapter 5, an experimental investigation established that an increase in pump pulse duration caused an increase in LC laser threshold and a decrease in slope efficiency. The results were obtained having corrected for the fluorescence emission that was found to accompany the LC laser. This chapter further explores the consequences of increasing the pump pulse length on LC laser performance. There is little theoretical work on the temporal characteristics of LC lasers, and even less experimental evidence, as, historically, the pump pulse duration could not be varied. This chapter aims to experimentally determine the effect of pump pulse peak power and pump pulse length on LC laser pulse length. Two photodiodes are introduced to the experimental arrangement to measure the temporal profiles of the emission from the LD and LC laser. The results presented in this chapter offer a significant contribution to the understanding of the temporal characteristics of LC lasers.

6.1.1 Chapter structure and nomenclature

The first investigation in this chapter explores the effect of *pump pulse peak power on LC laser pulse length.* The threshold of a DCM-doped LC laser was measured, and the pulse length was measured as a function of the ratio of pump energy (E_{pump}) to threshold energy (E_{th}), henceforth referred to as R (i.e. $R = E_{pump}/E_{th}$). This was then repeated for different pump pulse lengths.

The ability to vary the pump pulse duration is exploited further in the second investigation in which *the effect of pump pulse length on LC laser pulse length for a constant R* was measured.

The term *pulse energy* is only used in this chapter when discussing and comparing previously published work by other authors and when quoting values measured on the energy meter. As all previous literature has used a *fixed* pulse duration, any changes in energy have been due to a change in *peak power*, although this is rarely explicitly stated. In this work however, both pulse duration *and* peak power are varied independently, therefore the term *pulse energy* is ambiguous. Thus, wherever possible, *pulse peak power* and *pulse duration/length* are used.

6.2 Theoretical background and motivation

6.2.1 Previous investigations into LC laser temporal dynamics

In the theoretical paper by Shtykov *et al.* (first introduced in Section 2.4.2.1 and referenced again in Section 5.2), a series of rate equations were derived to model the kinetic behaviour of an LC laser system [30]. The equations describe the laser's temporal characteristics, taking into account the populations of the laser dye singlet and triplet states and the radiative and non-radiative transition lifetimes. Furthermore, the authors of Ref. [30] used the model to generate hypotheses of LC laser behaviour, in anticipation that a semiconductor-based pump source would successfully induce LC lasing in the future. Given that the first successful demonstration of this was presented earlier in this thesis (Chapter 4), the theoretical model in Ref. [30] motivated much of the experimental work presented in this chapter.

Shtykov *et al.*'s differential rate equations were applied by Ortega *et al.* [39], who experimentally showed the effect of pump energy on LC laser pulse length, with theoretical verification using Shtykov *et al.'s* model. The experimental data in Ref. [39] were acquired using LC laser cells with similar specifications to those used in this thesis, namely the same dye (DCM), cell spacing (10 μm) and a similar dye concentration (1 % in Ref. [39] compared to 0.5 % used here)[24]. The pulse energy was increased by increasing the peak power, as opposed to increasing the pulse length, which remained at 14 ns throughout their work. As illustrated in Chapter 5, this distinction is important when comparing and explaining the data.

[24] The differences between Ortega *et al.'s* work and the work here was the liquid crystal (E7 compared to BL006 respectively) and their use of a transmissive cell geometry.

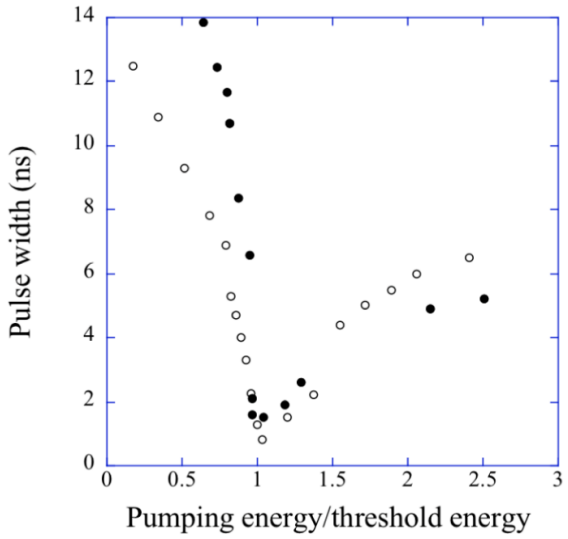

Figure 6.1. Data published by Ortega et al. in Ref. [39] *showing the experimental (black dots) and theoretical (white dots) effect of the pump energy (as a fraction of the threshold energy) on the output pulse length. The y-axis refers to the pulse length of the LC laser output.*

The authors of Ref. [39] found that the minimum LC laser pulse length occurred at threshold (Figure 6.1), below which the LC pulse length tended towards the pump pulse length (14 ns) used to induce LC laser emission. Above threshold, a gradual increase in LC laser pulse length was found with increasing pump pulse energy. The deviation between experimental and theoretical data was attributed to the rough estimation of values for some of the parameters used in the model and in the approximations used when measuring the pulse length.

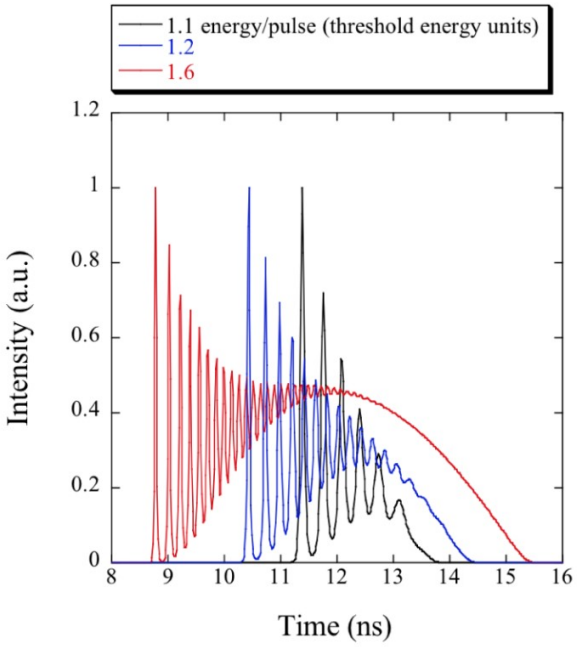

Figure 6.2. Simulated data from [39] *in which temporal profiles used to populate Figure 6.1 are shown for three different pump energies.*

A sample of the simulated data used for three of the data points in Figure 6.1 is shown in Figure 6.2, in which the spiking features are described by the authors as the result of mechanical and thermal disturbances as features on top of the laser emission. This is in contrast to the description provided in the original theoretical work by Shtykov *et al.* in which the spikes are described as laser emission and the broader feature is described as superluminescence (or amplified spontaneous emission). The experimental results presented in this chapter expand upon this and provide compelling evidence that explains the discrepancy between the two interpretations.

6.2.2 Energy level dynamics

The temporal dynamics of the four-level energy structure, typical of organic dyes used in LC lasers (and first presented in Chapter 2), is also important to consider when interpreting the results in this chapter. Each energy level in the singlet and triplet states has a characteristic lifetime and an associated rate of energy transfer from one energy level to another, either radiatively or non-radiatively.

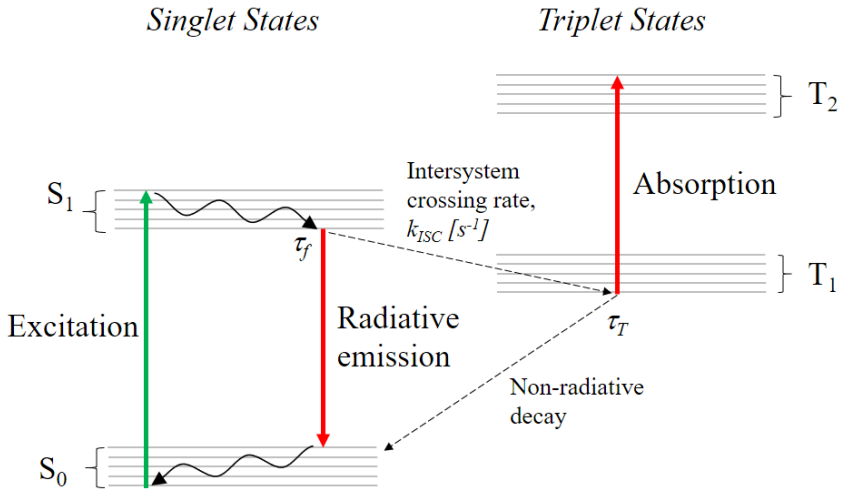

Figure 6.3. Jablonski diagram for a four-level laser with singlet and triplet energy states shown. τ_f is the fluorescence lifetime of the dye, τ_T is the triplet state lifetime and k_{ISC} is the rate of intersystem crossing from the excited singlet state to the ground triplet state.

The Jablonski diagram in Figure 6.3 shows the four-level energy structure for a typical organic dye, comprising singlet states S_1 and S_2, and triplet states T_1 and T_2. The singlet state lifetime (fluorescence lifetime, τ_f), triplet state lifetime (τ_T) and rate of intersystem crossing (k_{ISC}) are determined by the molecular structure of the organic dye[25]. Population of the triplet state is undesirable, as it removes energy from the lasing state [64]. Furthermore, the absorption spectrum between T_1 and T_2 often corresponds to the singlet fluorescence, thus introducing optical losses that would otherwise contribute to laser emission. This can eventually lead to quenching of the laser. The rate of transitions from S_1 to T_1 are dictated by the rate of intersystem crossing which, for organic gain media, falls within the range of $10^6 - 10^8$ s^{-1} [66], depending upon the concentration of dye molecules [132]. The rate of intersystem crossing is determined by the energy difference between S_1 and T_1, ΔE, whereby:

$$k_{ISC} \propto e^{-A\Delta E} \qquad \textit{Equation 2}$$

where A is a constant.

[25] They are also determined by concentration, temperature and environment (solvent), but can be considered constant within a given experiment.

With a few simplifying assumptions[26], the rate of triplet state population is given by:

$$\frac{dT_1}{dt} = k_{ISC}S_1 - \frac{T_1}{\tau_T} \qquad \textit{Equation 3}$$

where S_1 is the steady-state population of the lasing state and τ_T is the triplet state lifetime [66]. The triplet state lifetime can vary depending upon the concentration of oxygen present in the sample and typically ranges from 10^{-7} – 10^{-3} s (the oxygen quenches the triplet state, thus reducing its lifetime) [64]. For DCM, this is in the order of 10 – 100 μs. Comparison between the rate of intersystem crossing and the rate of depopulation of the triplet state ($1/\tau_T$) shows:

$$k_{ISC} \gg \frac{1}{\tau_T} \qquad \textit{Equation 4}$$

Therefore, under prolonged optical excitation, the population of T_1 increases, reducing the availability of molecules in the S_1 state for stimulated emission. Triplet state population is negligible when the pump source has a pulse duration much smaller than the duration of intersystem crossing [66]. Conversely, and of particular relevance to the work in this chapter, triplet state population is predicted to be strongly affected by long pump pulse durations. As the rate of intersystem crossing is an intrinsic property of the dye, the rate of population of the triplet state is constant, regardless of the pump pulse length. As intersystem crossing acts to non-radiatively depopulate the singlet state by populating the triplet state, the remaining energy in the pump pulse contributes only to spontaneous emission, as the population inversion required for stimulated emission cannot be achieved.

Based on this logic, it follows that the duration of the LC laser pulse, τ_{LCL}, can be approximated by:

$$\tau_{LCL} \approx \frac{1}{k_{ISC}} \qquad \textit{Equation 5}$$

[26] It is assumed that singlet state dynamics are much faster than triplet dynamics and that triplet state absorption causes the loss of a laser photon but not a significant loss of triplet population.

Since the rate of intersystem crossing is predicted to be dictated by the gain media (and not the pump parameters), it would be reasonable to expect that the LC laser pulse length is independent of pump pulse duration. Again, this is provided that the pump pulse duration is longer than the time taken for intersystem crossing to occur. It is only now that LD pumping has been demonstrated, that such an investigation is possible.

6.2.3 Other relevant studies into laser pulse temporal dynamics

Although it is believed that this is the first time an investigation into the temporal behaviour of LC lasers has been carried out with a pump source capable of varying the pulse length, some previous experimental work, either using different lasing mechanisms or different gain media, has been published. For example, Zhao *et al.* used a 450 nm LD pump source, similar to the one used in this work, to characterise the temporal performance of a DCM-based vertical external cavity surface-emitting organic laser (VECSOL) [112]. In a similar vein to the experimental method in this chapter, the authors of Ref. [112] varied the pump pulse length to observe the temporal shape of the VECSOL emission. With a pump duration up to 500 ns, an upper limit of the output pulse length of ~ 100 ns was concluded. However, the definition of laser emission in Ref. [112] appears to include fluorescence emission, despite a narrow-linewidth feature clearly present in their experimental data within the first few nanoseconds of pumping. Had the spectral data been simultaneously analysed by the authors, the presence of fluorescence would likely have been identified which, if accounted for, would have resulted in the calculation of a laser pulse length of approximately 3 ns (judging by the data they present). This analysis is in agreement with other studies, such as that by Lehnhardt *et al.* in which an organic solid-state laser was pumped with the same LD as in this work, with a pump pulse length of 70 ns resulting in a 3 ns output pulse. The short output pulse duration was attributed to triplet state population [133].

Despite the differences in laser cavity geometries and gain media, the consensus within the literature, whether based on experimental or theoretical evidence, is that the deleterious effect of a long pump pulse duration on laser emission is caused by singlet-to-triplet state energy transfer. As stated by Orazio Svelto with reference to dye lasers:

"*The duration of the pump pulse must be short enough to ensure that an excessive population does not accumulate in the triplet state*" [60].

The laser pulse temporal dynamics that have been investigated for different laser technologies, is, for the first time, experimentally explored for LC lasers in this chapter.

6.3 Investigation 1 - Measuring the effect of pump pulse peak power on liquid crystal laser pulse length

6.3.1 Experimental

Figure 6.4 shows the optical arrangement used to measure the temporal profile of the LD and LC laser emission using two photodiodes (*DET025A/M, Thorlabs*) connected to an oscilloscope *(WavePro 735Zi, LeCroy)*. The current monitor from the output of the LD driver electronics was also measured to compare the temporal profile of the electrical signal to the resultant optical signal from the LD. The photodiodes were interchangeable with the energy meter, depending upon the required parameter measurements. Channel 1 was used to compare the electrical pulse generated by the LD driver electronics to the resultant optical pulse on Channel 2, and Channel 3 measured the resultant LC laser pulse.

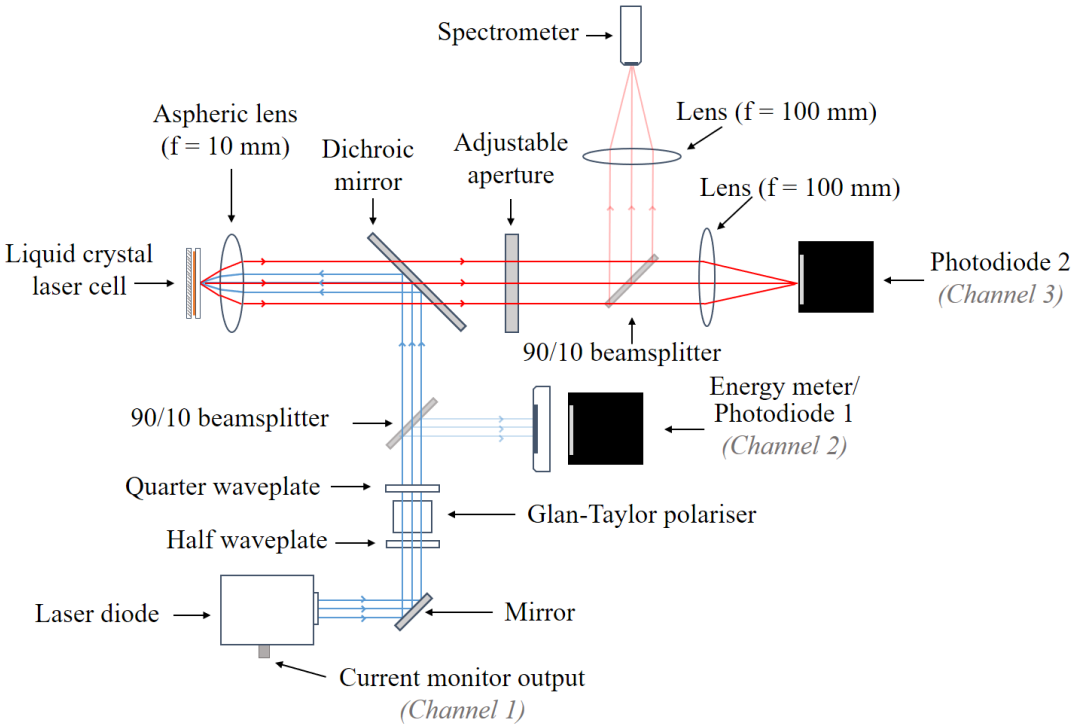

Figure 6.4. Optical arrangement for measuring the pump and LC laser pulse lengths. The energy meter (used to measure the pump energy) and photodiode 1 were interchangable depending upon the experiment. Channels 1-3 indicated correspond to the input on the oscilloscope used to analyse the driver electrical signal (Channel 1), pump laser (Channel 2) and LC laser (Channel 3).

For the first part of the investigation, the energy meter was positioned as shown in Figure 6.4, and photodiode 2 was connected to the oscilloscope which was set to measure the FWHM of the LC laser pulse. The combination of the LC laser emission detected by the spectrometer and the signal on photodiode 2 was used to determine threshold for the selected pump pulse length at a chosen cell position. The half-waveplate was rotated to increase the *pump peak power* incident upon the LC laser. The resultant energy[27] change was recorded when a narrow-linewidth signal was first detected by the spectrometer and pulses consistent with laser emission appeared on the oscilloscope. This value, E_{th}, was used for the remainder of the investigation to calculate R.

The reason for not using the LTS to determine the threshold, as presented in Chapter 5, was to minimise cell fatigue prior to taking R measurements. As the threshold was known to vary at

[27] The change in energy in this investigation was caused by an increase in peak power, as each data set had a fixed pulse length. The term *energy* is used because, firstly, this was the unit of measurement of the detector, and secondly, because this was the unit used in the work in Ref. [39], upon which this investigation builds.

different cell positions, the same cell position had to be used to acquire a full data set for all *R* values. Measuring threshold using the LTS required the same cell position to be pumped many times to populate an efficiency curve and would thus fatigue the cell prior to acquiring the experimental data. The method proposed here for determining threshold by observing the signals on the spectrometer and photodiode, required fewer pulses than for a full efficiency curve. In fact, Sanz-Enguita *et al.* state that this is a more accurate method of determining threshold compared to estimating the position of gradient change in an efficiency curve, and they use this method exclusively in their work [37]. By using the spectrometer *and* photodiode simultaneously to observe the onset of lasing, the systematic error was minimised. This method of determining threshold meant that it was important that the collection parameters (i.e. acquisition time and scaling) for the spectrometer were kept consistent throughout these experiments. While this method of determining threshold was not essential for the range of pump pulse lengths used in *this* investigation, when longer pump pulse lengths were required in the second investigation, this method was the only way to ensure reliable measurements, as longer pulse lengths resulted in rapid performance degradation. For consistency, the same method was therefore used for both investigations.

The LD pulse length was 12 ns and the repetition rate set to 1 Hz. The current was set to a maximum of 14 A and the half-waveplate rotated to reduce the pump energy (as measured on the energy meter) below threshold. Twenty pump pulses were recorded, the average energy value calculated by the Starlab software, and the average LC emission FWHM value measured by the oscilloscope. The ratio of this pump energy to the threshold energy was calculated and plotted against the measured LC emission pulse length. This process was repeated across a range of increasing pulse energies (i.e. increasing peak pulse powers), continuing above the threshold until a sufficient data set was collected. These measurements were repeated for different pump pulse lengths, with the aim of obtaining a deeper insight into the LC laser temporal characteristics.

6.3.2 Results

The results from the first part of the investigation are presented in Figure 6.5, showing the effect of pump energy (through adjustment of pulse peak power) on LC laser pulse length.

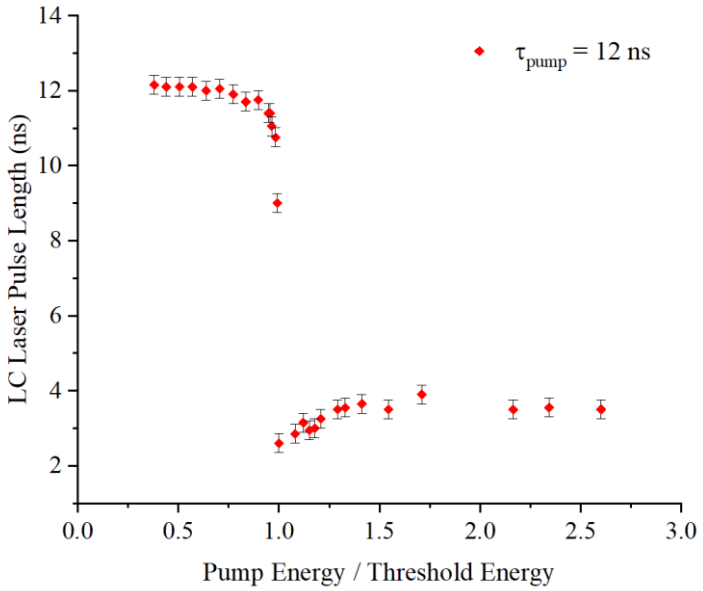

Figure 6.5. Measurement of LC laser pulse length as a function of the LD pulse energy/threshold ratio. A pump pulse length of 12 ns was used for this data set. The error bars are calculated from combining the rise and fall time of the detector (0.15 ns) and the 0.2 ns uncertainty in the pulse length measurement, resulting in an error of 0.25 ns.

In Figure 6.5, the pre-threshold LC laser pulse length is approximately equal to the pump pulse duration (12 ns) and drops to a minimum value at threshold. Above threshold, the LC laser pulse duration plateaus at approximately 3.5 ns as the pump energy increases. This behaviour was also found when the experiment was repeated with three further pump pulse durations (11 ns, 14 ns and 17 ns), as shown in Figure 6.6.

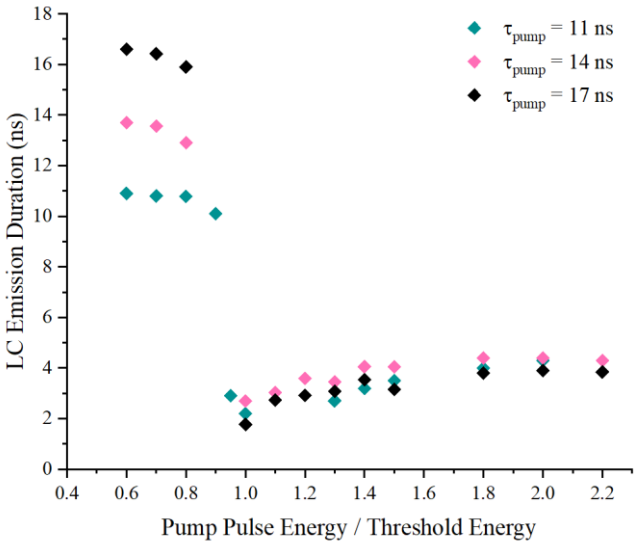

Figure 6.6. Effect of pump energy on LC laser pulse length below and above laser threshold using three different pump pulse durations.

6.3.3 Discussion

The *pre-threshold* results in Figure 6.5 are in agreement with Ortega *et al.* (Figure 6.1 [39]), for which the emission duration tends towards the pump pulse duration. Above threshold, however, the results differ. Unlike the published results, for which the LC laser pulse length continues to increase with increasing pump energy, the data in Figure 6.5 plateaux.

The plateauing effect can be explained by how the temporal data were interpreted. Likewise, the lack of plateauing in Figure 6.1 from Ref. [39] can be attributed to how the authors defined LC laser emission. As previously mentioned, the authors of Ref. [39] interpreted laser emission as temporally broad emission profiles, on top of which were a series of "spiking" features. In contrast, the authors of the original model in Ref. [30] interpreted this spiking as the "short laser generation pulses on a pedestal of superluminescence", where the superluminescence is also described as "intensified spontaneous emission".

An experiment was conducted with the aim of understanding the cause of the different interpretations. A LD pulse length of 11 ns was used to pump the LC cell. The resultant temporal emission from the cell was recorded (Figure 6.7a, red line). The fluorescence-only emission was also recorded (Figure 6.7a, black line, achieved by fatiguing the cell using a repetition rate of 100 Hz).

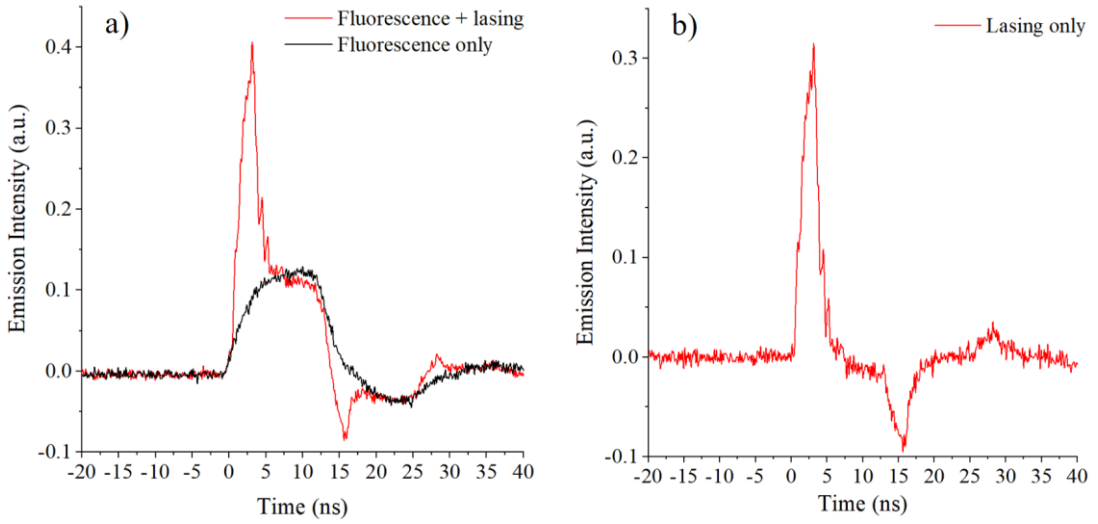

Figure 6.7. LC laser temporal profiles when pumped with an 11 ns pulse. The red line in a) shows the LC emission, with a short pulse lasting ~ 3 ns, after which the intensity drops for the remainder of the pump pulse duration. The black data show the fluorescence remaining when LC laser emission ceases after the cell is deliberately fatigued. The pulse in b) is the result of mathematically subtracting the fluorescence signal from the combined fluorescence and lasing signal.

When the fluorescence data were mathematically subtracted from the total emission (Figure 6.7b), a narrow-linewidth laser peak remained. The red experimental data in Figure 6.7a are analogous to the theoretical data in Figure 6.2, and by removing the fluorescence signal to display only laser emission in Figure 6.7b, this shows that the theoretical spiking *can* be attributed to laser emission. This agrees with the analysis presented in the original model [30].

This work therefore proposes that the LC laser emission experimentally demonstrated here corresponds to the spiking data Figure 6.2, and that the broad curve below the spiking is spontaneous emission. This definition explains the increasing trend in LC emission pulse length above threshold in Figure 6.1 compared to the plateauing behaviour above threshold in Figure 6.5; the authors of Ref. [39] have plotted what they have defined as lasing but what the experimental evidence here shows is spontaneous emission[28]. (Note: The negative signal that appears as a feature on the LC laser temporal profile in Figure 6.7 is unphysical and likely due to the response of the photodiode to an electrical reflection caused by an impedance mismatch, despite all precautions being taken to minimise this effect. It is therefore an electronics artefact,

[28] It should be noted that all lasers have some non-lasing transitions occurring alongside stimulated emission, and some authors may choose to include all emission as lasing. In this work, however, while there will be some on-axis spontaneous emission that cannot be removed, a distinction between stimulated emission and spontaneous emission is critical to the interpretation of the data.

rather than an optical phenomenon. Further work is needed to identify the exact cause of this, although it does not appear to affect the laser emission.)

With reference to the molecular energy levels (Section 6.2.2), as the pump pulse energy is increased (via peak power increase), the population of the excited singlet state (S_1 in Figure 6.3) also increases. Below threshold, the duration of the output emission is approximately the same as the duration of the pump pulse duration, as the peak power is not sufficiently high to form a population inversion from S_0 to S_1. At threshold, there is only *just* enough power to induce LC laser emission, thus resulting in a temporally short LC laser pulse. As the peak power is increased, multiple narrow laser pulses are produced, owing to the rapid excitation and de-excitation of the singlet state. This acts to increase the duration of the LC laser emission. However, as the peak power is increased further, a limit to the LC laser pulse duration occurs because of the intersystem crossing to the triplet state. As the rate of intersystem crossing is determined by the dye, increasing the pump pulse duration does not affect the maximum duration of the LC laser pulse. This explains the post-threshold plateauing at 3.5 ns for all three pump pulse durations in Figure 6.6.

An experimental equivalent to the mathematical removal of fluorescence post-experiment (Figure 6.7b) was achieved by using an aperture to block the fluorescence (the two methods are directly compared in Appendix H). Without the aperture (Figure 6.8, black line), the LC emission temporal profile was dominated by a broad signal caused by spontaneous emission. The laser emission was only visible as a narrow feature ontop of the broader curve (when $R \geq 1$). When the aperture was present, transmission was restricted to (mostly) laser emission (Figure 6.8, red line) evidenced by a narrow temporal profile which grew in intensity with increasing R, when $R \geq 1$. When $R < 1$, only a weak on-axis spontaneous signal was detected.

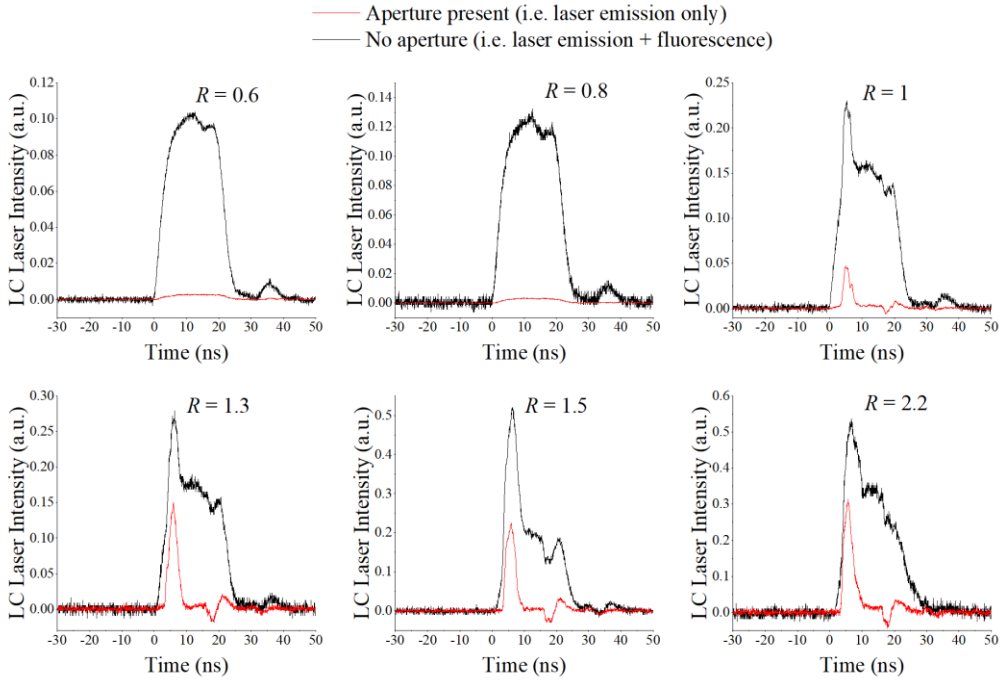

Figure 6.8. Evolution of LC emission temporal profiles with increasing pump peak power for a fixed pump pulse length of 17 ns. The black data show the emission detected by the photodiode when there is no aperture present; thus fluorescence and lasing are detected simultaneously. The red data show the laser emission after having attenuated the fluorescence with an aperture.

Figure 6.8 shows the temporal equivalent to the spectral data presented in Chapter 5 for validating the introduction of an aperture to the experimental arrangement. This substantiates Chapter 5's conclusions that the aperture was needed to attenuate the fluorescence signal. By removing the fluorescence with the aperture, is was possible to measure the LC laser pulse length *during the experiment*. This method was used for acquiring the data shown in Figure 6.5 and Figure 6.6.

There is one caveat to the data presented in Figure 6.5 and Figure 6.6. As highlighted in Chapter 5, when the threshold was measured as a function of pump pulse length, the peak height of the pump pulse remained approximately constant, and thus the rise time of the pump pulse was also approximately constant. However, for the temporal data used to plot the graphs in Figure 6.5 and Figure 6.6, this was not the case. As mentioned in Section 5.2, Shtykov *et al.* theoretically plotted the LC laser threshold for a varying rise time of a hypothetical semiconductor pump source [30]. They showed that an increase in rise time caused the LC laser threshold to increase. Experimentally, however, this is not possible; the pump pulse length and the rise time cannot both remain constant for an increase in pulse peak power, nor

can the rise time be independently controlled. Thus, in Figure 6.5 and Figure 6.6, each data point uses the same threshold energy. *R* values for which the threshold was calculated for the rise time associated with that specific pump peak power would ideally be used. However, as this was also the case in the original work by Ortega *et al.*, it remains a valid comparison. The effect of increasing the LD peak power on the rise time for a constant pulse length is shown in Figure 6.9, with a) showing the temporal shape of the pump as the peak power was increased and b) highlighting the increasing trend in the rise time gradient[29]. This temporal data for an increasing current and constant pump pulse length is analogous to the increasing energy data used to plot Figure 6.5 and Figure 6.6.

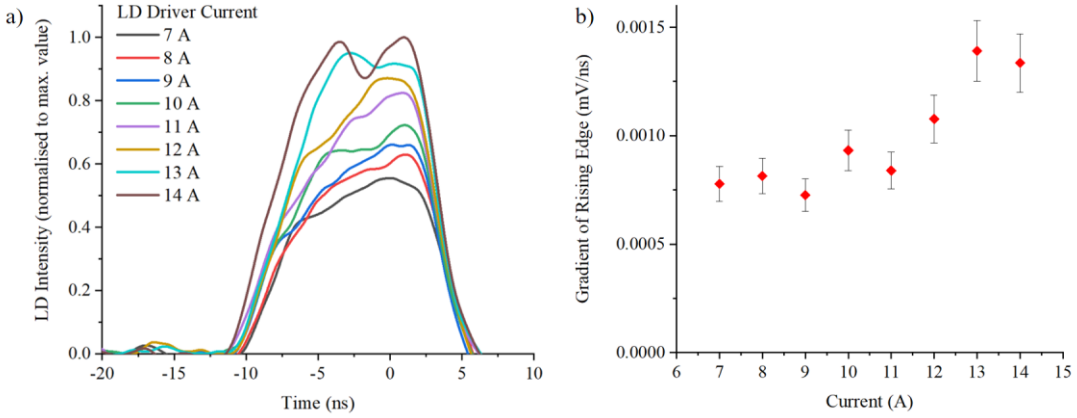

Figure 6.9. a) Laser diode pulse shape for an increasing current with a constant pulse length. b) Highlights the increase of the rise time gradient with current.

6.3.4 Summary

The effect of pump pulse energy on LC laser pulse duration was investigated. It was found that LC laser pulse length was minimum at threshold and plateaued at approximately 3.5 ns as the pump pulse peak power was increased. Moreover, the same LC laser pulse duration was reached when a further three pump pulse durations were tested. This suggested that the LC laser pulse length has an intrinsic upper limit. The following investigation expands upon this previously undocumented result.

[29] The rise time *gradient* was used instead of the rise time, as the exact time taken to reach the peak was ambiguous.

6.4 Investigation 2 - Measuring the effect of pump pulse length on liquid crystal laser pulse length

6.4.1 Experimental

The second investigation used a larger range of pump pulse lengths to investigate the effects on LC laser pulse length. In order to maintain consistency between data sets of different pump pulse lengths, the same *R* value was used throughout. The maximum *R* common to all pump pulse lengths was $R = 2.2$ (i.e., the maximum pulse energy achievable by all pulse durations was just over double the threshold energy).

As before, LC laser threshold was determined using the spectrometer and photodiode to detect LC laser emission, and the corresponding pump energy value recorded. Once the threshold for each pump pulse length had been determined, a calibration table was made for setting the current that would give a pump pulse energy corresponding to $R = 2.2$. This avoided having to measure the energy at the LC sample each time the pump pulse length was changed, thus enabling uninterrupted data acquisition.

The data were then recorded across nine pump pulse lengths, ranging from 11 ns to 94 ns. The pump pulse length and current corresponding to a pump energy value of $R = 2.2$ were set on the LD controller. The average pump energy value and LC laser pulse length were recorded for three different cell positions for each pump pulse length (i.e. twenty-seven cell positions in total).

6.4.2 Results

A sample of the LC laser temporal profiles across the full range of pump pulse lengths after removing the fluorescence are shown in Figure 6.10 for a DCM-doped cell and a C504-doped cell. A near-identical LC laser pulse length for each example is clearly present throughout, with a slightly longer LC laser pulse length for the C504 cell.

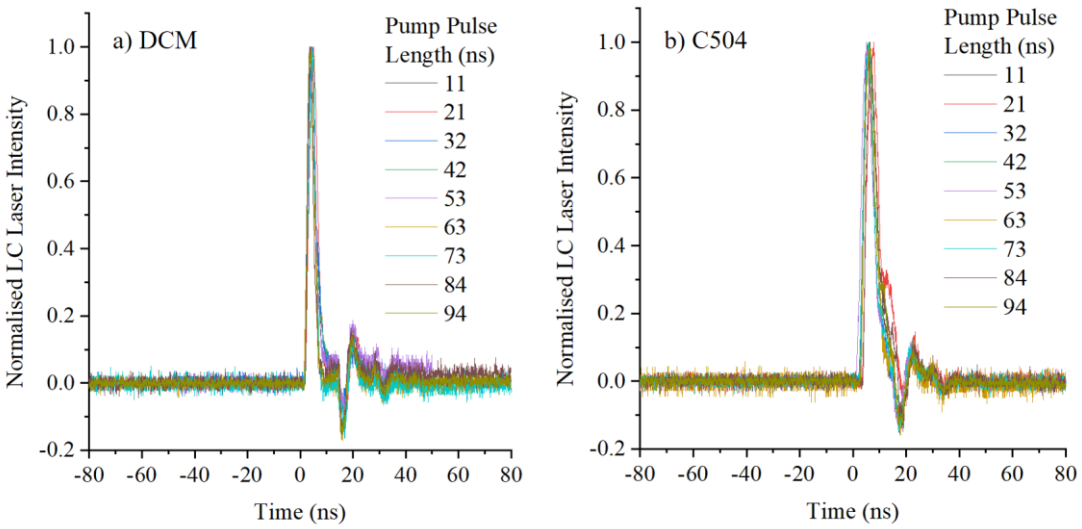

Figure 6.10. LC laser pulses for varying input pulses with durations ranging from 11 ns - 94 ns for cells doped with a) DCM and b) C504.

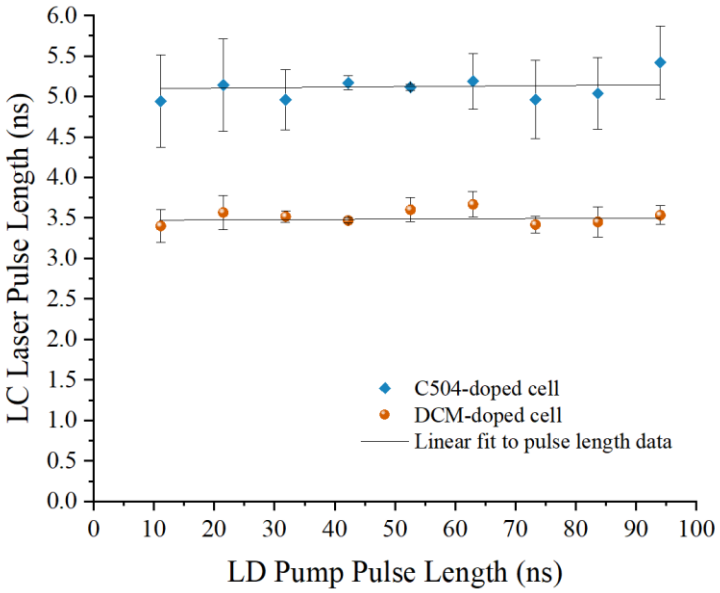

Figure 6.11. LC laser pulse length as a function of pump pulse length for a DCM-doped cell (orange circles) and a C504-doped cell (blue diamonds). Note that there are no data present for pump pulses shorter than 11 ns, as the LD driver electronics were limited to pulse lengths greater this.

Figure 6.11 highlights the approximately constant LC laser pulse lengths shown in Figure 6.10. The error bars on this data show the standard deviation of the mean LC laser pulse length for each pump pulse length, with the lines of best fit plotted in black. The average measured LC laser pulse length was 3.5 (± 0.1) ns for the DCM-doped laser cell and 5.2 (± 0.2) ns for the C504-doped cell. A different value for the DCM- and C504-doped cells was to be expected,

based on the theory presented in Section 6.2, which states that the temporal characteristics are determined by the gain media.

6.4.3 Analysis

Figure 6.10 and Figure 6.11 provide clear evidence of an upper limit to the pulse length emitted from an LC laser. The independence of LC laser pulse length with respect to input pulse length (for the range of input pulse lengths used in in this work) is in good agreement with the theoretical hypothesis provided by Forget *et al.* [66] in Section 6.2.2. This is believed to be the first time the existence of an upper limit to the pulse duration of an LC laser has been presented. The theoretical analysis used to explain the behaviour in the first investigation (i.e. the conclusions that triplet state population is responsible for there being an upper limit to the duration of an LC laser pulse) is validated by the results presented here.

Equation 5 shows that the output pulse length from the laser can be estimated by the inverse of the rate of intersystem crossing to the triplet state. The rate of intersystem crossing was unknown for the dye-doped chiral nematic mixtures used in this investigation. However, the measured LC laser pulse length of 3.5 ns for 0.5 $\%_{wt}$ of DCM laser would imply an intersystem crossing rate of ~ 3×10^8 s^{-1} using this approximation, which is within the typical literature range [66]. The theoretical work by Shtykov *et al.* used a rate of intersystem crossing of 5×10^7 s^{-1} for DCM which would correspond to $\tau_{LCL} \approx 20$ ns. However, this was for a different dye concentration and LC, and no reference was provided for this value. The theory also predicts that the plateauing behaviour would not be expected for pump pulse durations *less* than this upper limit of the LC laser pulse, as was discussed in Section 6.2, i.e., for DCM:

$$\tau_{pump} \geq 3.5\ ns, \quad \tau_{LCL} = 3.5\ (\pm\ 0.1)\ ns \qquad \textit{Equation 6}$$

$$\tau_{pump} < 3.5\ ns, \quad \tau_{LCL} \approx \tau_{pump} \qquad \textit{Equation 7}$$

This hypothesis is tested in Section 6.4.4 by using the 532 nm Q-switched pump source with a pulse length of < 1.3 ns.

The results are also in agreement with previously published data for other laser systems (Section 6.2.3). An upper limit of 3.5 (± 0.1) ns is similar to the pulse lengths presented for

the DCM-based lasers in Refs. [112] and [133] although, as already discussed, the former did not distinguish fluorescence from lasing and concluded a pulse duration of 100 ns.

The same approach as the first investigation for removing the fluorescence to isolate the laser emission was used in this investigation. An example of the LC emission with and without an aperture when pumped with a pulse length of 94 ns is shown in Figure 6.12. This further illustrates the effect of the aperture on the temporal characteristics of the LC emission.

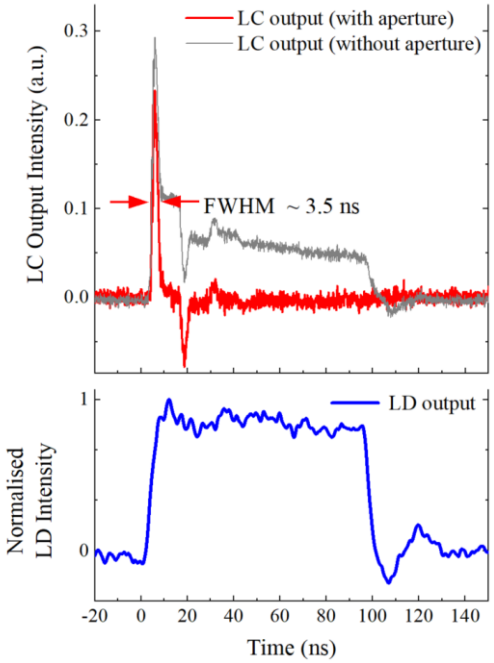

Figure 6.12. Temporal characteristics of the LC emission when pumped with a 94 ns pulse. Lasing and fluorescence can be seen (black data) when there is no aperture present, with the fluorescence lasting for the duration of the pump beam (blue data). When the aperture is present, the fluorescence is blocked, resulting in only laser emission (red data).

The effect of a change in rise time with increasing pump pulse energy discussed for the first investigation (Figure 6.9) was not relevant here, as the pump pulse *length* was varied in this case, while the peak power remained approximately constant. Therefore, the rise time remained approximately constant for all pump energies, as highlighted in Figure 6.13.

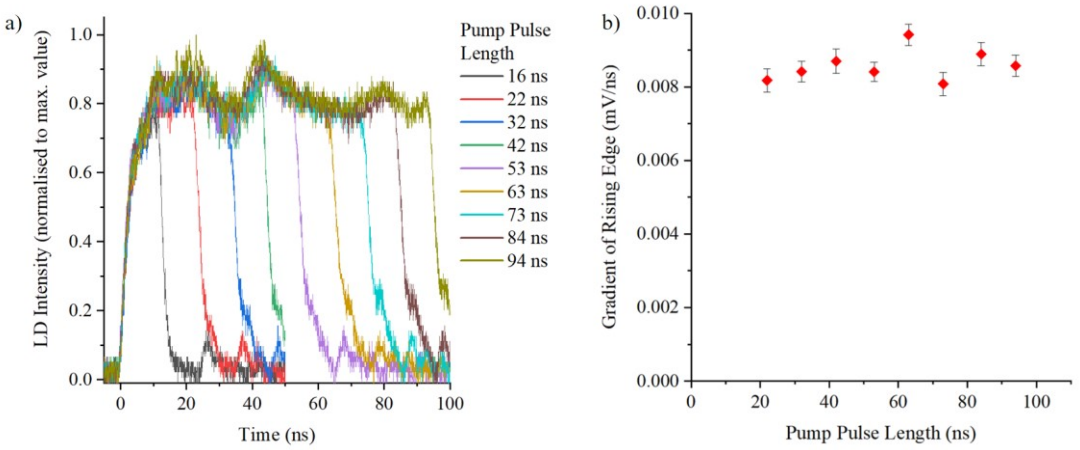

Figure 6.13. a) Pump pulses used to populate Figure 6.11 for R = 2.2, with b) showing the near-constant gradient of the pump pulse rise time.

6.4.4 Comparison with a Q-switched laser

It was expedient to compare the temporal results to the regime in which a pump pulse duration was *shorter* than that of the LC laser upper pulse length limit. However, the shortest possible pulse length that the LD driver electronics could produce was 8 ns, thus preventing such an investigation. Ideally, a pump source with a variable pulse length < 3.5 ns would be used, to allow the characterisation of the resultant LC laser pulses. This would offer further insight into the fundamental performance limitations of LC lasers, which could have implications for potential LC laser applications requiring sub-nanosecond pulses. It was possible, however, to gain some insight into the temporal behaviour of the DCM-doped LC laser in this shorter pump pulse length regime by using the < 1.3 ns, 532 nm Q-switched laser introduced in Chapter 4.

An optical configuration similar to that shown in Figure 6.4 was used, but with different waveplate and dichroic optics coated for use with a 532 nm laser source. The photodiodes were positioned as before to measure the pump beam and LC laser beam temporal profiles (Figure 6.14).

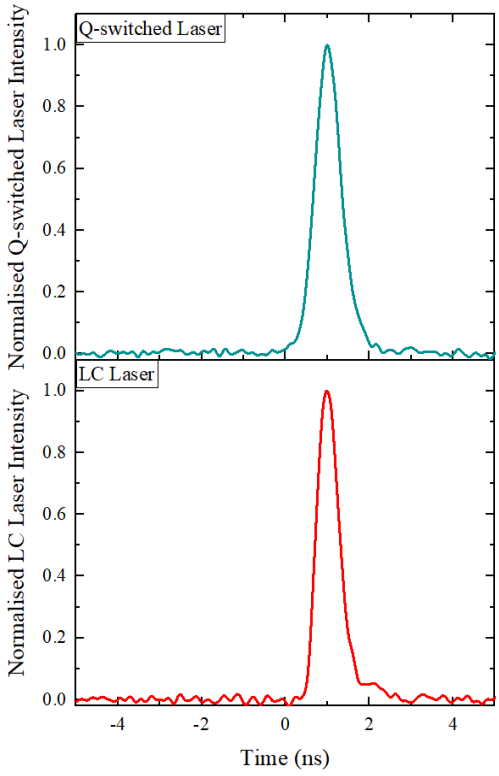

Figure 6.14. Temporal signal of the 532 nm Q-switched pump laser (top) and the resultant LC laser emission (bottom) showing near-identical profiles.

The FWHM of the 532 nm temporal profile was measured to be 0.73 ns, resulting in a slightly shorter LC laser pulse length of 0.65 ns, accompanied by what appears to be a very weak fluorescence signal. This data imply that when the LC laser is pumped with a pulse length *shorter* than the upper limit previously found, the LC pulse length instead follows that of the pump. This is in agreement with Equation 7 and with the literature, which shows that triplet state population is negligible if the duration of the pump pulse is less than the time taken for intersystem crossing [66].

A range of pump pulse lengths in addition to the Q-switched pulse presented above would ideally be used to form a larger data set. In particular, the lower limit to the pump pulse length would offer further insight into the performance limitations. However, this is beyond the capabilities of the LD driver electronics available at the time of writing.

6.4.5 Summary

This investigation verified the results from the first investigation, proving the existence of an upper limit to the LC laser pulse duration. It was shown that the LC laser pulse length was independent of the pump pulse length, provided that the pump pulse length exceeded the LC laser's upper limit. The reason for the existence of an upper limit to the LC laser pulse duration can be attributed to laser quenching caused by triplet state population. A Q-switched laser was used to prove the hypothesis that, when the pump pulse duration was *less* than the characteristic upper limit to the LC laser pulse length, the LC laser pulse length occurred over a similar timescale to the pump.

6.5 Comments on liquid crystal laser stability

A body of work worthy of future investigation is the LC laser output stability as a function of pump pulse duration, repetition rate and pulse energy. As the aim of the work in this chapter was focussed on investigating temporal characteristics of a single pulse, the stability was only measured in the context of optimising the experimental method. It was observed that, as the pump pulse length was increased, the cell's ability to reproduce LC laser emission diminished with consecutive pump pulses. This can be seen in Figure 6.15, in which a) consecutive LC laser pulses of equal intensity are seen when τ_{pump} = 11 ns, b) gradual decrease in LC laser intensity is seen when τ_{pump} = 42 ns and c) immediate LC laser pulse extinction occurs after only one pump pulse when τ_{pump} = 94 ns. After LC laser emission is extinguished, only fluorescence emission persists for a duration equal to the pump pulse length. This meant that cell alignment relative to the focussed pump spot had to be carried out using the shortest possible pump pulse length to acquire accurate data for longer pump durations.

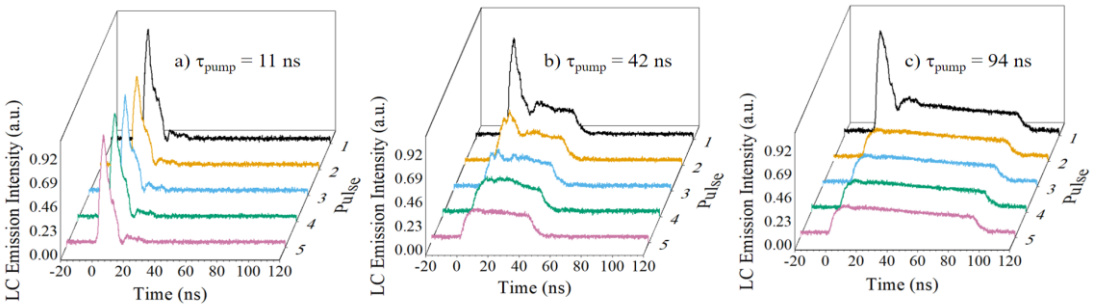

Figure 6.15. LC emission intensity for consecutive pulses when pumped using pulse lengths of a) 11 ns, b) 42 ns and c) 94 ns, all pumped at 1 Hz. As the pump pulse duration is increased, it can be seen that there is an increase in the rate of LC laser performance degradation. In the case of τ_{pump} = 94 ns, only one LC laser pulse is emitted, after which only fluorescence is produced.

Observations made during the work in this chapter showed that, even when pumped with a pulse duration of 11 ns at 1 Hz, the LC laser performance eventually degraded, although this was in the order of tens of minutes rather than seconds, with the degradation occurring more quickly at higher repetition rates and at higher energies. The cause of this behaviour can be explained based on the work carried out by Khoo *et al.* [134] and Morris *et al.* [32] in which the timescales of different degradation processes were analysed. As the triplet state lifetime of organic dyes is of the order of microseconds [93], the LC laser's inability to recover between consecutive pulses 1 second apart is unlikely due to triplet state population. Khoo *et al.* suggested that, at fluences > 1.8 mJ mm^{-2}, flow effects of the LC molecules can occur [134]. However, as the fluence of the pump pulse used in this work was < 0.125 mJ mm^{-2}, flow effects can be discounted.

Optical reorientation is also an unlikely source, as this is proportional to the pulse energy [32], and Q-switched pump sources which have pulse energies several orders of magnitude higher than those emitted from the LD can successfully pump LC lasers at higher repetition rates without impacting the stability [13]. The director reorientation relaxation time is also two orders of magnitude shorter than the repetition rate used here.

Since the performance degradation rate increases with increasing pulse lengths with consecutive pulses at 1 Hz, and since lasing cannot be recovered, the most likely reason for this behaviour can be attributed to dye bleaching, in which permanent damage to the dye molecules can occur with increasing exposure to the excitation source [135]. A more detailed study similar to [134] and [32] but which would include pump pulse duration would be needed to verify this. Based on this evidence however, for practical applications requiring high

repetition rates, short pump pulses are required not only to mitigate triplet state population within a single pulse, but also to prevent non-recoverable performance degradation between consecutive pulses.

6.6 Conclusions

The aim of this chapter was to investigate the temporal characteristics of an LC laser by exploiting the LD's ability to vary the pump pulse length. This is the first time that an experimental study into the effect of pump pulse length on LC laser pulse length has been possible, as the typical method of Q-switched pumping prohibits this. The principal investigations in this chapter successfully achieved the aims set out in Section 6.1 and its conclusions are summarised below.

The LC laser pulse duration plateaus as the pump energy is increased above threshold.
The first known study into the temporal performance of LC lasers under varying pump peak powers for multiple pulse durations was undertaken. The results were compared to, and expanded upon, previous experimental and theoretical work by other research groups. This led to the conclusion that an increase in pump energy (by increasing the peak power) from below LC laser threshold resulted in a minimum LC laser pulse length occurring at threshold, beyond which the LC pulse length increased and eventually plateaued. The principal outcome of this experiment found that when *different* pump pulse lengths were used across a 6 ns range, the LC laser pulse length tended towards the *same* LC laser pulse length above threshold, regardless of the pump pulse length. This is believed to be the first time such an observation has been made.

The LC laser pulse length is independent of the pump pulse length for long pump pulse durations.
Multiple LC laser pulse lengths were measured for pump pulse durations spanning a 90 ns range, whist maintaining a constant ratio of pump pulse energy-to-threshold throughout. A constant LC laser pulse length of 3.5 (± 0.1) ns for the DCM-doped cell was found, irrespective of the LD pump pulse length. The experiment was repeated with a C504-doped cell, for which a constant pulse length of 5.2 (± 0.2) ns was measured. This demonstrated, for the first time, the existence of an upper limit to the pulse length of an LC laser and that, if the pump pulse

length exceeded this, the remainder of the optical energy within the pump pulse resulted in fluorescence from the LC cell. The conclusions from this experimental work are in good agreement with the theory of organic dyes, whereby the duration of laser emission is limited by the rate of intersystem crossing from the excited singlet state to the lowest triplet state.

A 532 nm Q-switched laser with a pulse length shorter than the LC laser upper pulse length limit showed that the LC laser pulse length was similar to that of the pump. This may be generalisable for pump regimes in which the pulse length is *below* the characteristic upper limit of the LC laser pulse duration, but could not be tested in this work due to the limitations of the LD driver electronics. This could have practical implications for applications requiring sub-nanosecond pulse lengths, for example, fluorescence lifetime imaging [22]. For this temporal regime, the pump pulse length would need to be similar to the desired LC laser output pulse length. Conversely, as discussed by Chénais *et al*., a combination of a low intersystem crossing rate, low triplet-triplet cross-section, low overlap of the triplet absorption with the stimulated emission wavelength and a short triplet state lifetime would enable longer LC laser pulse lengths or CW LC laser emission [136].

6.6.1 Opportunities for future work

Some work has been done in an attempt to reduce the effect of triplet state population, for example, by adding oxygen to quench triplet state absorption, as the population of triplet states is the principal barrier preventing stable CW emission from an LC laser [31], [37]. It may be the case that alternative gain materials, impervious to triplet state population and thermal fatigue, are ultimately required if one wishes to achieve CW LC laser emission. An example of this could be the use of quantum dots as the gain media, which has shown promising results in LC hosts [137], [138]. Research into this and other methods would be an interesting area to pursue in future work.

The fact that the LC laser performance degraded more rapidly with increasing pump pulse length is a further indicator that the pump pulse length ought to be minimised when optimising LC lasers. This is in addition to the detrimental effect a long pump pulse duration has on threshold and efficiency. The extent to which the LC laser pulse length can be reduced would be an insightful topic for further investigation.

The development of a comprehensive theoretical model, which explores the temporal dynamics of LC laser emission from a reflective cell (with a variable duration and peak power) is also worthy of future work. This would expand upon the work by Shtykov *et al.* and would enable LC laser performance predictions based on the different pump parameters. This theoretical work is currently in progress within the group, and preliminary results[30] show a strong correlation with the experimental data presented in this chapter.

The intention of the work in this chapter was not only to contribute to the understanding of the temporal dynamics of LC lasers at a fundamental level, but also to gain a better insight into the optimum performance towards commercialisation. As mentioned in the introduction to this thesis, LC lasers have yet to find their place in a commercial setting. The success of LD pumping is expected to be a significant a step towards achieving this, and the work presented here, investigating the temporal dynamics, suggests that LC lasers could offer solutions in applications requiring nanosecond-or-less pulse durations. This could include, for example, fluorescence imaging or optoacoustic imaging, as both techniques require pulse lengths and energies achievable with LC lasers [139]. If LC lasers are to be considered a disruptive technology in such applications, however, the lab-based bench-top arrangement presented so far in this thesis must first be optimised and consolidated. It is therefore the topic of the final chapter to unveil the first LD-pumped LC laser prototype and demonstrate its performance capabilities.

[30] Unpublished at the time of writing. Part of the work towards the doctorate of Ieva Pakamorytė, School of Engineering, University of Edinburgh. Thesis submission expected 2025.

Chapter 7

Developing a diode-pumped liquid crystal laser prototype

"It is truly an amazing feeling when you know that you have built something that no one else ever has – and it actually works."

Donna Strickland

7.1 Introduction

For a new technology to succeed in the consumer market, it must offer an improvement compared to currently available competing technologies. For lasers, this could be, for example, an improvement in cost, size, wavelength range, pulse energy, average power, repetition rate, pulse duration or spectral linewidth, or the ability to combine functionalities that are otherwise mutually exclusive. The principal motivation for achieving LD pumping of LC lasers was to reduce the size and cost of the combined LC laser and pump source, towards commercialising this technology. Having demonstrated LD pumping, and found that optimum LC laser performance is achieved by minimising the pump pulse duration, this chapter exploits the LD pumping breakthrough and wavelength accessibility of LC lasers by developing the world's first diode-pumped LC laser (DPLCL) prototype. The expectation is that the device will be significantly smaller and cheaper than, for example, supercontinuum lasers and OPOs, whilst improving upon the previous examples of LC laser demonstration systems and improving upon the wavelength limitations of Q-switched lasers and LDs.

The design process is described and exemplified using computer aided design (CAD) and the engineering challenges are presented towards demonstrating a compact, portable and low-cost DPLCL. Optical and optomechanical components were selected to optimise LC laser performance whilst ensuring that the small footprint and low cost criteria were fulfilled. A spinning cell configuration was incorporated into the prototype design to maximise the average power output. Experimental results obtained from testing the completed prototype are presented and the results from a preliminary investigation in which the prototype was applied to fluorescence imaging are reported.

The development of the first diode-pumped LC laser prototype device presented in this chapter is published in the proceedings of SPIE *11987, Laser Resonators, Microresonators, Beam Control XXIV*, vol. 1198703, no. March, p. 12, 2022; "Advancing multi-wavelength liquid crystal laser microcavities in a compact prototype device using a laser diode pump source".

7.1.1 Competing laser technologies

This section provides a brief summary of laser systems with similar attributes to LC lasers. This was conducted to identify competing technologies and gaps in the market that LC lasers have the potential to fill.

It is difficult to compare the cost of different of laser systems, as most manufacturers do not provide this without a specific enquiry. However, laser performance parameters can be obtained. Table 7.1 provides examples[31] of tuneable/wavelength-selective pulsed laser systems, based on different technologies, such as solid-state lasers, dye lasers, supercontinuum sources and optical parametric oscillators. These lasers are capable of producing pulse energies in the mJ regime, often across a broad tuning range. However, this comes at the expense of size, complexity and cost. Most of the lasers in Table 7.1 would not be considered portable and require separate power supplies, controller units and water cooling apparatus. As a rough estimate, based on a discussion with a laser sales representative[32], the lasers in Table 7.1 range from tens of thousands to hundreds of thousands of pounds.

[31] This is by no means an exhaustive list; its purpose is simply to highlight the range of high-performance lasers available at the time of writing, for comparison to other technologies, including LC lasers.
[32] Conversation with Elaine Blackwood from Photonic Solutions Ltd, September 2018.

Table 7.1. Specifications of tuneable laser systems available on the market (as of July 2022). Note that this is a very limited selection and is provided simply to give examples of the lasers available.

Manufacturer	**Model**	**Dimensions (mm)**	**Wavelength Range (nm)**	**Pulse Energy (mJ)**	**Repetition Rate (kHz)**	**Variable Repetition Rate**	**Pulse Duration (ns)**	**Pulse Duration Selectivity**	**Laser technology**
Quantel	*QF-Qxy24-ILO(4)*	137 × 76 × 38	808, 915, 940, 980	< 2	< 6	Yes	80 – 130	Yes	Multiple laser diodes
Sirah Lasertechnik	*Credo Ti:Sa-10kHz*	650 × 494 × 280	690 - 950	0.68	3 - 10	Not given	28 - 50	Not given	Q-switch-pumped solid state laser
Sirah Lasertechnik	*Credo Dye Laser*	1110 × 537 × 312	380 - 920	< 1.05	< 10	Not given	4 – 35	Not given	Dye laser
OPOTEK	*Opolette 355*	305 × 178 × 124	410 - 2400	< 9.4	20	No	5	No	OPO
NKT Photonics	*SuperK Compact*	220.5 × 93 × 367	450 – 2400	Not given	0.001 – 20	Yes	< 2	No	Supercontinuum

An alternative to the high-performance tuneable pulsed systems in Table 7.1, is individual laser systems with fixed wavelengths, such as the Q-switched lasers developed by CrystaLaser. These lasers offer repetition rates from 1 – 100,000 Hz, and wavelength-dependent fixed pulse durations of 10 – 40 ns and pulse energies of 0.2 – 600 μJ. The lack of tuning capability of these lasers compared to those in Table 7.1 enables a smaller footprint (85 × 50 × 36 mm for the CrystaLaser systems), passive cooling and a lower cost. However, this is typically accompanied by a reduction in output energy and, in some cases, range of repetition rate. Furthermore, there are large gaps in the wavelengths available, for example in the yellow – red region of the spectrum between 532 and 657 nm (Figure 7.1).

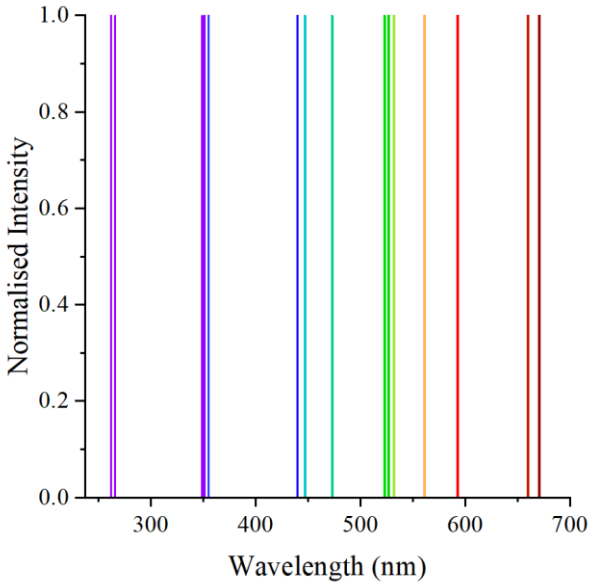

Figure 7.1. Available wavelengths from the Q-switched laser manufacturer, CrystaLaser.

A lower cost and smaller scale alternative to fixed wavelength Q-switched lasers is LDs, such as the 445 nm LD used as the pump source in this thesis. At centimetres in size (including driver circuitry), and at a consumer cost < £100, with the ability to emit wavelengths ranging from 375 nm to 3,330 nm, LDs offer many advantages over more complex systems [140]. However, the wavelengths within this range are discrete and, again, do not cover wide regions of the visible spectrum, particularly in the same range as with Q-switched laser technology (Figure 7.2).

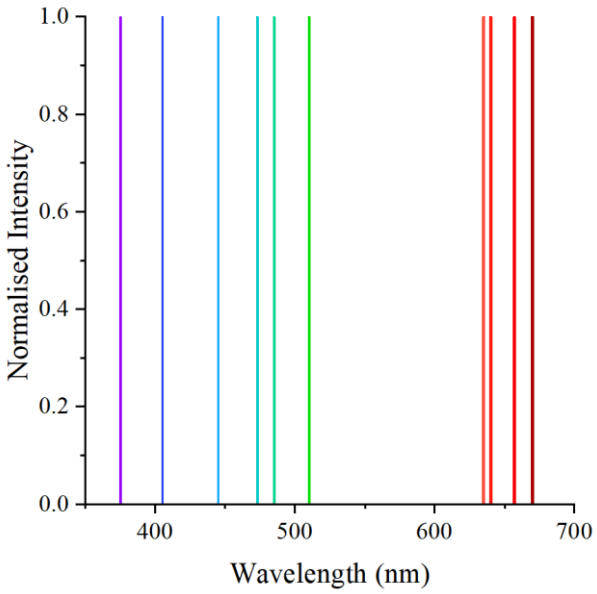

Figure 7.2. Common LD wavelengths in the visible range of the spectrum [140].

7.1.2 Summary of previous LC laser demonstration systems

There has been limited historical success in demonstrating LC laser-based devices. A portable LC laser demonstration system, based upon a Q-switched pump source, was demonstrated by Hands *et al.* in 2012, in which wavelengths spanning 450 – 850 nm were achieved using a gradient pitch LC laser cell on a motorised linear translation stage (Figure 7.3a) [40]. This had a smaller footprint than the two examples below, but did not have a spinning cell arrangement, so the repetition rate was limited to < 5 kHz.

Varanytsia *et al.* published a paper entitled "Small footprint cholesteric liquid crystal laser" in 2019, in which a Q-switched laser was used to pump LC laser cells (Figure 7.3b) [42]. The Q-switched pump was a simplified 1064 nm laser, which required a frequency doubling crystal to produce 532 nm. The dimensions of the pump were 24 × 40 × 105 mm, but when the frequency doubling crystal and beam steering mirror were added, this increased the footprint to 170 × 40 mm. This was *before* taking into account the LC laser cell and its associated alignment and focussing optics. Moreover, this arrangement required a 900 V power supply and custom-built pulsing circuitry, and had a repetition rate of just 1 Hz. No cost was provided for the assembly of the pump source and LC laser, nor for the associated optics.

A Q-switch-based demonstration unit was built by M. Normand, also in 2019, in which the pump could be swapped between a 440 nm Q-switched laser and a 532 nm Q-switched laser [41]. This incorporated a spinning cell arrangement and was capable of producing 3.5 mW of average power (the highest published power thus far) with a pump repetition rate of 10 kHz. It also demonstrated colour-switching at different wavelengths. The cost of this system, however, was > £20,000 (440 nm pump) and > £10,000 (532 nm pump) and required multiple power sources for the pump laser, spinning cell arrangement and microcontroller. The laser head (Figure 7.3c) had a footprint of 250 × 190 × 100 mm and a separate power supply unit of a similar size.

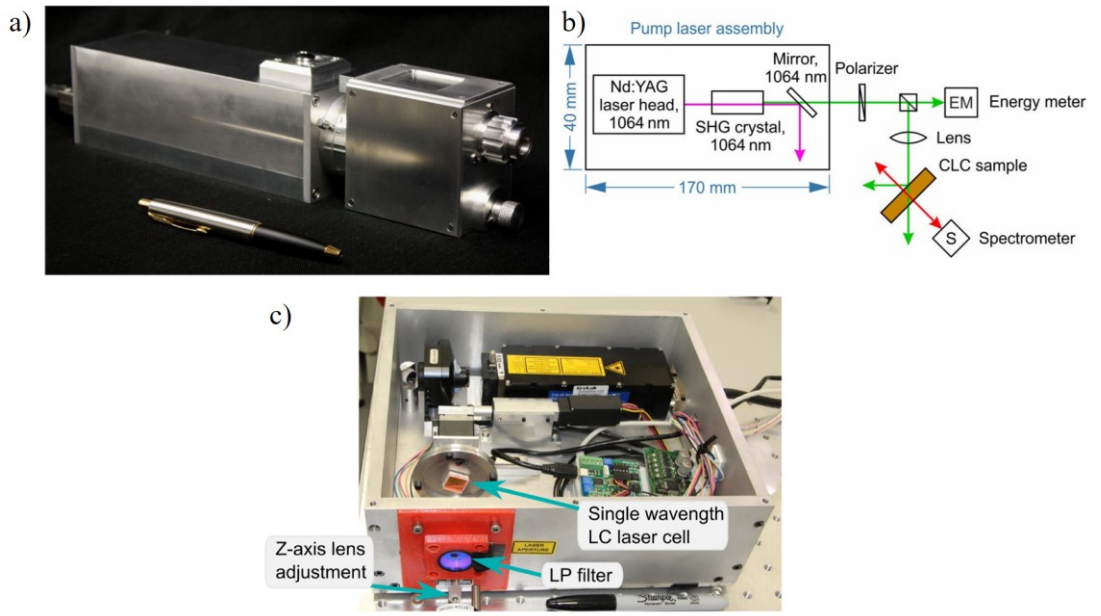

Figure 7.3. Previous portable/small-footprint LC laser demonstration systems, all based on Q-switched pump sources. a) is taken from Ref. [40] *, b) from Ref.* [42]*, and c) from Ref.* [41].

As yet, there has been no evidence of an inexpensive, compact LC laser device, capable of producing laser emission across the visible spectrum at repetition rates > 10 kHz.

7.1.3 Aims & design criteria

The primary aims of this work were, firstly, to design and manufacture a low-cost, portable LC laser system and, secondly, to demonstrate this in an application-based setting. To achieve this, the following objectives were set, whereby the prototype device would be designed to:

1. Utilise LD pumping;
2. Be as high-power as possible, to maximise visual effect, whilst also complying with laser safety regulations for public demonstration without the use of safety goggles;
3. Be capable of producing wavelengths spanning the visible range;
4. Be sufficiently small to fit on a desktop for demonstration at trade shows, conferences and to external stakeholders;
5. Be smaller (and/or more functional) than previous LC laser demonstrator systems;
6. Demonstrate a unique combination of capabilities not seen in competing laser systems;
7. Be a flexible platform, compatible with potential future upgrades and capable of integration with alternative pump sources;
8. Be capable for subsequent application in a variety of fields such as biomedical imaging, fluorescence microscopy, holography etc.

7.2 Prototype design

7.2.1 Performance requirements

To fulfil design objectives 1, 2 and 3, the 445 nm LD used in previous chapters was utilised for this work, at a repetition rate maximised to produce a high average power whilst minimising the risk of damaging the laser cell. At repetition rates > 10 Hz, performance degradation occurred. For the highest pump pulse energy of 100 nJ/pulse at a pulse length of 11 ns, assuming a 5 % slope efficiency based on experimental evidence, at this repetition rate the average output from form an LC laser was 50 nW. An increase in repetition rate by at least three orders of magnitude was required to compensate for the modest pulse energy, to achieve average powers in the microwatt regime. This power was desirable as it has been shown to be sufficiently high to generate fluorescence images [23], [141], and could therefore fulfil the

final design objective. A spinning cell configuration was therefore incorporated into the prototype design to enable a high repetition rate output [13].

The LD driver electronics specifications state that the maximum achievable repetition rate is current and pulse length dependent, and is higher in the presence of an active cooling system. For the highest current (15 A) and the longest pulse duration (100 ns) used in this work, the electronics can deliver the maximum repetition rate (2 MHz) without the need for active cooling. The evidence presented in the previous chapters has highlighted the preference of minimising the pump pulse duration for maximising LC laser performance. Therefore, assuming that the pump pulse duration never exceeds 100 ns, a cooling mechanism is only required when using a current of 50 A at a repetition rate > 10 kHz. In anticipation of such a scenario, an active cooling mechanism was considered for the prototype to prevent overheating and irreversible damage to the electronics. The electronics do not have an integrated cooling mechanism, and passive cooling via contact with a heat sink is not possible due to the air gap between the electronics and base plate onto which they are mounted. Therefore, an active mechanism, such as a fan, was desirable.

The combination of a compact size and broad wavelength range of LC lasers is arguably their most compelling feature in comparison to other tuneable laser systems. The ability to demonstrate this wavelength selectivity was therefore a key feature for including in the prototype. This required a quarter-waveplate if the 445 nm pump wavelength overlapped with the N*LC bandgap.

Although the purpose of the prototype was to demonstrate LD pumping, optional use with other pump sources was considered advantageous for highlighting the capabilities of LC lasers. For example, an application may require a wavelength uniquely deliverable by the LC laser, but at a higher pulse energy than possible with the LD. Easy replacement of the pump source with minimal disruption to the optical layout was therefore considered a necessary feature of the prototype design. Easy access to all optical components was also required, as optics such as the dichroic mirror would need to be replaced to accommodate a change in pump wavelength.

The design criteria are summarised in Table 7.2.

Table 7.2. Specification criteria for the LCL prototype.

Prototype Feature	Specification Target
Primary pump source	Laser diode
Emission wavelength	Selectable across visible spectrum > 445 nm
Polarisation control	Adjustable quarter-waveplate
Repetition rate	> 10 kHz
Average power	≥ 10 μW
Peak power control	Current
Dimensions	Minimised
Weight	Minimised
Specific design features	Modular design with easy access to optics Active cooling mechanism

7.2.2 Laser diode pump and driver electronics

The 445 nm Nichia LD and the PicoLAS driver electronics introduced in Section 4.4.1 were selected for use in the prototype. The LD pump had been shown to enable LC laser emission across much of the visible spectrum and the electronics were capable of delivering the high currents and nano-scale pulse durations required to overcome LC laser threshold, in a compact package. Both were therefore incorporated in the design of the prototype and fulfilled the design objective of building a prototype with an LD pump source.

7.2.3 Liquid crystal laser configuration

On-axis pumping was used throughout this thesis, whereby a dichroic mirror was used to reflect the pump beam onto the LC laser cell and transmit the resultant LC laser emission. The alternative, off-axis configuration, removes the need for a dichroic mirror, but requires an additional lens to focus the LC laser and a beam dump to absorb the reflection of the pump beam from the LC laser cell. Both arrangements (Figure 7.4) were considered for the prototype.

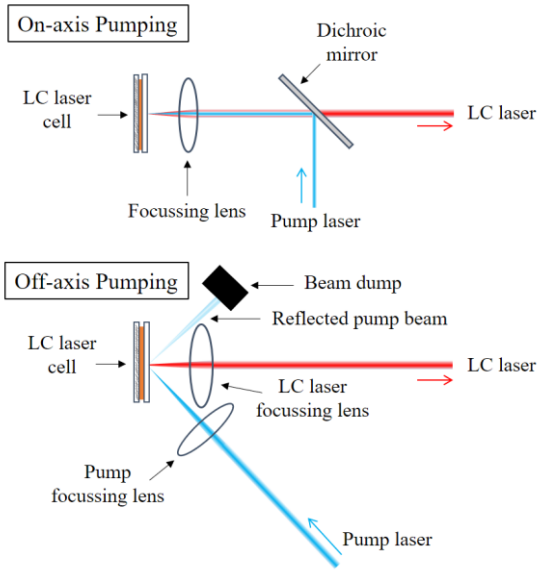

Figure 7.4. On-axis (top) and off-axis (bottom) pumping configurations.

Although an aspheric lens is typically less expensive than a dichroic mirror, the proximity of the two lenses relative to the laser cell can make this configuration awkward. It was therefore decided to use the on-axis configuration in the prototype, which had been successfully demonstrated in the bench-top experimental arrangements.

The use of a dichroic mirror with the on-axis configuration meant that, if this were the only mirror used to steer the pump beam, the pump source would need to be perpendicular to the output beam (Figure 7.5a). Consequently, pump beam alignment could not be optimised by adjusting the *xy* axes of the dichroic, as this would require access to the dichroic during operation which would present a laser safety hazard. An additional mirror was therefore included in the design that was mounted in an adjustable mirror mount to enable safe adjustment of the pump beam position (Figure 7.5b).

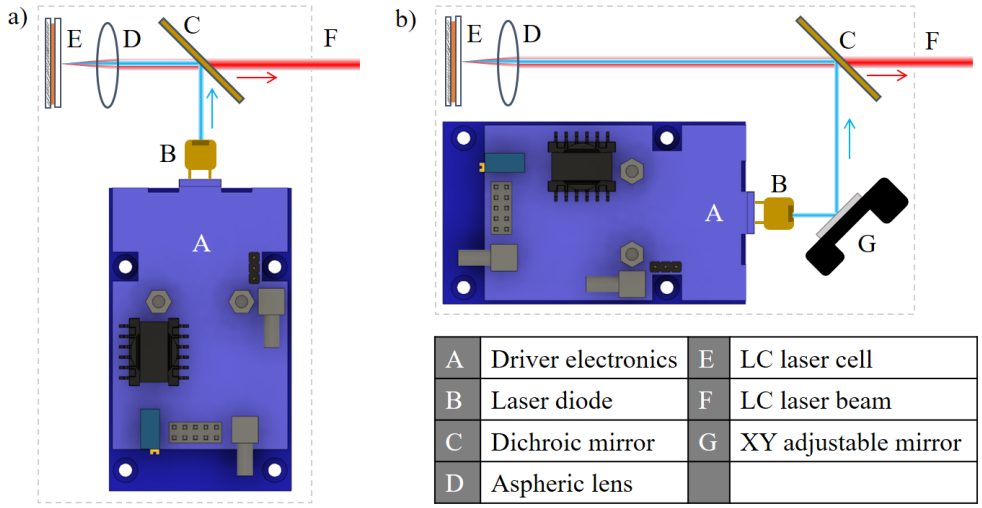

A	Driver electronics	E	LC laser cell
B	Laser diode	F	LC laser beam
C	Dichroic mirror	G	XY adjustable mirror
D	Aspheric lens		

Figure 7.5. Configuration of pump source relative to LC laser cell comparing a) a perpendicular arrangement with b) a parallel arrangement with a beam-steering mirror.

7.2.4 Optical components

The first demonstration of the LD pumping used a microscope objective to focus the pump beam and the resultant LC laser beam from the reflective laser cell. This was because the experimental arrangement had multiple uses, including using a white light source to measure the bandgap. However, with a weight of 0.64 kg, and larger and more expensive than the LD driver electronics, inclusion of the microscope objective in the prototype would not have fulfilled the design objective of developing a small footprint and low-cost device. An alternative to the microscope objective was therefore sought, that could focus the pump beam to a spot small enough to achieve the fluence required for LC lasing, in a compact and inexpensive package. The focal length of the lens also had to be minimised to reduce the size of the device.

Spherical lenses were first tested with focal lengths of 15 mm (*LA1540-AB*) and 25.4 mm (*LA1951-AB*). However, only amplified spontaneous emission was achieved, with the emission dominated by fluorescence. It could be seen by eye that the pump spot at the focus appeared to be distorted and was not as small as with the microscope objective. This was likely due to the simplicity of the lenses, as the multi-element design of the microscope objective compensated for optical distortions such as spherical aberrations that the single spherical lenses could not [142]. This can be seen in the top 2D ray diagram (*WinLens3DBasic, v1.2.11*) of Figure 7.6, in which the peripheral rays are focussed closer to the lens than the central rays.

The spot size is therefore larger (and the fluence is therefore smaller) at the focus than if all rays were focussed at the same point.

A single-element aspheric lens can be used to achieve improved focussing compared to a spherical lens. The more complex shape of the lens corrects for spherical aberrations, resulting in a smaller focus spot. This is shown in the bottom diagram of Figure 7.6, in which an aspheric lens (with the same focal length as the spherical lens) is simulated. The geometrical difference in the lenses can be seen to affect how well the light is focussed.

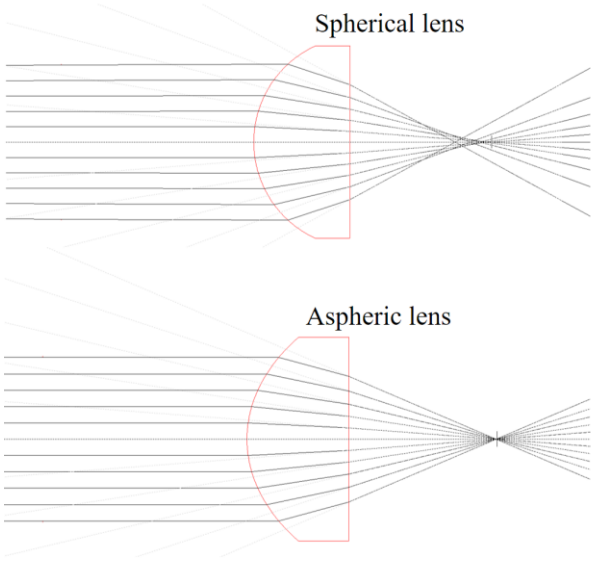

Figure 7.6. Comparison between a spherical lens (top) and aspheric lens (bottom), showing the effect the lens shape has on the lens' ability to focus.

As the most compact solutions were desired for building the prototype, two aspherical lenses with focal lengths of 8 mm *(ACL108U-A, Thorlabs)* and 10.5 mm *(ACL1210U-A, Thorlabs)* with diameters of 10 mm and 12.0 mm respectively were selected for testing. Each one was positioned in front of the LC laser cell, which was mounted on the *xyz* stage. Whilst undergoing pumping, the cell's *z*-axis position was adjusted and the LC emission signal was observed on the spectrometer. LC laser emission was detected at the optimum *z*-axis position for both aspheric lenses. The only apparent difference was the sensitivity to the *z*-position; the 8 mm focal length lens was the more sensitive, with a change < 10 µm determining whether the fluence was sufficiently high to overcome LC laser threshold. The 10.5 mm focal length lens was also sensitive to its position relative to the laser cell along the *z*-axis, but to a lesser extent. This behaviour was to be expected because of the small depth of focus associated with short

focal length lenses. By simulating the cross section of a circular laser spot at different positions along the *z*-axis (Figure 7.7), the difference in spot area can be seen for different aspheric lens focal lengths.

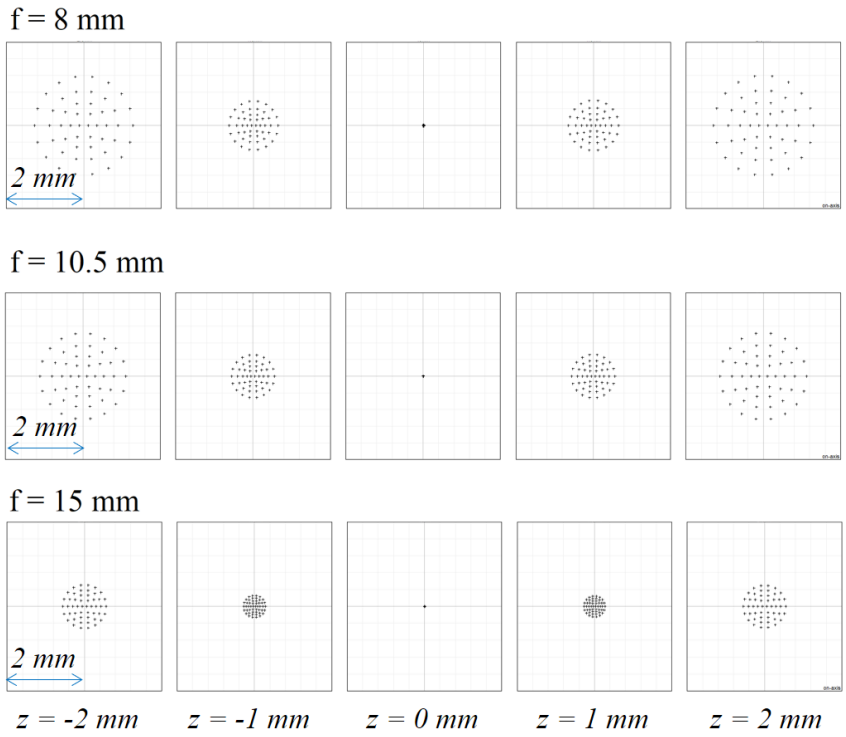

Figure 7.7. Spot size of circular laser profile at different z-axis positions for the 8 mm lens (top) and 10.5 mm lens (middle) with a 15 mm lens (bottom) simulated for comparison, highlighting the smaller depth of focus with decreasing focal length.

The sensitivity to cell-lens spacing for producing LC laser emission could have been reduced further by using a lens with a longer focal length. However, for minimising the prototype footprint, the 10.5 mm focal length lens was selected. The larger depth of focus of this lens compared to the 8 mm focal length lens was also expected to compensate for any changes in cell-lens spacing during operation (e.g. changes caused by vibrations from the motor). The spot size of the LD at the focal point of the 10.5 mm lens was measured using the knife-edge technique (Section 3.3.3) and found to be 41.6 (± 0.2) µm in the *x*-axis and 24.4 (± 0.8) µm in the *y*-axis.

When operating in an on-axis pumping configuration, the lens not only had to focus the pump spot onto the LC laser cell, but ideally it would also collimate the LC laser output emission; the lens would be chosen such that the converging LD rays would match the divergence of the

LC laser output. However, to maximise the fluence (and thus the output intensity of the LC laser beam), minimising the spot size at the focus was the priority. Should the lens be insufficient for collimating the LC laser emission, additional optics would be required at the output of the device.

In all of the experimental arrangements presented thus far, three polarisation optical components have been used: a half-waveplate to control the intensity of the linearly polarised pump beam by rotating the plane of polarisation relative to a Glan-Taylor linear polariser; and a quarter-waveplate to convert the linearly polarised pump beam to circular polarisation and thus mitigate pump beam reflection by the N*LC photonic bandgap (Section 3.3.1). One of the benefits of the LD pump source was the ability to control the pulse energy via the current delivered by the driver electronics. This eliminated the need for the half-waveplate and Glan-Taylor polariser; saving space and cost and reducing the optical losses. A half-inch quarter-waveplate *(WPQ05ME-445, Thorlabs)*, coated for 445 nm, was selected for integration with a manually adjustable rotation mount *(RSP05/M, Thorlabs)*. Additional waveplates with different anti-reflective coatings would be required if an alternative pump source with a different wavelength were to be used with the LC laser module.

7.2.5 Spinning cell requirements

A spinning cell was required to maximise the repetition rate and hence the average power of the DPLCL prototype. This required a motor to which the laser cell had to be attached. There were two motors considered for spinning the cell. The first was a DC motor *(MM10, Multicomp Pro)* and the second, a stepper motor *(4416, Adafruit)*. Before the motors were tested, the motor requirements were considered, based on the maximum possible repetition rate that could be achieved within the performance limitations of the driver electronics and LC laser cell performance parameters.

The *effective repetition rate* is defined as the frequency at which a particular cell position is pumped as it is spun. This therefore defined the frequency at which the motor needed to rotate to ensure consecutive pump spots did not overlap. As previously discussed, for a static cell, a repetition rate exceeding 10 Hz was shown to result in LC laser performance degradation caused by the relatively long pulse duration limited by the driver electronics. Therefore, a

spinning cell would need to rotate ten times per second for the same position of the cell to be pumped at an effective repetition rate of 10 Hz, i.e. the motor would need to spin at 600 rpm.

To determine the repetition rate of the pump permissible with this spinning cell, the cell dimensions and the pump spot diameter were considered. The cells used in this work had dimensions of 15 × 15 × 6 mm. Once the spacer-glue lines were applied to bond the substrates together, the active area of the cell was reduced to approximately 12 × 12 mm. For a spinning cell, this resulted in a maximum lasing circle or 'pump ring' of circumference 37.7 mm. The short-axis diameter of the elliptical LD pump spot after the aspheric lens was 25 µm. Therefore, a maximum of 1508 spots in one rotation could undergo optical excitation without overlapping. Thus, for an effective repetition rate of 10 Hz, the motor would need to rotate at 600 rpm, and a spot size of 25 µm would enable a repetition rate of 15 kHz[33]. This is summarised in Figure 7.8 and was used to determine the specifications required for the motor.

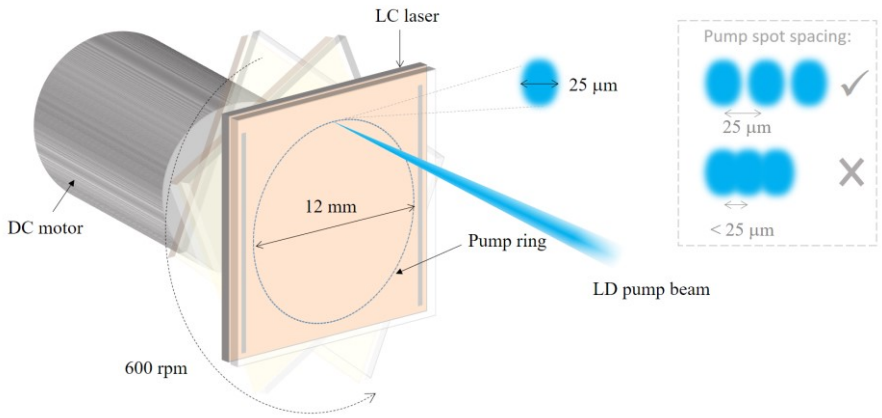

Figure 7.8. Spinning cell on a DC motor showing the relative dimensions of the active area of the cell and long-axis of the elliptical spot size.

DC motors are often used in hobby kits, as they are inexpensive and easy to use. Their speed can be controlled with pulse width modulation (PWM) or simply by adjusting the applied voltage. Their mechanical and electrical simplicity enables high revolutions speeds with little associated noise; both desirable properties for spinning the LC laser cells. However, they do not have the ability to record their position. For example, if a laser cell contained multiple regions, each with a different DDN*LC mixture for generating different laser wavelengths, a

[33] This differs from the 20 kHz rep rate published in Ref. [146], in which the microscope objective was used to focus the pump beam to a smaller spot, thus enabling more spots per rotation, compared to the arrangement here with the aspheric lens.

DC motor could not be programmed to move to a specific wavelength, without additional sensors.

One solution is to use a stepper motor with an encoder. A stepper motor moves in discrete steps with a pre-defined resolution, by using PWM to control the motor's speed. The encoder enables the precise location of the motor's position to be identified, and the exact rpm value at any given time to be known, based on a pre-defined reference point.

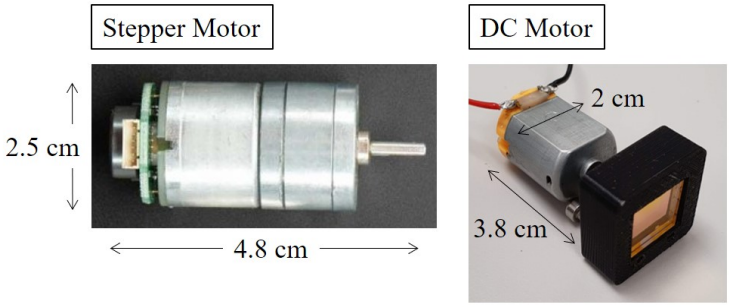

Figure 7.9. Stepper motor and DC motor used for comparing motor performance parameters. An LC laser cell is mounted in a 3D-printed cell holder and attached to the shaft of the DC motor.

A DC motor and a stepper motor were tested to determine which was the more suitable for use in the prototype. Each was selected based on minimising size and cost. A 3D-printed LC laser cell mount was made to attach to the shaft of each motor and an Arduino microcontroller was connected to a motor driver PCB to control the DC motor (see Section 7.2.8). The Arduino was also used to control the stepper motor with PWM.

It was immediately apparent that the stepper motor was significantly noisier than the DC motor, as well as being larger and heavier. The maximum speed of the stepper motor was 350 rpm, as measured by the encoder, which is lower than the target requirement of 600 rpm. A magnet was attached to the shaft of the DC motor to use with a Hall sensor for comparing its speed to the stepper motor. The supply voltage was controlled via a potentiometer and, when maximised, resulted in a speed of > 2,500 rpm.

The DC motor was selected for use in the prototype, as it was able to exceed the required revolution speed, it generated very little noise, and its compact size and less complex electrical configuration were more suitable for the fulfilling the cost and size requirements of the device.

7.2.6 Cooling mechanism

The maximum repetition rate possible using the spinning cell was 15 kHz. The LD driver specifications stated that a repetition rate of 15 kHz was not sufficiently high to warrant active cooling. If 100s of kHz or MHz repetition rates were realised in the future, by improvements in the materials or larger spinning cells for example, then thermal damage could pose a risk to the LD and electronics. An active cooling mechanism was therefore desirable in anticipation of this improved performance.

Cooling mechanisms such as water-cooling and thermoelectric cooling are often used to remove heat from a laser cavity. However, as cooling was not essential for the proposed DPLCL configuration, these options were rejected as they would have added to the cost and complexity of the prototype. A small fan *(F310R-05LC, Farnell)* was selected instead as the active cooling mechanism. Not only was it small enough not to impact the device dimensions, but its low power consumption meant that it did not require its own power supply and could be powered via the supply for the driver electronics.

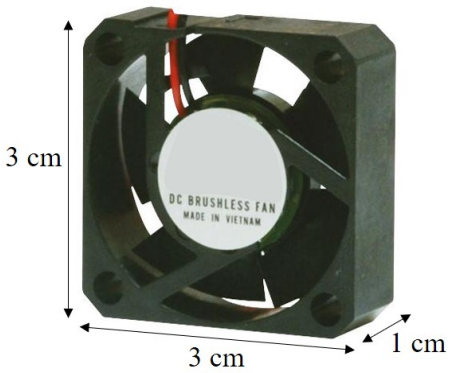

Figure 7.10. Small 5 V cooling fan used in the prototype in anticipation of higher repetition rate pumping.

7.2.7 Cell mounting and adjustment

The optical bench-top arrangement used throughout the work in this thesis used a 10 μm precision *xyz* stage mounted with the LC laser cell, in order to control the cell's position relative to the focussing lens. This enabled different cell positions to be tested for measuring thresholds, efficiencies, wavelength variation etc. by manually adjusting the *xy* axes, while the

position relative to the focal point of the pump beam was optimised with the *z*-axis adjustment. A similar system for adjusting the cell position was required for the prototype.

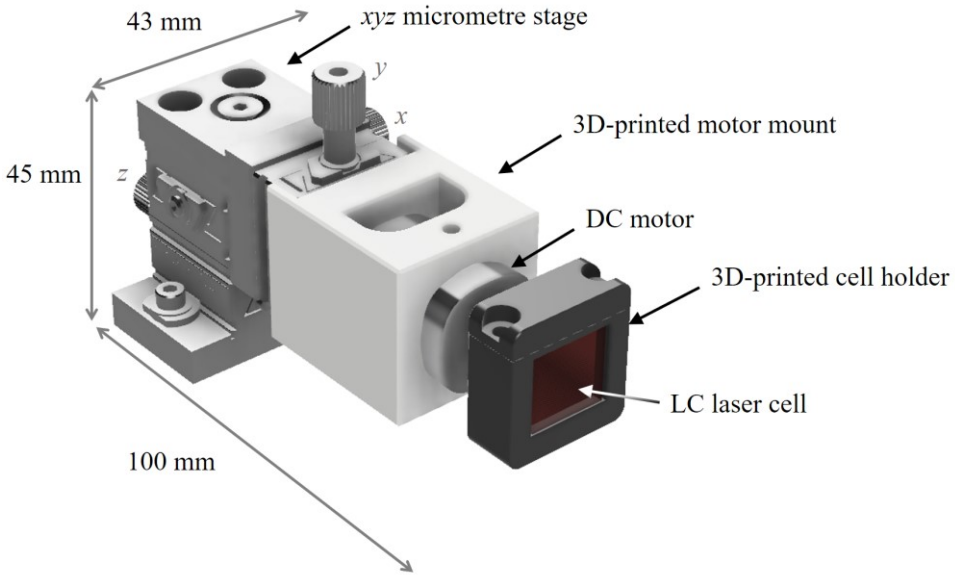

Figure 7.11. 3D rendering of xyz micrometre stage for adjusting the LC laser cell relative to the focussed pump beam. The 3D-printed motor mount and cell holder are shown, securing the motor and LC laser cell respectively.

An off-the-shelf *xyz* stage *(DT12XYZ/M, Thorlabs)* was a compact solution for positioning the LC laser cell, with a range of travel of 12.7 mm in all three axes (Figure 7.11). This allowed the full area active area of the LC laser cell to be pumped, given that the diameter of the pump ring was 12 mm. The design of the prototype had to be such that the adjustment thumbscrews could be easily accessed during operation to optimise the cell position (Section 7.2.9.3). 3D-printed parts were custom-built[34] to secure the motor onto the *xyz* stage and to secure the LC laser cell to the motor shaft. The top section of the LC laser cell holder was removable to allow the LC laser cell to be easily replaced, either for changing the emission wavelength or for replacing a fatigued/damaged cell (Figure 7.12). A spring was incorporated into the design to minimise movement of the cell inside the holder when spinning.

[34] The two 3D-printed parts were built with the assistance of Mark Mason from the mechanical workshop, University of Edinburgh.

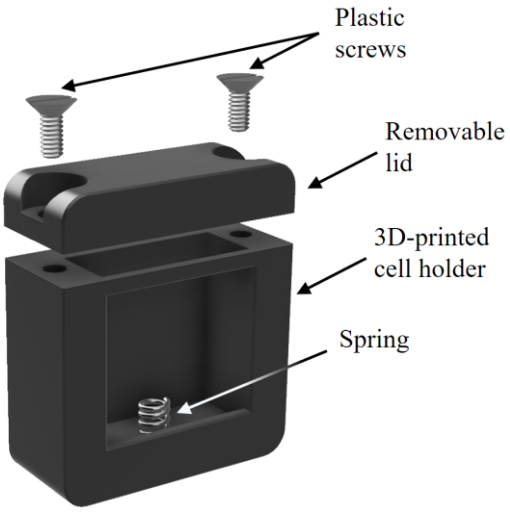

Figure 7.12. Exploded-view drawing of 3D-printed LC laser cell holder

7.2.8 Electrical design[35]

7.2.8.1 Electronics system control

Having established the suitability of a DC motor (*MM10, Farnell)* for the spinning cell configuration, the control system for the motor and LCD was designed. The purpose of this was to allow the user to control the motor speed, while also being able to monitor the rpm output displayed on an LCD. A motor driver *(102514, Cytron)* was incorporated with an Arduino Nano microcontroller (*ABX00033, Arduino*) to regulate the 6 V supplied by 4 × AA batteries. This voltage was varied with a potentiometer to control the speed of the motor. A Hall sensor (*WAV-9522, Waveshare*) was connected to an Arduino Uno microcontroller (*A000066, Arduino*) and used to measure the rotational speed of a magnet attached to the motor shaft as a function of the potentiometer rotational position. With the speed of the motor calibrated for a given potentiometer position, the Arduino Nano was programmed to display the speed on the LCD. The code for the Arduino Nano and Arduino Uno is given in Appendix I.

[35] The majority of the work in Section 7.2.8 was outsourced. The power supply and distribution were designed and built by Richard Scott, Iain Gold and Jamie Graham – all of whom are staff in the electronics workshop at the University of Edinburgh. The design and component selection for the motor control was based on conversations with Iain Gold, and the programming of the Arduino Nano and Arduino Uno was carried out with the assistance of Ieva Pakamorytė.

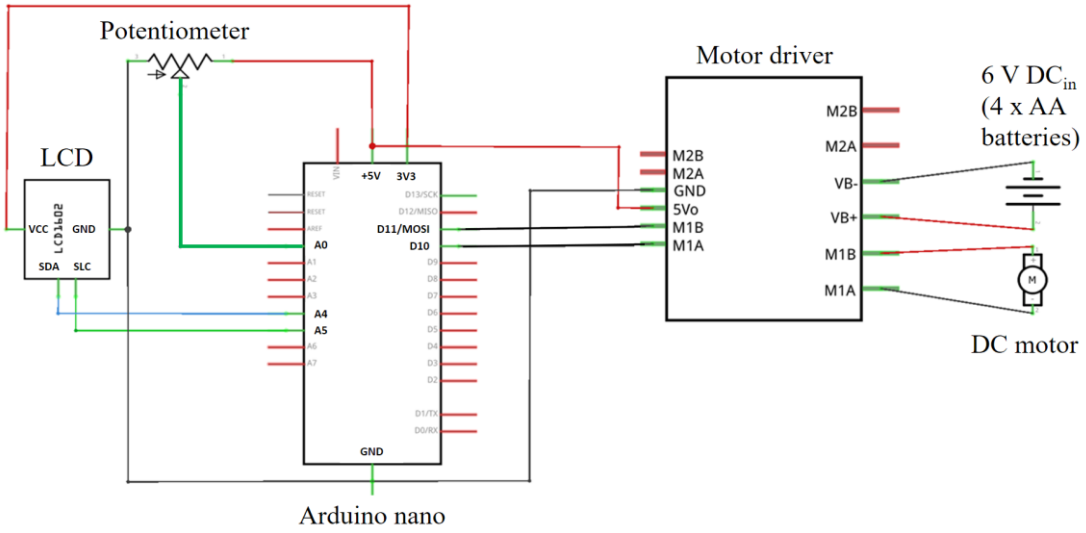

Figure 7.13. Electronic schematic showing the circuitry used to regulate the voltage supplied to the DC motor, with the potentiometer used control the motor speed and the resultant rpm displayed on the LCD.

Figure 7.13 illustrates the electrical layout of the control circuitry for varying the speed of the DC motor and displaying the speed in rpm on the LCD. The AA batteries powered the DC motor and LCD via the motor driver and Arduino Nano.

7.2.8.2 Power supply

In addition to the motor, the LD driver electronics and the cooling fan required a power source. The fan needed a 5 V supply and the driver electronics required a 15 V supply which also powered the LD controller unit. The electronics were designed such that a single supply could be used to power both the driver electronics and the fan. A series of Zener diodes was used to distribute the mains voltage between the fan and driver electronics, with minimal disruption to the supply required for the driver electronics. The power to all electrical components in the prototype was distributed through a PCB (Figure 7.14).

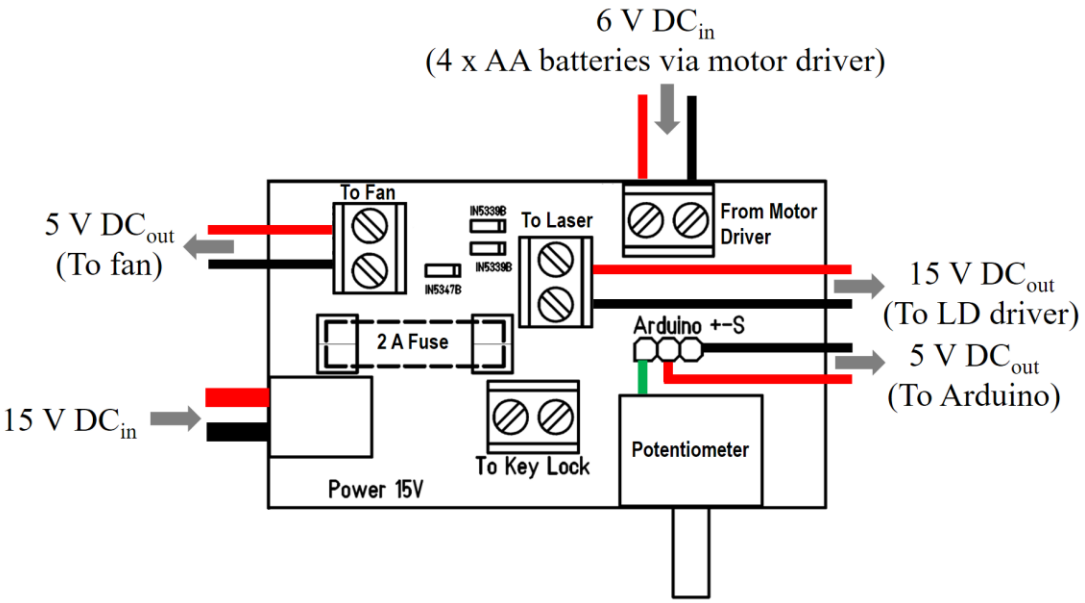

Figure 7.14. Power distribution PCB for all electrical components in the LC laser prototype. (PCB design courtesy of Richard Scott and Iain Gold, electronics workshop, University of Edinburgh).

The PCBs and power supplies were designed to be housed in a control module separate from the laser as this would minimise the size of the laser. Moreover, some applications require lasers to be controlled from a distance, for example, outside an optical enclosure or behind a laser safety screen. As an objective of the prototype was to demonstrate its versatility and small footprint, the accompanying electrical control had to also meet these criteria. The electrical configuration was therefore designed to require only one mains power supply, which would power the driver electronics and fan. The component arrangement is shown in Figure 7.15.

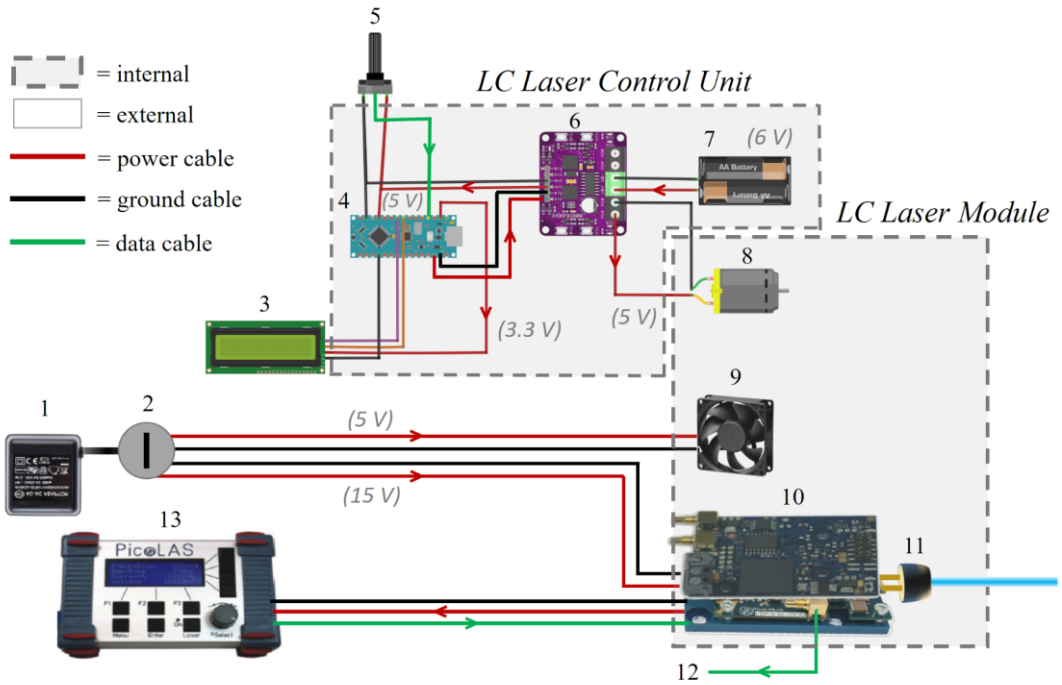

	Part description	Input Voltage (V)	Powered via	Part number
1.	DC power supply	230	**Mains***	-
2.	Key switch	-	-	*S286A-1*
3.	LCD	3.3	Arduino nano	*104056*
4.	Arduino Nano	5	Motor driver	*ABX00033*
5.	Potentiometer	-	-	*102841*
6.	Motor driver	6	**4 x AA batteries***	*102514*
7.	4 x AA battery pack	-	-	-
8.	DC motor	5	Motor driver	*MM10*
9.	Cooling fan	5	DC power supply	*F310R-05LC*
10.	Driver electronics Signal generator	15 15	Signal generator DC power supply	*LDP-V-50-100-V3.3* *PLCS-21*
11.	445 nm laser diode	≤ 100 V	Driver electronics	*NUBM44*
12.	SMA current monitor output	-	-	-
13.	Driver electronics controller	(not known)	Signal generator	PLB-21

* Power sources for other components

Figure 7.15. Pictorial configuration (top) of all prototype components connected to either the mains power supply or the 4 × AA battery supply. (Power distribution PCB not shown to simplify diagram.) The areas in grey contain components located inside the laser module or the laser control module, and the areas in white are external. The table (bottom) provides details of the components, their input voltages, the component through which they are powered, and their part numbers.

7.2.9 Laser head module design

Fusion 360 software (*v2.0.13377, Autodesk)* was used to design the mechanical assembly for the prototype. Fusion 360 specialises in 3D design and allows computer aided design (CAD) drawings by component manufacturers to be imported. This feature was used for creating realistic renderings of design concepts and accurate dimensional analysis of components' positions within the laser modules. This section presents the design considerations that led to the final prototype.

7.2.9.1 Module 1 – laser diode driver electronics and fan

A modular design was desirable for enabling different pump sources to be used with the LC laser cells. The LD pump source therefore had to be easily separated from the beam delivery optics.

Preliminary sketches were made that included the main components required in the prototype in different configurations. One example (Figure 7.16) was for a 'stacked' configuration. This had three modules: the first contained the LD and LD driver electronics (the combination henceforth referred to simply as the LD), the second contained the quarter-waveplate and the mirror on the *xy* mount and the third contained the dichroic mirror, focussing lens, LC laser cell, motor and *xyz* stage. This design fulfilled the objective of developing a compact device, as it had a small footprint of 220 × 80 mm. The LC module could be removed to access the pump and there would be access to the *xy* mirror from the side of the second module during operation to optimise the beam alignment. However, this arrangement would be difficult to integrate with an alternative pump source, and the potential danger of a vertical beam could cause laser safety issues. As the flexibility of using different pump sources was one of the key requirements of the prototype, the stacked option was discarded.

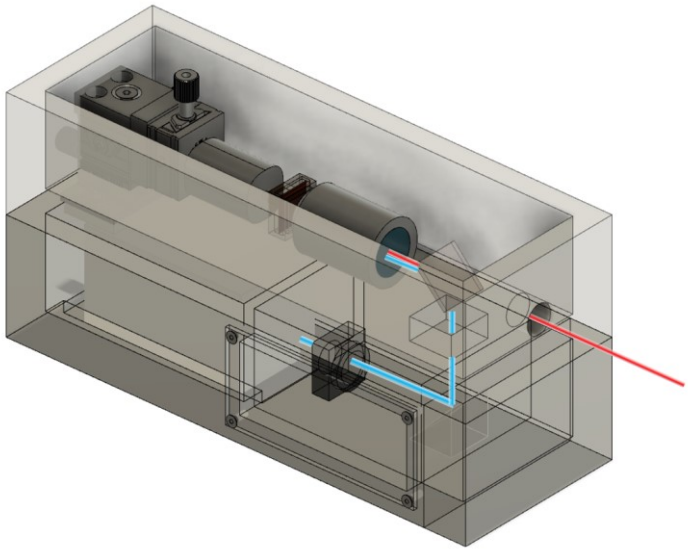

Figure 7.16. One concept for the LC laser prototype for which the LC laser module was stacked on top of the pump source and some of the delivery optics.

The concept of having three separate modules was developed further but with all modules on the same plane. Module 1 again contained the LD but also included the cooling fan. In order to minimise the footprint, the first idea was that the fan would need to be mounted above the horizontally positioned LD, as opposed to behind it (Figure 7.17). However, as access would be required to the LD via a lid, the fan could not be positioned here. Also, if anything were accidentally dropped inside the fan from above it could cause permanent damage to the electronics underneath.

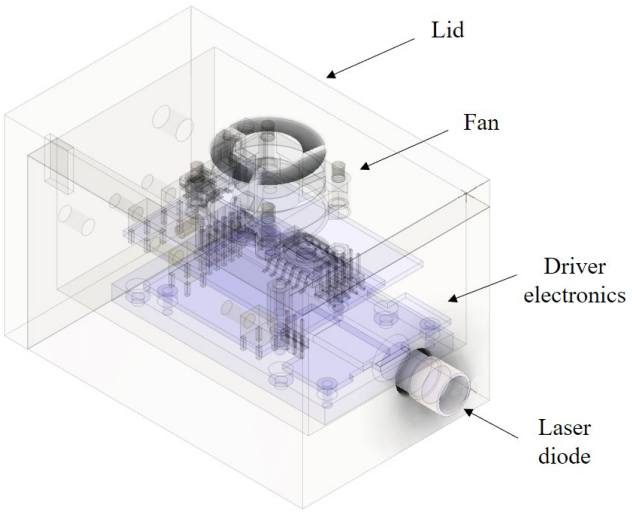

Figure 7.17. Concept for LD module with electronics mounted horizontally on the bottom and the fan positioned on the lid above.

An alternative solution was designed in which the electronics were mounted on the inner side face of the module with the fan on the opposite side (Figure 7.18). The module was also designed such that the sides were removable for mounting the electronics. This can be seen in the plan view in Figure 7.18, whereby the sides are formed by two L-shaped components. The base of the module was designed to contain a recess for a table clamp to secure the module to an optical bench. The LD was designed to protrude from Module 1 for easy access to the LD lens for adjusting the focus.

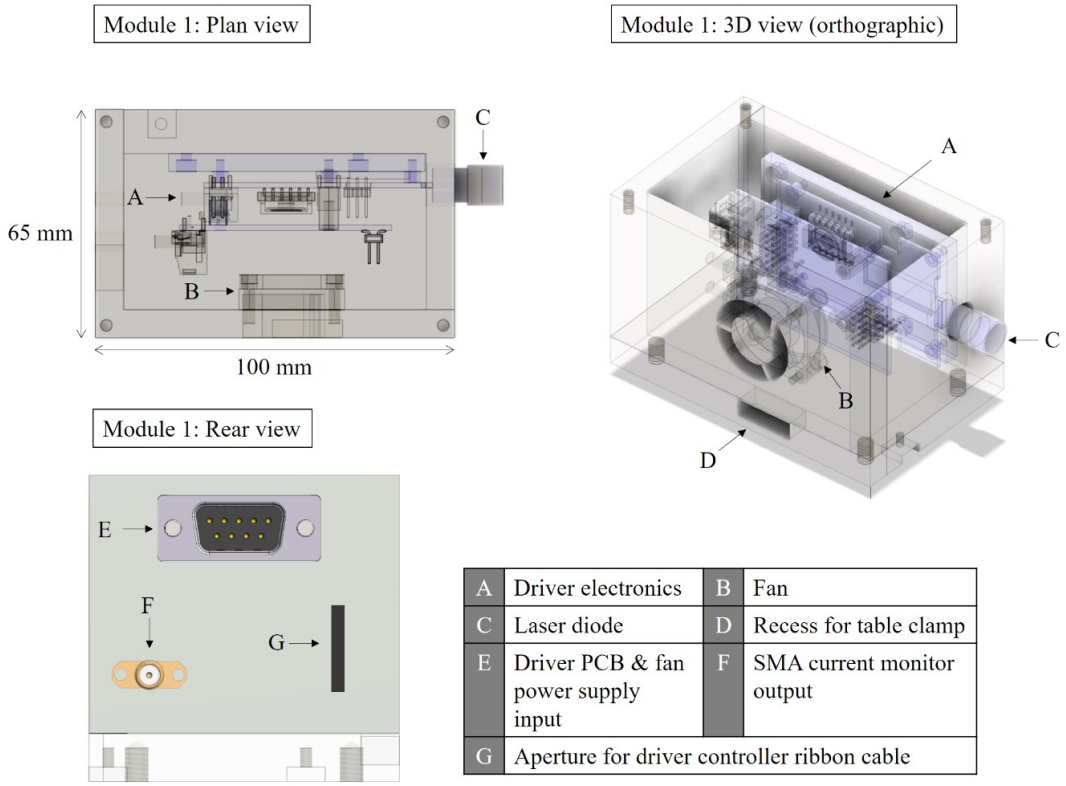

A	Driver electronics	B	Fan
C	Laser diode	D	Recess for table clamp
E	Driver PCB & fan power supply input	F	SMA current monitor output
G	Aperture for driver controller ribbon cable		

Figure 7.18. Plan view and orthographic 3D view of revised design of Module 1, in which the driver electronics are mounted on the inside side face with the fan on the opposite face. The rear view shows the electrical connections to the power supply, current monitor and driver controller.

7.2.9.2 Module 2 – polariser, beamsplitter and mirror

A concept for the second module, Module 2, was to include all remaining components i.e. the beam delivery optics, LC laser, motor and *xyz* stage. However, this again limited the flexibility for use with a different pump source. It also limited future experiments that might require more space between the beam steering optics and the LC laser, for example, for additional

polarisation control. It was decided that Module 2 would be designed to control the alignment and polarisation of the LD beam and a third module, Module 3, would contain the LC laser. Module 2 (Figure 7.19) was designed to include the quarter-waveplate (*WPQ05ME-445, Thorlabs*), aluminium mirror (*BB05-E02, Thorlabs*) in an *xy* mirror mount, and a 90/10 beamsplitter (*BSN04, Thorlabs*). The beamsplitter would reflect 10 % of the pump out of the device, to monitor the pump intensity, duration and/or wavelength. It could be easily removed to maximise the LC laser emission.

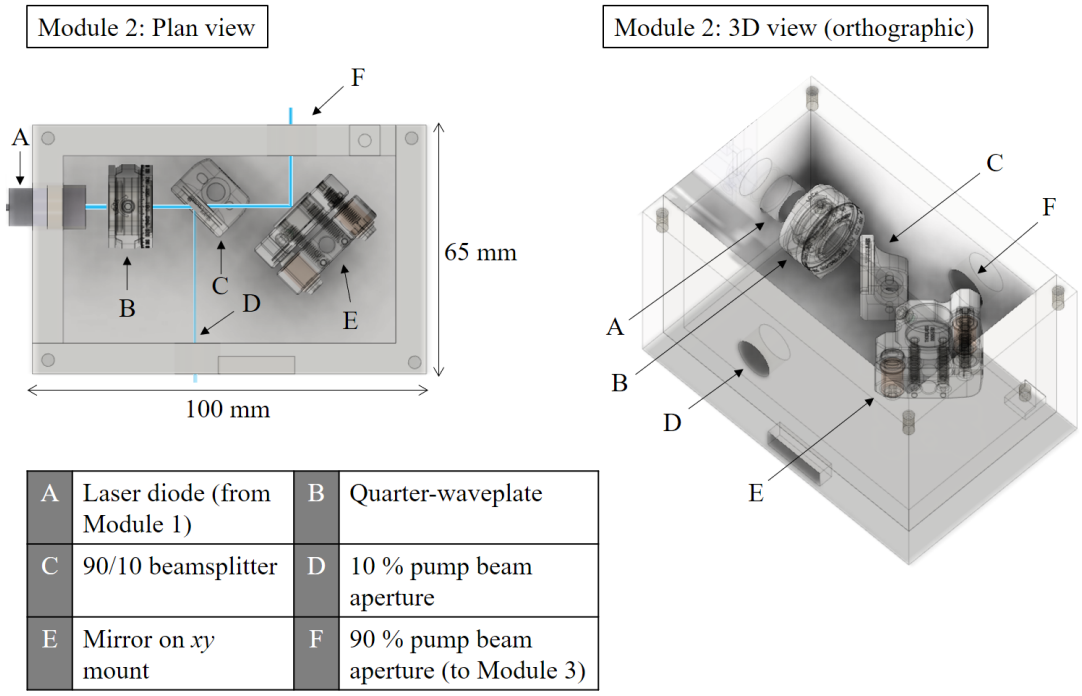

A	Laser diode (from Module 1)	B	Quarter-waveplate
C	90/10 beamsplitter	D	10 % pump beam aperture
E	Mirror on *xy* mount	F	90 % pump beam aperture (to Module 3)

Figure 7.19. Plan view and orthographic 3D view of Module 2.

The design of Module 2 incorporated an aperture through which the protruding LD mount containing the LD lens from Module 1 would be inserted. The quarter-waveplate was positioned immediately after the LD with its orientation controlled manually with the module's lid removed. The front surface of the beamsplitter would reflect 10 % of the pump beam, while 90 % would be transmitted onto the mirror. The pump beam would then be reflected from the mirror at a 90 ° angle through another aperture into Module 3. As per Module 1, the sides of Module 2 were removable to optimise the beam alignment. The CAD drawings of the optomechanics in Figure 7.19 were imported from the manufacturers to accurately simulate the dimensions and to position each component relative to the others and to the module.

7.2.9.3 Module 3 – liquid crystal laser

Module 3 (Figure 7.20) was designed with the same components as described for the third module in the stacked configuration. The dichroic mirror (*86-383, Edmund Optics*) was positioned to reflect the pump beam through the aspheric lens (*ACL1210U-A, Thorlabs*) and onto the LC laser cell. The LC laser cell was housed inside a 3D-printed mount which was attached to the DC motor. This was secured onto the *xyz* stage by the 3D-printed motor mount. This configuration allowed the position of the cell to be optimised by adjusting the three micrometre screws on the *xyz* stage, all of which were designed to be accessible through apertures in the module. Once the cell position relative to the aspheric lens was optimised for maximum LC laser intensity, the emission was focussed by the aspheric lens and transmitted by the dichroic mirror and through the output of the module.

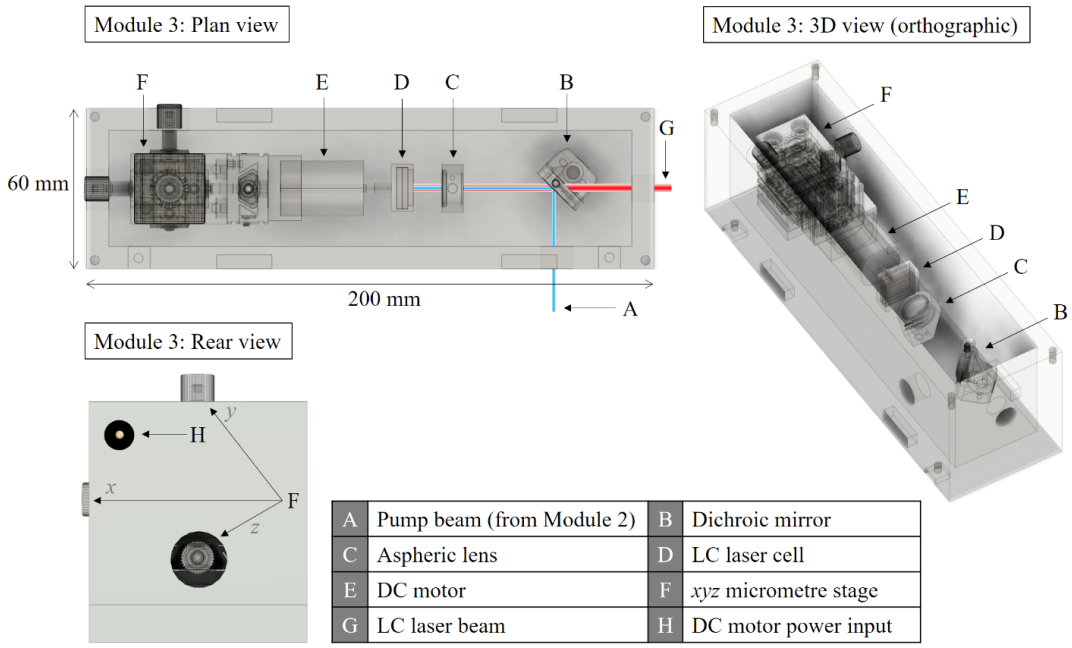

A	Pump beam (from Module 2)	B	Dichroic mirror
C	Aspheric lens	D	LC laser cell
E	DC motor	F	*xyz* micrometre stage
G	LC laser beam	H	DC motor power input

Figure 7.20. Plan view, orthographic 3D view and rear view of Module 3.

Countersunk brackets were incorporated into the modules' bases for securing them together. A lid was designed for using all three modules together, in addition to individual lids for each module, should they be separated for individual use.

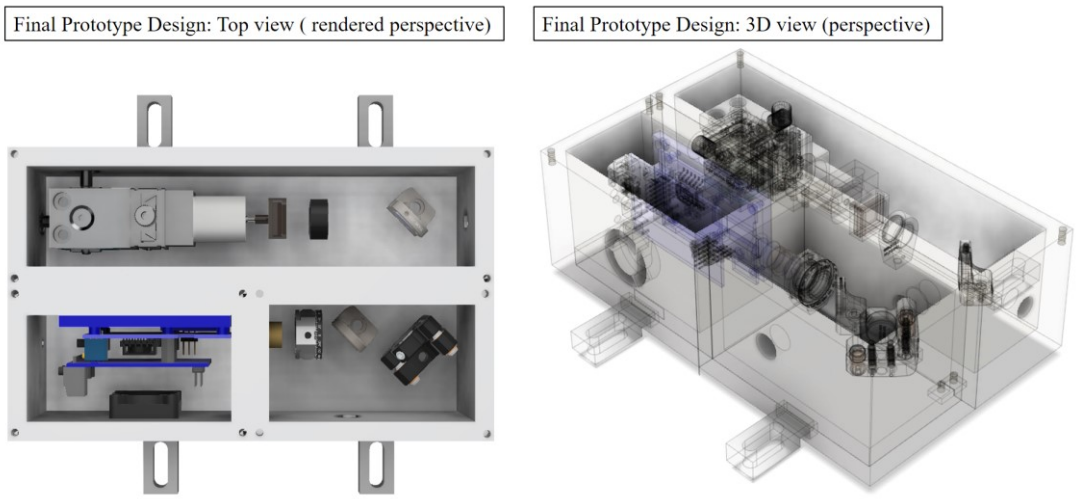

Figure 7.21. Final prototype design, showing a rendered top view and a transparent 3D view of all three modules, including the table clamps.

It can be seen from the top view in Figure 7.21 that the spacing between components was minimised as much as possible. The length of Module 3 was dictated by the combined lengths of Modules 1 and 2, and the width of Module 3 was designed to accommodate the full range of travel of the LC laser in the *x*-axis. The next stage was to build and test the performance of the final prototype design; a 1:1 scaled rendering of which can be seen in Figure 7.22.

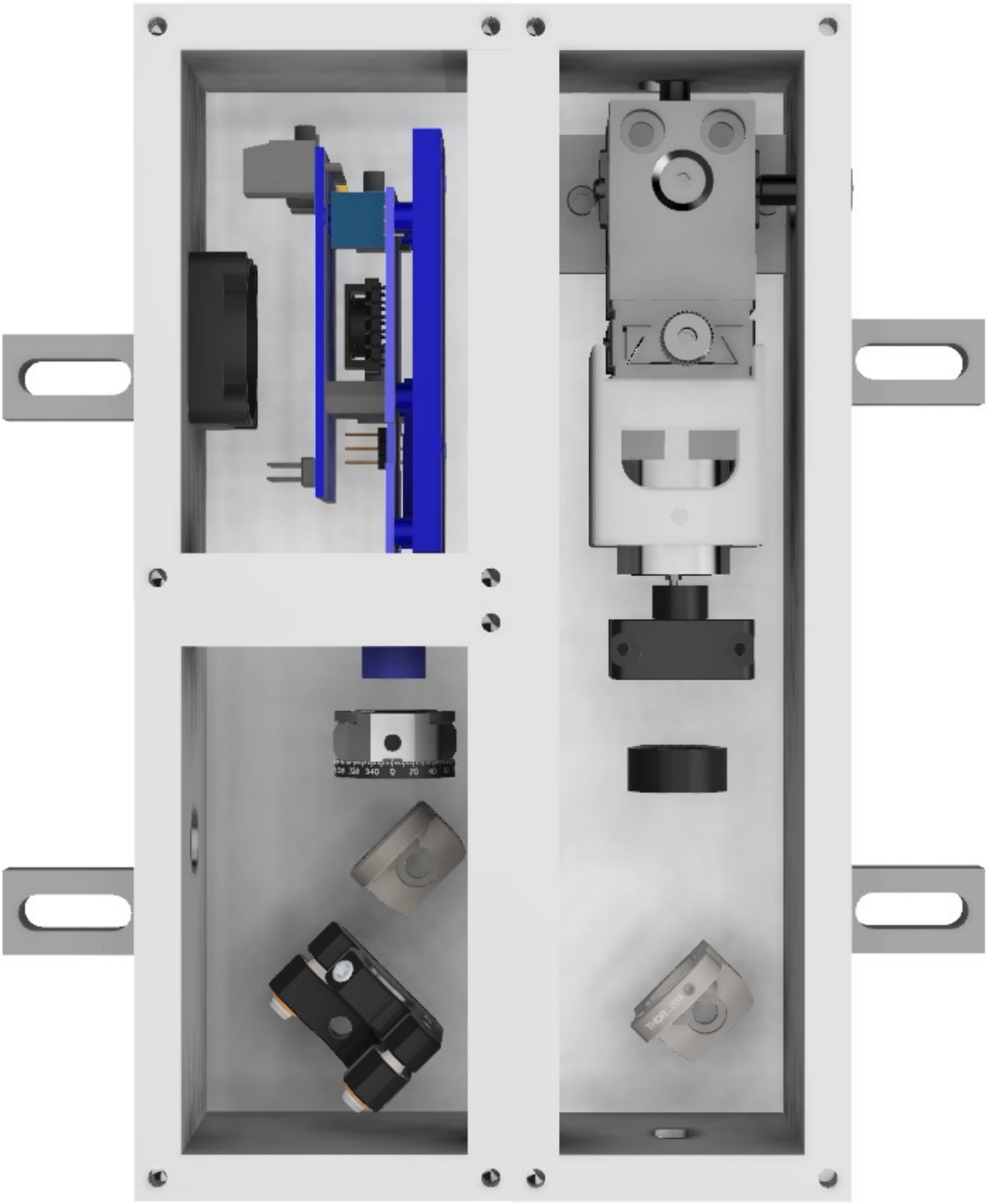

Figure 7.22. 3D perspective rendering of final prototype with a 1:1 scale (when printed on A4 scale).

7.3 Prototype build and testing

7.3.1 Test prototype

A test version of the prototype was built in acrylic[36] (Figure 7.23a) to verify the alignment, construction and usability, and to make any necessary modifications to the design prior to the final build in aluminium. The optical components we were aligned and LC laser emission was confirmed. Figure 7.23b shows the test device during operation, emitting an LC laser beam at 600 nm from a spinning cell.

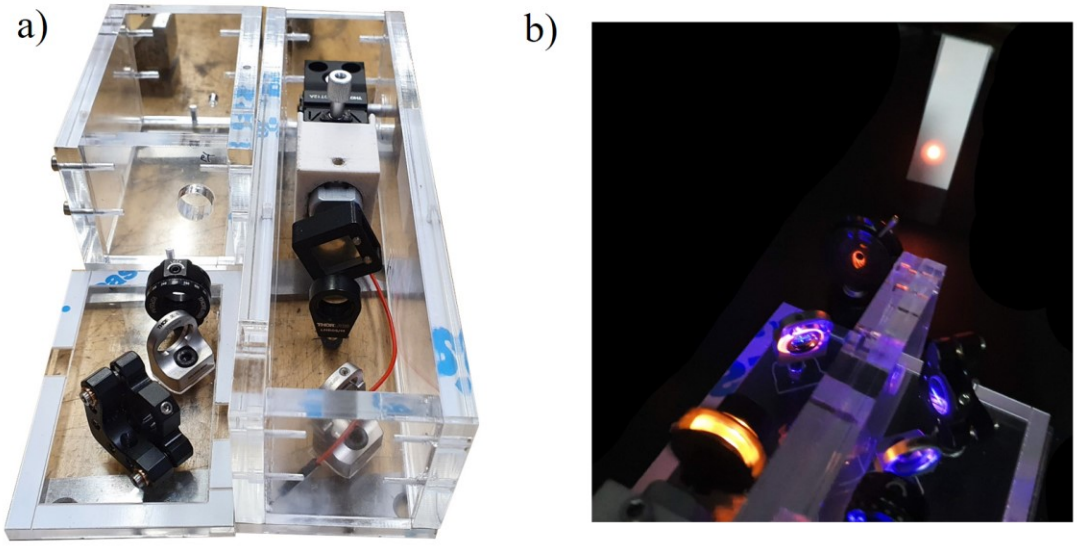

Figure 7.23. Test version of the prototype built using acrylic with a) showing the test system during construction before the electronics were added and b) showing the device working with the spinning cell producing 600 nm LC laser output.

Some modifications were made to the design to improve the functionality for the final version. This included:

- Adding stronger brackets underneath the system to secure the individual modules more robustly;
- Tapping M6 holes in the base to allow optical posts to be added for height adjustment;
- Adding a recessed space on the inner sides of the LC laser module on either side of the LC laser cell holder to ensure maximum *xy* travel and;

[36] The manufacture of the mechanical parts was carried out by Mark Mason in the mechanical workshop at the University of Edinburgh.

- Modifying the cell holder design to reduce the mass for minimising the vibrations of the cell during spinning.

7.3.2 Final prototype

The final working system is shown in Figure 7.24, with the electronics module shown in Figure 7.25 and the device specifications stated in Table 7.3.

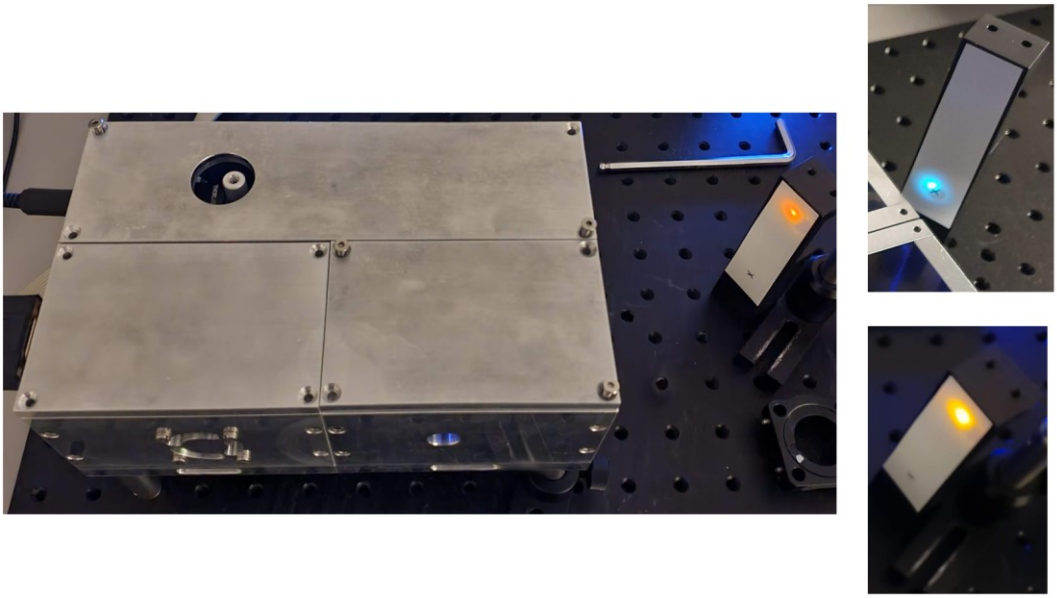

Figure 7.24. Final working prototype with LC laser emission at 600 nm. Posts have been screwed onto the base to raise the laser for experimental purposes. The images on the right show additional wavelengths at 480 nm (top) and 574 nm (bottom).

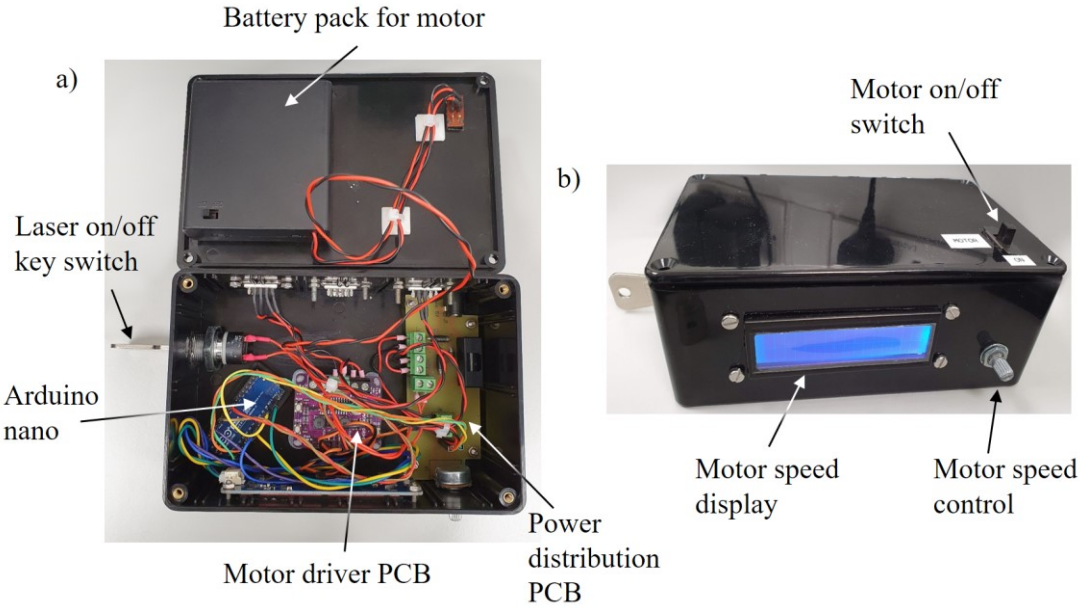

Figure 7.25. LC laser power module showing a) internal components and b) front-top view with the LCD and motor speed control.

Performance data were acquired using a DCM-doped LC laser cell emitting at 600 nm, to obtain the performance specifications. For a current of 14 A, the LC laser energy was measured as 4 nJ/pulse. An average power of 40 nW was therefore expected for a repetition rate of 10 Hz without spinning the cell. This was verified (Figure 7.26) with data acquired for 1 minute, resulting in an average power of 40.7 (± 0.7) nW.

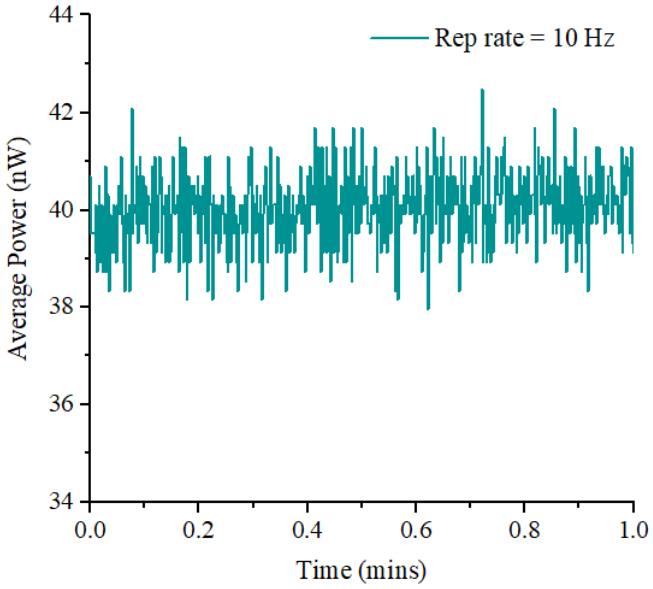

Figure 7.26. Average power of a static LC laser cell pumped at 10 Hz for one minute.

Based on the static cell data, the spinning cell arrangement was expected to result in an average power of 60 μW, when pumped at a repetition rate of 15 kHz with the cell spinning at 600 rpm. As can be seen in Figure 7.27, an average power of 52 μW was measured. However, the pulse-to-pulse variation caused a fluctuation of ± 40 μW; a percentage error of 77 % compared to 1.7 % for the static regime.

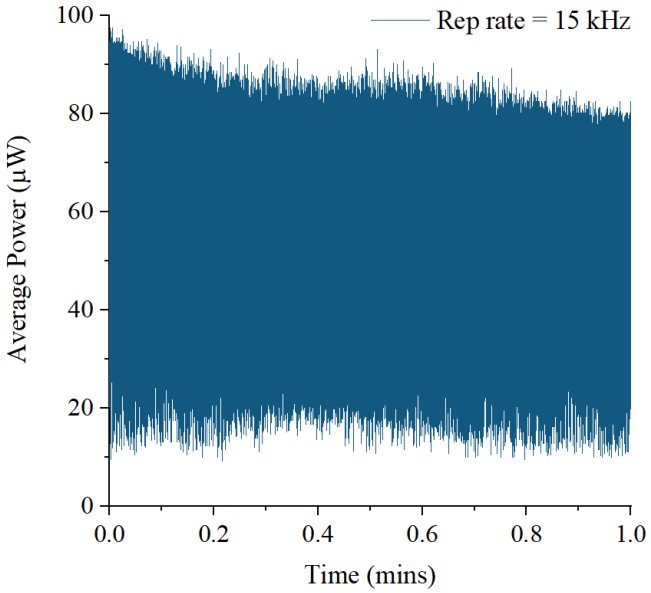

Figure 7.27. Average power of a spinning cell pumped at 15 kHz.

The pulse-to-pulse variation in average power for the spinning cell pumped at 15 kHz was not caused by the pump pulse fluctuations, as this was measured to show a power variation < 1 % over the same data acquisition timescale. The power disparity between pulses was also too large to be attributed to a variation in LC alignment across the cell area, especially as the cell had been well-made and appeared to show a uniform LC texture. The reason for the power fluctuation was found to be due to the sensitivity of the focal point of the pump spot relative to the spinning cell. As the cell was spun, either it did not remain perfectly perpendicular to the pump beam or there was a small movement of the cell in the *z*-axis, likely caused by movement in the motor shaft or a poor tolerance in the 3D-printed cell mount. This power fluctuation was unexpected, as the aspheric lens was anticipated to accommodate for movement in the z-axis. Clearly, however, the depth of focus of the lens was not sufficiently large to account for this movement. A higher tolerance in the mounting mechanics would therefore be required to improve the power stability. Alternatively, a longer focal length lens could be used to compensate for z-axis displacement of the cell during spinning, provided that

the spot size at the focus was still minimised. The focal length of an alternative lens could not be increased by more than 20 mm to ensure the lens could still fit within the footprint of the LC laser module. Nonetheless, the data showed than an average power of > 90 μW was feasible with this cell when pumped at 15 kHz, with a more stable output possible with minimal disruption to the prototype design.

The spectral stability of the LC laser, on the other hand, was excellent throughout the cell rotation, with *no variation* observed (outside the < 0.5 nm resolution limit of the spectrometer). This was further validation that the cell had been well fabricated and that the power fluctuations were not caused by poor cell quality.

To test that the prototype was capable of delivering multiple wavelengths (and thus fulfil design objective 3), four different LC laser cells were used. The blue, green and red emitting cells were the same as those presented in Section 4.5.4. An additional cell was fabricated with a 0.5 wt% DCM concentration and a chiral concentration of 4.6 wt%. This was designed to emit at 575 nm to address the wavelength gap inaccessible with laser diodes and Q-switched lasers and thus fulfil design objective 6. The emission spectra from all four cells in shown Figure 7.28, in which emission at 574 nm was achieved, along with emission at 480 nm, 530 nm and 610 nm.

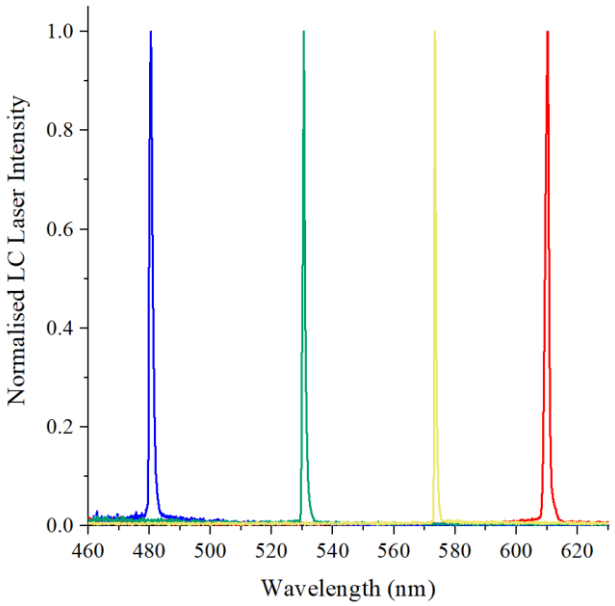

Figure 7.28. Prototype LC laser emission spectra, with each wavelength obtained using a different LC laser cell.

Table 7.3. Diode Pumped LC Laser Specifications

Parameter	Value/Description	Unit
Mode of operation	Pulsed	-
Repetition rate	1 – 15,000	Hz
Motor speed	0 - 600	rpm
Supplied pump source	Laser diode	-
Supplied pump wavelength	445	nm
Laser diode current	6.5 - 14	A
LC laser wavelength	480 - 610[37]	nm
Wavelength tuneable	No	-
Wavelength selective	Yes	-
Polarisation	Linear	-
Maximum average power (@ 14 A & 15 kHz)	< 100	μW
Laser diode cooling	Air	-
Driver current monitor / trigger out	Yes – SMA connector	-
Size (L × W × H)	20 × 12.5 × 7	cm
LC laser head weight	2.8	kg

The optical losses in the pump beam delivery (without the 90:10 beamsplitter) were measured and found to be 8.0 % (See Appendix F for details). This took into account losses from the quarter waveplate, aluminium mirror, aspheric lens and dichroic mirror. With the addition of the 90:10 beamsplitter, a further 10.9 % loss was introduced, such that the total losses between the pump and the laser cell were 18.0 %. The quarter waveplate and dichroic mirror were optimised for use with the 445 nm LD pump. If a pump source with a different wavelength were used, both optics would need to be changed.

As discussed in Section 7.2.4, the primary purpose of the aspheric lens was to focus the pump beam to the smallest possible spot to induce LC lasing; it was not chosen for its ability to perfectly collimate the LC laser output. When an LC laser beam is emitted from a cell, it is divergent [143] but the aspheric lens used here collected this emission and reduced the divergence. The divergence of the resultant LC laser beam appeared to be negligible over a

[37] This is the wavelength range tested so far. Longer wavelengths ought to be possible using other dyes or FRET.

distance < 1 m after the output. However if a perfectly collimated beam were required, additional optics at the output of the LC laser module would be needed. A beam profile camera would be useful for quantitative analysis of the divergence.

7.3.3 Laser safety classification

Lasers are given a safety classification depending upon their performance specifications. The British standard has eight classifications [144]: Class 1, 1C, 1M, 2, 2M, 3R, 3B and 4, with Class 4 the most dangerous. A Class 2 laser is designated to lasers that emit in the visible range (400 – 700 nm) with an average power up to 1 mW. Given that the work in this chapter has shown LC laser power levels < 100 μW in the visible range, the prototype would be expected to be designated a Class 2 classification, provided it is operated with the lid on and without the beamsplitter in-situ, to prevent exposure to the LD pump beam. This fulfilled the 2nd design objective, whereby laser safety regulations are adhered to for public demonstration purposes.

7.3.4 Comparison to previous demonstration systems

The prototype laser head footprint was 200 × 125 × 70 mm. The total cost of all prototype components, including the driver electronics, LD, optics, optomechanics and LC laser cell was £2,930.06 (a full bill of materials can be found in Appendix J). More than half of the cost was for the LD electronics supplied by PicoLAS (the driver PCB, signal generator PCB and LD controller; £1,600 in total). If the PCBs were to be mass-produced, they would be expected to be significantly cheaper. Compared to the demonstrator in Ref. [41], the prototype was cheaper by > £7,000 and > £17,000 (depending upon choice of pump source), it required fewer power supplies and it had a smaller footprint. The average power of the prototype was lower than the unit in Ref [41], which was expected due to the disparity in peak power between the Q-switched pump and LD pump sources. However, the more advanced design of this prototype enables integration with higher pulse energy pump sources (fulfilling the 7th design objective), should an application require it. The repetition demonstrated by the prototype (15 kHz) was higher than all previous demonstration systems in Refs. [40]–[42] and is believed to be the highest repetition rate reported to-date.

The DPLCL prototype is believed to be the least expensive LC laser demonstrated to-date, in addition to delivering the highest repetition rate and an overall improvement in functionality (and thus fulfilling design and performance criteria 4 and 5).

7.4 Fluorescence microscopy imaging with the prototype

A previous demonstration of LC laser technology was carried out using a Q-switch-pumped demonstration unit, in which fluorescent-labelled mouse kidney samples were successfully imaged in a microscopy lab [41]. A similar demonstration with the DPLCL was sought as a proof of concept to showcase the capabilities of the prototype in medical imaging. The prototype was taken to the Institute of Genetics and Molecular Medicine in Edinburgh with the aim of integrating it with a microscopy arrangement to record fluorescence images of non-biological samples doped with a high quantum-yield fluorophore. If successful, the investigation would be repeated with biological samples tagged with a common fluorescent biomarker. As the lasers typically integrated with microscopes for medical imaging are large and expensive, this investigation aimed to demonstrate fluorescence imaging using a significantly smaller and lower-cost laser source.

The microscopy work in this section was made possible by D. Dickinson, whose PhD is concerned with applying LC lasers to fluorescence microscopy (expected completion: summer 2023). The microscope arrangement and sample preparation was carried out by D. Dickinson as part of her research that follows on from the work by M. Normand [41].

7.4.1 Fluorescence imaging: configuration and methodology

A microscope (*Zeiss, Axioskop 2*) with a ×10 magnification objective was used for imaging nematic LC droplets *(BL006, Merck)* doped with the dye Ph660 *(Exciton)* and mixed in glycerol in a ratio of 4:96. A dye-doped nematic LC was used to demonstrate the imaging capabilities of the prototype, as this material is easier and less expensive to prepare than a biological sample and has a higher fluorescence intensity. The mixture was stirred at 1000 rpm for 10 minutes to break up the droplets in the glycerol, and then pipetted onto a glass slide and secured with a cover slip.

A Q-switch-pumped LC laser (QSPLCL) demonstration unit [41] was first aligned with the microscope to ensure the optics were correctly positioned and to record an image of the sample for comparison with the LD pumped LC laser. The QSPLCL was then replaced with the prototype, with the alignment optimised by adjusting two beam steering mirrors. The laser emission was coupled into the microscope, reflected by a dichroic mirror (*ET632/60m, Chroma*) and focussed onto the sample stage. The fluorescence signal was then detected either visually through the eyepiece or on a PC screen connected to a camera at the microscope output. This arrangement is represented in Figure 7.29.

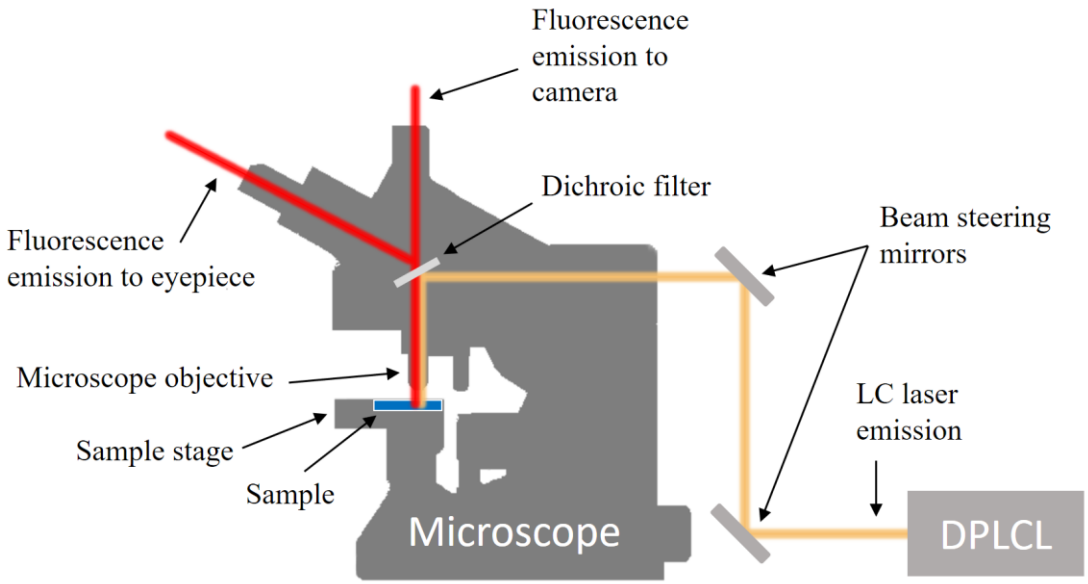

Figure 7.29. Diagram of the fluorescence imaging arrangement with the LC laser coupled into the back of the microscope and focussed onto the sample. A dichroic filter was used to reflect the LC laser beam onto the sample and transmit the fluorescence emission for detection at the eyepiece or camera.

The LC laser alignment was carried out with the laser cell static (as opposed to spinning) and with the pump repetition rate set to 50 Hz; sufficiently high to observe the LC laser emission but without rapidly fatiguing the cell. Optimum alignment was confirmed by maximising the intensity of the laser emission at the output of the microscope objective. The sample was placed on the sample stage, the LC laser motor was set to 300 rpm and the repetition rate of the LC laser was set to 15 kHz. Based on previous measurements, this produced an average power of approximately 50 μW.

7.4.2 Results and discussion

The dye-doped droplets were illuminated and the resultant fluorescence recorded on the camera. An obvious fluorescence signal was detected (Figure 7.30a), albeit with a slightly lower intensity than when illuminated with the QSPLCL (Figure 7.30b). The droplet formations in the two images differ because the slide had to be removed to align each laser beam and replacing the cell in the same position would have been unnecessarily time-consuming. The images are representative of the whole cell so are valid for qualitative comparison.

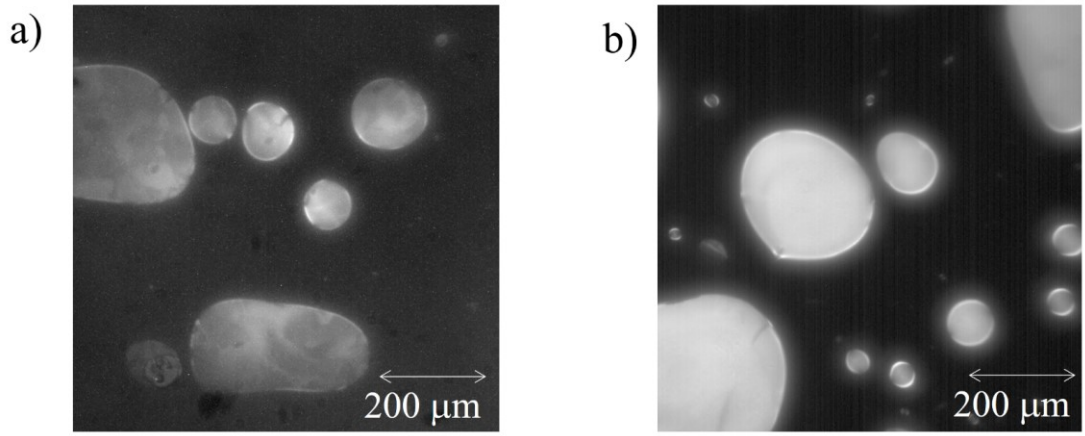

Figure 7.30. Fluorescence imaging of dye-doped LC droplets when illuminated with the a) DPLCL and b) QSPLCL.

The higher intensity of the QSPLCL-illuminated sample compared to the DPLCL-illuminated sampled was attributed to the higher pulse energy. Nonetheless, the results from this experiment show much promise for fluorescence imaging, especially considering that the peak absorption of Ph660 did not overlap with the emission wavelength of the LC laser (Figure 7.31).

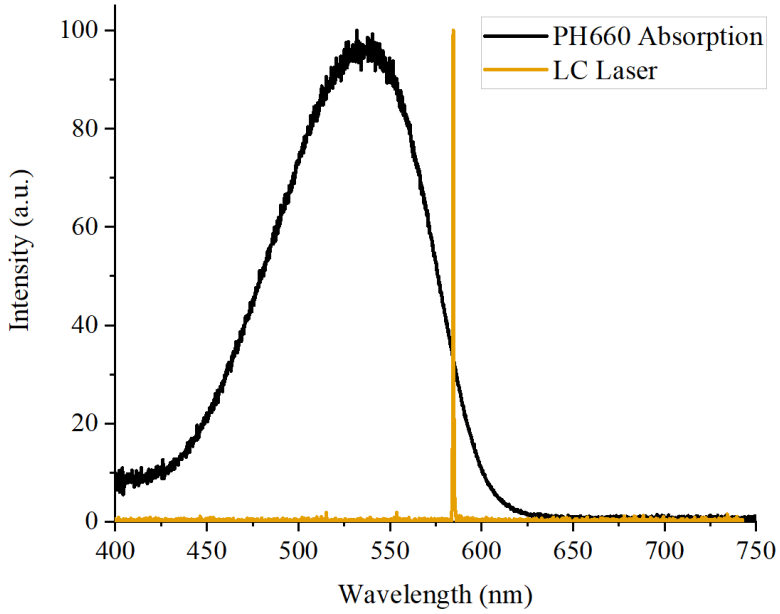

Figure 7.31. Absorption spectrum of PH660 (black line) and LC laser emission (orange line).

An attempt to extend the demonstration by imaging a real biological material was made by illuminating a sample of HeLa cells[38] tagged with the fluorescent protein, BOBO-3, the absorption and fluorescence spectra of which are shown in Figure 7.32. The cells were confined in a fixing agent and kept at 2 °C in a well plate. The sample remained in a fridge until the microscope and laser were set up, at which point the well plate was placed under the objective for imaging.

[38] HeLa cells are the most common human cancer cells used in cancer research [160]. They were obtained from a cervical cancer patient, Henrietta Lacks, in 1951 (without her permission) and were found to be able to replicate indefinitely in a culture, earning them the name "immortal" cells. This property enables constant reproducibility and was first used in the development for the polio vaccine.

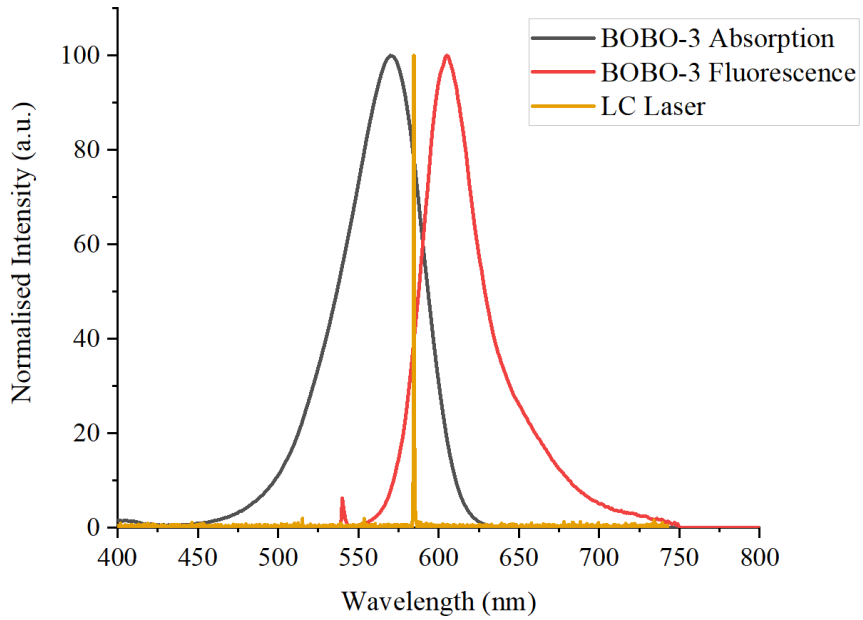

Figure 7.32. Absorption (black line) and emission (red line) spectra of BOBO-3 fluorescent protein with the emission spectrum of the LC laser (orange line).

At 585 nm, the LC laser cell emission was 15 nm longer than the peak absorption of BOBO-3. Despite this non-optimum wavelength, imaging of the HeLa cells with this LC laser was attempted.

Figure 7.33 below shows the fluorescence image of the HeLa cells when illuminated with the 585 nm LC laser when pumped with the Q-switched laser at 1 kHz.

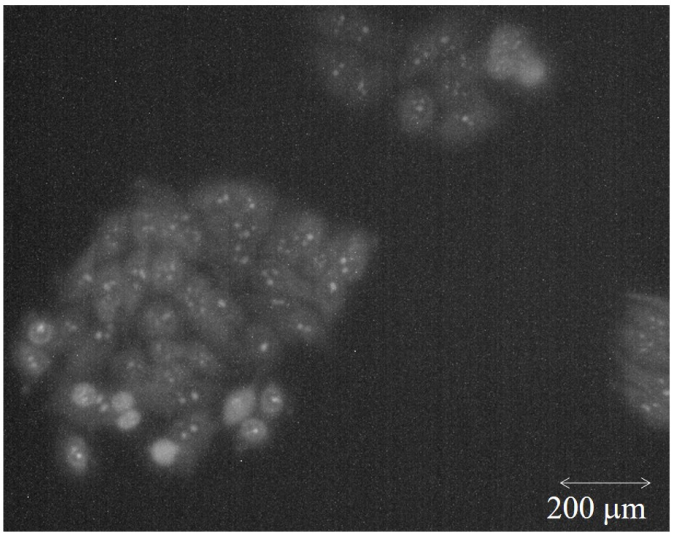

Figure 7.33. HeLa cells fluorescing under illumination by the Q-switch-pumped LC laser with an emission wavelength of 585 nm.

The average power emitted from the spinning LC laser under Q-switched pumping was approximately 0.3 mW. This was an order of magnitude greater than the DPLCL. When the QSPLCL was replaced with the DPLCL prototype, as per the previous experiment with the droplets, a similar image could not be achieved. Despite being able to see the laser beam at the output of the objective, it was apparent that the intensity was not sufficiently high for the microscope system to detect any fluorescence signal from the sample.

One possible reason for the better results with the dye-doped droplets compared to the HeLa cells (in addition to the different pump powers) was likely due to the way in which the samples were confined. As mentioned, the HeLa cells were suspended in a fixing agent and remained in the well plate for imaging. The cover of the well plate was plastic and at least 2 mm thick. Furthermore, the HeLa cells were suspended in the fixing agent, effectively making them a 3-dimensional sample. This was in contrast to the dye-doped droplets, which were confined between a glass slide and a 0.17 mm cover slip and could therefore be considered 2-dimensional. Not only did this make it easier to focus the laser on the sample, but the media through which the laser travelled was a hundred times thinner, and therefore scattered the light less. Fixed samples would therefore be desirable for future investigations of HeLa cells, or any other relevant mammalian cell samples.

Incorporating the prototype with the microscope arrangement (Figure 7.34) provided the opportunity to test some of the features incorporated in the design process. For example, the

ability to adjust the height was required for optimising the alignment into the microscope, and external access to position the LC laser cell enabled safe adjustment during operation. The small footprint allowed easy integration with the microscope and left ample space on the breadboard for additional optics for future experimental modifications.

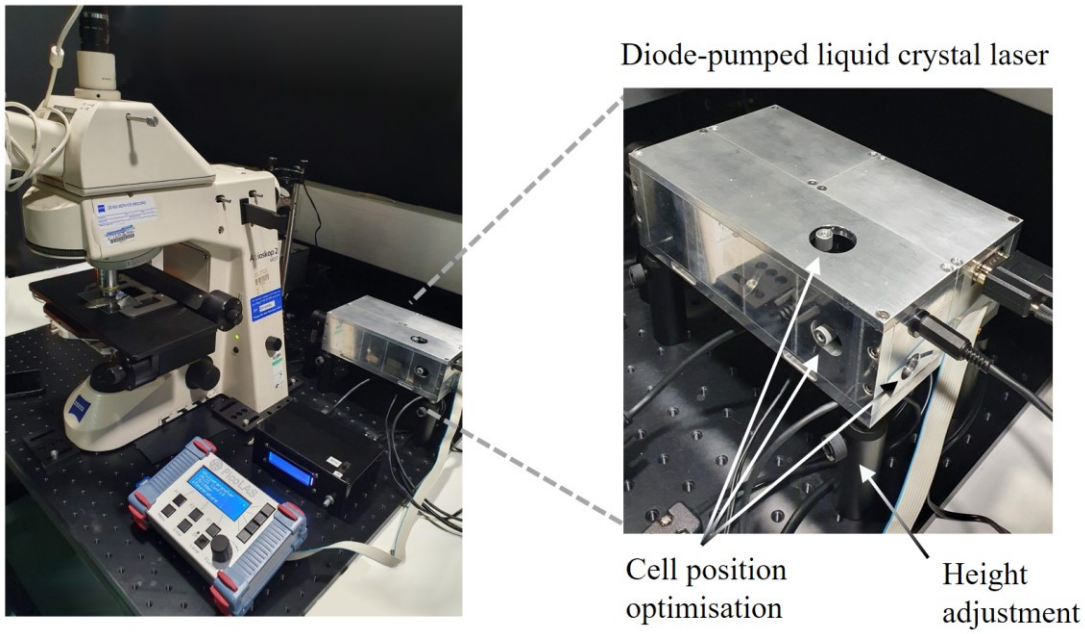

Figure 7.34. Photograph of microscope arrangement with features of the LC laser prototype highlighted.

To minimise the disruption to D. Dickinson's work, the preliminary investigation discussed in this section was time-limited and used DCM-doped LC cells that were not fully optimised for the absorption of PH660 nor BOBO-3. Only one biomarker-tagged sample and one LC laser cell were used. With more time, additional samples would be tested with different biomarkers using a range of LC laser emission wavelengths. Optimising the biomarker-wavelength combination would be expected to improve upon the results presented here. The fact that dye-doped droplet samples showed a strong fluorescence is encouraging evidence towards medical imaging using a DPLCL and is worthy of future work.

7.5 Conclusions

The culmination of fabricating low-threshold LC laser cells, achieving LD pumping and gaining a deeper insight into the performance requirements for successful LC laser emission was achieved in the demonstration of the first diode-pumped LC laser prototype device. The aim of this work was to develop a device that demonstrated many of the advantages that LC lasers offer over competing technologies. To achieve this, eight design and performance criteria were set, all of which were successfully delivered. Evidence of their success is stated below.

1. **Utilising LD pumping**
   The 445 nm LD, combined with PicoLAS electronics, was used as the primary pump source in the design and demonstration of an LC laser prototype and was shown to successfully induce LC laser emission.

2. **Delivering as high power as possible, to maximise visual effect, whilst also complying with laser safety regulations for public demonstration without the use of safety goggles**
   By delivering a current of 15 A to the LD pump and pulsing it at a repetition rate of 15 kHz (restricted by the optical configuration), an average power of > 90 μW was achieved. A laser safety classification of Class 2 is expected for this power level for emission in the visible range of the spectrum, meaning that the prototype can be demonstrated in a non-lab-based environment without the need for laser safety goggles (provided the pump beam is not exposed).

3. **Producing wavelengths spanning the visible range**
   The 445 nm LD successfully induced LC laser emission at wavelengths ranging from 480 nm to 610 nm, including at 574 nm – a wavelength within a region of the visible spectrum typically inaccessible with many competing LC laser technologies, including Q-switched lasers and LDs.

4. **Minimising the footprint to fit on a desktop for demonstration at trade shows, conferences and to external stakeholders**

   A laser head footprint of 200 × 125 mm was designed and built, which incorporated the LD pump source, polarisation and beam steering optics, an LC laser mounted on a DC motor, and alignment optimisation mechanics. Compact and customised optomechanics were used to minimise the size and weight of the device. The LD driver controller and LC laser head electronics controller were both smaller than the laser head and could be easily disconnected for transportation. The compact and durable design of the prototype and controllers enabled easy portability for demonstration purposes outside of a lab environment.

5. **Being smaller (and/or more functional) than previous LC laser demonstrator systems**

   The spinning cell arrangement enabled a repetition rate of 15 kHz – the highest frequency to-date in a demonstration unit. Furthermore, the prototype was designed such that only one mains power supply was required, in addition to a simple battery unit for powering the DC motor. The prototype is also believed to be the lowest cost LC laser device produced to-date.

6. **Demonstrating a unique combination of capabilities not seen in competing laser systems**

   The design of the prototype allowed application-specific wavelength customisation, achieved by using multiple LC laser cells designed to emit at different wavelengths, which can be easily exchanged by the user. Alternatively, the spinning cell architecture has also been shown to enable fast colour switching [13]. The combination of wavelength customisability integrated with an inexpensive, portable device capable of delivering a kHz repetition rate is believed to be unique.

7. **Proving a flexible platform that would be compatible with potential future upgrades and capable of integration with alternative pump sources**

   The prototype was designed to be modular, such that the LC laser could be separated from the LD pump source. This allows an alternative pump source to be used with the LC laser, should an alternative pump wavelength or pulse energy be required. Easy access to the optical configuration allows the user to customise the optical arrangement, for example, to add a beamsplitter for simultaneously measuring the pump LC laser beams. The

prototype was designed to be height adjustable, to allow integration with pre-existing optical arrangements. This was demonstrated when the prototype temporarily replaced a more complex laser in a microscopy lab.

8. **Demonstrating the application of LC lasers, for example, in biomedical imaging, fluorescence microscopy, holography etc.**
   A sample of dye-doped nematic LC was successfully imaged by the prototype. This investigation was a proof of concept for a medical imaging application of the LC lasers, in addition to demonstrating the prototype's ability to be integrated in a pre-existing experimental arrangement.

Developments to the design and functionality of the prototype could be made to improve its performance. The average power fluctuations (with an error of 77 %) that were measured when pumping a spinning cell at 15 kHz were attributed to *z*-axis displacement of the cell during spinning. Using an alternative aspheric lens with a longer depth of focus, or improving the tolerance of the optomechanics would be expected to improve this.

Imaging the dye-doped nematic droplets was accomplished with the prototype, whilst the attempt at imaging HeLa cells was unsuccessful due to the insufficient power (and a non-optimised optical configuration). The μW-scale power output from the DPLCL is a fundamental limitation of the LD pumping technique. A priority for future work would be to increase the power output if DPLCLs are to be considered for use in biomedical imaging. A maximum current of 14 A was used here. Increasing the current delivered to the LD would increase the peak power and therefore increase the average power with high repetition rate pumping. Although a current of 50 A was possible with the driver electronics, the risk of damaging the LD with this current was considered too high here. Furthermore, this would only produce a three-fold improvement in peak power and would still fall short of the milliwatts demonstrated with the Q-switch-pumped LC laser [13]. The 15 kHz repetition rate could be increased if the pump spot size could be reduced further, enabling more pulses per cell rotation. A larger cell diameter would achieve the same result, but would be detrimental to the size of the device. A more complex dynamic configuration could be introduced, such that the circular motion of the spinning cell would be combined with a linear motion, thus utilising the full area of the cell. This could however, introduce mechanical noise and result in an increase in size, weight and cost of the device.

Based on the achievements listed above, the DPLCL prototype was deemed fit for purpose, not only as an advocate for the success of LD pumping, but also for showcasing LC laser technology as a viable alternative to competing laser systems. This was exemplified by successful demonstration of the prototype in a fluorescence imaging application. While further developments are recommended to improve the performance, the objectives set out at the beginning of this work were all successfully met.

Chapter 8

Conclusions and future work

"The moment that you rest, thinking that you have attained the level you desire, a part of your mind enters a phase of decay. You lose your hard-earned creativity and others begin to sense it. This is a power and intelligence that must be continually renewed or it will die."

Robert Greene

8.1 Introduction

This chapter concludes the thesis by summarising the main results and highlighting the key achievements with reference to the research aims set out in Chapter 1. Limitations of the work are discussed to motivate future research and some anticipated consequences of this research are considered.

8.2 Research achievements

The primary aim of this thesis was to achieve the historically elusive and much sought-after goal of producing LC laser emission using a semiconductor-based pump source. The fabrication of LC laser cells was prioritised at the beginning of this work, to produce well-made cells, capable of delivering low threshold and high slope efficiency LC laser emission. A reflective cell geometry was used throughout this work, as this has shown improved performance compared to transmissive cells [69]–[71], [94]. This geometry was therefore more likely to succeed in demonstrating LC laser emission under optical excitation from an alternative, lower power pump source, compared to the standard method of Q-switched pumping.

A 445 nm LD was selected as the most likely semiconductor-based emitter to overcome LC laser threshold; firstly, this wavelength is absorbed by many of the dyes typically used as the gain media in LC lasers and secondly, this LD has been shown to withstand high currents in pulsed operation [104]. Driver electronics capable of delivering high currents (3 – 50 A), variable repetition rates (1 Hz – 2 MHz) and variable pulse durations (12 ns – 10 μs) were used to power the LD. By using this combination of LD and driver electronics to pump a well-made LC laser cell (doped with the high quantum yield organic dye, DCM) in an optimised optical arrangement, band-edge LC laser emission was successfully demonstrated [145]. This was evidenced by a narrow spectral linewidth (< 1.5 nm), low threshold behaviour (12.3 nJ/pulse), a distinct gradient change in slope efficiency and the linear polarisation expected from a reflective cell; performance characteristics commonly observed with Q-switched pumping. Furthermore, red, green and blue LC laser wavelengths were demonstrated using the same LD pump source.

This novel contribution to the field of LC laser research is a significant milestone in LC laser development, with the ability to now exploit the wavelength-selectability of LC lasers in a significantly smaller and lower cost arrangement compared to the previous Q-switched laser pumping regime.

Another advantage of this long-awaited breakthrough is the ability to vary the pump pulse duration. This enabled investigations not previously possible with the fixed pump pulse lengths associated with Q-switched pump sources.

The first part of this investigation was to determine the effect of pump pulse duration on LC laser threshold and slope efficiency, within the limitations of the pump durations deliverable by the driver electronics. Custom-built software was designed to automate the data acquisition for threshold and slope efficiency measurements, in which the LC laser output energy was measured as a function of the pump pulse energy. During this investigation, it was found that the increase in pulse energy associated with an increase in pulse duration did not result in an increase in LC *laser* emission and instead increased the *fluorescence intensity*. The presence of fluorescence distorted the slope efficiency measurements such that a clear change in gradient, indicative of LC laser threshold, could not be identified. This was resolved by introducing an aperture to the optical arrangement to block the off-axis fluorescence emission and to primarily allow detection of only on-axis laser emission.

With the aperture in place, the effect of pump pulse duration on LC laser threshold and slope efficiency was measured for different pump pulse lengths ranging from 16 ns to 94 ns. An increase in threshold and decrease in slope efficiency was found for an increase in pump pulse length. This was the first time such an investigation has been conducted, and unequivocally showed that, within the confines of the pump durations available with this equipment, the shortest pulse duration maximised LC laser performance. The cause of this behaviour was qualitatively attributed to an increase in the population of triplet states in the organic dye with increasing pump pulse duration. The results of this investigation are an important contribution to the understanding of LC laser performance, for several reasons. Firstly, they corroborate the limited theoretical and anecdotal evidence published at the time of writing [29], [30]. Secondly, the results show that minimising the pump pulse duration improves LC laser performance, thus enabling a quantitative approach for pump source selection. And thirdly,

the results motivate future work in exploring the lower limit of LC laser thresholds using pump sources with sub-nanosecond pulse lengths.

The second investigation explored the temporal characteristics of LC lasers. An investigation into the effect of pump energy (by changing pump peak power) on LC laser pulse length found that the LC laser pulse duration was minimum at threshold, increased above threshold, and then plateaued thereafter. The measurement of pump energy *vs.* LC laser pulse length was repeated for different pump pulse durations, resulting in the same plateauing affect above threshold at *the same* LC laser pulse duration, for all pump pulse durations. This is believed to be the first time this behaviour has been observed and warranted further investigation.

The LC laser pulse length was measured again, this time as a function of pump pulse length (with pulse energies exceeding threshold by the same amount for all pulse lengths tested). It was found that the LC laser pulse length was unaffected by the pump pulse length, and remained the same for all pump pulse lengths tested. The LC laser pulse length was found to be 3.5 (± 0.1) ns for a cell doped with 0.5 wt% of DCM. Theoretical exploration of the molecular dynamics of organic dyes led to the conclusion that the rate of intersystem crossing from the singlet state to the triplet state was responsible for the existence of an upper limit to the LC laser pulse duration. As the rate of intersystem crossing is dye-dependent, the investigation was repeated for a second dye, Coumarin-504, in which the same behaviour was observed, with a slightly longer pulse duration of 5.2 (± 0.2) ns. This is believed to be the first time that the existence of an upper limit to the pulse length deliverable from an LC laser has been identified. For a pump source with a pulse duration *shorter* than this upper limit, it is predicted that the LC laser pulse duration will follow that of the pump source. This hypothesis was tested using a 532 nm Q-switched pump laser with a pulse duration of 0.73 ns, which resulted in an LC laser pulse of 0.65 nm.

From one perspective, the results from this investigation implied that a pump source of *nanosecond or higher* durations can induce nanosecond-scale laser emission, provided the peak power of the pump is sufficiently high to overcome LC laser threshold. On the other hand, an LC laser pulse of *any* duration *shorter* than the upper limit of the LC laser pulse is achievable, and is dictated by the duration of the pump pulse. Both scenarios could have profound implications for dye-based LC lasers. The constant upper limit to an LC laser pulse duration could be employed as a pulse shortening mechanism for longer pulse length lasers,

albeit at a longer wavelength than the pump source. Alternatively, the ability for LC lasers to produce sub-nanosecond pulse durations across the visible spectrum could be applied in applications such as fluorescence lifetime imaging. The lower limit of LC laser pulse lengths could not be identified in this work due to the limitations of the LD driver electronics, available pump sources, and detection equipment, but would be worthy of future investigation. The results from this investigation fulfilled the second aim of this thesis, which set out to explore performance characteristics previously not possible from the fixed pulse durations of Q-switched laser sources.

The motivation for demonstrating LD pumping was to bring the commercialisation of LC lasers closer to realisation. Having successfully achieved LD pumping, a working prototype device was developed to incorporate this breakthrough, in a low-cost, small footprint system, with emission wavelengths spanning the visible spectrum at high repetition rates.

Prototype design and performance criteria were proposed at the beginning of the development process, and included: utilising a LD pump source; exhibiting advantages over competing technologies; showing performance improvements compared to previous LC laser demonstration units; enabling safe use in a non-lab-based environment for demonstration purposes; demonstrating wavelength selectivity at wavelengths not achievable with comparable technologies; and demonstrating LC laser technology in an application-based setting.

All of the performance and design objectives were met, with the demonstration of the first diode-pumped LC laser device [146]. This fulfilled the final aim of this thesis. Wavelengths spanning > 100 nm were demonstrated, including in the yellow region of the spectrum which is typically difficult (or, in some cases, not yet possible) to achieve with competing technologies and has been shown to be particularly useful, for example, in ophthalmology for treating diabetic retinopathy [147]. The highest reported repetition rate for LC lasers, 15 kHz, was achieved using a spinning cell arrangement, and produced an average power of 52 μW. Although this was accompanied by power fluctuations of ± 40 μW, improvements in the tolerance of the optomechanics and/or the depth of focus of the lens used to focus the pump beam would be expected to greatly reduce this effect. The prototype was designed to have a modular arrangement to enable optical excitation from alternative pump sources, and the small footprint of 200 mm × 125 mm enabled integration with pre-existing optical arrangements.

This was demonstrated in a fluorescence imaging environment, in which the LC laser emission was coupled into a microscope and successfully used to image dye-doped nematic droplets. This also demonstrated the application potential of LC lasers as an alternative to the larger and more expensive lasers typically used in fluorescence imaging systems.

The performance of the prototype could be enhanced further with additional development. This could include: using improved LD and LD driver technologies, such that shorter pulse lengths would improve the pulse-to-pulse stability and higher currents would enable higher LC laser peak powers; employing Förster energy transfer to extend the wavelength range to the near infrared region of the spectrum [15]; and improving the optical delivery to enable higher repetition rate pumping with improved power stability. The success of the first diode-pumped LC laser prototype, designed, built and demonstrated in this work, offers an exciting new opportunity for future evaluation in a range of potential applications and showcases the advantages LC laser technology offers over competing laser systems.

8.3 The future of liquid crystal lasers

8.3.1 Application potential

The advantages of LC lasers in terms of cost, size and wavelength accessibility are accompanied by challenges in terms of limited output power, repetition rate and stability. LC lasers in their current form are unable to deliver high powers and are therefore better suited for low power applications, such as fluorescence imaging [41] or medical diagnostics [28], in which low-power is preferable (and sometimes essential). The ability to access the full visible spectrum could enable the targeting of particular fluorophores that would otherwise rely on multiple laser sources, LEDs or supercontinuum lasers, all of which have significant limitations. Another interesting application for LC lasers is in holographic imaging. Preliminary investigations into holographic imaging with LC lasers have shown promising results, in which an 84 % reduction in speckle was reported [28]. These examples warrant further investigation with LC lasers, in addition to identifying other applications that could benefit from the advantages LC lasers offer. There are many ways in which LC laser technology could be developed towards fulfilling its application potential. The following sections highlight key areas worthy of future investigation.

8.3.2 Pulse duration

As mentioned in Section 8.2, investigation into the lower limit of the LC laser pulse duration was not possible in this work due to the experimental limitations. However, if such work were undertaken, this would not only offer further insight into the behaviour of LC lasers in the sub-nanosecond regime from an intellectual perspective, but could provide a solution for applications that require a compact tuneable laser source with short pulse durations. For example, PicoLAS, who manufacture the driver electronics used in this work, have recently introduced a new bespoke service that may be able to deliver a similar current but over a shorter pulse duration (albeit with a fixed pulse length). The same LD could be used, but with a pulse length ≤ 1 ns, which could enable higher repetition rates (and hence higher average powers) but with a more stable output than was possible in this work.

The modular design of the prototype presented in this work was primarily to enable LC laser pumping with pump sources other than the 445 nm LD, if required. For example, should LD driver electronics not meet the requirements needed to investigate sub-nanosecond pumping, alternative laser sources such a picosecond or femtosecond lasers could be used. It is unlikely that an incremental study into pulse duration like the one undertaken in this thesis would be possible with such lasers, as the pulse duration of more complex ultrashort pulsed systems cannot typically be varied. Nonetheless, it could offer an insight into the behaviour of LC lasers in the sub-nanosecond regime.

8.3.3 Repetition rate

In addition to independently controlling the pulse length, the LD driver electronics used in this work were capable of delivering a repetition rate up to 2 MHz. The LC laser architecture would need to be redesigned to achieve such high repetition rates, however, and would likely not be practical using a spinning cell configuration. For example, for a 2 MHz repetition rate pump with a spot diameter of 20 μm to achieve an *effective* repetition rate of 100 Hz (i.e. the number of times per second that the same cell position is pumped), an LC laser cell diameter of 12 cm spinning at ~ 6000 rpm (i.e. 100 Hz) would be required. This would produce milliwatts of average power, but with obvious impracticalities, such the requirement of a large device to accommodate a large laser cell, and the fast spinning possibly causing centrifugal effects

within the LC. Dynamic pumping could overcome the challenges of a spinning cell arrangement by using previously demonstrated holography techniques [148] or by scanning mirrors to translate the pump beam across the active area of a static cell. However, while this could enable high repetition rate pumping, the position of the output beam would vary, unless an optical configuration could combine the output to a single spot. As discussed below (Section 8.3.5) high repetition rate pumping will likely only succeed if inorganic gain media are introduced to LC laser technology.

8.3.4 Peak power

Apart from the pump pulse length, the peak pulse power of the LD used in this work was the main difference in the pump performance compared to a Q-switched pump source. The peak power could be increased by increasing the current from 15 A (the maximum current tested in this thesis) to 50 A (the maximum current deliverable by the electronics). However this is only a modest increase and would still be lower than the peak power offered by Q-switched lasers. The peak power of the LD pumping technique could be increased by combining the emission from arrays of laser diodes to a single spot (as exemplified by Wang *et al.* [130]). When accompanied by an increase in current delivered to the LDs, this could offer at least one order of magnitude improvement in peak power. However, depending upon the number of LDs and the complexity of the driver electronics, this may result in a negligibly small improvement in size and cost compared to a Q-switched pump laser. While it is not desirable to increase the pump peak power indefinitely due to detrimental thermal and dye molecule reorientational effects, higher power LDs would be advantageous. More work is needed in semiconductor-based material development to enable higher currents and/or more efficient devices to produce higher powers.

8.3.5 Alternative gain media

Many of the challenges regarding the temporal limitations of LC lasers (i.e. long pump pulse lengths and high repetition rate pumping) are caused by the energy level structure of the organic dyes incurring triplet state population, as discussed throughout this thesis. If there were a way to prevent performance degradation of the dye or to replace the dye with an inorganic emitter, this could remove the need for spinning the laser altogether and even lead to CW

operation. Adding triplet state quenchers to the dye [149]–[151] or integrating quantum dot technology with LCs [137], [138], [152], [153] are possible solutions to overcome temporal limitations. Both would be worthwhile research topics for the future development of LC lasers.

8.3.6 Fabrication

The ability to produce LC laser emission with a semiconductor-based pump source could present an exciting opportunity regarding the manufacture of LC lasers. The mass production of semiconductors is well established, and the increase in popularity of gallium nitride (GaN) over silicon [154] is particularly relevant, as this is the material used in the 445 nm LD. It is conceivable that a single, monolithic device could be manufactured in which the LC laser emitter is fabricated directly on top of the semiconductor. Furthermore, electrical tuning of LC lasers where the laser cell is made from ITO-coated substrates has been demonstrated [155]. Thus a microscale tuneable LC laser could be achieved.

The LC laser fabrication process is currently performed manually on a cell-by-cell basis. However, it ought to be possible to upscale this for mass manufacture, as the process is similar to that used for manufacturing displays. LC lasers could be more efficiently and effectively fabricated in large scales, as per display manufacturing, or through wafer-scale fabrication approaches.

Methods such as using thermally conductive substrates, antireflective coated substrates and polymer templating have demonstrated high slope efficiencies, with the current record claiming a slope efficiency of 60 % [71]. This is an order of magnitude increase compared to the slope efficiencies demonstrated in this work, and highlights the impact that improved fabrication techniques can have on LC laser performance.

8.4 Concluding remarks

The unique intellectual and practical contributions to LC laser development reported in this thesis are anticipated to not only bring the commercialisation of LC lasers closer to realisation, but also to motivate further research in field. The benefits of LC lasers in applications such as holography (through a reduction in speckle), medical imaging (through improved precision in

fluorophore targeting) and displays (by improving the range of perceivable colours), highlight the breadth of possibilities this technology offers. With continuing technological improvements, interdisciplinary research collaborations, and financial investment, LC lasers are on the cusp of becoming a disruptive technology in the compact, wavelength selective/tuneable laser market.

Bibliography

[1] T. H. Maiman, "Stimulated Optical Radiation in Ruby," *Nature*, vol. 187, no. 4736, pp. 493–494, 1960.

[2] B. P. Abbott *et al.*, "Observation of gravitational waves from a binary black hole merger," *Phys. Rev. Lett.*, vol. 116, no. 6, pp. 1–16, 2016.

[3] J. Wilson and J. Hawkes, *Optoelectronics*, 3rd ed. Prentice Hall, 1998.

[4] D. E. Murnick, "Laser applications in nuclear physics: Present and future," *Hyperfine Interact.*, vol. 24, no. 1, pp. 1–17, Aug. 1985.

[5] T. Gaumnitz *et al.*, "Streaking of 43-attosecond soft-X-ray pulses generated by a passively CEP-stable mid-infrared driver," *Opt. Express*, vol. 25, no. 22, pp. 27506–27518, Oct. 2017.

[6] F. Lureau *et al.*, "High-energy hybrid femtosecond laser system demonstrating 2 × 10 PW capability," *High Power Laser Sci. Eng.*, vol. 8, 2020.

[7] M. A. Noginov *et al.*, "Demonstration of a spaser-based nanolaser," *Nature*, vol. 460, p. 1110, Aug. 2009.

[8] L. S. Goldberg and J. M. Schnur, "Tunable internal feedback liquid crystal dye laser," 3771065, 1973.

[9] I. Ilchishin, E. Tikhonov, V. Tishchenko, and M. Shpak, "Generation of a tunable radiation by impurity cholesteric liquid crystals," *JETP Lett*, vol. 32, no. 1, pp. 24–27, 1980.

[10] J. P. Dowling, M. Scalora, M. J. Bloemer, and C. M. Bowden, "The photonic band edge laser: A new approach to gain enhancement," *J. Appl. Phys.*, vol. 75, no. 4, pp. 1896–1899, 1994.

[11] V. I. Kopp, B. Fan, H. K. M. Vithana, and A. Z. Genack, "Low-threshold lasing at the edge of a photonic stop band in cholesteric liquid crystals," *Opt. Lett.*, vol. 23, no. 21, p. 1707, 1998.

[12] H. J. Coles, S. M. Morris, A. D. Ford, P. J. W. Hands, and T. D. Wilkinson, "Red-green-blue 2 D tuneable liquid crystal laser devices," *Liq. Cryst. XIII*, vol. 7414, pp. 741402-1-741402–21, 2009.

[13] M. C. Normand, P. Chen, C. Can, and P. J. W. Hands, "Overcoming repetition rate limitations in liquid crystal laser systems," *Opt. Express*, vol. 26, no. 20, p. 26544, 2018.

[14] A. Munoz, P. Palffy-Muhoray, and B. Taheri, "Ultraviolet lasing in cholesteric liquid

crystals," *Opt. Lett.*, vol. 26, no. 11, pp. 804–806, 2001.

[15] P. J. W. Hands *et al.*, "Wavelength-tuneable liquid crystal lasers from the visible to the near-infrared," *Liq. Cryst. XV*, vol. 8114, p. 81140T, 2011.

[16] Y. Watanabe, M. Uchimura, F. Araoka, G. I. Konishi, J. Watanabe, and H. Takezoe, "Extremely low threshold in a pyrene-doped distributed feedback cholesteric liquid crystal laser," *Appl. Phys. Express*, vol. 2, no. 10, pp. 85–87, 2009.

[17] Y. Takanishi, Y. Ohtsuka, G. Suzaki, S. Nishimura, and H. Takezoe, "Low threshold lasing from dye-doped cholesteric liquid crystal multi-layered structures.," *Opt. Express*, vol. 18, no. 12, pp. 12909–12914, 2010.

[18] X. Zhan, H. Fan, Y. Li, Y. Liu, and D. Luo, "Low threshold polymerised cholesteric liquid crystal film lasers with red, green and blue colour," *Liq. Cryst.*, vol. 46, no. 6, pp. 970–976, 2019.

[19] J. Xiang *et al.*, "Electrically tunable laser based on oblique heliconical cholesteric liquid crystal," *Proc. Natl. Acad. Sci.*, vol. 113, no. 46, pp. 12925–12928, 2016.

[20] J. De Lin *et al.*, "Widely tunable photonic bandgap and lasing emission in enantiomorphic cholesteric liquid crystal templates," *J. Mater. Chem. C*, vol. 5, no. 13, pp. 3222–3228, 2017.

[21] T. J. MacGillivray, E. Trucco, J. R. Cameron, B. Dhillon, J. G. Houston, and E. J. R. Van Beek, "Retinal imaging as a source of biomarkers for diagnosis, characterization and prognosis of chronic illness or long-term conditions," *Br. J. Radiol.*, vol. 87, no. 1040, 2014.

[22] C. Dysli, S. Wolf, M. Y. Berezin, L. Sauer, M. Hammer, and M. S. Zinkernagel, "Fluorescence lifetime imaging ophthalmoscopy," *Progress in Retinal and Eye Research*. 2017.

[23] K. Nienhaus and G. U. Nienhaus, "Genetically encodable fluorescent protein markers in advanced optical imaging," *Methods Appl. Fluoresc.*, vol. 10, no. 4, 2022.

[24] J. W. Dobrucki and U. Kubitscheck, "Fluorescence Microscopy 3 . 1 Contrast in Optical Microscopy," 2019.

[25] A. K. Sreedhar and B. L. Sharma, "Light Emitting Diodes.," vol. 1, no. March 2015, pp. 1–13, 1973.

[26] S. M. Morris, P. J. W. Hands, S. Findeisen-Tandel, R. H. Cole, T. D. Wilkinson, and H. J. Coles, "Polychromatic liquid crystal laser arrays towards display applications," *Opt. Express*, vol. 16, no. 23, p. 18827, 2008.

[27] J. Someya *et al.*, "Laser TV: Ultra-Wide Gamut for a New Extended Color-Space

Standard, xvYCC," *SID Symp. Dig. Tech. Pap.*, vol. 37, no. 1, p. 1134, 2006.

[28] P. J. W. Hands, C. M. Brown, D. K. E. Dickinson, S. M. Morris, and J. Lin, "Liquid-Crystal Lasers : Recent Advances and Future Opportunities," *Soc. Inf. Disp.*, vol. 53, no. 2, pp. 440–443, 2022.

[29] W. Cao, P. Palffy-Muhoray, B. Taheri, A. Marino, and G. Abbate, "Lasing thresholds of cholesteric liquid crystals lasers," *Mol. Cryst. Liq. Cryst.*, vol. 429, pp. 101–110, 2005.

[30] N. M. Shtykov and S. P. Palto, "Modeling laser generation in cholesteric liquid crystals using kinetic equations," *J. Exp. Theor. Phys.*, vol. 118, no. 5, pp. 822–830, 2014.

[31] J. Ortega, C. L. Folcia, and J. Etxebarria, "Upgrading the performance of cholesteric liquid crystal lasers: Improvement margins and limitations," *Materials (Basel).*, vol. 11, no. 1, pp. 1–24, 2017.

[32] S. M. Morris, A. D. Ford, M. N. Pivnenko, and H. J. Coles, "The effects of reorientation on the emission properties of a photonic band edge liquid crystal laser," *J. Opt. A Pure Appl. Opt.*, vol. 7, no. 5, pp. 215–223, 2005.

[33] A. Varanytsia and P. Palffy-Muhoray, "Thermal degradation of the distributed-feedback cavity in cholesteric liquid crystal lasers," *Liq. Cryst. XVII*, vol. 8828, no. September 2013, p. 88281F, 2013.

[34] J. Etxebarria, J. Ortega, C. L. Folcia, G. Sanz-Enguita, and I. Aramburu, "Thermally induced light-scattering effects as responsible for the degradation of cholesteric liquid crystal lasers," *Opt. Lett.*, vol. 40, no. 7, p. 1262, 2015.

[35] G. E. Nevskaya, S. P. Palto, and M. G. Tomilin, "Liquid-crystal-based microlasers," *J. Opt. Technol.*, vol. 77, no. 8, pp. 473–486, 2010.

[36] A. Chanishvili *et al.*, "Laser emission from a dye-doped cholesteric liquid crystal pumped by another cholesteric liquid crystal laser," *Appl. Phys. Lett.*, vol. 85, no. 16, pp. 3378–3380, 2004.

[37] G. Sanz-Enguita, J. Ortega, C. L. Folcia, I. Aramburu, and J. Etxebarria, "Role of the sample thickness on the performance of cholesteric liquid crystal lasers: Experimental, numerical, and analytical results," *J. Appl. Phys.*, vol. 119, no. 7, 2016.

[38] A. Muñoz *et al.*, "Continuous wave mirrorless lasing in cholesteric liquid crystals with a pitch gradient across the cell gap," *Opt. Lett.*, vol. 37, no. 14, p. 2904, 2012.

[39] J. Ortega, C. L. Folcia, G. Sanz-Enguita, I. Aramburu, and J. Etxebarria, "Kinetic behavior of light emission in cholesteric liquid crystal lasers: An experimental study," *Opt. Express*, vol. 23, no. 21, p. 27369, 2015.

[40] P. J. W. Hands, S. M. Morris, M. M. Qasim, D. J. Gardiner, T. D. Wilkinson, and H. J. Coles, "Continuous wavelength-tuning across the visible spectrum with a compact and inexpensive liquid crystal laser," *Abstr. from 24th Int. Liq. Cryst. Conf. (ILCC 2012), Mainz, Ger.*, 2012.

[41] M. C. Normand, "Towards Biomedical Imaging with Liquid Crystal Lasers," University of Edinburgh, Degree of Doctor of Philosophy, Supervisor: Philip J. W. Hands, 2019.

[42] A. Varanytsia, T. Guo, and P. Palffy-Muhoray, "Small footprint cholesteric liquid crystal laser," *Appl. Opt.*, vol. 58, no. 4, p. 739, 2019.

[43] F. Reinitzer, "Beitrage zur Kenntniss des Cholesterins," *Monatshefte für Chemie*, vol. 9, no. 1, pp. 421–441, 1888.

[44] P. Collings and M. Hird, *Introduction to Liquid Crystals*. Taylor & Francis, 2004.

[45] O. Lehmann, "Über fliessende Krystalle," *Zeitschrift für Phys. Chemie*, vol. 4U, no. 1, pp. 462–472, 1889.

[46] G. A. DiLisi, *History*. Morgan & Claypool Publishers, 2019.

[47] G. W. Gray, K. J. Harrison, and J. A. Nash, "New family of nematic liquid," *Electron. Lett.*, vol. 9, no. 6, pp. 130–131, 1973.

[48] H. S. Nalwa, *Handbook of Advanced Electronic and Photonic Materials and Devices*. Academic Press, 2001.

[49] "Global Liquid Crystal Display (LCD) Market – Industry Trends and Forecast to 2029," *Data Bridge Market Research*, 2022. [Online]. Available: https://www.databridgemarketresearch.com/reports/global-liquid-crystal-display-lcd-market. [Accessed: 09-Sep-2022].

[50] D. Andrienko, "Introduction to liquid crystals," *J. Mol. Liq.*, vol. 267, pp. 520–541, 2018.

[51] D. J. Mulder, A. P. H. J. Schenning, and C. W. M. Bastiaansen, "Chiral-nematic liquid crystals as one dimensional photonic materials in optical sensors," *J. Mater. Chem. C*, vol. 2, no. 33, pp. 6695–6705, 2014.

[52] I. C. . Khoo, *Liquid Crystals*, 2nd ed. Wiley-Interscience, 2007.

[53] S. J. Woltman, G. D. Jay, and G. P. Crawford, "Liquid-crystal materials find a new order in biomedical applications," *Nat. Mater.*, vol. 6, no. 12, pp. 929–938, 2007.

[54] G. Hegde and L. Komitov, "Periodic anchoring condition for alignment of a short pitch cholesteric liquid crystal in uniform lying helix texture," *Appl. Phys. Lett.*, vol. 96, no. 11, 2010.

[55] S. G. Lipson, H. Lipson, and D. Tannhauser, *Optical Physics*, Third. Cambridge, 2001.

[56] M. Mitov, "Cholesteric liquid crystals with a broad light reflection band," *Adv. Mater.*, vol. 24, no. 47, pp. 6260–6276, 2012.

[57] J. Guo *et al.*, "Polymer stabilized liquid crystal films reflecting both right- and left-circularly polarized light," *Appl. Phys. Lett.*, vol. 93, no. 20, pp. 1–4, 2008.

[58] L. Arissian and J. C. Diels, *Lasers: The Power and Precision of Light*. Wiley, 2011.

[59] P. W. Milonni and J. H. Eberly, *Lasers*. Wiley, 1988.

[60] O. Svelto, *Principles of Lasers*, 5th ed. Springer Science & Business Media, 2010.

[61] V. I. Kopp, Z.-Q. Zhang, and A. Z. Genack, "Lasing in chiral photonic structures," *Prog. Quantum Electron.*, vol. 27, no. 6, pp. 369–416, 2003.

[62] C. T. Wang *et al.*, "Electrically assisted bandedge mode selection of photonic crystal lasing in chiral nematic liquid crystals," *Appl. Phys. Lett.*, vol. 112, no. 4, 2018.

[63] S. M. Morris, A. D. Ford, C. Gillespie, M. N. Pivnenko, O. Hadeler, and H. J. Coles, "The emission characteristics of liquid-crystal lasers," *J. Soc. Inf. Disp.*, vol. 14, no. 6, pp. 565–573, 2006.

[64] SNAVELY BB, "Dye Lasers," *Spie J*, vol. 8, no. 4, pp. 119–125, 1970.

[65] O. G. Peterson, J. P. Webb, W. C. McColgin, and J. H. Eberly, "Organic dye laser threshold," *J. Appl. Phys.*, vol. 42, no. 5, pp. 1917–1928, 1971.

[66] S. Forget and S. Chenais, *Organic Solid State Lasers*. Springer, 2013.

[67] C. V. Shank, "Physics of dye lasers," *Rev. Mod. Phys.*, vol. 47, no. 3, pp. 649–657, 1975.

[68] Y. Zhou, Y. Huang, T.-H. Lin, L.-P. Chen, Q. Hong, and S.-T. Wu, "Direction controllable linearly polarized laser from a dye-doped cholesteric liquid crystal," *Opt. Express*, vol. 14, no. 12, p. 5571, 2006.

[69] K. Amemiya *et al.*, "Enhancement of laser emission intensity in dye-doped cholesteric liquid crystals with single-output window," *Jpn. J. Appl. Phys.*, vol. 44, no. 6 A, pp. 3748–3750, 2005.

[70] Y. Zhou, Y. Huang, A. Rapaport, M. Bass, and S. T. Wu, "Doubling the optical efficiency of a chiral liquid crystal laser using a reflector," *Appl. Phys. Lett.*, vol. 87, no. 23, pp. 1–3, 2005.

[71] C. Mowatt, S. M. Morris, T. D. Wilkinson, and H. J. Coles, "High slope efficiency liquid crystal lasers," *Appl. Phys. Lett.*, vol. 97, no. 25, pp. 1–4, 2010.

[72] O. G. Peterson, S. A. Tuccio, and B. B. Snavely, "Cw operation of an organic dye solution laser," *Appl. Phys. Lett.*, vol. 17, no. 6, pp. 245–247, 1970.

[73] D. P. Benfey *et al.*, "Continuous-wave visible diode-pumped dye laser," *Visible UV Lasers*, vol. 2115, no. June 1994, p. 204, 1994.

[74] T. Dadalyan *et al.*, "Tuning the lasing wavelength of dye-doped chiral nematic liquid crystal by fluid flow," *Liq. Cryst.*, vol. 44, no. 2, pp. 372–378, 2017.

[75] P. Chen, "Multi-wavelength liquid crystal laser for 3D displays," University of Edinburgh, Degree of Master of Science, Supervisor: Philip J. W. Hands, 2018.

[76] A. Chanishvili *et al.*, "Widely tunable ultraviolet-visible liquid crystal laser," *Appl. Phys. Lett.*, vol. 86, no. 5, pp. 1–3, 2005.

[77] S. Furumi, "Self-assembled organic and polymer photonic crystals for laser applications," *Polym. J.*, vol. 45, no. 6, pp. 579–593, 2013.

[78] J.-D. Lin, H.-L. Lin, H.-Y. Lin, G.-J. Wei, and C.-R. Lee, "Wide-band tunable photonic bandgap device and laser in dye-doped liquid crystal refilled cholesteric liquid crystal polymer template system," *Proc. SPIE - Int. Soc. Opt. Eng.*, vol. 10125, no. February 2017, 2017.

[79] T. H. Lin, Y. J. Chen, C. H. Wu, A. Y. G. Fuh, J. H. Liu, and P. C. Yang, "Cholesteric liquid crystal laser with wide tuning capability," *Appl. Phys. Lett.*, vol. 86, no. 16, pp. 1–3, 2005.

[80] G. Chilaya *et al.*, "Reversible tuning of lasing in cholesteric liquid crystals controlled by light-emitting diodes," *Adv. Mater.*, vol. 19, no. 4, pp. 565–568, 2007.

[81] G. Chilaya, A. Chanishvili, G. Petriashvili, R. Barberi, M. P. De Santo, and M. A. Matranga, "Different Approaches of Employing Cholesteric Liquid Crystals in Dye Lasers," *Mater. Sci. Appl.*, vol. 02, no. 02, pp. 116–129, 2011.

[82] G. Chilaya *et al.*, "Light control of cholesteric liquid crystals using azoxy-based host materials," *Mol. Cryst. Liq. Cryst.*, vol. 453, no. 1, pp. 123–140, 2006.

[83] M. Ozaki, M. Kasano, T. Kitasho, D. Ganzke, W. Haase, and K. Yoshino, "Electro-tunable liquid-crystal laser," *Adv. Mater.*, vol. 15, no. 12, pp. 974–977, 2003.

[84] S. Furumi, S. Yokoyama, A. Otomo, and S. Mashiko, "Electrical control of the structure and lasing in chiral photonic band-gap liquid crystals," *Appl. Phys. Lett.*, vol. 82, no. 1, pp. 16–18, 2003.

[85] B. Park *et al.*, "Electrically controllable omnidirectional laser emission from a helical-polymer network composite film," *Adv. Mater.*, vol. 21, no. 7, pp. 771–775, 2009.

[86] H. Lu *et al.*, "Wide tunable laser based on electrically regulated bandwidth broadening in polymer-stabilized cholesteric liquid crystal," *Photonics Res.*, vol. 7, no. 2, p. 137, 2019.

[87] C. Mowatt, S. M. Morris, M. H. Song, T. D. Wilkinson, R. H. Friend, and H. J. Coles, "Comparison of the performance of photonic band-edge liquid crystal lasers using different dyes as the gain medium," *J. Appl. Phys.*, vol. 107, no. 4, 2010.

[88] B. B. Snavely, "Flashlamp-Excited Organic Dye Lasers," *Proc. IEEE*, vol. 57, no. 8, pp. 1374–1390, 1969.

[89] S. M. Morris, A. D. Ford, M. N. Pivnenko, O. Hadeler, and H. J. Coles, "Correlations between the performance characteristics of a liquid crystal laser and the macroscopic material properties," *Phys. Rev. E - Stat. Nonlinear, Soft Matter Phys.*, vol. 74, no. 6, pp. 1–5, 2006.

[90] J. Schmidtke and W. Stille, "Fluorescence of a dye-doped cholesteric liquid crystal film in the region of the stop band: Theory and experiment," *Eur. Phys. J. B*, vol. 31, no. 2, pp. 179–194, 2003.

[91] L. Penninck, J. Beeckman, P. De Visschere, and K. Neyts, "Light emission from dye-doped cholesteric liquid crystals at oblique angles: Simulation and experiment," *Phys. Rev. E - Stat. Nonlinear, Soft Matter Phys.*, vol. 85, no. 4, pp. 1–7, 2012.

[92] F. Araoka *et al.*, "How doping a cholesteric liquid crystal with polymeric dye improves an order parameter and makes possible low threshold lasing," *J. Appl. Phys.*, vol. 94, no. 1, pp. 279–283, 2003.

[93] H. A. Montejano, F. Amat-Guerri, A. Costela, I. García-Moreno, M. Liras, and R. Sastre, "Triplet-state spectroscopy of dipyrromethene·BF2 laser dyes," *J. Photochem. Photobiol. A Chem.*, vol. 181, no. 2–3, pp. 142–146, 2006.

[94] F. Araoka and H. Takezoe, "Towards highly-efficient liquid crystal microlasers," *Org. Photonic Mater. Devices XIII*, vol. 7935, no. February 2011, p. 79350A, 2011.

[95] S. S. Anufrik, V. V. Tarkovsky, G. G. Sazonko, and M. M. Asimov, "New laser dyes based on 3-imidazopyridylcoumarin derivatives," *J. Appl. Spectrosc.*, vol. 79, no. 1, pp. 46–52, 2012.

[96] T. H. Lin *et al.*, "Electrically controllable laser based on cholesteric liquid crystal with negative dielectric anisotropy," *Appl. Phys. Lett.*, vol. 88, no. 6, pp. 2–5, 2006.

[97] Y. Wang *et al.*, "Dependence of lasing threshold power on excitation wavelength in dye-doped cholesteric liquid crystals," *Opt. Commun.*, vol. 280, no. 2, pp. 408–411, 2007.

[98] C.-R. Lee, J.-D. Lin, T.-S. Mo, C.-T. Horng, H.-Y. Sun, and S.-Y. Huang, "Performance evolution of color cone lasing emissions in dye-doped cholesteric liquid crystals at different fabrication conditions," *Opt. Express*, vol. 23, no. 8, p. 10168,

2015.

[99] M. Meyer, J. C. Mialocq, and B. Perly, “Photoinduced intramolecular charge transfer and trans-cis isomerization of the DCM styrene dye. Picosecond and nanosecond laser spectroscopy, high-performance liquid chromatography, and nuclear magnetic resonance studies,” *J. Phys. Chem.*, vol. 94, no. 1, pp. 98–104, 1990.

[100] S. L. Bondarev, V. N. Knyukshto, V. I. Stepuro, A. P. Stupak, and A. A. Turban, “Fluorescence and electronic structure of the laser dye DCM in solutions and in polymethylmethacrylate,” *J. Appl. Spectrosc.*, vol. 71, no. 2, pp. 194–201, 2004.

[101] T. Förster, “Transfer mechanisms of electronic excitation,” *Discuss. Faraday Soc.*, vol. 27, no. 10, pp. 7–17, 1959.

[102] M. Berggren, A. Dodabalapur, R. E. Slusher, and Z. Bao, “Light amplification in organic thin films using cascade energy transfer,” *Nature*, vol. 389, no. 6650, pp. 466–469, 1997.

[103] A. D. Ford, S. M. Morris, and H. J. Coles, “Photonics and lasing in liquid crystals,” *Mater. Today*, vol. 9, no. 7–8, pp. 36–42, 2006.

[104] H. Wenzel, P. Crump, A. Pietrzak, X. Wang, G. Erbert, and G. Tränkle, “Theoretical and experimental investigations of the limits to the maximum output power of laser diodes,” *New J. Phys.*, vol. 12, 2010.

[105] Y. Yang, G. A. Turnbull, and I. D. W. Samuel, “Hybrid optoelectronics: A polymer laser pumped by a nitride light-emitting diode,” *Appl. Phys. Lett.*, vol. 92, no. 16, pp. 2006–2009, 2008.

[106] S. D. Stranks *et al.*, “Enhanced Amplified Spontaneous Emission in Perovskites Using a Flexible Cholesteric Liquid Crystal Reflector,” *Nano Lett.*, vol. 15, no. 8, pp. 4935–4941, 2015.

[107] T. Kozaki, T. Yanamoto, T. Miyoshi, Y. Fujimura, S. Nagahama, and T. Mukai, “52.3: High - Power InGaN Blue - Laser Diodes for Displays,” *SID Symp. Dig. Tech. Pap.*, vol. 36, no. 1, p. 1605, 2005.

[108] T. Kozaki, H. Matsumura, Y. Sugimoto, S. Nagahama, and T. Mukai, “High-power and wide wavelength range GaN-based laser diodes,” *Nov. In-pl. Semicond. Lasers V*, vol. 6133, no. February 2006, p. 613306, 2006.

[109] M. H. Chen, S. C. Hsiao, K. T. Shen, C. C. Tsai, and H. C. Chui, “The spectral mode evolution in a blue InGaN laser diode,” *Optik (Stuttg).*, vol. 186, no. April, pp. 41–45, 2019.

[110] M. H. Chen, S. C. Hsiao, K. T. Shen, C. C. Tsai, and H. C. Chui, “Single longitudinal

mode external cavity blue InGaN diode laser," *Opt. Laser Technol.*, vol. 116, no. March, pp. 68–71, 2019.

[111] D. Stefańska, M. Suski, A. Zygmunt, J. Stachera, and B. Furmann, "Tunable single-mode cw energy-transfer dye laser directly optically pumped by a diode laser," *Opt. Laser Technol.*, vol. 120, no. January, p. 105673, 2019.

[112] Z. Zhao, O. Mhibik, M. Nafa, S. Chénais, and S. Forget, "High brightness diode-pumped organic solid-state laser," *Appl. Phys. Lett.*, vol. 106, no. 5, pp. 2–7, 2015.

[113] O. A. Burdukova, M. V. Gorbunkov, V. A. Petukhov, and M. A. Semenov, "Diode-pumped dye laser," *Laser Phys. Lett.*, vol. 13, no. 10, 2016.

[114] D. Stefanska, M. Suski, and B. Furmann, "Tunable continuous wave single-mode dye laser directly pumped by a diode laser," *Laser Phys. Lett.*, vol. 14, no. 4, 2017.

[115] O. Burdukova, M. Gorbunkov, V. Petukhov, and M. Semenov, "Diode pumped tunable dye laser," *Appl. Phys. B Lasers Opt.*, vol. 123, no. 3, pp. 1–4, 2017.

[116] O. Burdukova, V. Petukhov, and M. Semenov, "Highly efficient tunable pulsed dye laser longitudinally pumped by green diodes," *Appl. Phys. B Lasers Opt.*, vol. 124, no. 9, pp. 1–5, 2018.

[117] Y. Ruan, "Heating and Cooling System for Liquid Crystals," University of Edinburgh, Degree of Master of Science, Supervisor: Philip J. W. Hands, 2016.

[118] S. M. Morris, A. D. Ford, B. J. Broughton, M. N. Pivnenko, and H. J. Coles, "Liquid crystal lasers: coherent and incoherent microsources," in *Emerging Liquid Crystal Technologies*, 2005, vol. 5741, no. April 2005, p. 118.

[119] J. Stöhr and M. G. Samant, "Liquid crystal alignment by rubbed polymer surfaces: A microscopic bond orientation model," *J. Electron Spectros. Relat. Phenomena*, vol. 98–99, pp. 189–207, 1999.

[120] R. Ozaki, T. Shinpo, and H. Moritake, "Improvement of orientation of planar cholesteric liquid crystal by rapid thermal processing," *Appl. Phys. Lett.*, vol. 92, no. 16, pp. 1–4, 2008.

[121] M. Schadt, K. Schmitt, V. Kozinkov, and V. Chigrinov, "Surface-Induced Parallel Alignment of Liquid Crystals by Linearly Polymerized Photopolymers," *Jpn. J. Appl. Phys.*, vol. 31, no. 7 R, pp. 2155–2164, 1992.

[122] R. Ozaki, T. Shinpo, M. Ozaki, and H. Moritake, "Lasing in cholesteric liquid crystal oriented by acoustic streaming," *Jpn. J. Appl. Phys.*, vol. 47, no. 2 PART 2, pp. 1363–1366, 2008.

[123] H. Coles and S. Morris, "Liquid-crystal lasers," *Nat. Photonics*, vol. 4, no. 10, pp. 676–

685, 2010.

[124] W. J. Marshall, "Two methods for measuring laser beam diameter," *J. Laser Appl.*, vol. 22, no. 4, pp. 132–136, 2010.

[125] H. K. C. Bahr, C. Bahr, E. M. Guyon, D. Langevin, and H. E. Stanley, *Chirality in Liquid Crystals*, 1st ed. Springer, 2001.

[126] Y. Matsuhisa *et al.*, "Low-threshold and high efficiency lasing upon band-edge excitation in a cholesteric liquid crystal," *Appl. Phys. Lett.*, vol. 90, no. 9, pp. 2005–2008, 2007.

[127] A. Stylogiannis, L. Prade, A. Buehler, J. Aguirre, G. Sergiadis, and V. Ntziachristos, "Photoacoustics Continuous wave laser diodes enable fast optoacoustic imaging," *Biochem. Pharmacol.*, vol. 9, pp. 31–38, 2018.

[128] "Nichia LED/LD." [Online]. Available: https://led-ld.nichia.co.jp/en/product/ld_industry.html. [Accessed: 02-Jul-2022].

[129] S. Klinkhammer *et al.*, "Continuously tunable solution-processed organic semiconductor DFB lasers pumped by laser diode," *Opt. Express*, vol. 20, no. 6, p. 6357, 2012.

[130] H. Wang, Y. Kawahito, R. Yoshida, Y. Nakashima, and K. Shiokawa, "Development of a high-power blue laser (445 nm) for material processing," *Opt. Lett.*, vol. 42, no. 12, p. 2251, 2017.

[131] J. Herrnsdorf *et al.*, "Micro-LED pumped polymer laser: A discussion of future pump sources for organic lasers," *Laser Photonics Rev.*, vol. 7, no. 6, pp. 1065–1078, 2013.

[132] A. M. Taleb, B. T. Chiad, and Z. S. Sadik, "Spectroscopic study of DCM as an active medium for luminescent solar concentrators," *Renew. Energy*, vol. 30, no. 3, pp. 393–398, 2005.

[133] M. Lehnhardt, T. Riedl, T. Weimann, and W. Kowalsky, "Impact of triplet absorption and triplet-singlet annihilation on the dynamics of optically pumped organic solid-state lasers," *Phys. Rev. B - Condens. Matter Mater. Phys.*, vol. 81, no. 16, 2010.

[134] I. C. Khoo, R. G. Lindquist, R. R. Michael, R. J. Mansfield, and P. LoPresti, "Dynamics of picosecond laser-induced density, temperature, and flow-reorientation effects in the mesophases of liquid crystals," *J. Appl. Phys.*, vol. 69, no. 7, pp. 3853–3859, 1991.

[135] A. Diaspro, G. Chirico, C. Usai, P. Ramoino, and J. Dobrucki, "Photobleaching," *Handb. Biol. Confocal Microsc. Third Ed.*, pp. 690–702, 2006.

[136] S. Chénais and S. Forget, "Recent advances in solid-state organic lasers," *Polym. Int.*, vol. 61, no. 3, pp. 390–406, 2012.

[137] S. G. Lukishova, L. J. Bissell, J. Winkler, and C. R. Stroud, "Resonance in quantum dot fluorescence in a photonic bandgap liquid crystal host," *Opt. Lett.*, vol. 37, no. 7, p. 1259, 2012.

[138] L. J. Chen, J. De Lin, and C. R. Lee, "An optically stable and tunable quantum dot nanocrystal-embedded cholesteric liquid crystal composite laser," *J. Mater. Chem. C*, vol. 2, no. 22, pp. 4388–4394, 2014.

[139] S. H. Yun and S. J. J. Kwok, "Light in diagnosis, therapy and surgery," *Nat. Biomed. Eng.*, vol. 1, no. 1, 2017.

[140] S. Haiyin, *Guide to Handling Laser Diode Beams*. Springer Netherlands, 2015.

[141] K. Chen, R. Yan, L. Xiang, and K. Xu, "Excitation spectral microscopy for highly multiplexed fluorescence imaging and quantitative biosensing," *Light Sci. Appl.*, vol. 10, no. 1, 2021.

[142] C. S. Adams and I. G. Hughes, "Optics f2f," *Optics f2f*. 2018.

[143] C. L. Folcia, J. Ortega, and J. Etxebarria, "Spot profile and beam divergence in cholesteric liquid crystal lasers," *Liq. Cryst.*, vol. 48, no. 3, pp. 1–9, 2020.

[144] "BSI Standards Publication Safety of laser products of laser products," 2014.

[145] C. M. Brown, D. K. E. Dickinson, and P. J. W. Hands, "Diode pumping of liquid crystal lasers," *Opt. Laser Technol.*, vol. 140, p. 107080, 2021.

[146] C. M. Brown, D. K. E. Dickinson, and P. J. W. Hands, "Advancing multi-wavelength liquid crystal laser microcavities in a compact prototype device using a laser diode pump source," *SPIE 11987, Laser Reson. Microresonators, Beam Control XXIV*, vol. 1198703, no. March, p. 12, 2022.

[147] K. Aflalo, M. Ben-David, A. Stern, and I. Juwiler, "Theoretical investigation of using a yellow (577nm) laser for diabetic retinopathy," *OSA Contin.*, vol. 3, no. 11, p. 3253, 2020.

[148] S. M. Wood *et al.*, "Adaptive holographic pumping of thin-film organic lasers," *Opt. Lett.*, vol. 38, no. 21, pp. 4483–4486, 2013.

[149] M. Ahmad, M. D. Rahn, and T. A. King, "Singlet oxygen and dye-triplet-state quenching in solid-state dye lasers consisting of Pyrromethene 567–doped poly(methyl methacrylate)," *Appl. Opt.*, vol. 38, no. 30, p. 6337, 1999.

[150] L. Zhao *et al.*, "Singlet-Triplet Exciton Annihilation Nearly Suppressed in Organic Semiconductor Laser Materials Using Oxygen as a Triplet Quencher," *IEEE J. Sel. Top. Quantum Electron.*, vol. 22, no. 1, pp. 26–34, 2016.

[151] A. S. D. Sandanayaka *et al.*, "Improvement of the quasi-continuous-wave lasing

properties in organic semiconductor lasers using oxygen as triplet quencher," *Appl. Phys. Lett.*, vol. 108, no. 22, 2016.

[152] J. Mirzaei, M. Reznikov, and T. Hegmann, "Quantum dots as liquid crystal dopants," *J. Mater. Chem.*, vol. 22, no. 42, pp. 22350–22365, 2012.

[153] Supreet and G. Singh, "Recent advances on cadmium free quantum dots-liquid crystal nanocomposites," *Appl. Mater. Today*, vol. 21, 2020.

[154] D. Athow, "How GaN is changing the future of semiconductors," *Techradar*, 2022. [Online]. Available: https://www.techradar.com/uk/news/how-gan-is-changing-the-future-of-semiconductors. [Accessed: 13-Jul-2022].

[155] H. Yu, B. Y. Tang, J. Li, and L. Li, "Electrically tunable lasers made from electro-optically active photonics band gap materials," *Opt. Express*, vol. 13, no. 18, p. 7243, 2005.

[156] A. Boudrioua, M. Chakaroun, and A. Fischer, "Organic Lasers," in *Organic Lasers*, Elsevier, 2017, pp. 95–130.

[157] N. P. Barnes and B. M. Walsh, "Amplified spontaneous emission - Application to Nd : YAG lasers," *IEEE J. Quantum Electron.*, vol. 35, no. 1, pp. 101–109, 1999.

[158] P. I. H. Bastiaens and A. Squire, "Fluorescence lifetime imaging microscopy: Spatial resolution of biochemical processes in the cell," *Trends Cell Biol.*, vol. 9, no. 2, pp. 48–52, 1999.

[159] T. K. Mavrogordatos *et al.*, "Density of photon states in dye-doped chiral nematic liquid crystal cells in the presence of losses and gain," *Phys. Rev. E - Stat. Nonlinear, Soft Matter Phys.*, vol. 86, no. 1, pp. 1–7, 2012.

[160] J. R. Masters, "HeLa cells 50 years on: the good, the bad and the ugly," *Nat. Rev. Cancer*, vol. 2, no. 4, pp. 315–319, 2002.

Appendices

Appendix A
Laser cell fabrication

Below are the details for laser cell fabrication in the cleanroom, and the process for making the dye-doped chiral nematic liquid crystal laser (DDN*LC) mixture. The cell fabrication process is for the case of a reflective cell geometry in which aluminium coated substrates are used. Any steps involving the aluminium-coated substrates can be ignored if a transmissive cell is required, in which case two plane glass substrates are used instead. The two different types of substrate will henceforth be referred to as "coated" and "glass" respectively.

The process was carried out as follows:

Cleaning

1. Submerge the coated substrates in a beaker of IPA and place in an ultrasonic bath filled with de-ionised (DI) water for 10 minutes (refreshing the chemical after 5 minutes).
2. Store in DI water until needed to prevent particle contamination.
3. Dissolve approximately fifty potassium hydroxide (KOH) pellets in DI water.
4. Wipe the surfaces of the glass substrates with a lint-free tissue soaked in the KOH solution. Rise with DI.
5. Clean the glass substrates using the following Piranha procedure under a fume hood: Mix a 3:1 ratio of sulphuric acid (H_2S0_4) and hydrogen peroxide (H_20_2), by slowly adding the 50ml of H_2O_2 to 150ml of H_2SO_4, using a thermometer to monitor the temperature of the solution. This should not exceed 70°C.
6. Submerge the glass substrates in the solution for 10 minutes.
7. Remove and rinse thoroughly in DI water. Store in DI water.

Spinning

1. Remove the polyimide (PI) from the freezer several hours before needed.
2. Mix a 1:1 ratio of PI with solvent N-Methyl-2-pyrrolidone (NMP) by adding 1.5 ml of each into a vial with a magnetic stirrer and place on an unheated hotplate to stir for 20 minutes at 100 rpm.

3. Once mixed, use a syringe to extract the solution, attach a filter to the syringe, then deposit the mixture into another vial. Leave for 1 hour to allow bubbles to leave.
4. Prepare the spin-coater by setting it to spin at 500 rpm for 5 seconds, immediately followed by 4000 rpm for 60 seconds.
5. Remove a cleaned substrate from the DI water, dry with the nitrogen gun, then place the substrate onto the spin-coater. (When coating the glass substrates, use a pen to mark an arrow on the side of the substrate pointing to the surface to be coated with PI.)
6. Clean a plastic pipette with a nitrogen gun then draw up a small volume of the PI mixture into the pipette. Deposit 2-3drops (just enough to cover top surface) onto the substrate.
7. Close the lid of the spin-coater, activate the vacuum to hold the substrate in place, then start the spinning process.
8. Once spinning is finished, remove the substrate and place it in a covered dish to prevent contamination.
9. Repeat this process for all substrates.

Curing

1. Carry out a pre-bake at 80°C for 5 minutes on a hotplate
2. Bake the glass substrates at 220 °C for 1.5 hours and the coated substrates at 140 °C for 3 hours.

Rubbing

1. Set the rubbing machine to a roller speed of 200 rpm, for 3 passes at a speed of 2 mm/s.
2. Place a substrate on the centre of the vacuum plate then beginning the rubbing process.
3. Do three passes per substrate and repeat for all substrates, making a mark on the side of the substrate with a pencil to show the rubbing direction.
4. Clean each substrate with an ionised nitrogen gun.

Gluing & UV-Curing

1. Add 2 wt% spacers to NOA68 glue inside a syringe. Stir and degas.
2. Attach the syringe with a 0.2 mm tip to the gluing machine.

3. Program glue dispenser with the following settings: pressure = 1.2 bar, point dispense = 0.2 s, Line speed = 8 mm/s.
4. Select the required program or create a new program to set the glue pattern parameters.
5. Place the substrate under the first position of the program and press start.
6. Remove the substrate from the machine and carefully place the second substrate ontop to form the cell, ensuring that the rubbing directions are anti-parallel and that the PI-coated surfaces are on the inside facing each other.
7. Gently press down, enough that the glue spreads evenly but without so much force as to crush the spacers.
8. Place the cell in the UV oven for 3 × 60 seconds to cure the glue.
9. Remove and store in a sealed container. The cell is now ready for filling with the dye-doped chiral nematic liquid crystal mixture.

Appendix B
Making the dye-doped chiral nematic liquid crystal laser mixture

The mixture used to form the DDN*LC is comprised of three components:

BL006 Nematic LC
BDH1281 high twisting power chiral dopant
Organic dye (e.g. DCM)

Making the chiral nematic liquid crystal

The first stage is to dissolve the chiral dopant in the LC. The total mass of the mixture depends upon the number of cells being filled with the mixture, but for approximately ten cells, a mass of LC of 200 mg is sufficient.

1. Clean an amber glass vial with nitrogen. (An amber vial is used to prevent UV damage of the laser dyes.)
2. Weigh the vial and zero the scale.
3. Add the desired mass of LC to the vial, then add the required mass of chiral dopant that will result in a photonic bandgap with the bandedge at the required spectral position for lasing.
4. Add a magnetic stirrer to the solution and place on the hotplate at 140°C, stirring at 200 rpm for 2 hours.
5. Place the mixture in an oven set to 100 °C and leave for at least 8 hours.
6. Remove the mixture from the oven.

If measurement of the bandgap position is required, at this stage of the process, use a glass pipette to extract a small volume of the chiral nematic and fill a pre-fabricated transparent Instec cell placed on a hotplate at 100 °C. Cool on the hotplate from 100°C to room temperature in increments of 0.3°C/min, rubbing the surface with a piece of soft plastic (e.g. a pen lid or plastic tweezers) to promote uniform alignment of the LC with the rubbed polymer layers.

Adding the dye

1. Place the chiral nematic mixture on a hotplate at 100 °C, ideally immediately after removing the mixture from the oven.
2. Add the desired mass of dye to the mixture.
3. With the hotplate set to 100 °C, set the stirrer to 200 rpm for at least 2 hours
4. Place the mixture in the oven for another 8 hours at 100 °C.

Filling the cell

1. Place an empty cell on the hotplate and set to 100 °C.
2. Remove the DDN*LC from the oven.
3. Use a glass pipette to extract a small volume of DDN*LC from the vial and use capillary action to transfer the mixture from the vial to the cell gap.
4. Ensure that the cell is filled fully with DDN*LC.
5. Set the hotplate to cool from 100 °C to room temperature in increments of 0.3 °C/min.

Appendix C
Equipment and materials

Cleaning Chemicals		
Chemical	**Model & Manufacturer/Supplier**	**Purpose**
Isopropyl Alcohol (IPA)	*Sigma Aldrich*	Cleaning Al-coated substrates
Potassium hydroxide (KOH)	*Fisher Scientific*	Cleaning uncoated substrates
N-Methyl-2-Pyrrolidone (NMP)	*OM Group Ultra Pure Chemicals Ltd*	Solvent for PI
Sulphuric acid (H_2SO_4)	*Gower Chemicals LTD*	Cleaning uncoated substrates

Laser Cell Parts		
Component	**Model & Manufacturer/Supplier**	**Purpose**
Glass substrates	*LAS-033024, Laser 2000*	Form LC laser cell
Polyimide (PI)	*SE-1410, Nissan Chemical Industries*	Coat inner surfaces of LC laser cells
UV-curable glue	*NOA68, Norland*	Glue substrates together
Spacer spheres	*Nanjing Jianzun Glass Microsphere Plant Company Ltd*	Form gap between substrates
Torr seal	*TS10, Varian*	Seal LC laser cell to contain dye-doped chiral nematic LC
Liquid crystal	*BL006, Merck*	Liquid crystal
Chiral dopant	*BDH-1281, Merck*	From chiral LC

Laser Dyes	
Dye	**Supplier**
4-(Dicyanomethylene)-2-methyl-6-(4-dimethylaminostyryl) -4H-pyran (DCM)	Exciton
Coumarin 504 (C504)	Exciton
Coumarin 540A (C540A)	Exciton

Cleanroom Equipment		
Tool	**Model & Manufacturer/Supplier**	**Purpose**
Ultrasonic bath	*SW12, Clifton*	Part of process for cleaning glass substrates
Hotplate	*1000-1 Hotplate, Electronic Micro Systems*	Pre-cure PI
Spin coater	*LIT-016, Polos*	Cover one surface of substrate in even layer of PI
Oven 1	*Junior Oven, Tennay*	Cure PI on Al-coated substrates
Oven 2	*VT 5050 EK, Heraeus*	Cure PI on uncoated substrates
Cloth rubbing machine	*HO-IAD-BTR-01, Holmarc*	Form alignment layer
Robotic gluing machine	*JR-2304N, Nordson EFD with JR2000N desktop robot, Janome.* *7018395 stainless steel tips, Nordson*	Make glue lines to glue substrates together
UV curing oven	*UV-1250, Loctite*	Cure NOA68 adhesive

Prep. Lab Equipment		
Tool	**Model & Manufacturer/Supplier**	**Purpose**
Balance	*PAS214C, Fisher Scientific*	Weighing DDN*LC constituents
Vials	*C4015-2W, Fisher Scientific*	Container for DDN*LC
Hotplate	*11-302-50 SHP, Fisher Scientific*	Heating and stirring DDN*LC
Oven	*Hotbox Oven (with fan), Sanyo Gallenkamp*	Heating DDN*LC

Appendix D
Optimising the DCM concentration

The concentration of dye in the cells varies throughout this thesis within the range of 0.5 wt% – 1.5 wt% and was based on a combination of literature values claiming optimum concentration [29], [87], and experimental evidence. The slope efficiency and threshold were used to determine the optimum dye concentration. Figure 0.1 shows results from an investigation for determining the optimum concentration of DCM in BL006. The optimum concentration was approximately 0.5 wt%, although other cells presented in this thesis appeared to work equally well with concentrations of 1.5 wt%. This disparity is likely caused by the variation in cell fabrication which, as highlighted in Chapter 3, was the dominant factor in determining the quality of the laser emission.

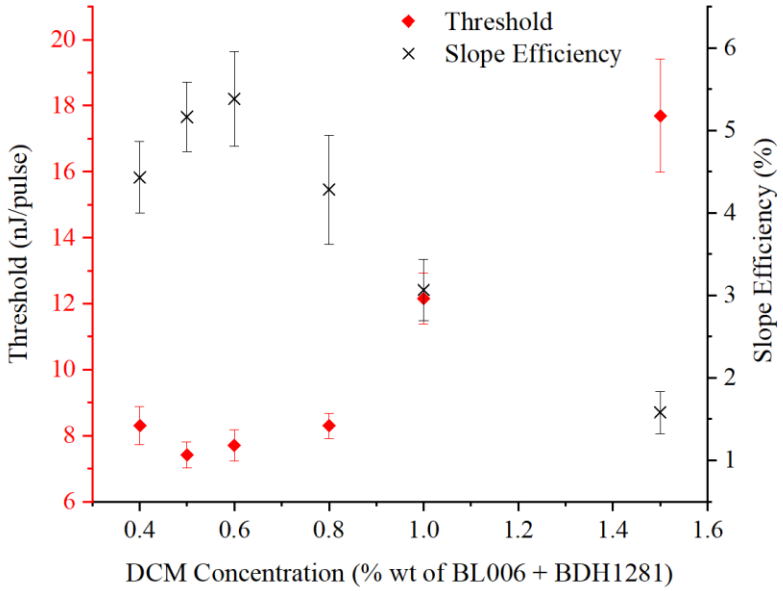

Figure 0.1. Experimental evidence showing the optimum concentration of DCM at ~ 0.5 wt%.

Appendix E

Least squares fit algorithm for the laser test software

The algorithm for determining the threshold and slope efficiency was developed and programmed by Ieva Pakamoryte as part of an Equate Scotland summer project during which she developed the laser test software (LTS).

In order to determine the threshold of an LC laser, the equations of the pre-threshold slope efficiency and post-threshold slope efficiency were needed, as it is at the point of intersection of these lines that corresponds to the laser threshold.

The least squares fit (chi-squared, χ^2) values for the data were needed. This is a statistical line to minimize the difference between experimental data and the theoretical best fit ($\chi^2 = 0$ is the ideal case).

$$\chi^2 = \sum_{i=1}^{N} \frac{[y_i - y_h(x_i)]^2}{\sigma_i^2} \qquad \textit{Equation 8}$$

where N = number of data points, σ_i = known uncertainty in each measurement, i denotes experimental data and h denotes theoretical/expected data.

For this work, y_i is a data point which is the mean energy value obtained in the time duration selected on the energy meter software and y_h is the corresponding expected point on the fitted line.
So, $y_h = mx + c$. This affects χ^2 so the aim is to find values of *m* and *c* that minimise χ^2. In order to do this, take the partial derivatives of χ^2 with respect to *m* and *c* and set them to zero. This leads to:

$$\chi^2 = \sum_{i=1}^{N} [y_i - (mx + c)]^2 \qquad \textit{Equation 9}$$

where the uncertainties, σ_i, are assumed to be the same for each data point and thus do not affect the χ^2 calculation.

Equating derivatives to zero and rearranging gives equations for *m* and *c* that, for the chosen data set, give the line of best fit, where *m* is given by:

$$m = \frac{\frac{\sum x_i y_i}{N} - \frac{\sum x_i}{N}\frac{\sum y_i}{N}}{\frac{\sum x_i^2}{N} - (\frac{\sum x_i}{N})^2} \qquad \textit{Equation 10}$$

Then for *c*, use:

$$c = \bar{y} - m\bar{x} \qquad \textit{Equation 11}$$

where $\bar{x} = \frac{\sum x_i}{N}, \bar{y} = \frac{\sum y_i}{N}$

These values of *m* and *c* result in the equation of the straight line for the chosen experimental values. From this, the residual can be calculated from:

$$\chi^2 = \sum_{i=1}^{N} [\bar{y}_i - (m\bar{x} + c)]^2 \qquad \textit{Equation 12}$$

So, imagine a data set consisting of 10 data points (which are each an average number of pulses at that position on the LC laser cell:

Position	E_{in}	E_{out}
1	x_1	y_1
2	x_2	y_2
3	x_3	y_3
⋮	⋮	⋮
10	x_{10}	y_{10}

In order to find the two lines that form the data below and above threshold, the χ^2 for N-1 (9 in this example) needs to be calculated for each pair of permutations, i.e.:

$$\left.\begin{aligned} \chi^2_{1a} &= \sum_{i=1}^{2} [\bar{y}_i - (m\bar{x} + c)]^2 \\ \chi^2_{1b} &= \sum_{i=3}^{10} [\bar{y}_i - (m\bar{x} + c)]^2 \end{aligned}\right\} \text{Permutation 1}$$

$$\left.\begin{aligned} \chi^2_{2a} &= \sum_{i=1}^{3} [\bar{y}_i - (m\bar{x} + c)]^2 \\ \chi^2_{2b} &= \sum_{i=4}^{10} [\bar{y}_i - (m\bar{x} + c)]^2 \end{aligned}\right\} \text{Permutation 2}$$

etc.

For each permutation, the two χ^2 values are summed, i.e.:

$$\chi^2_{1a} + \chi^2_{1b} \quad , \quad \chi^2_{2a} + \chi^2_{2b} \quad , \quad \cdots \quad , \quad \chi^2_{10a} + \chi^2_{10b}$$

and whichever permutation result in the smallest value (i.e. whichever results in *m* and *c* values which minimise the difference between experimental and theoretical data points) is the one from which *m* and are used to determine the equations of the two lines – one below threshold and one above threshold.

Once the equations for these two lines are known, henceforth referred to as below (B) and above (A), they can be equated to zero and then rearranged to find the threshold and efficiency.

$$y_B = m_{(B)}x + c_{(B)} \qquad \textit{Equation 13}$$

$$y_A = m_{(A)}x + c_{(A)} \qquad \textit{Equation 14}$$

The LC laser slope efficiency is simply given by:

$$\boldsymbol{\eta = m_{(A)}} \qquad \textit{Equation 15}$$

The threshold is given by finding the x value which is the E_{in} value (i.e. x-axis value) where both lines intersect:

$$y_B = m_{(B)}x + c_{(B)} = m_{(A)}x + c_{(A)}$$

$$\Rightarrow \quad m_{(B)}x - m_{(A)}x = c_{(A)} - c_{(B)}$$

$$\Rightarrow \quad \boldsymbol{x = \frac{c_{(A)} - c_{(B)}}{m_{(B)} - m_{(A)}} = E_{th}} \qquad \textit{Equation 16}$$

Appendix F
Optical losses

Optical losses measured with laser diode pump set with the following specifications:

Current = 12 A

Pulse length (set) = 20 ns

Repetition rate = 10 Hz

Losses calculated from the change in laser pulse energy before and after each component.

Free-space optical arrangement

Component	***Percentage Loss (%)***
90/10 Beamsplitter	14.6
Aluminium-coated mirror	12.2
Dichroic mirror	9.2
Microscope objective	21.8
Polarisation optics	5.0

Prototype

Component	***Percentage Loss (%)***
90/10 Beamsplitter	10.9
Quarter waveplate	0.5
Aluminium-coated mirror	3.8
Dichroic mirror	2.3
10 mm aspheric lens	1.6

Appendix G
Comments on the laser testing software (LTS)

The LTS enabled fast, repeatable data acquisition. Without it, human error would have been more prevalent and data acquisition would have required significantly more time. However, there were some limitations to the software that had to be accounted for.

The LTS was designed to process live read-outs from the data file created by the Starlab software that records the lasers' pulse energies. The energy meters could detect pulse energies in the range of 15 pJ – 200 nJ and the Starlab software uses four different energy detection windows (W_1-W_4) within this range: W_1 = 15 pJ – 200 pJ, W_2 = 200 pJ – 2 nJ, W_3 = 2 nJ – 20 nJ and W_4 = 20 nJ – 200 nJ. The energy window was set prior to the LTS beginning data acquisition and could not be changed while in progress. If the laser energy falls below or exceeds the energy within the set detection window, it displays an error and the data file being recorded in real-time replaces numerical values with an error message. As the LTS relied on the data file for calculating mean energy values at different positions of the half-waveplate and plotted them to extrapolate the slope efficiency and threshold, if a laser pulse fells outwith the pre-set energy window, then the LTS could not produce reliable data. A full data set could therefore only be recorded and analysed if the pump and LC laser energies fell within their respective pre-selected energy windows on the Starlab software. This limited the range of data that could be collected and was problematic if the range of data had energy values across two energy windows.

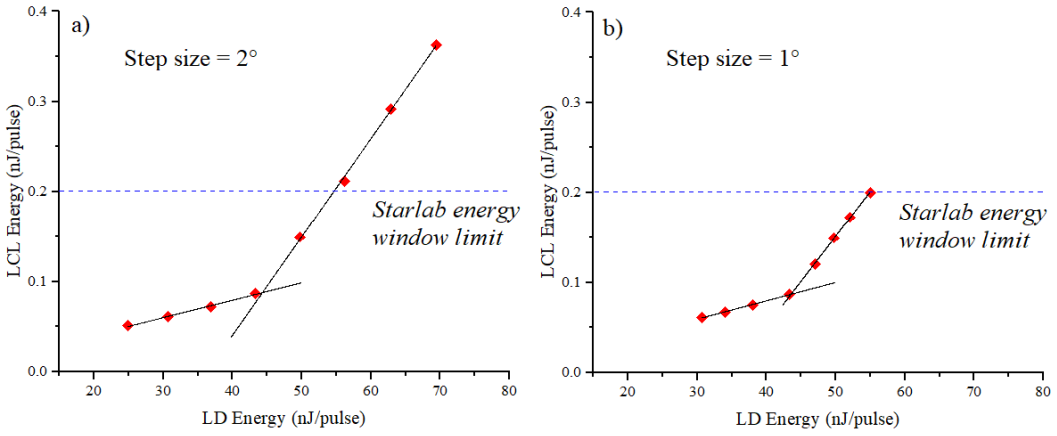

Figure 0.2. Hypothetical slope efficiency data demonstrating the limitation of the LTS. Example a) shows that only one data point above threshold would be possible within the limitation of the Starlab software for that chosen step size of 2 degrees (i.e. the angular difference in waveplate position to increase the pump pulse energy). This can be

resolved by reducing the step size to 1 degree as shown in b), thus allowing the same number of data points to be recorded but ensuring all are within the Starlab energy window.

For example, it may be the case that, across an angular range of 16 degrees of the half-waveplate, the LC laser output ranges from 50 pJ – 360 pJ, therefore crossing the 200 pJ energy boundary set by Starlab (Figure 0.2). Depending upon the threshold position, this problem could be resolved by adjusting the set step-size of the half-waveplate motor to reduce the range but still have sufficient data below and above threshold from which the slope efficiency could be calculated. Only when the threshold is at the exact boundary between the Starlab energy windows can the LTS not be used as there is no way to record data without changing the energy window.

The LTS's reliability was tested by manually calculating the threshold and slope efficiency of the same LC laser used throughout this chapter. The threshold was found by recording the pump energy at which the LC laser emission was detected on the spectrometer across a range of pump pulse lengths. The pump energy at the cell was adjusted by manually rotating the half-waveplate. The slope efficiency was found by calculating the gradient of the slope between this threshold energy and the maximum pump energy achievable for a given pulse length, again, by manually rotating the half-waveplate for maximum pump laser transmission. This resulted in near-identical threshold and slope efficiency values as calculated using the LTS, thus verifying its reliability. Any discrepancies between the values were within the error bars or each measurement. One caveat to this, is that there needed to be a sufficient *range* of data points, which also needed to be a sufficiently high step size apart, for an accurate slope efficiency calculation. If, for example, only three data points above threshold were recorded at only 0.1° apart, this would likely result in a significant underestimation in slope efficiency. If, at any point throughout the investigation, there was any doubt as to the accuracy of the values of threshold and slope efficiency calculated by the LTS, the measurement was repeated manually, which allowed a greater range of energy values to be measured as the Starlab energy windows limit could be changed without affecting the results.

Appendix H
Justification for mathematically removing the fluorescence signal

The method of post-processing the temporal data by mathematically subtracting the fluorescence emission from the total emitted light to show only laser emission (Figure 0.3a) was justified experimentally. In order to collect all of the light emitted from the LC laser cell for accurately measuring the temporal profile, the aperture was not present. By reinstalling the aperture to the optical arrangement, only on-axis emission was detected by the PD. This can be seen in Figure 0.3b, in which the addition of the aperture has little effect on the laser intensity and almost entirely removes the signal attributed to fluorescence. Comparison of Figure 0.3a to Figure 0.3b for a 94 ns pump pulse shows near identical results.

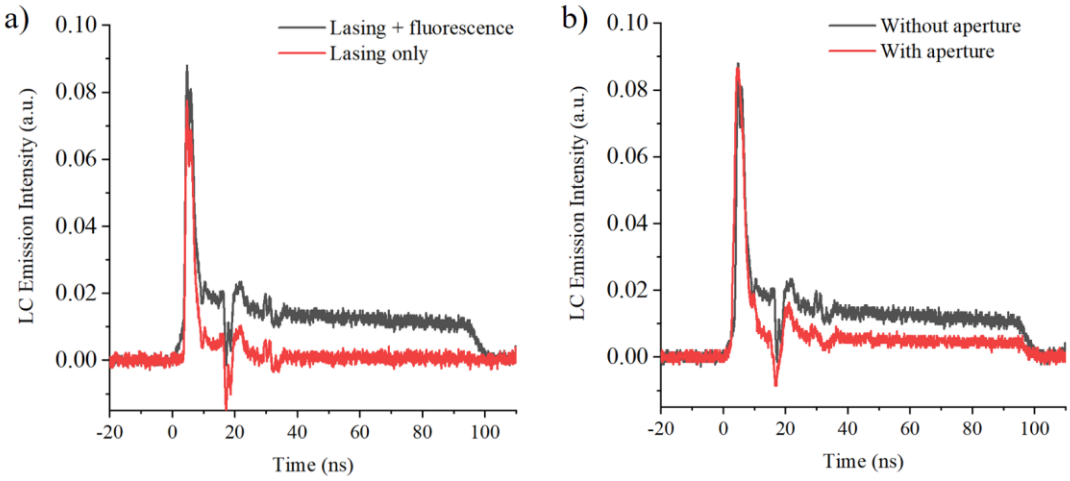

Figure 0.3. Removing of the fluorescence signal from the combined fluorescence-laser signal (black) to show only the laser signal (red) by a) mathematically subtracting the fluorescence post-measurement and b) using an aperture to attenuate all off-axis (fluorescence) emission during the experiment.

Appendix I
Arduino code for prototype

The Arduino coding was carried out by Ieva Pakamorytė, University of Edinburgh.

This code was used to program the motor and LCD for the prototype.

```
//include libraries for the motor driver & LCD respectively
#include "CytronMotorDriver.h"
#include "Waveshare_LCD1602_RGB.h"
#include <Wire.h>

// Configure the motor driver
CytronMD motor(PWM_PWM, 6, 9);   // PWM 1A = Pin 9, PWM 1B = Pin 10.

// Configure the LCD
Waveshare_LCD1602_RGB lcd(16,2);  //16 characters and 2 lines of show

// Defining the values for the potentiometer
int potPin = A0;
int potValue;
int last_motorValue = 0;

//For the hall sensor:
volatile uint32_t last_hall = 0;
volatile float hall_rpm = 0;

void setup() {
  // put your setup code here, to run once:

  // ***LCD ***
  // Initialises LCD
  lcd.init();
  lcd.setRGB(240,248,255);            // sets colour of LCD background
  lcd.setCursor(0,0);
  lcd.send_string("LC Laser");
  lcd.setCursor(0,1);
  lcd.send_string("Warming up...");

  delay(2000);
  lcd.clear();

  // *** POTENTIOMETER ***
  // This sets the potentiometer pin (A0 defined above) as the input
  pinMode(potPin, INPUT);

}
// This converts string to int
char buff[12];

// This void function tells the LCD what to display. It takes the global variable,
hall_rpm, (using the itoa() fn to convert
// a volatile float into a string) converts it to a buff format (which has 12
character spaces) with a base of 10.
// https://playground.arduino.cc/Code/PrintingNumbers/
void printHall() {
 }
void printRPM() {

    lcd.clear();
    lcd.setCursor(0,0);
    lcd.send_string("POT: ");
    lcd.setCursor(8,0);
    lcd.send_string(itoa(potValue,buff,10));

   }
```

```
int potentiometerRead () {

  potValue = analogRead(potPin);
  int curr_motorValue = map(potValue, 0, 1023, 0, 255);
  return curr_motorValue;
  }
// This is the error associated with fluctuations in the reading from the
potentiometer (noise).
// By including this error, it prevents the RPMs from being constantly updated and
only updates when the potentiometer is changed ie. when the motor speed is changed.
int potentiometerError = 2;

// The loop routine runs over and over again forever.
void loop() {

  int curr_motorValue = potentiometerRead();

  //Checks if the potentiometer has been moved ie. if the motor speed has changed. If
so, update the RPMs on the display. If not, keep the same RPMs unchanged.
  if (abs(curr_motorValue - last_motorValue) > potentiometerError)
    {
        //RPMs are recalculated here
        printRPM();

        motor.setSpeed(curr_motorValue); //set motors speed

        // Sets the previous motor value to the updated motor value after changing
the potentiometer
        last_motorValue = curr_motorValue;
     }
}
```

This code was used to program the Hall sensor for converting the potentiometer position to revolutions per minute of the motor.

```
volatile uint32_t last_hall = 0;
volatile float hall_rpm = 0;

// These let us convert ticks-to-RPM
float gearing = 20;
float encodermult = 12;

 void setup()
 {
   Serial.begin(9600);
   attachInterrupt(0, magnet_detect, FALLING);//Initialize the intterrupt pin
(Arduino digital pin 2)

 }
 void loop()//Measure RPM
 {
 }
 void magnet_detect()//This function is called whenever a magnet/interrupt is
detected by the arduino
 {

 uint32_t curr_hall = micros();

  if (last_hall < curr_hall) {
    float rev = curr_hall - last_hall;  // us
    rev = 1.0 / rev;            // rev per us
    rev *= 1000000;             // rev per sec
    rev *= 60;                  // rev per min
    hall_rpm = rev;
   }
last_hall = curr_hall;
  Serial.println(hall_rpm);
 }
```

Appendix J
Bill of materials for prototype

The list below details the parts required for the prototype build.

(Prices as of July 2022.)

Item	***Supplier***	***Part #***	***Cost (£)***
Aluminium enclosure	Richard Austin Alloys	6082T6	74.00
Laser diode	Endurance Lasers	NUBM44	40.00
Laser diode driver electronics	PicoLAS	LDP-V 50-100 V3.3	500.00
Laser diode pulse generator	PicoLAS	PLCS-21	640.00
Laser diode controller	PicoLAS	PLB-21	460.00
Beam splitter 10:90	Thorlabs	BSN04	87.65
Beam splitter mount	Thorlabs	POLARIS-B05G	29.95
Quarter waveplate	Thorlabs	WPQ05ME-445	238.58
Quarter waveplate mount	Thorlabs	RSP05/M	70.12
Broadband mirror	Thorlabs	BB05-E02	47.76
Mirror mount	Thorlabs	KS05K/M	79.86
Dichroic mirror	Edmund Optics	86-383	168.30
Dichroic mirror mount	Thorlabs	POLARIS-B05S	71.62
Aspheric lens	Thorlabs	ACL1210U-A	27.96
Aspheric lens mount	Thorlabs	LMR05/M	14.57
xyz stage	Thorlabs	DT12XYZ/M	295.00
5 V DC motor	Farnell	MM10	1.25
Fan	Farnell	F310R-05LC	7.07
Key switch	Farnell	S286A-1	10.37
Power box	Farnell	*BIM2006/26-BLK/BLK*	11.23
Arduino Nano	The PI Hut	ABX00033	12.50
Motor controller	The PI Hut	102514	4.00
LC display	The PI Hut	104056	9.50
LC laser cell	*Single cell estimate*	-	30.00
LC laser cell holder	*3D printed in-house*	-	-
		Total	**£2,931.29**